INVESTIGATION INTO SUBMICRON TRACK POSITIONING AND FOLLOWING TECHNOLOGY FOR COMPUTER MAGNETIC DISKS

by

BAOLIN TAN

A thesis submitted to the University of Plymouth

in partial fulfilment for the degree of

DOCTOR OF PHILOSOPHY

School of Electronic, Communication and Electrical Engineering

Faculty of Technology

October 1998

INVESTIGATION INTO SUBMICRON TRACK POSITIONING AND FOLLOWING TECHNOLOGY FOR COMPUTER MAGNETIC DISKS

by Baolin Tan

Abstract

In the recent past some magnetic heads with submicron trackwidth have been developed in order to increase track density of computer magnetic disks, however a servo control system for a submicron trackwidth head has not been investigated. The main objectives of this work are to investigate and develop a new servo pattern recording model, a new position sensor, actuator, servo controller used for submicron track positioning and following on a computer hard disk with ultrahigh track density, to increase its capacity.

In this position sensor study, new modes of reading and writing servo information for longitudinal and perpendicular magnetic recording have been developed. The read/write processes in the model have been studied including the recording trackwidth, the bit length, the length and shape of the transition, the relationship between the length of the MR head and the recording wavelength, and the S/N of readout. It has also been investigated that the servo patterns are magnetized along the radial direction by a transverse writing head that is aligned at right angles with the normal data head and the servo signals are reproduced by a transverse MR head with its stripe and pole gap tangential to the circumferential direction. It has been studied how the servo signal amplitude and linearity are affected by the length of the MR sensor and the distance between the shields of the head. Such things as the spacing and length of the servo-pattern elements have been optimised so as to achieve minimum jitter and maximum utilisation of the surface of the disk. The factors (i.e. the skew angle of the head) affecting the S/N of the position sensor have been analysed and demonstrated. As a further development, a buried servo method has been studied which uses a servo layer underneath the data layer, so that a continuous servo signal is obtained.

A new piezo-electric bimorph actuator has been demonstrated. This can be used as a fine actuator in hard disk recording. The linearity and delay of its response are improved by designing a circuit and selecting a dimension of the bimorph element. A dual-stage actuator has been developed. A novel integrated fine actuator using a piezo-electric bimorph has also been designed. A new type of construction for a magnetic head and actuator has been studied.

A servo controller for a dual-stage actuator has been developed. The wholly digital controller for positioning and following has been designed and its performances have been simulated by the MALTAB computer program.

A submicron servo track writer and a laser system measuring dynamic micro-movement of a magnetic head have been specially developed for this project.

Finally, track positioning and following on 0.7 μm tracks with a 7% trackwidth rms runout has been demonstrated using the new servo method when the disk was rotating at low speed. This is one of the best results in this field in the world.

Contents

List of Illustrations

Figure Page

LISTS OF ABBREVIATIONS AND SYMBOLS

ABBREVIATIONS

AC	Alternating Current
AE	Arm Electronics
A/D (ADC)	Analogue to Digital Convertor
BPI	Bits Per Inch
DC	Direct Current
DEMOD	Demodulator
DSK	DSP Starter Kit
DSP	Digital Signal Processor
DTM	Discrete Track Media
FCI	Flux Change Inch
FFT	Fast Fourier Transform
HDD	Hard Disk Drive
IBM	International Business Machines
IMC	Internal Model Control
IES	Integral-Error-Square
LQ	Linear Quadratic
LQG	Linear Quadratic Gaussian
LTR	Loop Transfer Recovery
MFM	Magnetic Force Microscope
MLSD	Maximum Likelihood Sequence Detection
MR	Magnetoresistance
PD	Peak Detection
PES	Position Error Signal
PLL	Phase Lock Loop
PR	Partial Response
PRML	Partial Response Maximum Likelihood
PZ	Piezoelectric ceramic
R/W	Read and Write
RZ	Return to Zero
S/N	Signal to Noise Ratio
SEM	Scanning Electron Microscope

SI	Serial Input
SO	Signal Output
SPM	Scanning Probe Microscope
SSTW	Submicron Servo Track Writer
TMR	Track misregistration
TPI	Track Per Inch
VCM	Voice Coil Motor
VSM	Vibrating Sample Magnetometer
WRTMR	Write-to-Read TMR
WWTMR	Write-to-Write TMR

SYMBOLS

a	the transition parameter; the arctangent parameter
a_{yp}	the transition width written by a single-pole head
a_{yr}	the transition width written by a ring head
b	the minimum servo pattern bit length
B_g	gap flux density
c	any constant for all r, x
C	capacitance
d	the head-media spacing
e	the readback voltage
f_r	resonant frequency
fi_{nd}	sensing function in output of inductive head
f_{MR}	sensing function in output of MR head
F	blocking force of PZ actuator
F_x	the driving force for PZ actuator in x axis
g	the gap length of the head
g (n, m)	the pattern offset at (n, m)
Gb/in^2	10^9 bits per Inch Square
h	the height of the magnetoresistor
H	magnetic field
H_0	the deep-gap field in oversteps; the reverse field in the MR film
H_2	the fields which would produce negative and positive remanent magnetization
H_b	the biasing field

H_c	the coercivity
H_{cr}	the remanence coercivity
H_d	the self-demagnetizing field
$H_{d,max}$	the maximum of demagnetizing field
H_h	the field of the head
H_x	the longitudinal field component
H_y	the perpendicular field component
I	the current magnitude
k	the number of cycles/cm
k (n, m)	the PES gain at (n, m)
k_t	torque constant
K_e	the sensitivity for measuring PES
L	the transition length; the position signal linearity; free length of PZ bimorph element
L_{min}	the minimum transition length
L_t	the total length of PZ bimorph element
m	mass
M	magnetization
M_r	remanent magnetisation (remanence)
M_x	the horizontal component of the magnetization vector
M_y	the vertical component of the magnetization vector
n	the sector index
N	the number of turns on the head
PE (n, m)	the total off-track error at (n, m)
r	track centre position
R_f	actuator force constant
S_T	the transition area per area unit
t	the pulse width of writing current per bit
v	the moving velocity
V	the speed of moving media
w	track width
x	the position of the head on disks
x_d	desired head location
X_s	the total stroke length in metres
z or Z	deflection of PZ actuator
Δz	a transverse region

Δz_{min}	the minimum transition width
δ	depth of focus; eddy current penetration depth; the coating thickness; thickness of a domain wall; thickness of a magnetic media
η	the efficiency of a write head
θ	the angle between the magnetization vector and the applied current
λ_{min}	the minimum wavelength
μ	relative magnetic permeability
μ_0	magnetic permeability of free space
ρ	the resistivity of the MR film
ρ_0	the normal resistivity
ρ_{max}	the maximum value of the change in resistivity

Acknowledgement

I would like to express my gratitude to all those people and organisations who have been associated with this project especially the following persons.

My supervisor Professor D. J. Mapps (Director of Studies), Dr. G. H. Pan and Mr. P. Robinson of the School of Electronic, Communication and Electrical Engineering at the University of Plymouth for their constant support, encouragement and guidance throughout the project.

Both members of the technical staff at the Centre for Research in Information Storage Technology for their support and friendship, in particular Mr. P. Brown without whose mechanical expertise and enthusiasm, many of the experiments in the work would not have been possible.

Professor W. W. Clegg of Manchester University, for his great help in the MFM observation.

Dr. R. Moate, Manager of the Electron Microscopy Centre at the University of Plymouth, for his help in SEM investigation.

Dr. D. Jenkins, Dr. P. Davey and Dr. R. Chandrasekar of the Centre for Research in Information Storage Technology at the University of Plymouth and Mr G. Quick in Xyratex Ltd. (former data storage division, IBM UK) for their many useful discussions.

Xyratex Ltd (former data storage division, IBM UK) for experience gained whilst working as development servo track writer engineer on advanced servo track writer for HDD for more than one year.

Mr. M. Abdin, Chairman of Dwight Cavendish Developments Ltd. for his strong support and the staff in this company for their friendship during the final correction of my Ph. D thesis.

Mr. P. Steven and Mrs. S. Steven for their constant friendship.

The National Computer Peripheral Equipment Research Institute in China, for their understanding and encouragement.

Most important of all my grateful thanks goes to my parents and wife, without whose unlimited support, patience, love and understanding this work would not have been possible.

AUTHOR'S DECLARATION

At no time during the registration for the degree of Doctor of Philosophy has the author been registered for any other University award.

This study was financed with the aid of research supports from The Centre for Research in Information Storage Technology, School of Electronic, Communication and Electrical Engineering at the University of Plymouth.

A programme of advanced study was undertaken, which included extensive reading of literature relevant to the research project, an advanced course on Applied Magnetism and Magnetic Recording and Modern Control Engineering, supervised training in Scanning Electron Microscopy and Magnetic Force Microscopy.

Four papers from this work have been presented at international conferences and published in the relevant journals. Copies of published papers are included in Publication of this thesis.

In addition the author attended The 6th MRM International Conference, July 1995, in Oxford, U.K. and The 2nd European Conference on Magnetic Sensors & Actuators, July 1998, in Sheffield, UK.

Signed..Baolin Tan.....

Date..18.2.99.....

To My Motherland

Chapter One

Background to the Investigation

1.1 Introduction

Magnetic recording technology is developing very fast towards higher information storage density, larger capacity, faster access, smaller volume and lower costs. For 30 years, up to 1990, the areal storage density of hard disk drives has increased about an order of magnitude per decade. Since 1992, the pace of this increase has picked up and currently is about 60% per year. Recently IBM has successfully demonstrated magnetic recording at an areal density of 3.1 Gb/in^2 with 1.5 μm trackpitch [Tsang et al., 1996]. The areal density in 2000 and 2005 may go up to 10 Gb/in^2 (bits per inch (BPI) = 400 k bits, tracks per inch (TPI) = 25 k tracks) and 100 Gb/in^2 (BPI = 1250 k bits, TPI = 80 k tracks) respectively [Wood, 1994]. Furthermore, Chou has made a disk with a recording bit size of 50 × 50 nm (TPI = 500 k) [Chou & Krauss, 1996]. In the Centre for Research in Information Storage Technology, University of Plymouth, hard disks with 10 Gb/in^2 are being researched by Mapps et al. [Mapps, 1995]. A bit density has been achieved of about 150,000 BPI in the production of hard disks, but the track density is lower about 15,000 TPI. So large increases in track density are anticipated in the 21 st century [Ottesen, 1994].

The increase in track density is limited by the track width of read and write heads and the accuracy with which the heads can be positioned. In the recent past, a number of

very narrow-track heads, e.g. a trackwidth of 1.2 μm, 1 μm, 0.4 μm have been developed [Takano et al., 1991] [Tsang et al., 1996] [Nakamura et al., 1994]. However, the study of a head position servo control system corresponding to the above heads is very late. The servo control system for a submicron track-width head has never been investigated.

In studying the head positioning and following on micron-sized tracks, Akagi used a laser-diode optical system fixed to the side of a magnetic head to obtain a servo signal on 1.5 μm of trackwidth on rigid disks [Akagi et al., 1991]. Mori developed a dual-stage actuator used to seek and follow on 1.5 μm magnetic tracks [Mori et al., 1991]. Watanabe achieved 5.2 μm track-seeking and following based on discrete track media using a servo signal reproduced by the data head [Watanabe et al., 1993]. More recently, Zhang reported a new method using etched patterns on hard disks to obtain head positioning of 4000 TPI [Zhang et al., 1994]. Fan described a rotary microactuator for fine positioning of recording heads with a stroke of ± 2.54 μm [Fan et al., 1994].

This project was proposed to meet the technical challenge of increasing track density. The aim of this work is to: (a) demonstrate a servo (positioning) measuring system, actuator and controller for ultra-high recording density (10 Gb/in^2) computer magnetic disks, and (b) to investigate the design and development of a dual-stage actuator and controller, with particular emphasis on the position measuring system. Following the introduction, the fundamental theories of magnetic recording and the principle of the computer hard disk drive are discussed. A systematic review is presented of an assortment of various servo control systems including the position measuring system, actuator and controller.

Chapter Two describes a new servo pattern recording/reading model suited for submicron servo track positioning and following. A systematic discussion of the model is presented in more detail and related to the main recording and reproducing performance parameters.

Chapter Three describes the development of the main experiments and equipment including the submicron servo track writer and real-time measuring system for submicron movement. Some experimental techniques for observation of the magnetic servo pattern, signal measuring and analysis (using MATLAB) are also given. The experimental procedure and some results are also described.

Chapter Four presents detailed results and discussion of the main investigation into the position measuring system. It contains four major parts as follows:

ℵ Performance of the new position sensor on longitudinal rigid disks. The major issues investigated included sensitivity, linearity and S/N ratio of the sensor and also the effect of servo Magnetoresistive head gap and length. ℑ Study of a new position sensor for perpendicular rigid disks. ℜ Study of a novel 'buried' servo with separate servo layer, including the effect of the gap and length of MR head, thickness and magnetic coercivity of the data and servo layers as well as thickness of the insulating layer, and servo and data frequency. ℘ Discussion of the design and result of the position measuring system.

Chapter Five presents detailed results and discussion of the investigation of a new dual-stage actuator. The mathematical model of the actuator is developed. Its main performance is measured and studied. A new 'bimorph' actuator is also discussed.

Chapter Six describes the design of the controller including simulation results. The initial hardware and algorithm employed in this design are given in more detail.

Chapter Seven presents the author's conclusions, together with a recommendation for further research.

1.2 Background to the Investigation

1. 2.1 Magnetic recording principles

1.2.1.1 Fundamentals of magnetic recording

The fundamental principles of operation of most magnetic recording products are similar in all cases including recorded servo information, which is depicted in Figure 1.1. As the writing current encoded by the information to be stored passes through the coil of the inductive head, it produces a magnetic field. If the field around the gap produced by the head is sufficient to overcome the coercive force of the media, the media will be magnetized by the head field, and a "recorded" magnetization in the media is formed. Thus a representation of the current waveform applied to the head (information) is stored in the media.

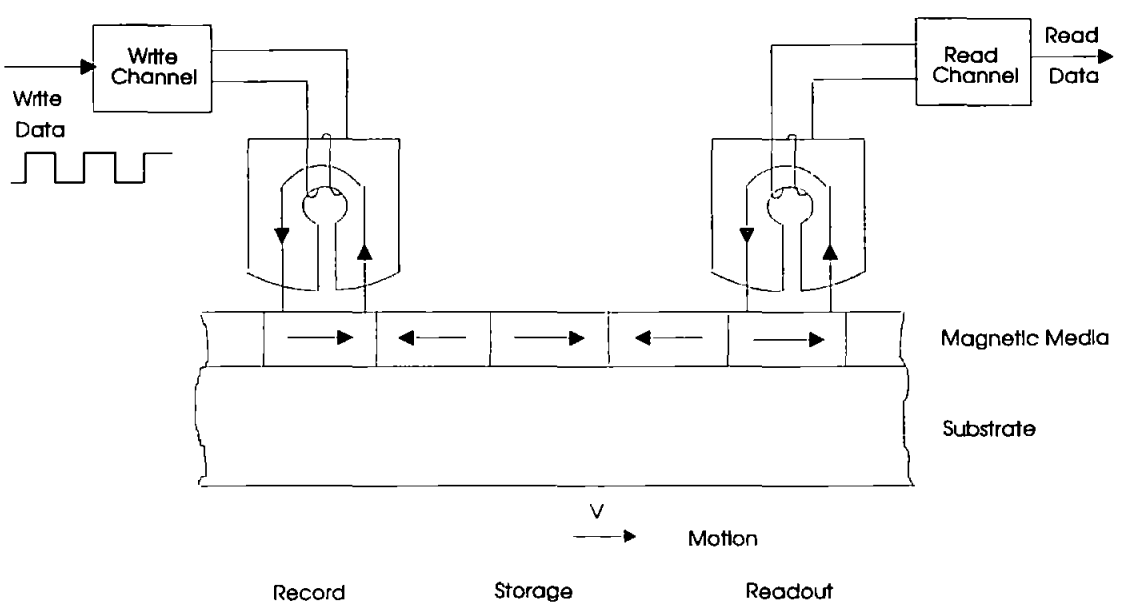

Figure 1.1 Diagram illustrating the fundamental magnetic recording configuration

Readout of previously-recorded information is accomplished by using the head to sense change of the magnetic stray fields produced by the recorded patterns in the media

when the recorded media is passed over the head. If the media is moved with respect to the head, the flux passing through the coil around the head will change in a manner which is representative of the recorded magnetization pattern in the media. By Faraday's Law of Induction, a voltage representative of the recorded information is thus induced in the coil and is proportional to the rate of change of this flux [Bertram & Mapps et al., 1994].

1.2.1.2 Theory of the magnetic recording process

In the writing (recording) process, the fringing field produced by the recording head magnetizes the media as the media is moved past the head. Karlquist presented the most commonly used analytical solution for the field in front of the write-gap of a ring head. As indicated by the co-ordinates in Figure 1.2, the longitudinal field component H_x and the perpendicular field component H_y of the head could be described by

$$H_x = \frac{NI}{2\pi g}\left[\tan^{-1}\left(\frac{x+\frac{g}{2}}{y}\right) - \tan^{-1}\left(\frac{x-\frac{g}{2}}{y}\right)\right] \tag{1-1}$$

$$H_y = \frac{NI}{2\pi g}\ln\left[\frac{\left(x+\frac{g}{2}\right)^2 + y^2}{\left(x-\frac{g}{2}\right)^2 + y^2}\right] \tag{1-2}$$

where N is the number of turns on the head and the contours of equal longitudinal field are described approximately by circles passing through the gap corners as shown in Figure 1.2, except at points of very near the gap corners.

In digital or saturation recording, some portion of the media see fields less than those required for saturation, because of the gradient. This is illustrated in Figure 1.2 where the contours for three different longitudinal fields are drawn. In the Figure 1.2 H_{cr}

is the remanence coercivity of the media, H_1 and H_2 are fields which would generate negative and positive remanent magnetization M_1 and M_2, respectively. H_1 and H_2 are dependent on the head field gradient. Note that smaller head-to-media spacing and thinner media both lead to narrower transitions being recorded, because the head field gradient is the sharpest near the pole tips of the head. Another factor, the demagnetizing field of the media itself produces transition region. However, those transition regions are expected as short as possible, in order to achieve higher recording bit density

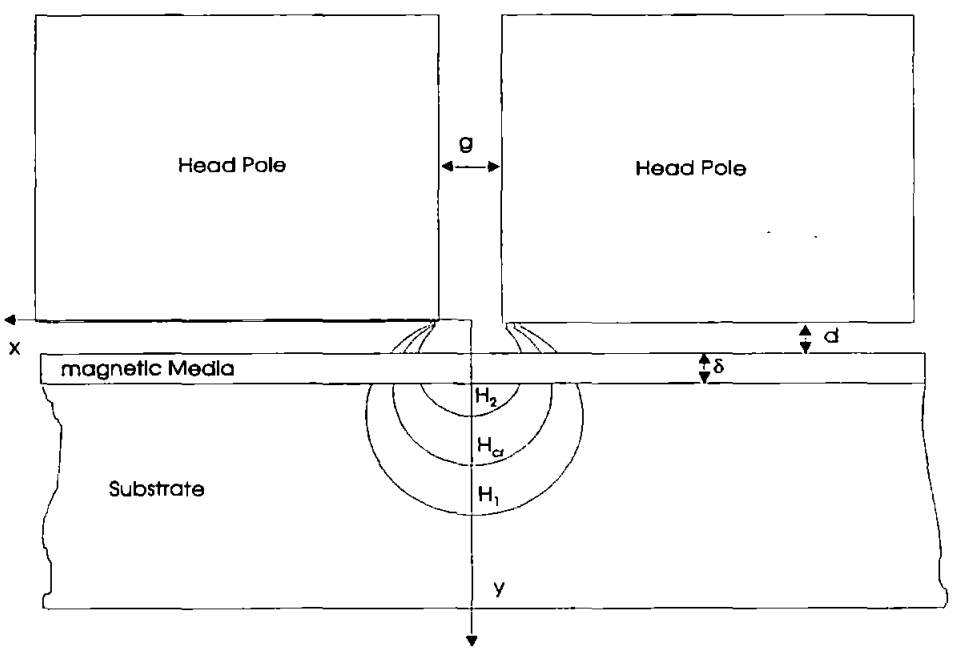

Figure 1.2 Diagram illustrating the constant longitudinal field contours in the gap region of a recording head [Bertram & Mapps et al., 1994]

A major target in designing the write process in digital magnetic recording is to write data on the media as closely as possible. The ideal situation for this is that the two discrete magnetization states in the media exhibit a step-like reversal upon switching the direction of writing current. In reality, however, such a reversal is strongly affected by the head field gradient, properties of the media, and for longitudinal recording in particular, by the self-demagnetizing nature in the recording transition. Such a transition

region eventually limits the ultimate recording density [Bertram & Mapps et al., 1994].

Taking into account the head field gradients, the non-linear M-H loop characteristics of the media and the demagnetising field, Williams and Comstock [Williams & Comstock, 1972] developed a model for the recording process as following.

(1) Longitudinal transition

A convenient approximation to the variation of recording media magnetisation along the x-direction (M_x) through a magnetisation reversal (recorded transition) in longitudinal recording media is [Williams & Comstock, 1972]]

$$M_x = \frac{2}{\pi} M_r \tan^{-1}\left(\frac{x}{a}\right) \tag{1-3}$$

where, a is the transition parameter, by which the transition length is defined as $L = \pi a$.

Figure 1.3 illustrates the arctangent transition model for longitudinal recording media.

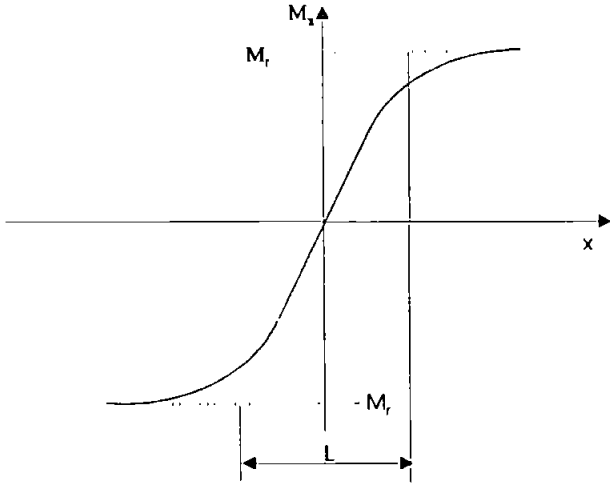

Figure 1.3 The arctangent transition model for longitudinal recording media.

The demagnetizing field for an arctangent transition can be calculated from the divergence of magnetization [Bertram & Mapps, et al., 1994].

$$H_d = \frac{2M_r}{\pi}\left[\tan^{-1}\left(\frac{a+\frac{\delta}{2}}{x}\right) - \tan^{-1}\left(\frac{a}{x}\right)\right] \tag{1-4}$$

where δ is the thickness of the magnetic medium.

The maximum value of demagnetizing field $H_{d,max}$ occurs at $x = a$ [Bertram & Mapps et al., 1994], this leads to

$$H_{d,\max} = \pm\frac{M_r\delta}{2\pi a} \tag{1-5}$$

From equation (1-5) it can be seen the maximum demagnetizing field in the longitudinal transition increases as the recording density increases. Accordingly the maximum demagnetizing field can not exceed the H_c of media and can only be equal to the H_c. For thin films, from eq. (1-5), we have:

$$a_{\min} = \frac{M_r\delta}{2\pi H_c} \tag{1-6}$$

It can be seen from equation (1-6) that a small value of transition length requires a high value of H_c and a thin media.

(2) Perpendicular transition

In perpendicular recording the media has a preferred orientation, or easy axis, in a direction normal to its plane [Iwasaki & Nakamura, 1977]. Thus the head field is magnetising the media in an upward direction against a background of downward magnetization. In perpendicular recording, bits of information are arranged as anti-parallel magnets (to each other) for every half-wavelength of signal.

One of the fundamental differences between perpendicular recording and longitudinal recording is the distribution of the demagnetizing field in the recording

transition on media. Figure 1.4 shows the demagnetizing field distribution for a longitudinal step-like transition and perpendicular step-like transition [Susuki & Iwasaki, 1982].

The expressions of the transition width written by a ring head or a single-pole on the perpendicular media are respectively [Mee, 1989]

$$a_{yr} = \frac{2}{0.3\pi}\left(d + \frac{\delta}{2}\right) - \frac{\delta}{2} \tag{1-7}$$

or

$$a_{yp} = \frac{4}{\sqrt{3}\pi}\left(d + \frac{\delta}{2}\right) - \frac{\delta}{2} \tag{1-8}$$

where d is the space between the head and the media, and δ is the thickness of the media. α_{yr} is the transition width using the ring head to write and α_{yp} is the transition width using the single-pole head to write.

Middleton and Wright have used the Williams-Comstock model to concluded accurately that a very narrow transition length could be realised in perpendicular recording [Middleton & Wright, 1982]. It should been noted that it is possible to realise a step-like transition (zero transition length) in perpendicular recording as d is reduced to zero, if only considering the transition demagnetization when d is reduced to zero. Therefore it is possible that the ultimate recording density for perpendicular recording would no longer be transition demagnetization limited [Mapps et al., 1993].

1.2.1.3 Theory of the readback process

The readback or reproducing process in magnetic recording relates to a head-media interaction which produces the readback voltage. As opposed to the recording process, the readback process can usually be modelled as a linear process. This is mainly because the flux density levels are so low in the reading head. The corresponding output voltages have been derived by other researchers such as Westmijze, Mee and Sebertyen.

The most common way to model the readback process is to use the principle of reciprocity which states that the flux produced by the following equation:

$$\Phi = \iiint M(r)H(r)d^3r \tag{1-9a}$$

where $M(r)$ is the magnetization distribution function in the medium, $H(r)$ is the head field function. For a magnetic recording head which produces the longitudinal field $H_x(x, y)$, a recording media with magnetization $M(x, y)$ and moving velocity (v) between the head and the media, the reproducing voltage and waveform can be calculated by Eq. (1-9b) as follows:

$$e = -N\frac{d\Phi}{dt} = -\mu_0 Wv\int_d^{d+\delta}\int_{-\infty}^{\infty}\int_{-W/2}^{W/2}\frac{\partial M_x(x-\bar{x},y)}{\partial x}H_x(x,y)dxdydz \tag{1-9b}$$

where W is the trackwidth of the head, μ_0 is the magnetic permeability of free space. N is the number of turns of coil of the head, and $\bar{x}$ is the movement in the track direction.

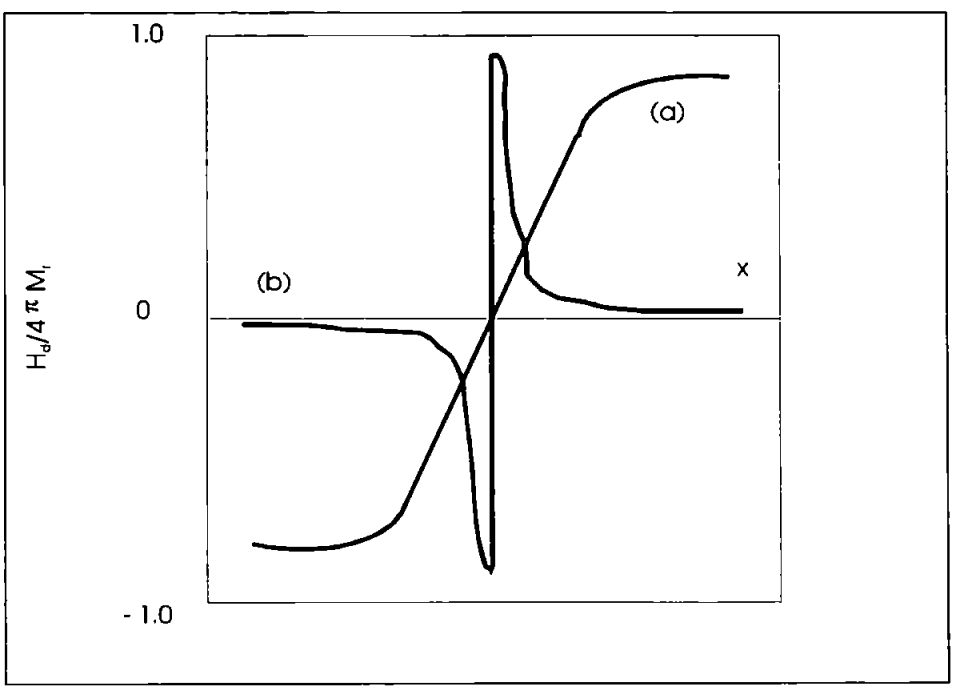

Figure 1.4 (a)The demagnetising field distribution for a longitudinal step-like transition. (b) and perpendicular step-like transition.

This expression shows that the readback voltage of the head is dependent upon the magnitude of the magnetization in the recording media being sensed, the relative head-media velocity, the track width and the number of the coil turns.

1.2.2 Data storage on rigid disks

A hard disk drive (HDD) is one of the most important peripheral storage devices to date. It consists of a write/read magnetic head, a disk with a thin magnetic coating, a head positioning and following (servo control) system, a data signal processing system and rotating disk system as shown in Figure 1.5. The write/read head records and reproduces data and servo information in circumferential tracks on the disk surface that rotates at a high speed. The data channel processes the analogue read signal and digital write current pulses. The high speed, accurate servo control system moves the head across the disk surface so that it can position and follow over the desired track.

The main components of the HDD, such as the magnetic head, the media, the data channel and the servo system, will be given in more detail as follows:

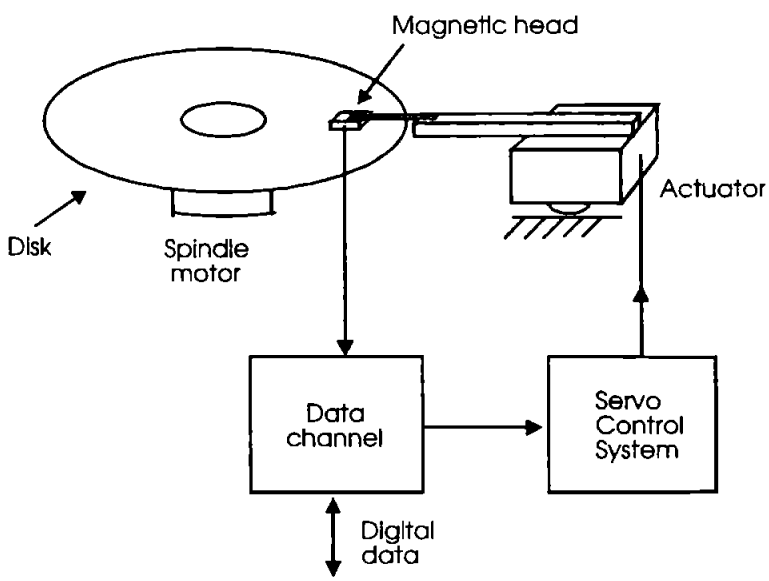

Figure 1.5 Schematic diagram showing the primary components of a rigid disk.

1.2.2.1 Magnetic head

Basic constructions of all ring heads are shown in Figure 1.6 (a). Early head cores were made of laminated mu-metal with the gap formed by a copper shim. Later, recording heads consisted of toroids of magnetically soft ferrite, such as NiZn-ferrite and MnZn-ferrite, with a few turns of wire for HDD around them [Warner, 1974]. For high density recording applications, however, ferrite can no longer be used, because when the deep gap field in the head approaches one-half the saturation magnetization of ferrite saturation of the pole tips of a ferrite head begins to occur [Jeffers, 1986].

This limitation has been overcome with the invention of metal-in-gap (MIG). The basic idea is simple by putting a magnetic metallic alloy with a much higher saturation flux density than the ferrite on the gap faces, the onset saturation in the gap corners will not occur until higher values of write current or deep-gap field. The use of MIG technology has extended the use of the ferrite heads.

The first operating thin-film head was built in 1970 [Romankiw et al., 1970], thin-film heads also utilise high-magnetization materials but they are made by means of photolithographic processes like those used to build semi-conductor devices. This gives them two significant advantages: they are inexpensive and easy to miniaturise.

In the continuing trend to narrower recorded track, it is necessary to find read element with great output. Magnetoresisitive (MR) sensors have been used as read head parts 1970s [Hunt, 1971]. In a MR head, the interception of magnetic flux leads to a modulation of the MR resistance through the magnetoresistive effect. This resistance modulation is in turn converted into a voltage signal by passing a sense current through the MR. It has two great advantages: the MR read head produces great output and output is independent of the head-media velocity. It has also two disadvantages:

embarrassingly sensitive to temperature changes [Mallinson, 1993], more susceptible to media noise than thin-film inductive head [Darragh, 1994].

Recently thin-film manufacturing techniques have been used to make dual heads, combining an inductive write head and an magnetoresistive (MR) read head in one structure [Tsang et al., 1990[1]] [Tsang et al., 1996] [Takano et al., 1991]. Because the read and write parts are distinct, each can be individually optimised for its function. For large readback sensitivity, for example, an MR film with a high magneoresistive coefficient is desirable. For the inductive write head, the choice of material and the fabrication method are basically the same as for a thin-film inductive head used for both reading and writing. For good performance at high density, however, the write-only head can be designed accurately such as with controlled pole-tip geometries, small throat heights, and narrow gaps.

(1) The Theory of Inductive Head

To date, almost all heads for hard disk drives (HDD), such as early ferrite heads and metal-in-gap heads, as well as the late thin film heads, have the same or similar structures. They are all ring structures with a small gap as shown in Figure 1.6 (a).

(a) Equivalent circuit of a head

Figure 1.6 (b) shows its equivalent magnetic circuit of a write head and Figure1.6(c) shows the equivalent circuit of a read head. Although the two equivalent circuits are different, the head efficiency for reading and writing [Mallinson, 1993] is

$$\eta = \frac{R_g}{R_c + R_g} \tag{1-10}$$

where R_g and R_c are two reluctances which appear for the gap and the core.

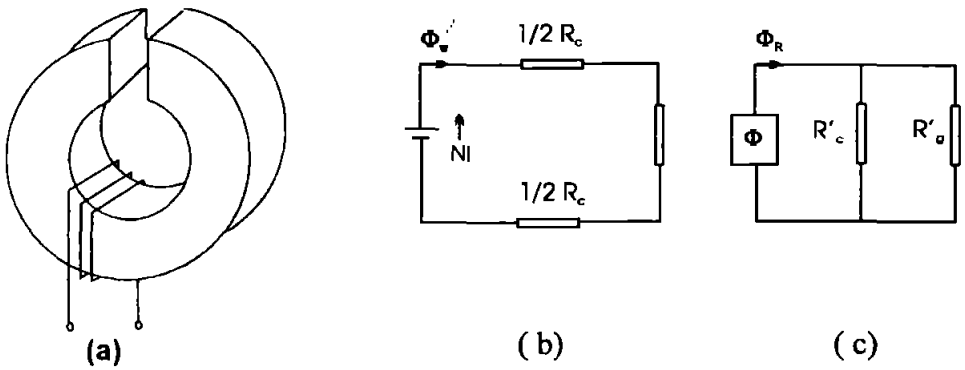

Figure 1.6 Showing a gapped ring head (a) its equivalent magnetic circuit of a write head (b) and its equivalent electric circuit of a read head (c).

For the analysis of a magnetic recording system, it is necessary to know the deep-gap field [Mallinson, 1993].

$$H_0 = \eta \cdot \frac{NI}{g} \tag{1-11}$$

where, H_0 is the deep-gap field in A/m and N is the number of turns, and I is the magnitude of current in amperes. NI is the magnetomotive force in amperes and g is the gap length in m.

(b) Fringing Field Shape

In Figure 1.7 [Mallinson, 1993] the H field is drawn in the region around the gap of a ring head. In Figure1.7, line (1) is the closest to the head, line (2) is at a distance y = 0.28g above the top of the head.

Figure 1.8 [Mallinson, 1993] shows the horizontal or x, component of the fringing field for four trajectories parallel to the top of the head shown in Figure 1.7. For trajectory 1 the field component H_x is sharply peaked above the gap corners. Mathematically, these peaks reach extremely high values, but in physical reality they are limited in magnitude by the saturation induction (B_s) of the magnetic material used in making the head.

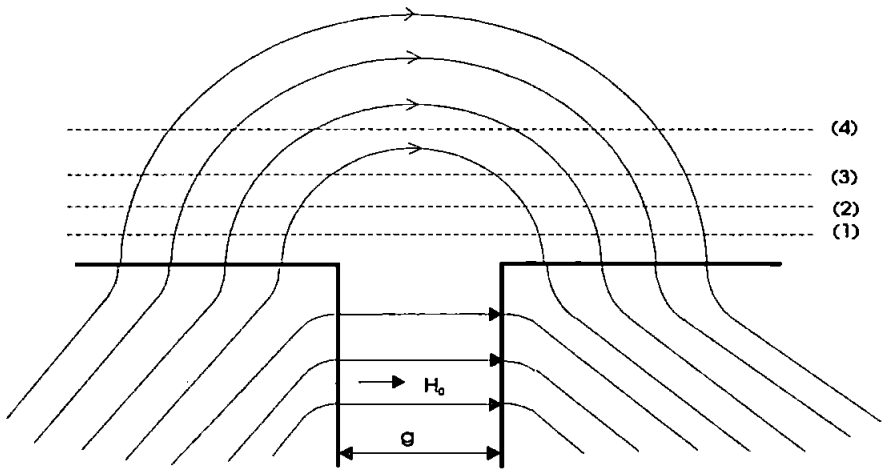

Figure 1.7 The magnetic flux flow (B field) adjacent to the gap of a ring head.

(c). The Karlqvist Approximation

The fringing field sharp of the head in Figure 1.7 may be computed using several more or less difficult techniques such as the Schwarz-Christoffel Conformal transformation, Fourier harmonic analysis, and numerical finite element or difference methods. For most practical purposes, however, Karlqvist's simpler approximation suffices. Except at points within about one-fifth of the gap length from the gap corners, the errors are negligible.

In Figure 1.8, for a deep-gap field of H_0 (see Equation 1-11) the horizontal field component can be expressed by the following equation

$$H_x = \frac{H_0}{\pi} \tan^{-1}\left[\frac{yg}{x^2 + y^2 - \left(g^2/4\right)}\right] \tag{1-12}$$

and the vertical field component can be expressed by the following equation

$$H_y = \frac{H_0}{\pi} \log_e \left[\frac{\left(x - g/2\right)^2 + y^2}{\left(x + g/2\right)^2 + y^2} \right] \qquad (1\text{-}13)$$

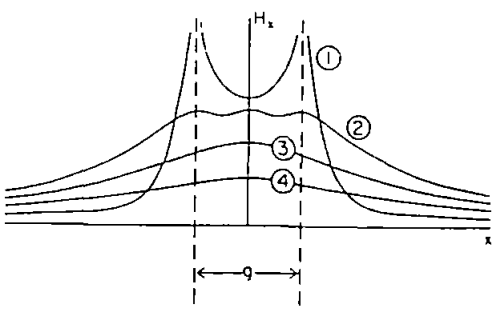

Figure 1.8 The longitudinal component of the fringing field above the gap of a ring head (1), (2), (3), (4) refers to Figure 1-7.

(d) Side-fringing fields

Experiment showed that the side-fringing fields of the recorded head limit to obtain high track density and reduce S/N, because they produce the side-write and erase-band [Herk & Bijl, 1980] & [Zhu & Ye, 1992]. The potential of an infinite-permeability head with a rectangular gap geometry shown in Figure 1.9 has been derived by several workers [Van Herk, 1977]. In here the head is assumed to be one-sided, extending to infinity in the z-direction. Calculated fields in the vicinity of the head edge are shown in Figure 1.10 [Lindholm, 1977]. It should be noted that the longitudinal field H_x begins to decrease from inside the physical width of the poles. Outside the poles the half width of the H_x peak in x direction is approximately proportional to distance z to the side of the

head, which indicates a lower resolution in reading off-track recorded information. The peak amplitude of the longitudinal field is approximately inversely proportional to the same distance. The results for a head with a one-sided, semi-finite width can be used to construct good approximations to the field for heads of finite width [Mee, 1989].

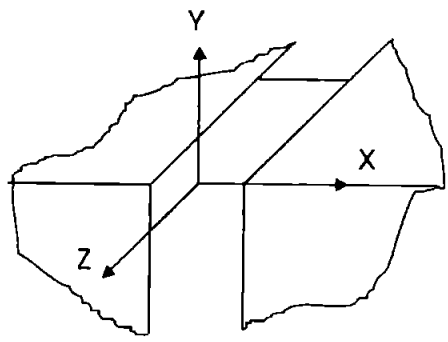

Figure 1.9 Polar and rectangular co-ordinate systems at the side of a semi-infinite head [Mee,1989].

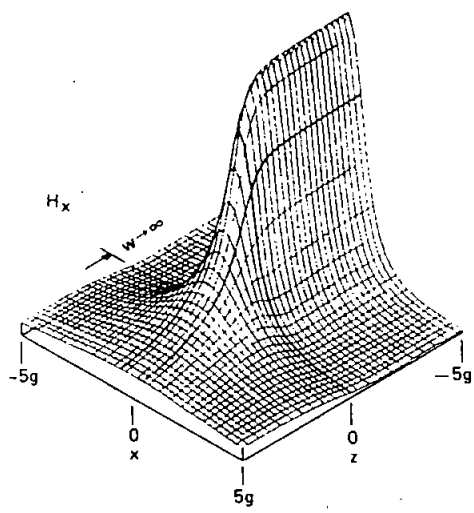

Figure 1.10 Showing the calculated field in the vicinity of the head edges for a semi-infinite-width head [Lindholm,1977].

(2) Theory of Magnetestoresistive Head

A magnetoresistive (MR) head for reproducing magnetic information is shown in the Figure 1.11. In the MR head, bias technique is to use a soft adjacent layer (SAL). Shielding the MR film not only prevents flux from transitions far from the gap from affecting the MR film but in some cases helps to increase the flux picked up by the MR film from a transition near to but not directly under it, because the shields help to conduct the return flux back to the recording medium. The resistivity of the MR film is dependent on the direction of magnetization. The relation of the resistivity and the angle between the magnetization and the easy axis can be expressed as:

$$\rho = \rho_0 + \rho_{max} \cos^2 \theta \qquad (1\text{-}14)$$

where, ρ_0 is the normal resistivity, ρ_{max} is the maximum value of the change in resistivity and θ is the angle between the magnetization vector and the applied current.

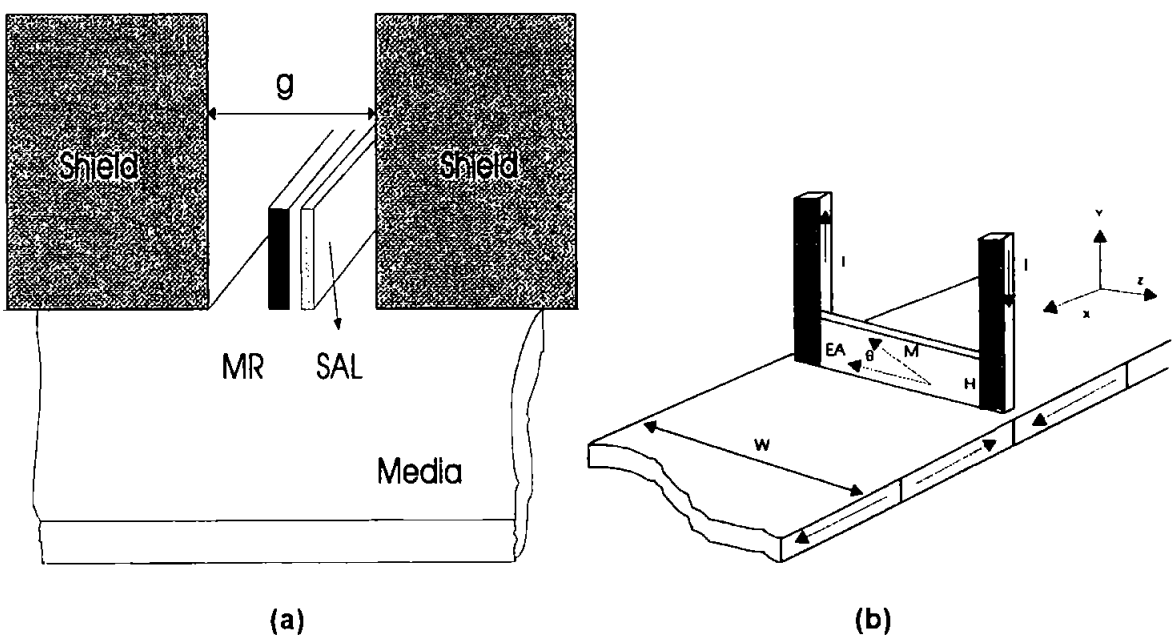

Fig. 1.11 (a) A shielded MR head for reproducing magnetic pattern [Mee, 1989]. (b) An unshielded MR head for reproducing magnetic pattern.

Another MR head, shown in Figure 1.11 (b) is unshielded, it is sensitive only to the vertical component H_y of the fringing field. The horizontal component plays almost no role because high demagnetizing fields force the magnetization to remain in the plane of the sensor film. The H_y, of course, varies exponentially with distance. The change from the medium in resistance of the sensor is just the average of the change throughout the volume, it follows that [Bertram & Mapps et al., 1994]

$$V = 2IR_0 \Delta\rho \frac{H_b}{\rho_0 H_0^2} \iint h_y(y,z) \frac{dy}{h} \frac{dz}{l} \tag{1-15}$$

where, h, l and t are the height, length and thickness of the magnetoresistor respectively, I is the constant current, $H_0 = H_k + N_y M_s$ (where H_k is the thin-film anisotropy field, N_y is the demagnetising factor in the vertical, M_s is the saturation magnetisation of the ideal (single domain) state of magnetisation), and H_b and H_o are the biasing field and the reverse field in the film of MR, respectively.

The biasing field is used to move the operating point to the linear part of the magnetoresistance curve as shown in Figure 1.12, thus avoiding positive and negative excursions of H_y about zero which both produce a negative change in resistance [Bertram & Mapps et al., 1994].

1.2.2.2 Magnetic recording media

There exists a wide variety of magnetic recording media. Particulate media includes gamma-ferric oxide, cobalt modified gamma-ferric oxide, chromium dioxide, metallic iron, and barium ferrite. Continuous media includes cobalt-phosphorus, nickel-cobalt-phosphorus, and cobalt-chromium thin metallic films. Today, although such

particular media are still widely used for tape and floppy disks, thin film media have almost entirely taken over the rigid disk business during the 1980's.

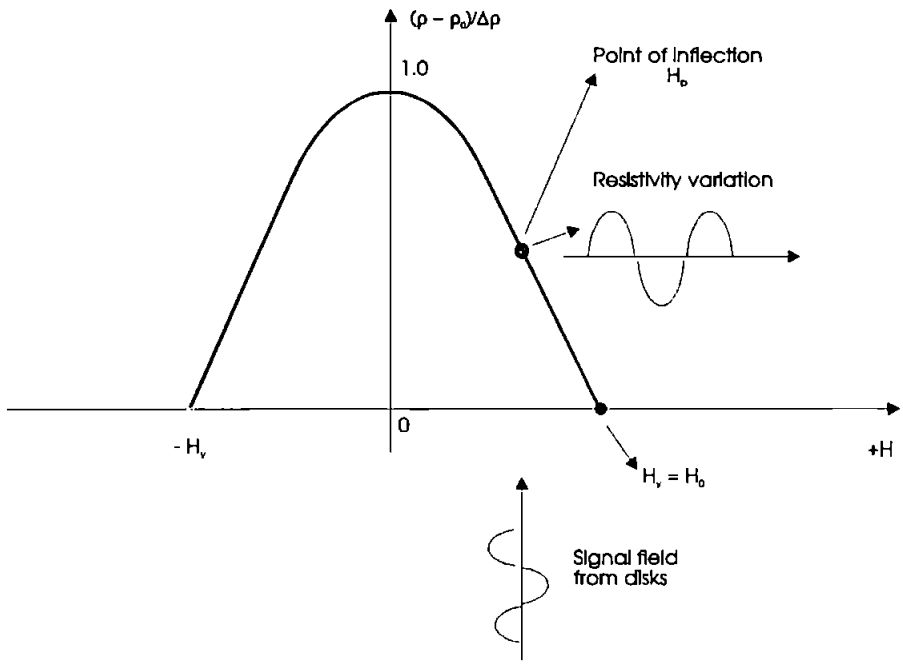

Figure 1.12 The magnetoresistive transfer characteristic used in magnetic recording [Bertram & Mapps et al., 1994].

(1) Longitudinal recording media

Thin film recording media generally have excellent magnetic and recording properties for high density recording. Because they are nearly 100% dense, they can be made to have the highest possible magnetization. Because of their high magnetization they can be made extremely thin and still provide adequate signal during readback. This helps to achieve the short transition in longitudinal media. Thin film media can also be made extremely smooth today. To achieve the smallest possible head-to-media spacing, smooth media are required.

Early thin film media was composed of a homogeneous film of Co-P or Co-Ni-P which is often sputtered on to the rigid disk surface. Other deposition methods (including electroplating, chemical plating and evaporation) are used for depositing magnetic films on aluminium or glass substrates.

Later, among the sputtered Co-based alloy are CoNiCr, CoPtNi, CoPtCr and CoCrTa. Some Co-alloys can also be sputtered ($CoNi+N_2$), or plated (CoNiP).

After significant noise reduction was achieved in thin film media with morphologically-decoupled magnetic grains by increasing the sputtering gas pressure [Yogi et al., 1990], media with high coercivity (1800~2120 Oe) has been developed for one and 2 Gb/in^2 [Yogi et al., 1990] [Futamoto et al., 1991]. In both cases the low noise (23.5 ~ 25 dB) is obtained by isolating the magnetic grains using a Cr underlayer so as to break the exchange coupling between the grains. The grain size is approximately 15 nm, and about 1000 grains are included in a magnetic bit.

A roadmap to achieve an areal density of 10 Gb/in^2 was published [Murdock et al., 1992]. The development of a longitudinal media for 10 Gb/in^2 recording has taken two paths in the last few years.

The improvement of Co alloy media such as CoCrTa, CoNiPt and CoPtCr, development of quaternary alloys such as CoCrTaPt, CoPtCrSi and others are examples of this approach continue and may be successful in achieving 10 Gb/in^2 density. The Ta, Cr, and B additives are thought to accumulate at the grain boundaries and break the exchange coupling between magnetic grains, thus achieving magnetic decoupling and low media noise [Zhu & Bertram, 1991]. Parker reported additional improvements in magnetic properties of hexagonal Co alloy media by using alternative underlayer films such as CrTi and CrV alloy [Parker et al., 1993].

Another possibility for 10 Gb/in^2 media is the development of new alternative materials with higher anisotropy than hexagonal Co alloys. The high anisotropy materials systems investigated in some detail include Cr/CoSm bilayer films and sputtered Barium Ferrite [Velu & Lambeth, 1991] [Velu & Lambeth, 1992]. Coercivities of Cr/CoSm media in the range of 3 kOe have been achieved (Barium Ferrite); and recent data shows little or no dependence on recording density up to 100 kFCI. However, it is necessary to research further the chemical stability of CoSm. Because sputtered longitudinal Barium Ferrite media has the high anisotropy and the mechanical hardness and wear resistance combined with its chemical stability many researchers are interested in it. Sui and Kryder [Sui & Kryder, 1993] [Sui & Kryder, 1994] have investigated CoTi doped longitudinal Barium Ferrite and have presented detailed studies in the microstructure and recording performance including S/N as well as tribological properties, and demonstrating that CoTi additives can be used to adjust the coercivity from 1400 Oe to nearly 4000 Oe. Ullah et al. have investigated the use of laser annealing to crystallise the Barium Ferrite films without degrading the conventional glass substrate [Ullah et al., 1994] & [Howard, 1994].

(2) Perpendicular recording media

In perpendicular recording, the plane of magnetization and easy axis of the media are normal to the plane of the disk (the surface of media film). To reduce demagnetising field is most important to increase the linear density in longitudinal recording media. However in perpendicular recording the demagnetising fields actually improve at high recording densities [Mapps & Pan, 1993]. The world record linear recording density (1040 kFCI) for magnetic disk recording has been demonstrated on a perpendicular film [Honda et al., 1996]. Due to thermal instabilities, longitudinal recording is not

expected to be able to achieve a 100 Gb/in^2 recording density. Perpendicular magnetic recording is more favourable at such a high density due to reduced demagnetising fields in the recorded transition and the ability to use thicker media.

The usual perpendicular material is a sputtered film of Co-Cr about 100 nm thick, which forms naturally into columns of about 50 nm in diameter, oriented normal to the plane of the disk. Other new perpendicular material are CoSm and Ba ferrite thin film [Mastsuoka et al., 1982] & [Chandrasekhar & Mapps, 1996].

1.2.2.3 Data channel

Today, the data channel is not only for data signal processing but also for some servo signal processing . The servo signal processing will be discussed in the next section.

The data channel consists of a preamplifier, AGC amplifier, filter/equaliser, data detector, clocking circuit; write precompensation and data coding circuits. In the Peak Detector (PD), the signal waveform is strobed at the centre of each bit and the sample value is compared with a threshold level. A "1" will result if the level is above the threshold level and a "0" will result if it is low. The peak detector is both robust and very simple to implement. Ten years ago the PD was used in almost all HDD. However, as the PD's very nature it performs best at low linear densities. When linear density increases, intersymbol interference and noise can cause both missing and peak shift bit errors. It is because of this the threshold is fixed at some level above the zero signal level.

An optimum detection process for correlated data uses threshold control based on the past present and 'future' data signal. The delay method can be used to obtain the

'future' data signal. In many ways, the data channel behaves just like a typical communication channel. Therefore sampled amplitude detection has been proposed for use in magnetic recording systems [Kobayashi & Tang, 1970] & [Wood et al., 1984]. Partial-response maximum-likelihood (PRML), demonstrates significant density increases over peak detection with the same physical recording system [Kobayashi & Tang, 1971]. Recently, an adaptive partial response data channel for HDD was investigated [Darragh, 1994].

1.2.2.4 Servo control system

In the HDD, there are two servo control systems. The spindle (disks) rotating control system and the servo system of the head position. The speed of the disk is controlled by comparing a Hall sensor on the motor to a stable reference clock. The accuracy of the speed is commonly ± 0.1%. The head servo control system, which is the key in this investigation, is discussed in the next section.

1.2.3 Servo control system of the magnetic head

1.2.3.1 An overview of the development of a servo system for a disk drive head

(1) Measuring Position System (servo)

Unlike the first optical disk, the track density of the first magnetic rigid disk drive, the IBM 350, was very low (20 TPI in 1956) and its servo system was very poor. The average access time (T_p) and accuracy of head positioning were 600 ms and 125 μm respectively. The track access method was that a single magnetic head first sought the disk address, then sought the track address. A motor and clutch were used as an actuator in the IBM 350. In 1960, the IBM 1301 used a hydraulic drive for the head-arm. This was a comb-type with one arm for each head on each surface of disk. Closed loop servo control was first used. This reduced the average time to 165 ms, and increased TPI and the positioning accuracy to 40 TPI and 50 μm respectively [Harker et al., 1981].

Stepper motors replaced hydraulics in the IBM 2311 (1964), which had a big volume and slow motion. The seeking velocity and track density as well as positioning accuracy increased twice using open-loop control. The IBM 3330 was produced in 1970, using the long voice coil motor as an actuator and using a servo surface as a position sensor system. Closed-loop servo control was used. The T_p and positioning accuracy were further reduced and increased by a factor of two respectively. The short voice coil motor was first used in the IBM 3340 in 1974. In order to reduce the track misregistration (TMS) which is produced by thermal track shift, a key technology i.e. sector servo + dedicated servo, was developed and successfully used for the IBM 3310 at the IBM Development Laboratory in Hurseley (England) in 1978. Digital control for the head servo system with closed-loop bandwidth in excess of 1 kHz only became feasible in the early 1980's. The first products in the marketplace that relied on a

processor for algorithmic computation of the control were the IBM 3380 models J and K [Workman, 1987].

While most of the early developments in rigid disk drives centred on 356 mm (14″) and 133 mm (5.25″) disks, more recently, disk drives with disks of 89 mm (3.5″), 65 mm (2.5″) and 33 mm (1.3″) diameter are utilising some technologies developed for high-capacity disk drives. Since 1980, many new companies have joined the HDD business and technology for small-size disk drives including new servo technology was quickly developed. The main servo technologies will be reviewed as follows:

(a) Embedded servo

Embedded servo, often called sector servo, was first utilised in small-size disk drives in 1978 [Commander and Taryor, 1980]. In 1981, HDDs (e.g. the D160) with embedded servos were developed [Maury, 1981]. The servo information needed for head positioning is provided by the data head itself. The technology allows less than 5% data capacity loss. The track density was as high as 1000 TPI. Positioning error was less than 3 μm. Nakanishi reported that four-phase servo pattern encoding, modified RZ recording for servo pattern writing (using compensated hybrid position signals) and optimal design of the number of servo sectors were utilised. Access times as fast as (servo surface accessing) 30 ms and positioning accuracy of 0.4 μm have been achieved [Nakanishi et al., 1983].

Ishii developed a new servo pattern encoding and position signal detecting method in 1987 [Ishii & Mizukami, 1987]. The servo pattern encoding is composed of a two-bit elements with magnetization reversal according to odd and even servo tracks. The position signal is detected by differentiating the two-bit pulses. This is effective in

suppressing elements with magnetization reversal according to odd and even servo tracks. The position signal is detected by differentiating the two-bit pulses. This is effective in suppressing undesirable lower frequency noise. With these techniques, a 5 dB S/N improvement of the position signal and high accuracy with ± 0.15 μm positioning errors were experimentally achieved.

In 1988, Jackson presented a novel way of formatting servo patterns to reduce the servo gain variations on a HDD because the servo gain varies with the position of the head on the disk, from disk to disk and from head to head. In this method, the servo patterns were written with the double write Dit Dah Dit pattern, in which the servo pattern can be written with width equal to W, the width of a multiple written servo track, and W made to vary with read track width R such that R plus W is kept constant (e.g. $2T$ (T is the track spacing)), therefore, the servo gain could keep at constant, because the servo Gain = $k\frac{2}{R+W-T}$, (where k and T are constant) [Jackson et al., 1988].

In order to improve the data rate of 'embedded' servo disk drives, a data head switching at a high rate is required. A control method of two degrees of freedom that compensates for the computation time delay and phase lag of filters was developed by Shishida. Head switching times were reduced by about 50% using this method [Shishida et al., 1993].

(b) Optical servo

An optical servo method is very attractive because it is able to both position and follow on tracks 1.6 μm wide and provide a continuous position error signal (PES). In 1980, Koshino first tried to use this method. In his study, optical patterns depicting the position of the data track were formed by colouring the anode oxidised surface layer of

an aluminium substrate, and by forming a magnetic film over that. Three optical fibres were imbedded in a hole in the central rail of a Winchester type ferrite head and were used to read the optical pattern. The positioning accuracy of the head was $\pm$ 0.3 μm [Koshino & Ogawa, 1980].

The application of optical disk technology to magnetic disk systems to obtain a high quality position signal with a track width 1.5 μm was successful demonstrated by Akagi in 1991 [Akagi et al., 1991]. In this method, a laser-diode optical system fixed to the side of a magnetic head obtained a high quality servo signal from a magnetic disk which had about 2000 pairs of pits formed on each track.

(c) Discrete tracks for servo

Discrete track media (DTM) for magnetic disks was primarily proposed to increase the track density [Lambert et al., 1987]. In 1990, Hua and Zhang first reported a head position control system using an etched servo disk [Hua & Zhang, 1989] [Zhang et al., 1991]. In this method, an etched area was formed in the adjacent media which is used for recording servo information in the track direction. Zhang et al., further studied a new method of the graphic head position (GHP) in which servo information is recorded on the etched graphic media [Zhang et al., 1994]. Discrete servo tracks were also used by Lambert [Lambert et al., 1991].

Wang proposed another servo method with an etched servo pattern [Wang et al., 1991]. The media of a half trackwidth along the track direction is etched. The servo head is an MR head with three electrodes having a central electrode two times as wide as the discrete track. Continuous servo signals can be obtained from the MR head on the discrete track on which data information is recorded. However, half the capacity is lost. The width of the centre electrode limits the trackwidth of the discrete track.

In another study of PERM (Pre-Embossed Rigid Magnetic) Disk, an embossed disk with discrete magnetic tracks and servo marks was made by etching the surface of a glass or plastic disk. Using the disks, a head positioning accuracy of 0.09 μm (rms) and a track density of 192/mm were demonstrated [Ishida et al., 1993] [Tanaka et al., 1994].

(d) Buried servo

Buried servo means that the servo information is recorded in a lower layer of a magnetic media whilst data is written on the surface of the media. It was proposed in the 1970's.

This is a continuous servo system that shares the surface area of the media with data on the same track, unlike a conventional media with a single head. A long-gap head records low-frequency servo signals deeply into the media coating, and a short-gap head then erases the surface portion to stabilise the servo amplitude. Short-gap read-write heads then write and read high-frequency data signals without interference. Using frequency-separation filters and an AC-biased pulse-write method, an inductive head reads servo signals while simultaneously writing data [Haynes, 1981]. In this method, the servo pattern consists of two single-frequency signals recorded deeply into the magnetic media below the area used for data. The servo signals are detected by synchronous detection techniques and provide a continuous head position error signal. The servo system uses this head position error signal to follow a given data track with a track width of 50 μm and to seek new data tracks [Hansen, 1981].

(2) Actuator

Before 1970 actuators in hard disk drives were driven by motor and magnetic power clutches, hydraulic cylinders and stepper motors. The actuator was made with a wire-wound cylindrical bobbin supported by a carriage and moving in a magnetic field structure similar to a loudspeaker (here referred to as a "voice coil motor"). It was the first linear voice coil motor (VCM). An ingenious rotary voice coil actuator was developed at the IBM development laboratory in Hursley (England) and used in the IBM3310 disk drives.

Two closed-loop linear actuators for high performance disk drives designed in the early 1970's are discussed in detail by Hiyane [Hiyane et al., 1972]. Both of these actuators were designed with a single magnetic path. They generate flux in a short air gap and operate in conjunction with a long coil. In 1974, two short-coil and long-gap actuators [Inoue et al., 1974] were developed. The magnetic flux paths for these two actuators were a single path design even though two different magnets were used.

In 1977 [Patel, 1977], a multiple-actuator system was invented with a single magnetic path for each actuator. In order to improve the performance of the linear actuator for a high performance servo systems, a dual path E-Core type actuator was patented. A dual path E-coil type linear voice coil motor was designed by Dong [Dong, 1983]. It has distinct advantages such as:

(1) Equal force constants in the push and pull directions;

(2) Evenly distributed flux lines with better orientation;

(3) Reduction in flux leakage so that the actuator is placed in closer proximity to the disk.

In order to reduce friction and stiction, an air bearing was used for the voice coil motor [Scranton et al., 1983].

The dynamic performance of the actuator was carefully studied by Fazzio [Fazzio et al., 1993] and a new method is used to reduce mechanical vibration.

In the past 20 years, actuators have not changed in basic theory, but they have changed from linear to rotary, and their volume has become smaller. However, following a narrow track requires a servo actuator with a high bandwidth. An actuator with a single voice coil motor is not good enough. A dual-stage actuator is an efficient way for achieving an increased bandwidth [Yen et al., 1990]. Mori reported a dual-stage actuator using a VCM rotary actuator as a coarse actuator and a piezoelectric actuator installed in a head-arm as a fine actuator. The actuator successfully follows on a 1.5 μm pitch track (17 kTPI).

(3) Controller

The IBM 3330 (1970) was the first production disk drive to incorporate a track-following feedback controller with an analogue servo. A sector (embedded) servo controller was first used in the IBM 3310. The IBM 3380 J or K first utilised a wholly digital controller for head position servomechanisms in 1987. Stich used adaptive control technology for a HDD controller [Stich et al., 1987]. The controller has an on-line adjustable gain characteristic for controlling movement of the actuator and an estimator that estimates actuator velocity and bias. Forward gain is estimated from position and coil current measurements and compared with a normal value to create an error signal used to adjust the controller and estimator gain characteristics.

Horowitz presented a new self-tuning control scheme for disk file track following servos [Horowitz & McCormick, 1991]. The main feature of the self-tuning control scheme is its ability to maintain a specified nominal performance in the presence of

variations in the dynamics of the various disk files that the control system is expected to operate on.

Another new digital servo controller was reported by Sir-Jayantha [Sir-Jayantha et al., 1991]. This controller employs a steady state Kalman filter-like full state estimator and a pole-placement technique.

Miu and Bhat (1991) presented analytical and experimental results, that deal with power optimal control strategies for the point-to-point slewing of motor-driven flexible structures which would result in zero residual vibration [Miu & Bhat, 1991].

A seek controller for a VCM which eliminates the control chattering and reduces the high frequency flexible excitation modes was discussed by Lee [Lee et al., 1993]. Results were presented which show the effectiveness of the controller.

Later, another adaptive time optimal controller was reported by Weerasooriya [Weerasooriya et al., 1994]. Controller adaptation is used to achieve time optimal seek performance on individual drives with different plant parameters. Implicit model identification is done through the use of overshoots of pre-determined seeks. Adaptation is facilitated through a small, off-line trained, neural network. Comparisons with a fixed parameter PTOS controller indicate the faster access of the proposed control scheme.

In 1995, Weerasooriya presented the new discrete-time linear-quadratic Gaussian control combined with loop transfer recovery (LQG/LTR) design of a disk drive track-following servo system. The servo compensatory designed through LQG/LTR consists of a Kalman filter for state estimation and state feedback for control. The desired tracking servo performance is first formulated through a frequency shaped return ratio of the Kalman filter and subsequently recovered at the output of the plant/compensator loop through the automatic design of a discrete-time linear quadratic (LQ) regulator [Weerasooriya & Phan, 1995].

Lee used Internal Model Control (IMC) structure to design a new controller for HDD. It is well known that one of the major problems in designing a high-performance disk drive servo controller is the difficulty imposed by the high-frequency characteristics of the actuator. In the method, a second order nominal model of the plant is used to design an H_2-optimal controller to attain minimum integral-error-square (IES) performance. Then to maintain robust stability at higher frequencies, sufficient roll-off at such frequencies is provided by an H_∞ optimisation procedure [Lee et al., 1995].

The earliest controller for a dual-stage actuator was in an optical disk drive. Inada developed the controller in 1983 [Inada et al., 1983]. In their study, the controller used a serial construction in which the output of a coarse actuator became the input of the fine actuator for track seeking. The output of the fine actuator was the input of the coarse actuator for track following. Using such a controller, stable and high speed accessing with accurate track following for tracks of 1.6 μm wide was achieved.

The study of a controller for a dual-stage HDD actuator was started by Yen [Yen et al., 1990]. His paper addressed the application of discrete- LQG/LTR method to the design of a track following controller for a dual-stage HDD actuator. Performance requirements for a state-of-the-art dual-stage actuator servo system were described in terms of the frequency response of the closed-loop tracking error rejection and the transfer function from the reference signal to the actuator input.

Mori et al., successfully developed a controller for dual-stage actuator by using a piezoelectric device for the fine actuator and VCM for coarse actuator. The dual-stage controller consists of a VCM controller and a piezo-controller. The feedback signal is supplied to both controllers. The output of the piezo-controller is added to the input of the VCM controller, which prevents the piezoelectric actuator from going to the end of its stroke. The servo system is designed so that the tracking error at 60 Hz decreases by

16 dB in the piezo servo system. The total decrease of the tracking error is 40 dB when both servo systems are used. The bandwidth of the VCM servo system is 250 Hz, with 1 kHz for the piezo servo system [Mori et al., 1991].

1.2.3.2 Basic system functions

The head-positioning servo system in a HDD provides a means for locating read-write heads in fixed radial locations over the disk surface and allowing the repositioning of these heads from one radial location to another. A block diagram of a typical head positioning servo system is shown as Figure 1.13.

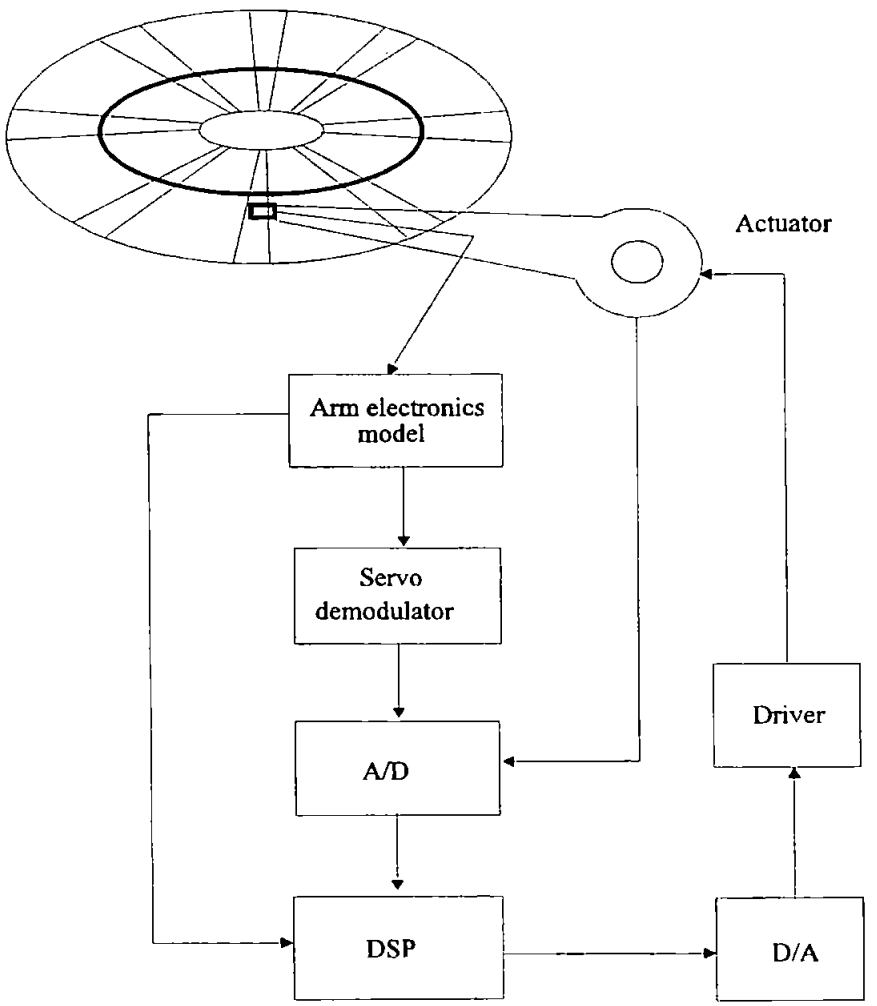

Figure 1.13 Block diagram of a typical head-positioning servo system.

Figure 1.13 indicates that on the rotating disk there are written equally-spaced sectors of servo information (e.g. 80 sectors); these are prewritten on the disk by servo track write (STW) during HDD manufacture only. This servo information takes up about 10% of the magnetic recording area on a disk surface. When the disk is rotating, the read/write head will cross servo information and servo pattern encoded data is read. As shown in Figure 1.13, this servo signal is amplified by the arm electronics module, output of the module is cascaded with the demodulator that converts the encoded servo pattern code data to a digital track address and an analogue position error signal (PES). The PES is converted and fed into the servo digital signal processor (DSP) (servo controller). The controller provides advanced accessing and tracking servo. The D/A converts the output of the servo DSP to an equivalent analogue value. The current power driver drives the actuator (VCM) to move in a direction to reduce the PES.

1.2.3.3 Position measuring system

The position measuring system for a HDD measures the real-time head position (or so-called position error signal) and the velocity of the head on the disk. In high track density recording, the accuracy of the position sensor is of great importance. It is possible to have a very good servo system, but still end up with mediocre tracking performance due to sensor errors.

(1) Principle of measuring position

The position error signal (PES) is a signal proportional to the relative difference of the positions of the centre of the servo head and the nearest track centre. Thus the position error signal is a periodic function of x (the x is the position of the centre of the servo head in radial direction) for stationary and ideal track centres [Oswald, 1974].

The position error signal results from two sources of motion: that of the head and also that of recorded servo patterns on the disk surface. A simple mathematical description of the position error signal is

$$PES = k_x (r\text{-}x) \tag{1-16}$$

where r is the track centre position references and k_x is the position gain [Mee, 1989].

Figure 1.14 shows the practical principle to produce the PES. In Figure 1.14, the peak amplitudes of $\overline{A}$ and $\overline{B}$ are the same, that is $PES = 0$, when the servo head is in a data track. The demodulation of the readback signal to obtain a position estimate is described as follows:

$$PES = \frac{\overline{A} - \overline{B}}{\overline{A} + \overline{B}} \tag{1-17}$$

where $\overline{A}$ and $\overline{B}$ are the peak amplitude estimates from the respective burst regions in Figure 1.14.

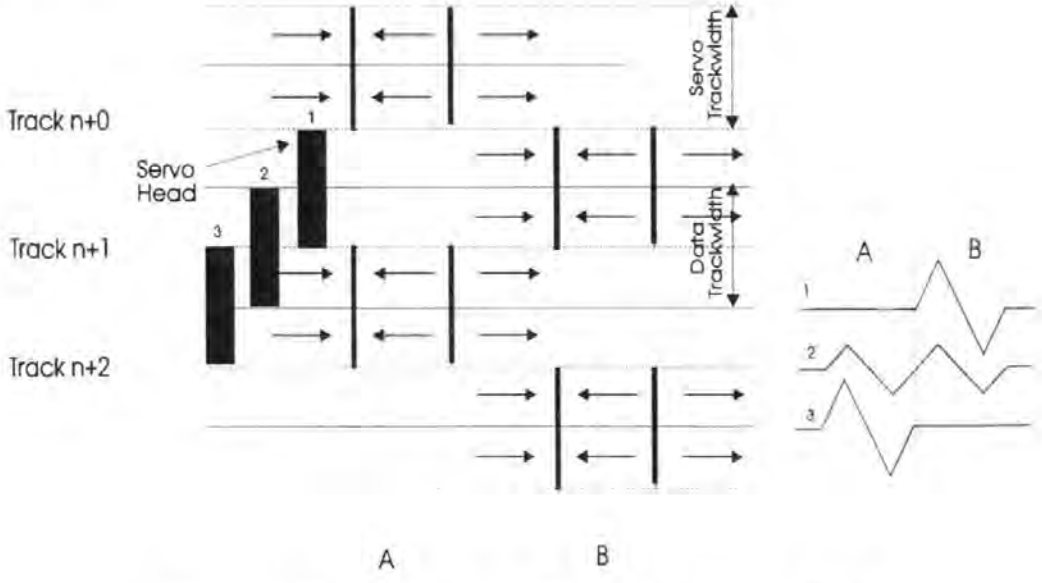

Figure 1.14 The scheme of demodulating PES.

Three basic types of demodulation are employed: peak detection, area detection and phase detection. Both peak detection and area detection are sensitive to the amplitude of the readback signal from the servo head. The benefits of phase detection are

that the servo signal frequency does not vary, the pattern is linear over four tracks and single bit disk defects usually do not have a significant effect on the servo position signal, since multiple cycles are averaged. Like phase detection, the peak detection will tolerate small disk defects since many cycles are used in the burst. However the amplitude of PES is not as linear as phase detection and there are two widely separated components in the pattern DC and the burst frequency. Area detection is less sensitive to disk surface defects and noise.

There are however physical defects and coercivity variations in the magnetic disk media. The recording head both produces side-erase bands and has an offset when writing the servo pattern. The sensitivity of the read head is not uniform across its width. The actual *PES* transfer function in the on-track following servo mode can be modelled as

$$PES(n,m) = Q(n,m) \bullet PE(n,m) + g(n,m) \qquad (1\text{-}18)$$

where, n is the sector index, m is the track index and the disk surface location is identified as (n,m). $Q(n,m)$ is the *PES* gain at (n,m), $g(n,m)$ is the pattern offset at (n,m) and $PE(n,m)$ is the total off-track error at (n,m) [Ottesen, 1994].

(2) Performance of the measuring position system

There are four main performance specifications when measuring the *PES*:

a) Sensitivity per unit of trackwidth;

b) S/N of *PES*;

c) Linearity;

d) Position accuracy.

(a). Sensitivity

Sensitivity is most important for servo systems and is affected by many factors. A simple description of the sensitivity for measuring *PES* is given by

$$K_e = \frac{V_{ps}}{x} \tag{1-19}$$

where V_{ps} is the magnitude of PES with off-track distance x and K_e is dependent on the sensitivity of the servo head. It is also dependent on H_c and M_r of media, head-disk interface, shape of servo pattern and detecting method. It will be further discussed in Chapter Four.

(b). S/N of PES

In the measuring position system, there are three types of noise to be considered: media (disk noise), servo/data head noise and electronic noise. Electronic noise originates in the first stages of electronic amplification of the reproduced signal, and it can be made almost negligible in most systems. The media noise is the main noise source in the system when recording trackwidth is reduced to micro size.

The wide-band signal-to-noise ratio in particulate media for longitudinal recording is expressed by [Mallinson, 1993],

$$(S/N)_w = \frac{nw\lambda_{\min}^2}{2\pi} \tag{1-20}$$

for a servo pattern, Eq. 1-20 can become

$$(S/N)_w = \frac{2nwL_{b\min}^2}{\pi} \tag{1-21}$$

where, n is the number of particles per unit volume, w is the track width, λ_{min} is the minimum wavelength, and L_{bmin} is the minimum servo pattern bit length.

Note that the Eq. 1-21 suggests that if the media noise is in PES limited, from *S/N* considerations, the best way to increase the *S/N* is to increase the servo bit length rather than to increase the servo trackwidth. Therefore the head servo system for submicron track is much more important in future.

The $(S/N)_w$ expression in metallic thin film media noise for longitudinal recording is

$$(S / N)_w = mw\delta L_{b\min} \tag{1-22}$$

where, δ is the thickness of the media.

It should be noted that the trackwidth is assumed to be fixed, so S/N of the PES can be increased by increasing the bit length of the servo pattern.

It should be noted that for longitudinal thin film media and for perpendicular films media, noise occurs mainly at the transition centres and occurs away from the transition centres respectively. However, both the longitudinal and the perpendicular media noise increases and decreases respectively with increasing recording density. [Beardsley & Zhu, 1991] [Pan, 1993]

(c). Linearity

The linearity of the measuring positioning system is obtained by analysing the superposition of mono-polar pulses, $m(x, y)$ and side-cross-talk [Ishii & Mizukami, 1987]. Here, the position signal linearity, L_L, is defined by:

$$L_L = \frac{L_{L1}}{L_{L0}} \tag{1-23}$$

where, L_{L0} and L_{L1} indicate the features of the position signal shape. L_{L0} is the interval between zero-crossing and a position signal peak. L_{L1} is the interval between zero-crossing and the point where the tangent to the position signal at point zero meets the 95% peak level.

(d). Position accuracy

Position accuracy as indicated by PES means the positioning accuracy of the track centre. It is dependent of the servo pattern writing accuracy. The process of recording a

servo position pattern on the disk is referred to as servo writing. Servowriting can generate write/write track mis-registration, which can not be removed by the servo system.

1.2.3.4 Actuators

Actuators are one part of a servo control system used to control the movement of the magnetic head across the disk surface and to maintain the heads on-track. They also minimise track misregistration during a read and write process.

A key performance parameter for HDD is the access time. The average access time is specified for the worst-case conditions, including lowest power supply voltage, largest movable mass, largest friction, and highest bias force from air movement and voice coil motor cable.

Another key performance parameter for a HDD actuator is the ability to follow tracks, i.e. the smallest resolution of the movement of the head. This ability can be effected by friction, stiction, wear debris on the way rails, and the response to external force disturbances, e.g. windage force resulting from air flow generated by the rotating disks and by forces resulting from the actuator voice-coil motor power cable [Mee, 1989].

A model of a rotary actuator suitable for use with a servo system to predict performance is developed below. Torque (M_m) for a rotary actuator with bearing-to-centre-of-force distance (R_b) is given by

$$M_m = B_g l_{coil} i R_b = k_t i \tag{1-24}$$

where, B_g is gap flux density, l_{coil} is length of coil wire in the gap flux region, i is coil current and k_t is torque constant [Mee, 1989].

The average power dissipated in the voice coil motor when doing seeks of average length $N_t/3$ (N_t is the total number of tracks on a disk.) [Mee, 1989] is

$$\overline{P_E} \cong \left(\frac{M}{K_f}\right)^2 \left(\frac{4}{3}\right) \frac{x_s^2}{\overline{\tau_{sk}}^4} \tag{1-25}$$

where, x_s is the total stroke length in meters, M is the movable mass of the actuator, $\overline{\tau_{sk}}$ is average seeking time and K_f is actuator force constant.

Therefore it is most important, for a chosen acceptable seeking time, to reduce the power dissipated to according to Eq. (1-25). Once the maximum power dissipation is fixed, it is necessary to have a large electromechanical bandwidth and large k_t, small movable mass of the actuator and small friction in order to reduce the average seeking time.

1.2.3.5 Controller

The function of the controller for a magnetic head is divided into seeking mode and following mode. The purpose of the seeking mode is to move the head from one track to another desired track in the shortest possible time. The purpose of the track-following mode is to keep the head on track in the presence of actuator disturbances such as bias forces, external vibrations, disk spindle bearing run-out and imbalance, and noise in the position measurement.

Figure 1.15 [Mee, 1989], shows a simplified and linearized functional block diagram of a controller with an analogue servo, where x_d is the desired head location, r is the position references of track centre, x is the position of the head in radial direction on the disk.

This system is a traditional position and velocity control system [Mee, 1989].

In the Figure 1.15, $\frac{1}{s}$ and $\frac{k_v}{s}$ are the transfer function of the actuator. The box (3) is a voltage-to-current converter with the maximum saturating current. The box (1) includes an integrator so that a servo control loop is constructed (type-1 position loop) whilst track following, whereas during any seek, box (1) output is zero because of the large transient in x_e. Boxes (4), (5) and (6) comprises an analogue velocity estimator which uses both the filtered integral of the acceleration (i) and the filtered derivative of the position (x_e).

Box 2 in Figure 1.15, which represents one quadrant of the system switching curve, is defined by following equation [Mee, 1989],

$$V_c = f(x_e) = Sgn(x_e)\sqrt{2a_{\max}|x_e|} \qquad (1\text{-}26)$$

where $a_{\max} = i_{\max}K_v$. In fact, the equation to minimum-time move problem is derived by applying the Pontrayaging maximum principle.

In the Figure 1.16, box (2) is a current driver, box (3) is the transfer function of the actuator, box (1) expresses a control-law, box (4) is a state estimator which estimates the position, the velocity and the bias force from the PES signal and the current through the VCM.

Figure 1.16 shows a sampled data sector servo implemented with an analogue-control structure. It is a discrete-time system. The essence of this design is the use of a state estimator to obtain continuous position, velocity and track-crossing pulses. The plant model must contain a model of the continuous-time position error signal with track-pulses [Stephens & Workman, 1986]. Once this is established, the estimator error is derived at the sampling intervals by subtracting the model output from the position error signal samples. An important feature added to the estimator shown in

Figure 1.16 is the state $\hat{f}$, which is the estimated bias force. In fact, practical actuators contain bias forces acting on them which must be overcome in order to track-follow successfully [Mee, 1989].

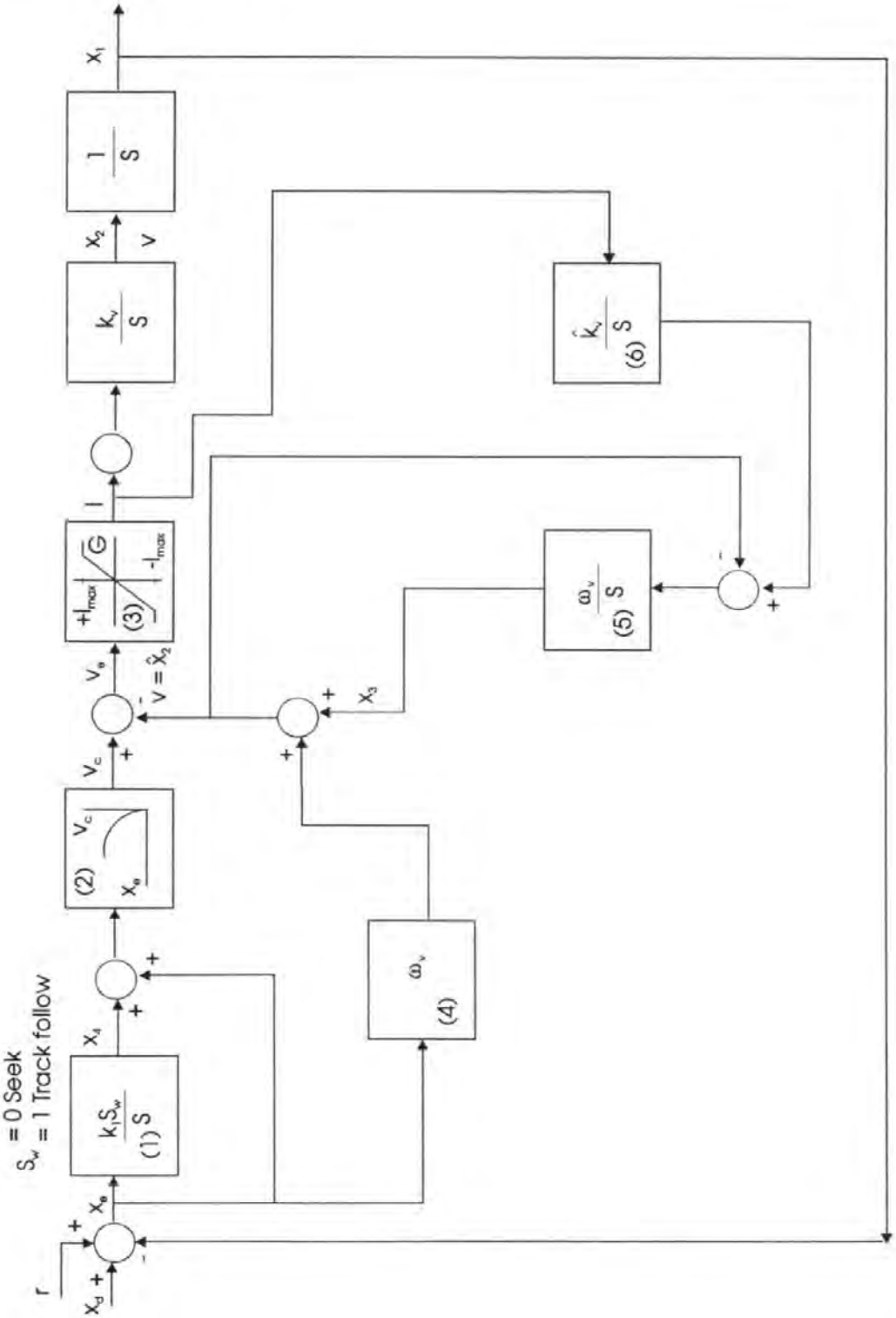

Figure 1.15 Block diagram of a controller with an analogue servo.

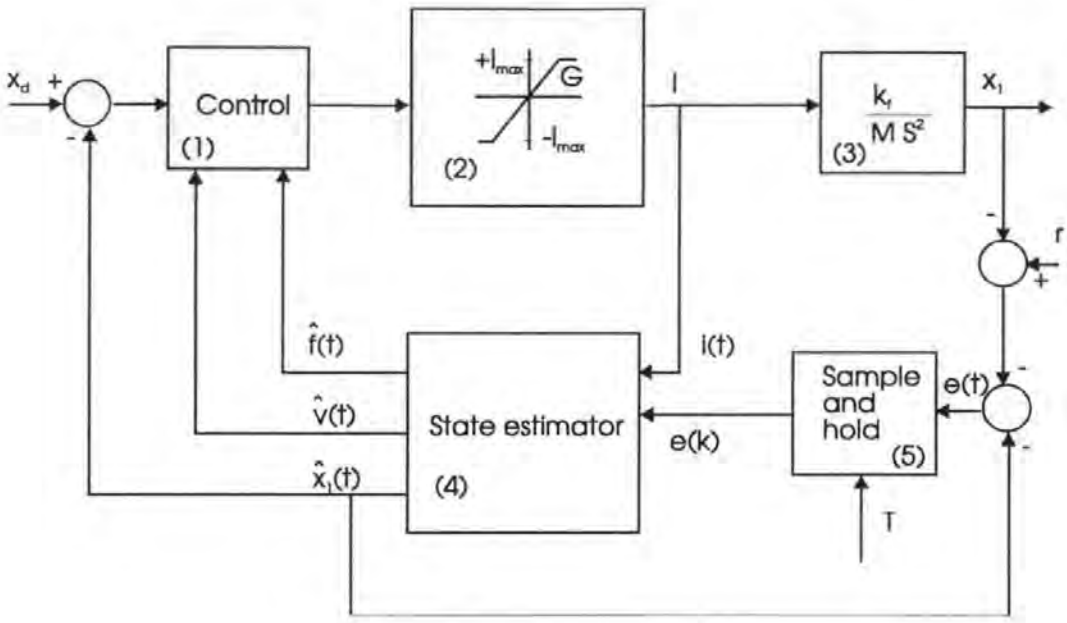

Figure 1.16 Sampled data sector implementation with an analogue-control structure. Copy from [Mee, 1989].

Figure 1.17 shows a wholly digital controller for a HDD. The only difference lies in the fact that the track following control is via a digital-control loop, rather than an analogue-control loop.

It should be noted that current feedback is the current through the VCM.

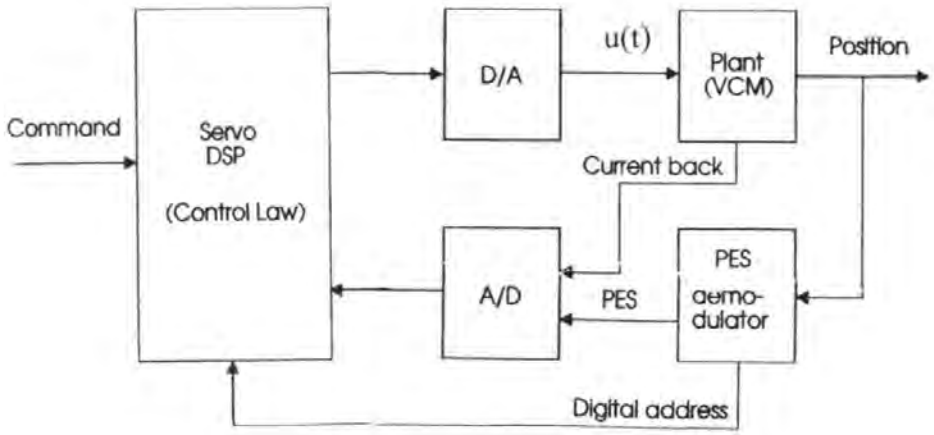

Figure 1.17 Block diagram of a digital discrete-time-control system.

The basic design procedure of the digital discrete-time-control system using state-space methods is shown as follows:

(1) Construct a digital state-space model for the plant from the point of the output ($u(t)$) as shown in Figure 1.17. Check the model using MATLAB.

(2) Design a state-space model of a control-law and check it by using MATLAB.

(3) Design a state-space model of an estimator.

(4) Combine the control-law and the estimator.

(5) Combine the digital state-space model for the plant and the controller, check it by using MATLAB.

(6) Place the complete state-space model in a design program executed by the DSP.

1.2.3.6 Position error sources

(1) Track misregistration

The track misregistration (TMR) means the offset between the actual data read head position and the track centre. It is not a number but a statistical distribution. The maximum track misregistration in a HDD has to be less than 12% of the track-to-track pitch [Mee, 1989]. The TMR has an approximate Gaussian normal distribution with mean zero. The TMR has two parts: the first is called write-to-read TMR which is the difference between the TMR of writing a track to the TMR of reading the same track (see Figure 1.18); the second is called write-to-write TMR which is the difference in relative head-to-track position between a recorded track and an adjacent track, resulting in track encroachment or track-to-track "squeeze", depending on the direction of the misregistration on the adjacent recorded track (See Figure 1.18) [Mee, 1989].

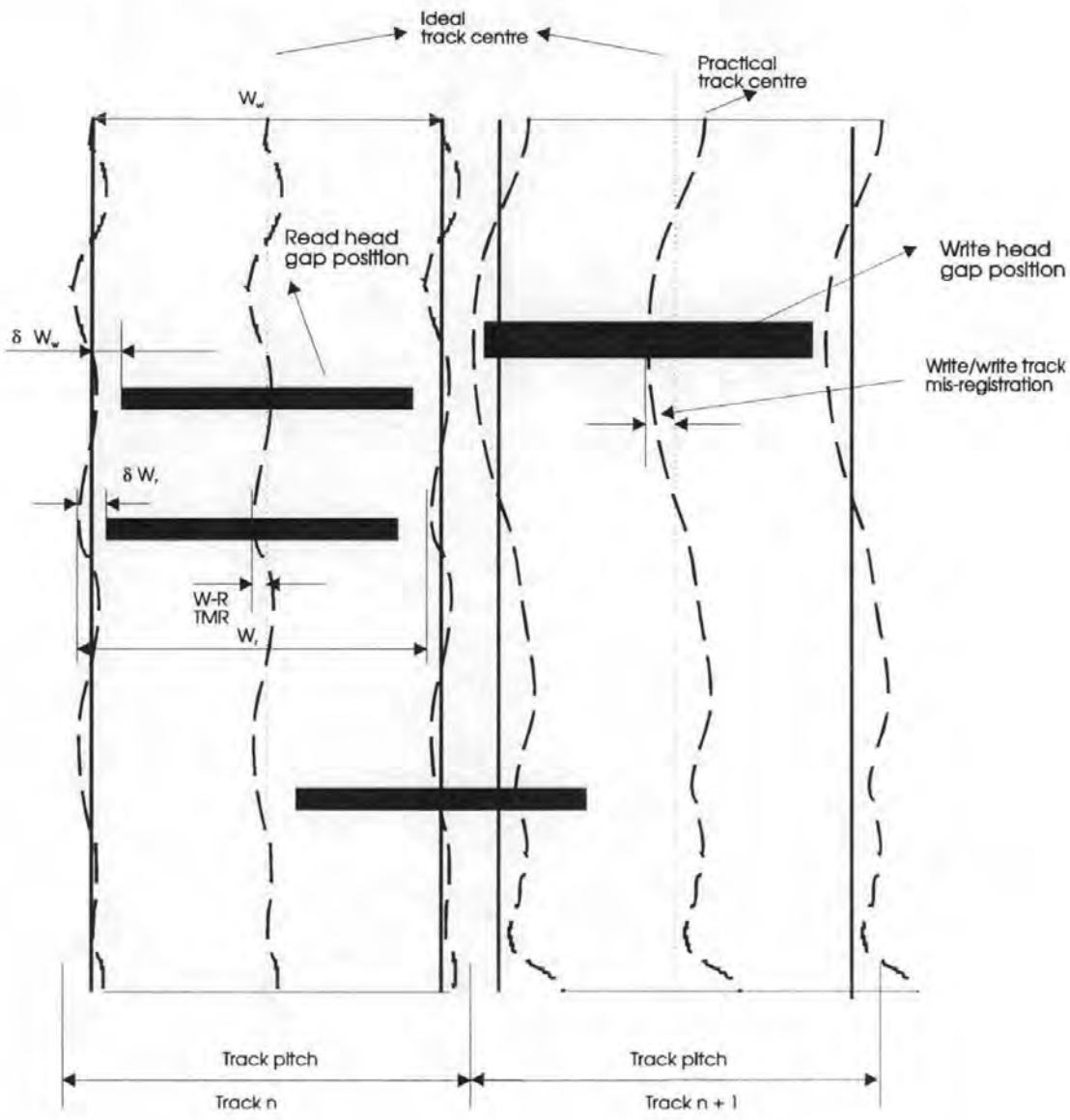

Figure 1.18 Illustration of various error modes arising from track misregistration

Some of the largest TMR components are listed below:

(a) Servo pattern linearity and accuracy caused by anomalies in the disk media, recording head, recording process, and the format of the servo pattern writing; these errors show up in the servo pattern demodulator as linearity and offset errors.

(b) Nonrepeatable spindle runout caused by the spindle bearing.

(c) Thermal shift due to mechanical misalignment between the data head and servo head.

(2) Radial Nonrepeatable Runout

Radial nonrepeatable runout is non-repeatable radial motion of the track or heads, which is produced by mechanical vibrations in the actuator, disk, and spindle assembly. The effect between the arm and the disk is due to flutter; resonant modes with motion perpendicular to the head arm and disk structures are induced by buffeting from the air carried along with the disks. In the case of the spindle, the nonrepeatable runout produces from dynamic spindle tilting [Mee, 1989]. Typical values for the total nonrepeatable runout following random seeks is 0.5 to 1.5 μm base-to-peak value. A significant contribution to nonrepeatable runout is from the spindle bearings. Naruse presented an analysis of the contribution of spindle ball bearings with deformed inner and outer bearing races to nonrepeatable runout [Naruse et al., 1983]. The frequency-separation of the radial nonrepeatable runout was measured by Richter [Richter & Talke, 1988]. Note that nonrepeatable and repeatable runout, within the bandwidth of the actuator servo system, could be followed by the servo head controlled by the servo system.

1.2.4 Summary

Magnetic recording principles are introduced and discussed in section 1. The main components of a hard disk drive (HDD), the magnetic head, the media, and the data channel are described and reviewed in the second section. In the third section, the profile of the head servo system is described and reviewed. The main performance of the head system is discussed by reviewing and discussing the technology. It is shown that the development of a position measuring system is of most interest to current HDD industrial research. A few new servo methods have been developed and reported. However,

because they use etch or stamp technology to make marks, grooves and lands on the surface of the disk for recording servo patterns, the surface of the disk would be not suitable for near-contact or contact recording which is the objectives of tomorrow's HDD's. On the other hand, adding etching and stamping processes will increase cost. More detail can be seen in sections 4.3.11 and 4.3.13. The current studies using a dual-stage actuator have produced exciting results, and it seems that it is quite possible to apply these methods in the development of a servo control system.

The author believes that this new technology and the development of the new measuring position system for a submicron track HDD. is the most important development for an ultra-high track density HDD. As J.C. Mallinson said, in his book on magnetic recording, "It is important to realise that the essence of the problem is not in the implementation of the servo feedback loop or the head actuator, for submicron track positioning and following . The basic problem is, where does the track error signal come from?" [Mallinson, 1993].

Chapter Two

A New Recording Mode

for the Magnetic Servo Patterns

2.1 Introduction

Three magnetic recording modes, namely for longitudinal recording, perpendicular recording and transverse recording have been used or studied in current magnetic recording systems. These three recording modes are schematically shown in Figure 2.1. (a), (b) and (c) respectively. In the longitudinal magnetic recording mode, as shown in Figure 2.1 (a), the recorded data and the servo patterns are magnetised along the media moving direction. The gap lengths of the recording head and the reproducing head are parallel to the direction of media motion [Mee, 1989]. In the perpendicular magnetic recording mode, the data and servo bits are magnetised perpendicular to the media plane. The gap lengths of the recording head and the reproducing ring head or the thickness of single pole head are parallel to the media moving direction [Iwasaki & Takemura, 1975]. In the transverse recording mode, the data bits are magnetised along a direction perpendicular to the recording track. The gap lengths of the recording head and the reproducing head are perpendicular to the direction of the recording track [Sauter et al., 1972].

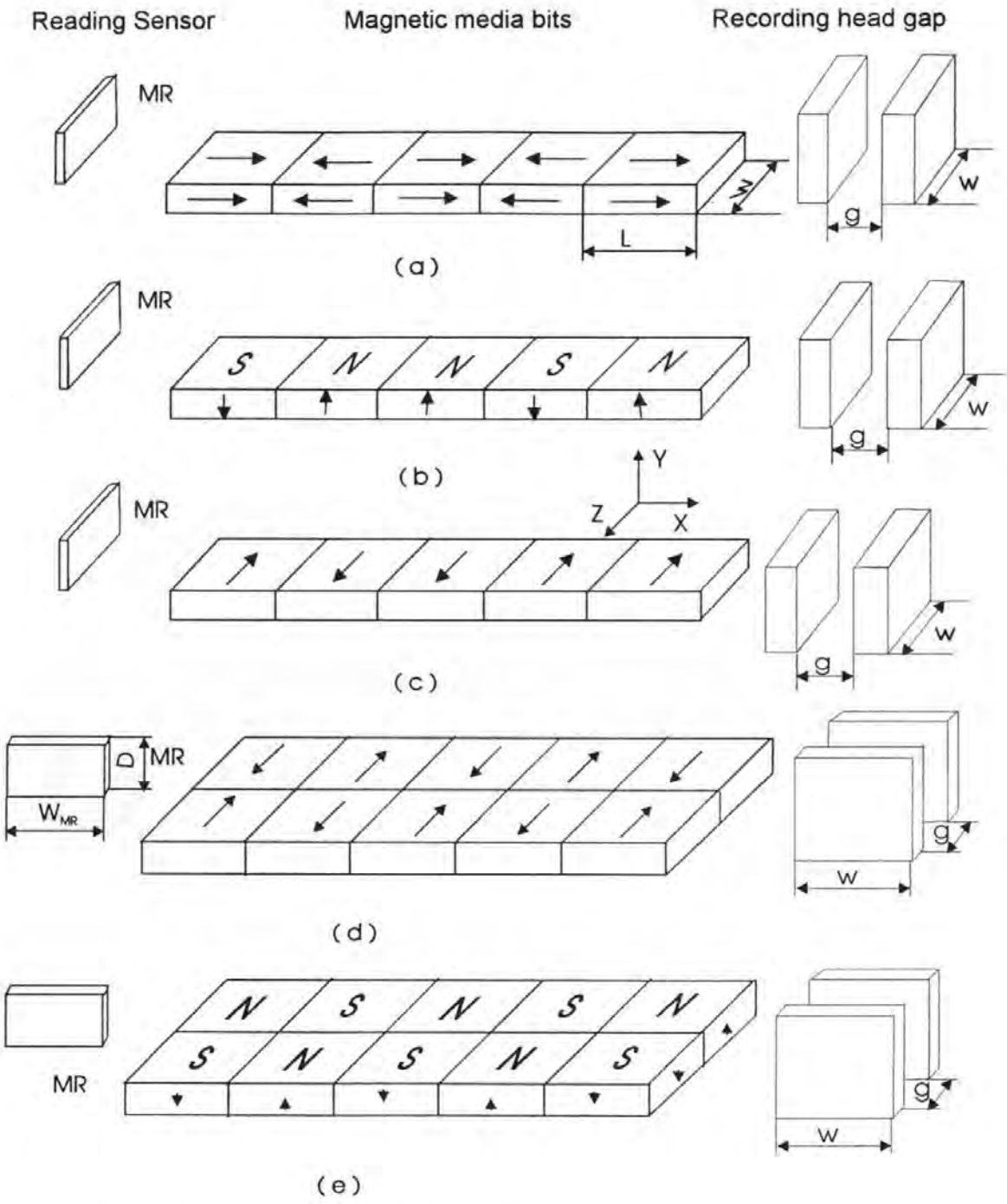

(a) The longitudinal magnetic recording mode
(b) The perpendicular magnetic recording mode
(c) The transverse magnetic recording mode
(d) The dual-transverse magnetic recording mode on longitudinal media
(e) The dual-transverse magnetic recording mode on perpendicular media

Figure 2.1 Reading and writing modes for magnetic recording.

Almost all commercial magnetic recording systems operate in the longitudinal recording mode at present. The perpendicular magnetic recording mode has been widely studied, but the transverse magnetic recording mode is still at its early development stage, though the transverse magnetic recording mode was proposed in the sixties, as a promising method to achieve high density magnetic recording [Machinski, 1967] [Sauter, 1971]. Only a few people have shown interest in it, partly due to successive improvements in longitudinal and perpendicular recording introduced by thin film technologies. Researchers took no further interest in the transverse magnetic recording mode, partly due to the fact that the reproduction of the recorded signal is very difficult. Sauter reported the results of an experiment in the transverse magnetic recording mode using a thin film recording head in 1972 [Sauter, et al., 1972], in which the recording densities with flux changes per inch (FCI) = 18.5 k and track per inch (TPI) = 0.5 k were obtained with the recorded bits being reproduced by optical methods rather than a magnetic read head. Desserre presented experimental results of transverse recording on a radially anisotropic disk in 1985 [Deserre, 1985]. In his work a radially anisotropic disk coated with Co-Sm media with coercivity of 300 Oe and thickness of 0.35 μm was developed. The simple reading and writing experiments made on the disk yielded recording densities of FCI = 10 k and TPI = 690. A hierarchical micromagnetic mode of longitudinal thin film media was employed by Miles et al. to investigate the high density performance of transverse recording [Miles & Middleton, 1991].

In these recording modes, the output of the reproducing head, $v(x)$, is proportional to the width of the head, i.e.

$$v(x) \propto w \cdot f(t) \tag{2-1}$$

where, $f(t)$ is the readout function per unit of head width and w is the width of the head.

In general, the head width is equal to or less than the recorded trackwidth and when recording trackwidth is reduced, so is the reading head width. Consequently the readout and the values S/N of the data and servo signals are reduced. Therefore in the above three magnetic reading modes, the head, when reading servo information, suffers from low S/N and poor linearity of the position error signal (PES). This problem becomes worse as the trackwidth reduces to submicron size [Akagi, et al., 1991].

On the other hand, it is well-known that there is an asymmetrical off-track response for a longitudinal read MR head [Zhu & Ye, 1992] [Lee et al., 1991]. If a MR head is used as a servo head, these phenomena will result in low both linearity and S/N of the position signal. More details will be given in the section 4.3.

2.2 The New Magnetic Recording Mode

The new dual-transverse read/write modes, for longitudinal media and perpendicular media are shown in Figure 2.1 (d) and (e). In these modes, the gap length of the write head is perpendicular to the direction of media motion. The MR head is aligned at a 90° angle compared with conventional heads in other modes. Information is recorded along the transverse direction of moving media.

The obvious advantage of the transverse MR reading mode is that the performance of the read head is no longer affected by the data track width in the direction of moving media. Further discussion on its advantage will be given in the Chapter Four.

2.3 Recording and Reproducing in the New Mode

Because the recording and reproducing processes are very different from those in conventional longitudinal magnetic recording, the aim of this section is to discuss mode's characteristics, such as recording trackwidth, shape of the transverse bit and the transition length, and the reproducing process including output voltage waveforms and the S/N ratio.

In this co-ordinate system, shown in Figure 2.2, the x co-ordinate has become the direction of recording trackwidth. The z co-ordinate is parallel to the recording track direction or moving media direction (unlike the usual case for magnetic recording). Hereafter, letters W (w) and L (l) indicate width x co-ordinate and z coordinate, respectively.

2.3.1 Recording trackwidth and bit length

The length (L_c) of a recorded bit in the track direction in the new mode is defined as:

$$L_c = v_z T \tag{2-2}$$

where, v_z is the speed of media motion and T is the pulse width of writing current per bit.

The recording trackwidth is defined by the write head trackwidth in conventional magnetic recording, although there is a side writing phenomenon which is much smaller than the head trackwidth. Figure 2.2 is a schematic diagram of transverse recording trackwidth. It should be noted that the recording track direction is perpendicular to the paper. In Figure 2.2 the equal magnetic field of H_x is shown by dotted line. Thus, the Karlqvist equation can be used in this case and its horizontal field component is expressed as:

$$H_x = \frac{NI}{g}\left[\frac{yg}{x^2 + y^2 - \left(g^2/4\right)}\right] \tag{2-2a}$$

When $H_x \geq H_c$, the magnetic state changes from $-M_r$ to $+M_r$ or vice versa. The track width can then be expressed as:

$$w_r = 2x_c = 2\sqrt{\frac{gy}{\tan\left(\frac{2gH_c}{NI}\right)} - y^2 + \frac{g^2}{4}} \tag{2-3}$$

where, H_c is the coercivity of a media, g is the gap length of the write head, I is write current and N is the number of turns of coils of the write head.

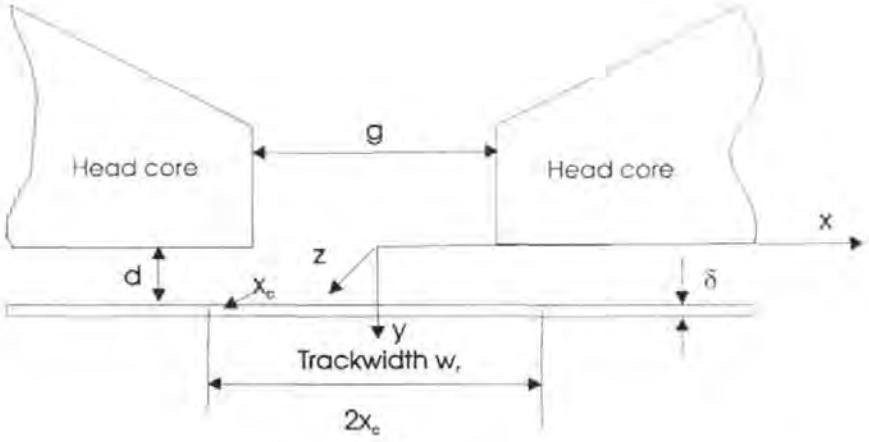

Figure 2.2 Schematic diagram of recording trackwidth *in transverse read/write model*

Equation (2-3) shows that the recorded trackwidth is dependant not only on the gap length (g) of the write head, but also on the magnitude of write current, the H_c of medium and the space (d) between the head and the medium.

Assuming the ideal contact recording condition, that is $d = 0$, it follows from, equation (2-3), $w_r = g$. However, it becomes more complicated in the case when $d > 0$, because the following effects must be considered:

(1) Effect of head - media spacing

When the calculation condition is given by: $g = 0.7$ μm, $H_c = 2000$ Oe, $N = 16$, $\eta = 0.7$ and $I_1 = 60$ mA or $I_2 = 80$ mA, the variation of the recording trackwidth with the head-medium spacing is shown in Figure 2.3. It can be seen from Figure 2.3 that the function is not monotonic and that W_{rmax} is not at $y = 0$, but $y = 0.32$ μm where H_x is equal to H_c and x has its maximum value. The trackwidth increases with the space before point B.

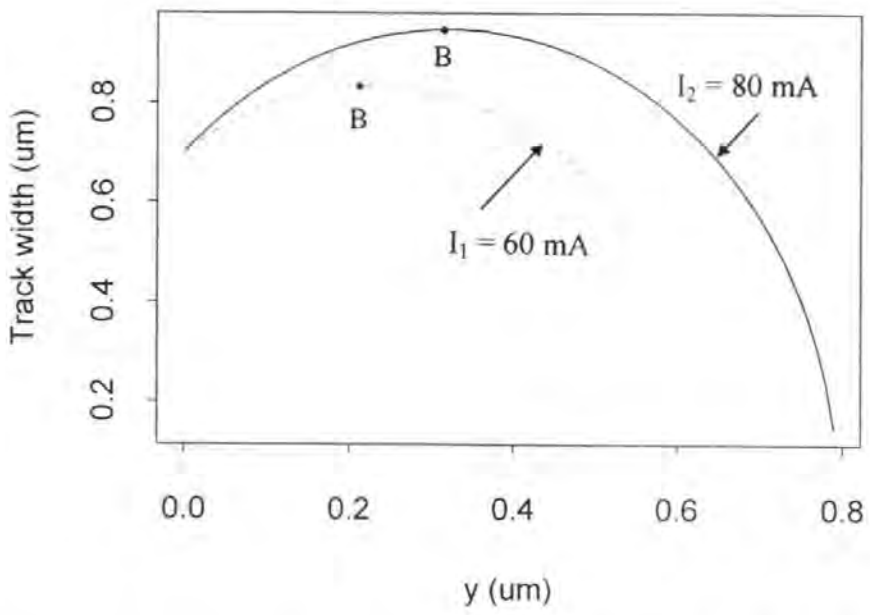

Figure 2.3 The recording trackwidth vs. space between the head and medium.

Therefore, it can be seen that in order to maintain a constant recorded trackwidth, low flying height and small changes of flying height are required.

(2) Effect of write current

From Figure 2.4, it can be seen that the trackwidth increases as the write current increases and that the gradient of the trackwidth curve becomes larger as H_c increases.

The magnitude of the write current must be greater than the value at point C to reduce gradient effects.

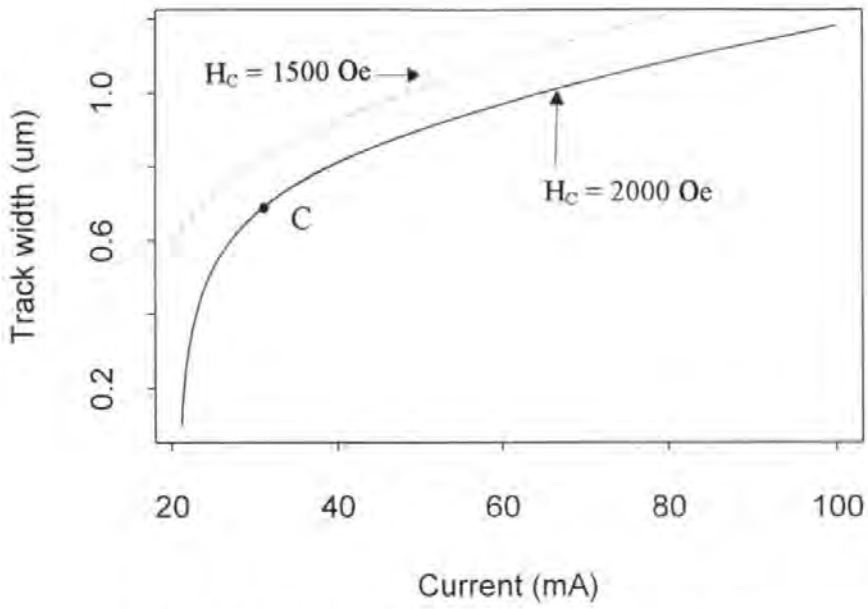

Figure 2.4 The recording trackwidth vs. the write current

(3) Effect of media coercivity H_c

Figure 2.5 shows the variation of trackwidth with the coercivity (H_c) of the media for two values of write current, when the spacing is 0.05 μm. The trackwidth reduces when the coercivity of media increases.

In summary, the transverse recorded track width is dependent not only on the gap length of the write head, but also on the magnitude of write current, the H_c of the media and the spacing between head and media. When the current reduces and the spacing or the H_c value increases, the trackwidth reduces. A written track with minimum variation of track can be achieved for a medium with given H_c by optimizing the spacing (or the flying height) and writes current.

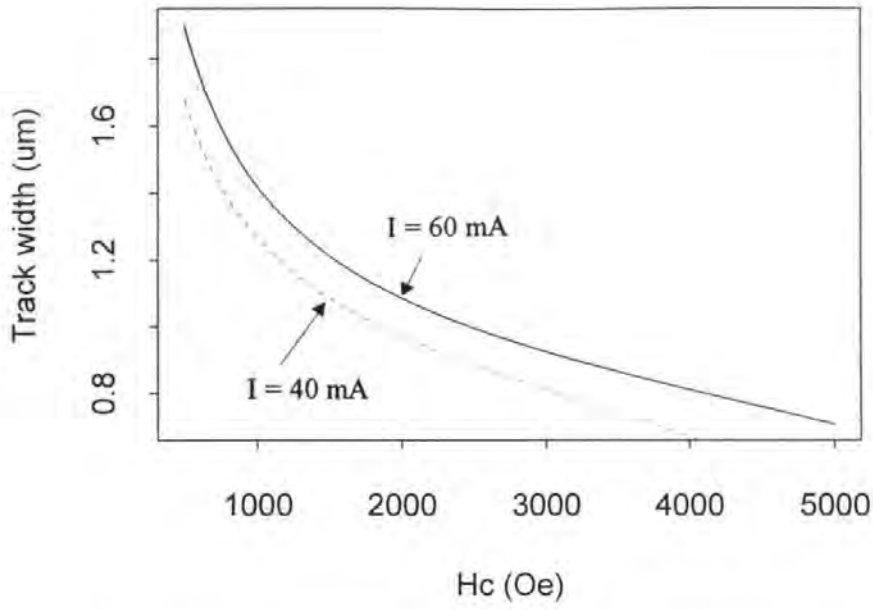

Figure 2.5 The recording trackwidth vs. the coercivity of the media

2.3.2 Calculation of minimum transition length

According to reference [Sauter et al., 1972], recording pattern in the new mode is separated by transition regions in the radial and circumferential direction, as are shown in Figure 2.6.

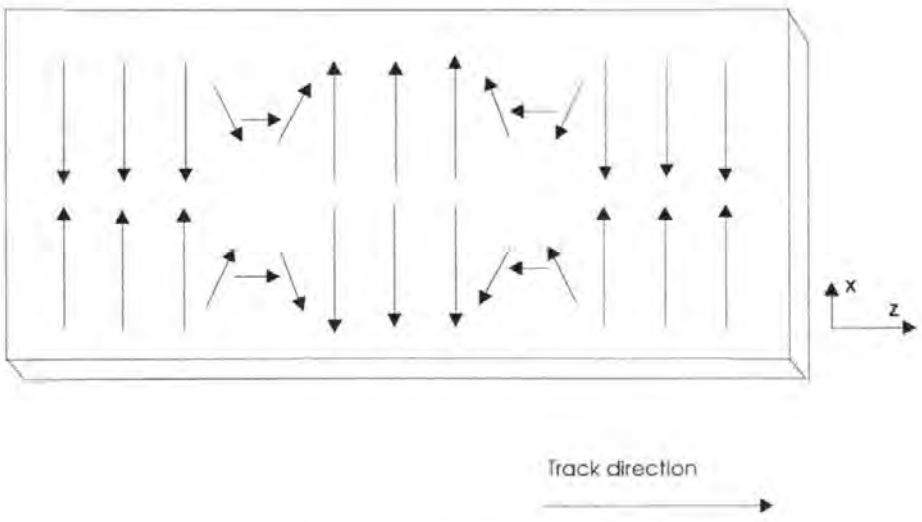

Figure 2.6 Description of the transition regions in the circumferential and the radial direction

The length of transitions in the circumferential (track) direction in this new mode is similar to that in the conventional transverse recording mode. The transition length was simulated by Miles and Middleton [Miles & Middleton, 1991]. According to their results, the transition length in the new recording mode is also shorter than that in the longitudinal recording mode. As we can see from Figure 2.6, the radial transition length in the new mode is similar to that between bit and bit in the longitudinal recording mode. Therefore the length in the model can be calculated as follows:

Referencing Mee's book [Mee, 1989], in order to simplify the calculation for the transition region length, the following five assumptions are taken:

(1) Only longitudinal writing-head fields are considered.

(2) The magnetization is uniform throughout the magnetic coating and to be longitudinally oriented only.

(3) The longitudinal demagnetizing field is treated in an approximate manner.

(4) The medium is in-plane isotropic.

(5) The transition is an arctangent transition.

The argument for assumption (4) is as follows:

Simulation and experimental results show that high media orientation ratio yields large transition noise and track edge noise at high track and bit recording density [Zhu et al., 1992], [Zhu, 1993] [Doerner et al., 1991] in longitudinal recording mode. From the noise view point, isotropic media is more preferable than anisotropic media in the new mode because the transition between track to track and the transition between bit to bit in the new recording mode are similar to the transition between bit to bit and the written edge of track in the longitudinal case. Therefore, isotropic media is used in this discussion. The specific form of an arctangent transition can be expressed by:

$$M_z(z) = \frac{2M_r}{\pi}\tan^{-1}\left(\frac{z}{a}\right) \tag{2-4}$$

and with the definition,

$$\Delta z = \pi a \tag{2-5}$$

where Δz is a length of transition region, a is called the arctangent parameter, M_r is the magnetization for each side of transition. Under the above five assumptions, the demagnetizing field can be expressed as [Mee, 1989]:

$$H_{dz\max} = 4M_r\left[\tan^{-1}\frac{\left(\frac{\delta}{2}+y_0\right)z_0}{z_0^2+a^2+a\left(\frac{\delta}{2}+y_0\right)} + \tan^{-1}\frac{\left(\frac{\delta}{2}-y_0\right)z_0}{z_0^2+a^2+a\left(\frac{\delta}{2}-y_0\right)}\right] \tag{2-6}$$

by differentiating H_{dz} with respect to z and letting $y_0 = 0$, it is found that H_{dz} obtains its maximum at

$$z_0 = \sqrt{a^2+\frac{a\delta}{2}} \tag{2-7}$$

The maximum value of H_{dz} is:

$$H_{dz\max} = 8M_r\tan^{-1}\left(\frac{\delta}{4a\sqrt{1+\frac{\delta}{2a}}}\right) \tag{2-8}$$

Inspection of the hysteresis loop reveals that, for a stable magnetization, demagnetizing fields cannot exceed the media coercivity [Chapman, 1963]. Therefore, according to Eq. (2-8), there will be a minimum value of the transition length allowed by demagnetization, which can be determined by $H_{dz,\,max.} = H_c$, that is

$$a_{\min} = \frac{\delta}{4}\left(\csc\frac{H_c}{8M_r}-1\right) \tag{2-9}$$

Than, the minimum transition length is

$$\Delta z_{\min} = \pi a_{\min} = \frac{\pi\delta}{4}\left(a\cos\left(\frac{H_c}{8M_r}\right) - 1\right) \tag{2-10}$$

when $\frac{\delta}{a} \leq 1$ (in the case of using ultra-thin medium), Eq. (2-10) can be simplified, that is

$$\Delta z_{\min} = 2\pi\delta\frac{M_r}{H_c} \tag{2-11}$$

A number of deductions can be made from Eq. (2-11). Firstly, the expression for the transition length in radial direction on in-plane isotropic magnetic media in new recording mode is similar to that in the conventional longitudinal recording. Secondly, the transition length is proportional to medium thickness and the value M_r. It is also inversely proportional to H_c. Thus for all media, it is necessary to keep M_r small, H_c high and δ small in order to achieve sharp transitions in the new mode.

2.3.3 Shape of the transverse bit

To study the shape of the recorded pattern we first need to consider the edge-fringing field of the write head. The edge field affects the written trackwidth, partially erases adjacent tracks, and increases the reading width of the head and the pickup of signals from adjacent track in longitudinal recording. A three-dimensional model of the head is used to study the field by Herk, Lindholm and et al. [Herk, 1977] [Lindholm, 1977].

In the model shown in Figure 2.7, the solid line is a geometrical construction for a conventional inductive recording head. In a Cartesian Coordinate System, labelled by (x', y', z'), the horizontal component of the field from the Karlqvist approximation is

$$H_{x'}(x', y') = \frac{NI}{g}\tan^{-1}\left(\frac{y'g}{x'^2 + y'^2 - (g^2/4)}\right) \tag{2-12}$$

Supposing that the dotted and solid lines in Figure 2.7 are geometrical construction of a conventional inductive recording head where length L is infinite, and that a new Cartesian coordinate system labelled by (x, y, z) is set up as shown in Figure 2.7, according to the Karlqvist approximation, we have the similar form with Eq. (2-12). The contribution (semi-infinite) of the top half ($z > 0$) of the construction to a point in the x-y plane ($z = 0$), according to the theory of linear superposition and supposing that the material of the head pole is isotropic, is

$$H_x(x,y) = \frac{1}{2} \cdot \frac{NI}{g} \tan^{-1}\left[\frac{yg}{x^2 + y^2 - \left(g^2/4\right)}\right] \tag{2-13}$$

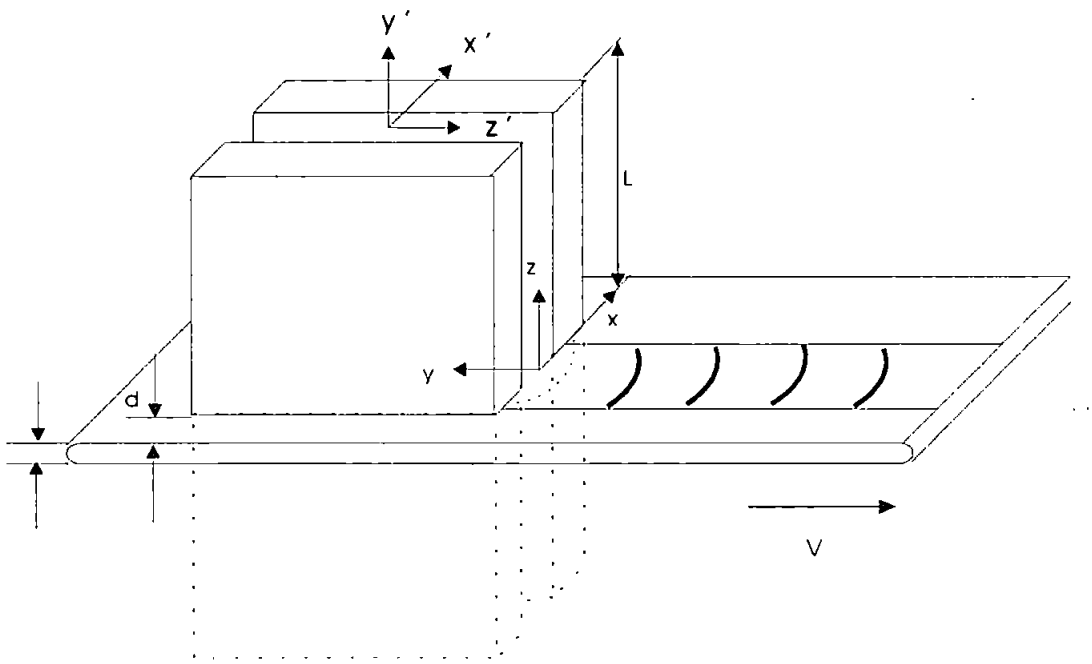

Figure 2.7 A three-dimensional model of the writing head and medium in transverse read/write mode.

When $H_x(x, y) \geq H_c$, the magnetization changes, that is:

$$H_c = \frac{NI}{2g} \tan^{-1}\left[\frac{yg}{x^2 + y^2 - (g^2/4)}\right] \tag{2-14}$$

which can be rewritten as:

$$\tan\left(\frac{2gH_c}{NI}\right) = \left[\frac{yg}{x^2 + y^2 - (g^2/4)}\right] \tag{2-15}$$

Assuming that $k = \tan\left(\frac{2gH_c}{NI}\right)$, Eq. (2-15) reduces to

$$x^2 + \left(y - \frac{g}{2k}\right)^2 = \left(\frac{g}{2}\sqrt{1 + 1/k^2}\right)^2 \qquad (2\text{-}16)$$

which represents a circle with radius equal to $\frac{g}{2}\sqrt{1 + 1/k^2}$. The displacement of off-centre of the circle is $\frac{g}{2k}$. It is noted that the leading edge of a bit is a sector of circle and is not a straight line as in the conventional recording. Simulation results show that the radius (R) of the circle is dependent on the gap length of the head (g), the H_c of the media and the write current, which is illustrated in Figures 2.8 and 2.9.

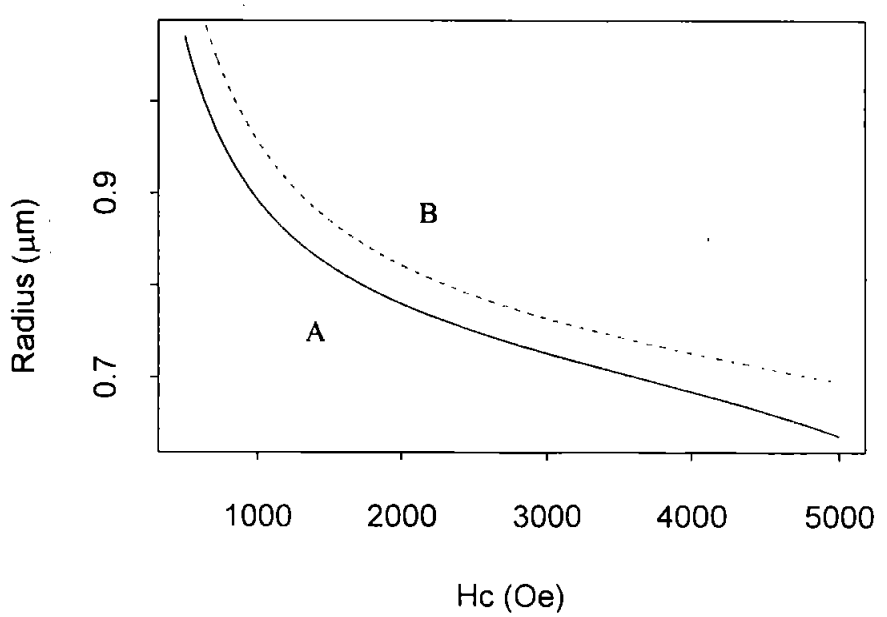

Figure 2.8 The relationship between the radius and the coercivity of media. Curve A for the write current is 60 mA; Curve B for the write current is 80 mA.

Simulation results in figure 2.8 shows the variation of the radius with the values H_c of the media with the write current equal to 60 mA for Curve A and 80 mA for Curve B, respectively, which indicates that R reduces as H_c increases. Figure 2.9 shows the

relationship between the radius and the write current with the value H_c of the media = 2000 Oe for the dotted curves **A** and 1500 Oe for the solid curve **B**, respectively.

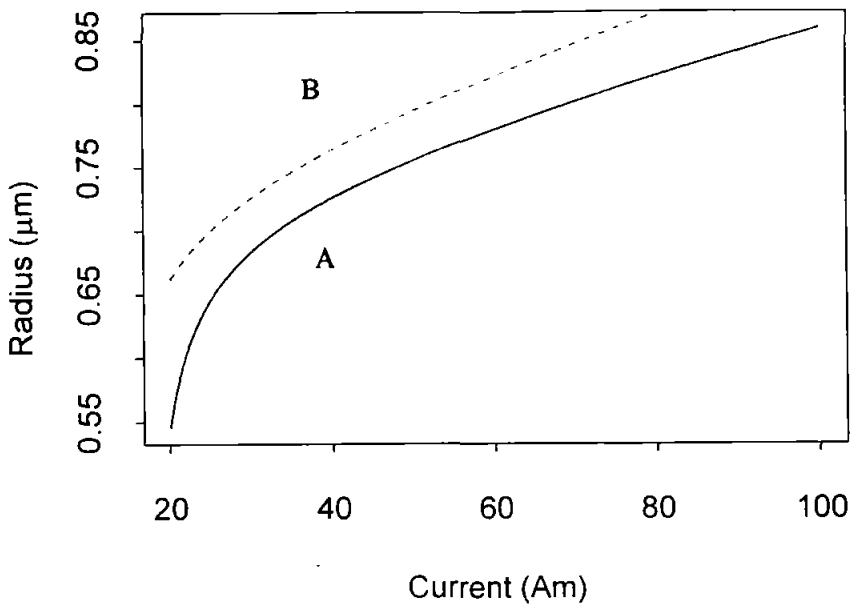

Figure 2.9 The relationship between the radius and the write current, Curve A for media coercivity of 2000 Oe; Curve B for media coercivity of 1500 Oe.

Though the above modelling and simulation are based on this special case, sufficient information can be provided to explain why the shape of a transition region is a curve and how parameters g, I and H_c affect it. It should be emphasised here that the radius r is very important and it will be discussed further in what follows:

It is well-known that the transition region is the main source of media noise (V_{mnoise}) in high density longitudinal recording and the noise is inversely proportional to the recorded wave-length (λ) {see Eq. (1-24)}(λ is inversely proportional to the number of transitions per unit length) when only considering in one dimension. Considering in two-dimension, thus,

$$V_{mnoise} \propto S_T \tag{2-17}$$

where, S_T is transition area per unit recording area. Supposing that the recording trackwidth is w and that the transition length is Δz, then transition area (S) is

$$S = 4\Delta z \cdot R \cdot \sin^{-1}\frac{w}{2R} \tag{2-18}$$

It can be seen from Eq. (2-18) that S is proportional to Δz and R, which means that reducing Δz and R will result in an increase in S/N of a MR head during readback.

2.3.4 Experimental observation of the recorded bits

The recording and reproducing experiments in the new recording modes were undertaken on the submicron servo track writer (SSTW) which will be explained in detail in Section 3.1.2. The read/write head is a commercial thin film/MR head. The length and width of the gaps of the read/write head are (0.7 μm and 4 μm)/(0.7 μm and 6 μm), respectively. The head was maintained at right angle to the normal data head when it reads or writes in the new mode. The head is moved by the positioner of SSTW. A 3.5" rigid disk (made by IBM) with in-plane isotropic longitudinal media of 1800 Oe and B-H loop squareness $s^* = 0.81$ was used in the experiment. The write/read circuit will be explained in detail in Section 3.2.

Figure 2.10 shows the magnetic force microscopy image of two transverse recorded tracks which are produced by the University of Manchester Information Storage Group. It can be seen that transition regions exist between the recorded bits and between the recorded tracks. It can also be seen that the shape of the transition regions between the bits in the track direction are curves and the shape between the bits in the transverse track direction are straight lines. The write currents for recording track ***A*** and for recording track ***B*** are 40 mA and 80 mA respectively. The results for both trackwidths show that the recorded trackwidth increases with write current, which coincides well with the above calculation and analysis.

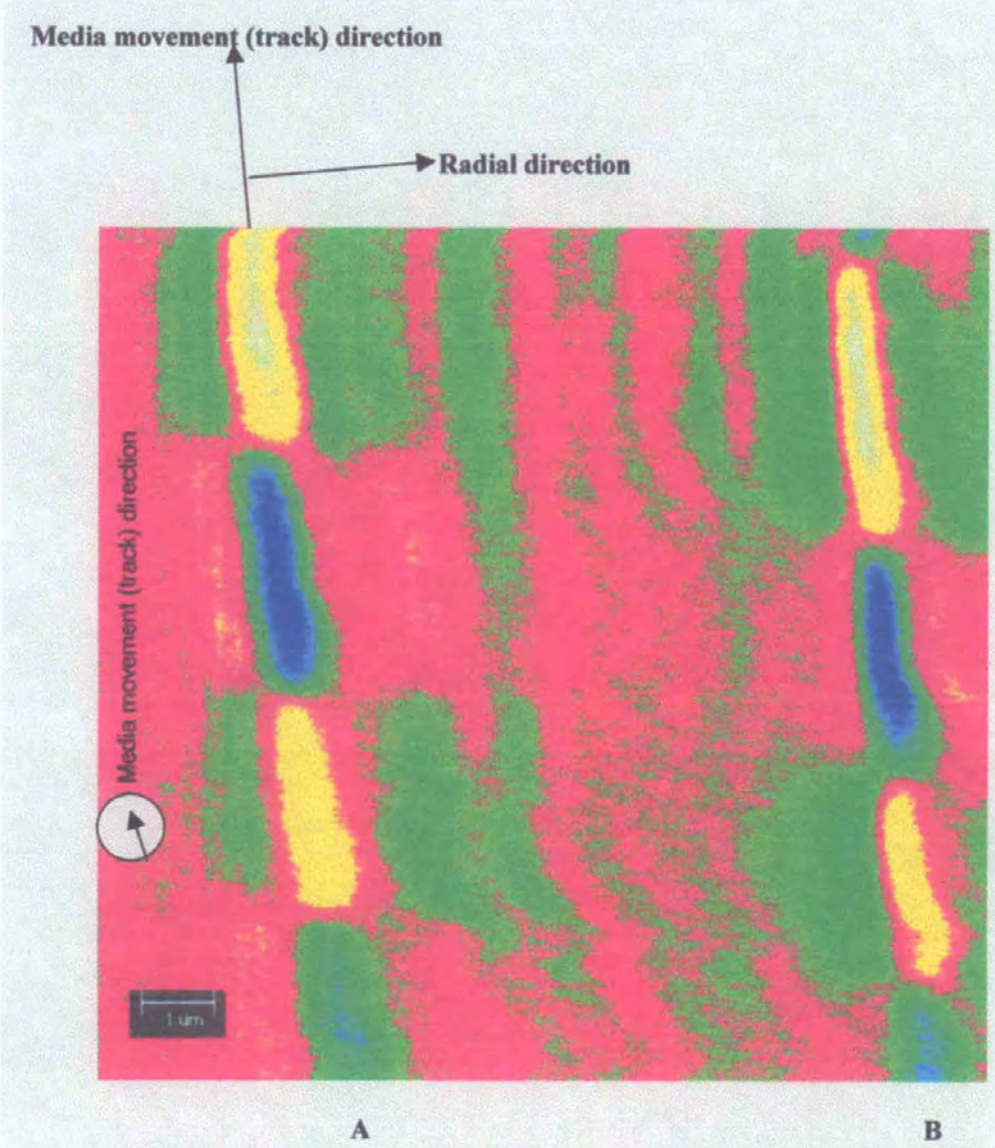

Figure 2.10 Magnetic force microscopy image of the transverse bits. (This MFM image was produced by Prof. Clegg of Manchester University. For writing conditions see Section 2.3.4).

2.3.5 Reproducing processes

As discussed in Chapter One, there are two ways by which the MR readout shown in Figure 2.1 (d) and (e) can be calculated, such as Eq. (1-15).

It is noted that it is very difficult to solve these two equations in general cases because a 3D transmission-line model would be needed. However a 2D model can be used for some special cases.

We consider a simple case, i.e. transverse unshielded MR reproducing signals on perpendicular media as shown in Figure 2.1 (e). Assuming that the recorded patterns in the media have been written with a perfect, undistorted sine wave of longitudinal magnetization, which has the same magnitude and phase angle throughout the coating depth, then it follows that

$$M_z = M_r \cdot \sin\frac{2\pi z}{\lambda} \tag{2-19}$$

Further, the fringing field produced by the medium can be obtained by integration over these poles, which gives the analytical expression for the vertical component of the fringing field by

$$H_y = -2\pi M_r \cos(2\pi z/\lambda) e^{-2\pi y/\lambda}\left(e^{\pi\delta/\lambda} - e^{-\pi\delta/\lambda}\right) \tag{2-20}$$

and supposing that the trackwidth is infinite, then Eq. (1-15) reduces to

$$V(\bar{z}) = I\alpha\Delta R(\bar{z}) = 2IR_0\frac{\Delta\rho_{\max}}{\rho}\cdot\frac{H_b}{H_0}\int_0^L\int_d^h H_y dz dy \tag{2-21}$$

if
$$k_v = -2\pi M_r\left[e^{\pi\delta/\lambda} - e^{-\pi\delta/\lambda}\right]2IR_0\frac{\Delta\rho_{\max}}{\rho}\frac{H_b}{H_0^2} \tag{2-22}$$

then,
$$V(\bar{z}) = k_{v1}\left[\sin\frac{2\pi(0-\bar{z})}{\lambda} - \sin\frac{2\pi(L-\bar{z})}{\lambda}\right] \tag{2-23}$$

$$k_{v1} = k_v\left(e^{-2\pi d/\lambda} - e^{-2\pi h/\lambda}\right) \tag{2-24}$$

where, L is the length of the MR in the track direction, h is the height of the MR, M_r is the peak sinusoidal remanence, δ is the coating thickness, d is the head-media spacing, and λ is the recording wavelength.

It is noted that the output of the MR head is proportional to the coercivity of the media, the current and the parameters of the MR material and that the output of the MR head is not dependent upon the head-media speed.

It is interesting to study the behaviour of the length of the MR head (L) and recording wavelength λ. To this end, by using the Newton-Raphson method to solve numerically Eq. (2-23), we have

$$V_{max} = k_{vl}, \qquad when\ L = (n/2)\lambda \tag{2-25}$$

$$V_{min} = 0, \qquad when\ L = n\lambda \tag{2-26}$$

where n = 1, 2, 3.....

In Figure 2.12, both the numerical result (that the output of the MR head varies with L/λ) and the experimental ones are shown by line **A** and line **B** respectively (λ is the recording wavelength, L is the length of the MR head in track direction in the new mode). Comparison between the numerical results (calculating it according to Eq. (2-23)) and the experimental ones shows that good agreement is obtained, except for the regions near points where $L/\lambda = n$, which is due to the fact that an anisotropic flux propagation has occurred in the MR head in these regions. In other words, it is due to that the magnetic centre offsets from the physical centre of the MR head, and the output is not equal to zero near points where $L/\lambda = n$.

In the above experiment, conditions were same as Section 2.3.4, except (1) the writing signal frequencies change from 31.4 kHz (n = 0.1) to 942 kHz (n = 3) by step of n = 0.1, (2) a 3.5" glass disk coated with CoCrTa single layered perpendicular media

with coercivity of 2000 Oe [Mapps et al., 1993] was also used. Note that when reproduced the head must be moved a gap (e.g. 4 μm in the experiment) between the gap of the write head and the gap of the read head in radial direction, after writing recording bits.

Further, it is seen that the extreme values of the output of the MR head in the longitudinal recording media are the same as those obtained by Eq. (2-25) and Eq. (2-26). In fact the outputs of the MR head in longitudinal recording and the new mode are the same when the ratio of L to λ is optimised, which can be demonstrated by the following experimental results.

Figure 2.13 shows a waveform reproduced by a shielded MR head with trackwidth equal to 4 μm on a track on which recorded patterns have a trackwith of 4 μm and bit length of 0.7 μm on a 3.5" rigid disk with longitudinal recording media of coercivity 1800 Oe (note that 1 Oe ≅ 79 A/m), which was rotating at 3600 rpm. Figure 2.14 shows a waveform reproduced by same MR head on a track with 0.7 μm trackwidth and 4 μm bit length on the same disk in the new read/write mode. It is noted that in both cases the experimental conditions are the same, except the speed of the medium (300 rpm). The result shows that the readouts for both are approximately the same, whereas the trackwidth for the new mode reduces from 4 μm to 0.7 μm.

In order to remove the effects of different flying heights of the MR head and different medium moving speed, the gain of the amplifier for Figure 2.13 has been increased by 62%. This was found by experiment to be the adjustment needed to equalize the outputs for the longitudinal recording mode at the different flying heights.

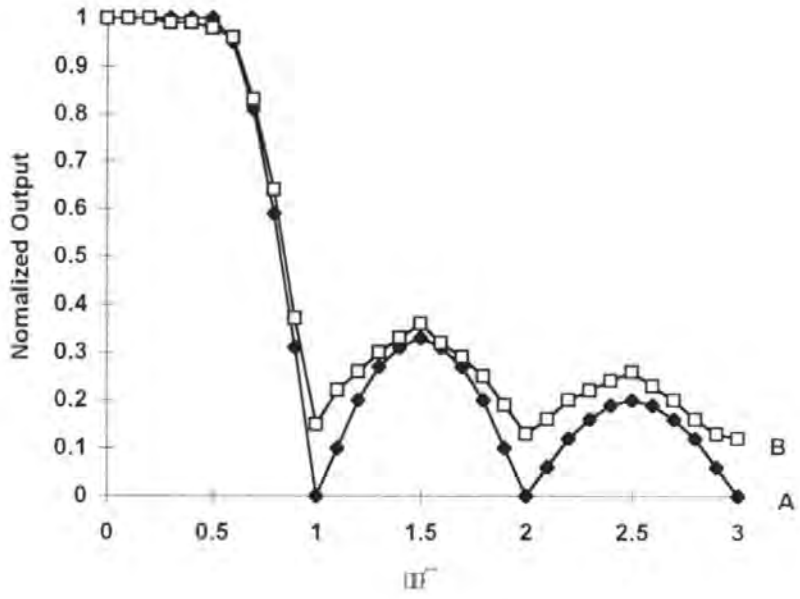

Figure 2.12 Comparison of relationship between the MR sensor length and recording wavelength, B for theoretical results and A for experimental results.

increased by 62%. This was found by experiment to be the adjustment needed to equalize the outputs for the longitudinal recording mode at the different flying heights.

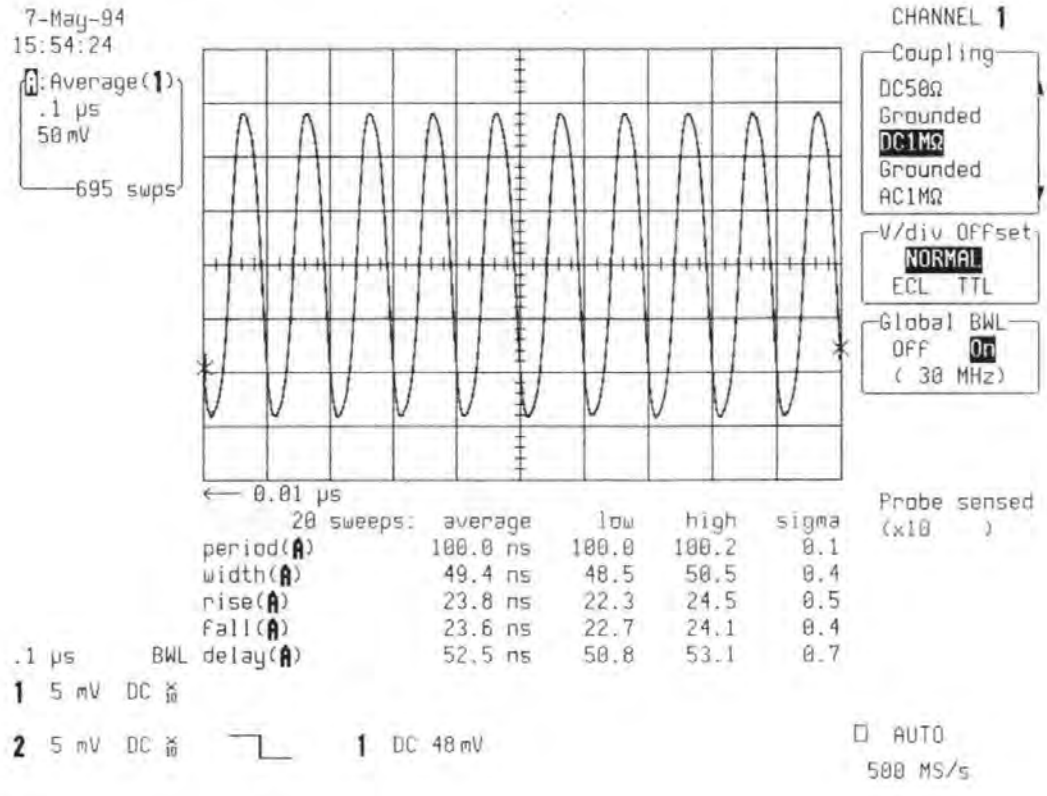

Figure 2.13 Waveform reproduced by the MR head in the longitudinal recording mode on longitudinal media.

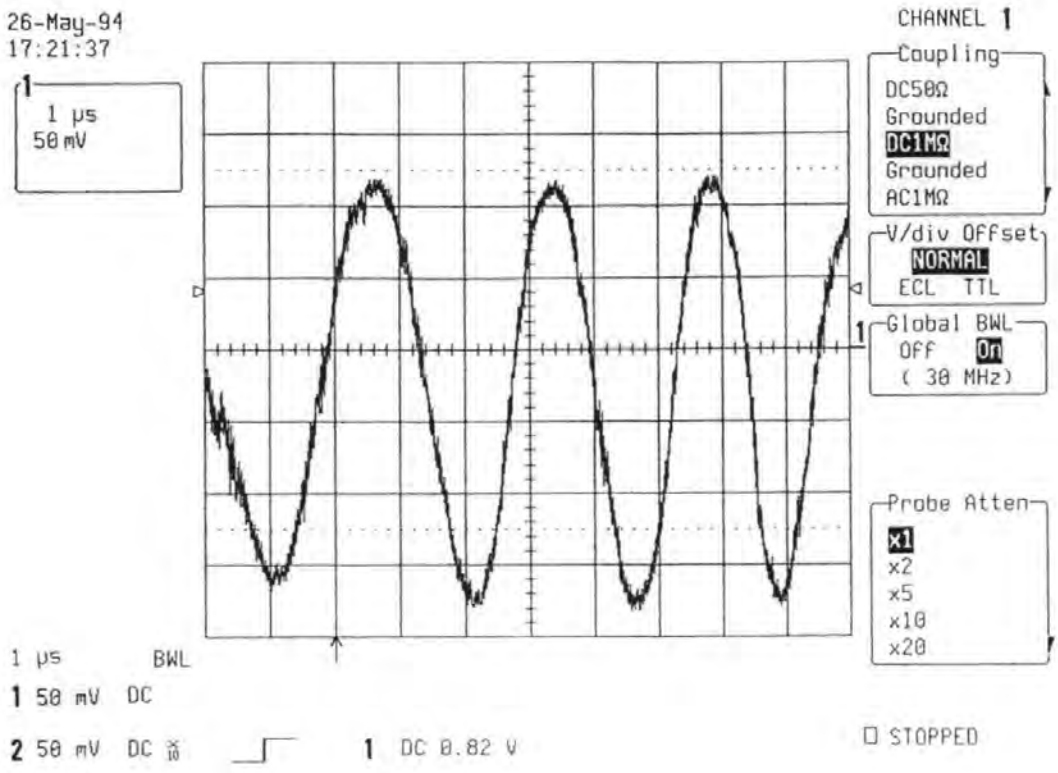

Figure 2.14 Waveform reproduced by the MR head in new transverse read/write mode on longitudinal media.

2.3.6 Signal/noise ratio of the output in the new recording

In this section S/N of the readout in the new mode on longitudinal media will be discussed (comparison with the experiment results can be seen in section 4.3.7).

As discussed in Chapter One, the readouts of an inductive head and a MR head on the thin film media in conventional recording mode are expressed by Eq. (1-9b) and Eq. (1-15). However these equations have to be changed in the new mode. In the new mode, the effective read width of the MR head does not reduce when recording bit length is greater than the MR length, even though the data trackwidth is reduced, while the effective read width for the inductive head is reduced from the head's trackwidth to the length of the gap in the new mode, that is,

$$S_{MR} \approx L_{MR} \cdot f_{MR}(t) \tag{2-27}$$

$$S_{ind} \approx g \, f_{ind}(t) \tag{2-28}$$

where, f_{MR} and f_{ind} are sensing functions in the output of the MR head and inductive head respectively. S_{MR} is the signal level of output of MR head and S_{ind} is the signal level of output of an inductive head. The inherent noise for both heads does not change. Therefore the S/N of the output of the MR head is independent of the trackwidth of the recorded track, but is roughly proportional to the MR length in the ideal case. We have,

$$S/N \propto L_{MR} \cdot f_{SMR}, \qquad \text{when } L > \lambda / 2 \tag{2-29}$$

In the new mode, the S/N of the output of the inductive head is dependent on the gap length of the head and is lower than that in longitudinal recording. It can be expressed by the following equation

$$(S/N)_{id} \propto (S/N)_{il} \cdot g / w_h \tag{2-30}$$

where, w_h is trackwidth of an inductive head and $(S/N)_{il}$ is the S/N of the inductive head in longitudinal recording.

Figure 2.15 shows a readout of an inductive head with 5 μm trackwidth and 0.25 μm gap length on rigid disks in the new mode. It is not practical because of very low S/N. That is why the early readback experiment with transverse recording was not successful.

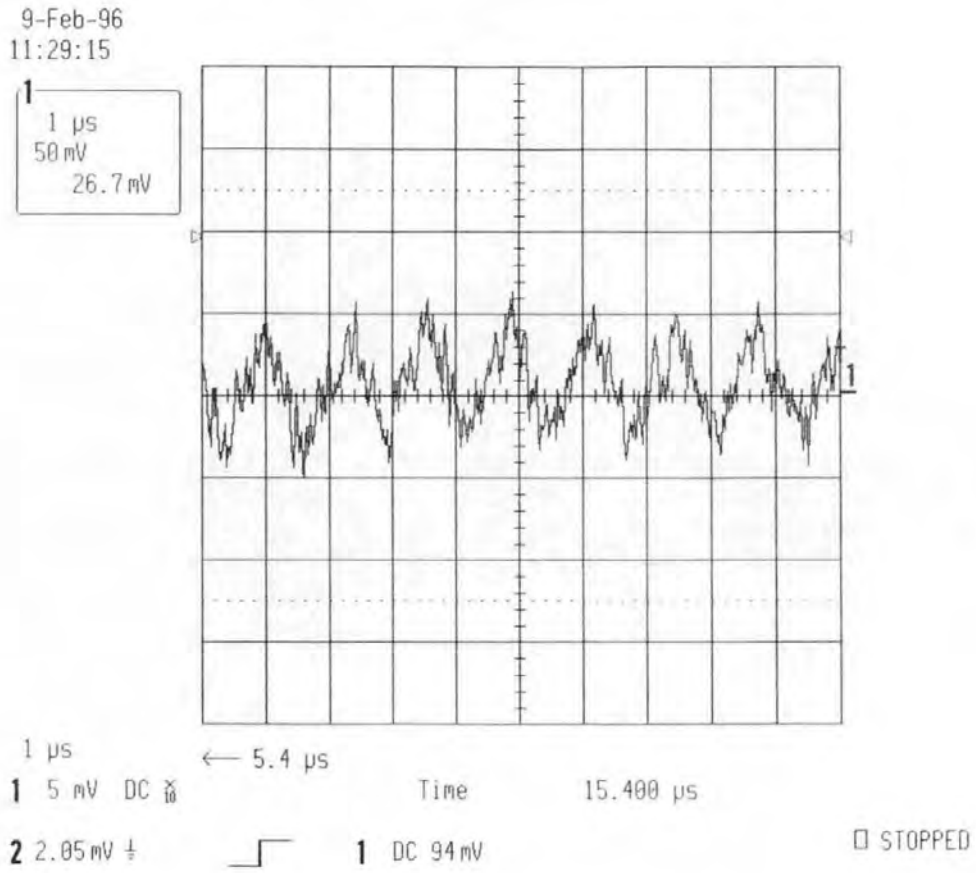

Figure 2.15 Readout of an inductive head in new transverse read/write mode on longitudinal media.

2.4 Summary

Three kinds of magnetic recording modes were reviewed in section 2.1.

In section 2.2 the new recording/reproducing mode was introduced and described, to obtain servo (position) signal with high quality when recording trackwidth is reduced to submicron size.

In section 2.3 the recording process for the new mode is investigated. Unlike the conventional recording model, the recorded track width in the new mode is mainly dependent on the gap length (g) of the write head, magnitude of the write current, H_c of the medium and the space between the head and the medium. There is a transition region between tracks, which is similar to that between bits in longitudinal recording. So in theory, the limitation of TPI in the new model equals the limitation of BPI in longitudinal recording.

A track of width 700 nm was recorded on rigid disks with in-plane longitudinal media of coercivity 2000 Oe, by a head with g = 700 nm. The three-dimensional model of the edge of gap in the write head was simply set up to study the transition region from bit to bit. Results show that the magnitude of the write current strongly affects the width of the transition region because of the component of the head field in the track direction. The shape of the edge is a dual-curve and must be symmetrical with the centre of the track. Some results were observed by MFM, and microscope indicated by ferro-fluid. In the reproduce process, when the length of the MR equates to one or half of recording wavelength, the MR head output respectively is maximum or zero in the experiment and computer simulation. Finally, a better S/N can be expected (for the same number of bits/in^2). It is found that the S/N of the output of the MR head is independent of the trackwidth of the recorded track, but it is proportional to the MR length, as the L and g of the MR head are less than the recording bit length and track width, respectively.

Therefore, the number of TPI is limited by the width of the zig-zag walls in the new mode. However, the same limitation applies to longitudinal recording for the bit density and on the new mode for the track density. It is a great advantage for reading and writing bits or servo patterns for submicron tracks, because the readout of the MR head is proportional to the length of the MR in the track direction and is no longer limited by the trackwidth of the recorded track, even the number of BPI is limited by the length of MR head. It seems that the new model is a potential candidate for reading and writing a submicron-servo-pattern as it is not necessary to have high BPI for recording a servo pattern. Further discussion will be carried out in Chapter Four.

Chapter Three

Experimental Development

This chapter describes the development of a submicron servo track writer, measuring systems and associated equipment for this project. The main measuring and observing systems and equipment used in the project are also discussed. The major experimental techniques are described in detail.

3.1 The Submicron Servo Track Writer System

3.1.1 Introduction

The submicron servo track (pattern) writer system (SSTW) was developed by the author using a "Spin Stand" disk testing station installed at CRIST facility. This station had been manufactured by Speake and Co. Ltd. for a disc manufacturer [Speake, 1985]. It had been developed into a Hard-disk Experimental Test Station by N. Darragh. The Hard-disk test station was used in his Ph. D project, "An Adaptive Partial Response Data Channel for Hard Disk Magnetic Recording" [Darragh, 1994]. Further hardware and software development were carried out by the author, designed mainly to convert the system for recording submicron servo tracks on rigid disks and for all recording experiments and signal analysis in this project. It is the fundamental experimental tool for this project. Moreover, it is a powerful and effective development system for the HDD industry. To date, the servo track writer can be offered by only a few companies in the world, and there is no submicron servo track writer on the market. The best servo track writer presently is only able to record 3 μm trackwidth. The servo track writer is shown in Figure 3.1.

Figure 3.1 Photograph of submicron servo track writer system

The operation of the system can be described as follows. The servo patterns are written on one side of disk surfaces. In our project, the servo pattern is written by a transverse inductive write head mounted on the servowriter to perform this task. The servowriting process is a repetitive process of writing a track, test the track and moving the head to the next track. The process is repeated until all tracks are written. The process of writing the servo pattern is relatively straight forward, but since it must be precisely done, the system can become quite complicated.

In order to position with submicron accuracy and write perfectly pre servo patterns in both radial and circumferential directions of a disk that is running at high speed (for example 3600 rpm), many techniques have to be employed. There are two bases of position on the disk, one for radial and one for circumferential position systems. An encoder or servo pattern generator supplies the correct servo code to the head for writing on the disk, and the disk rotating system is mounted on air bearing spindle.

3.1.2 The submicron servo track writer system

Figure 3.2 is a schematic diagram of the Submicron Servo Track Writer (SSTW) system. As shown in Figure 3.1 & 3.2, the main aspects are the head positioning system, angular clock subsystem, servo pattern generator, testing subsystem, spindle, clamp and control computer. In order to suppress any external vibration being transmitted to the head/disk interface, all of these are mounted on a granite bed supported on air cushion. The granite bed and mechanical assembly are placed within a class 100 air booth which itself is located within a class 1000 clean room facility, so that the disk and head will not become contaminated with dirt particles.

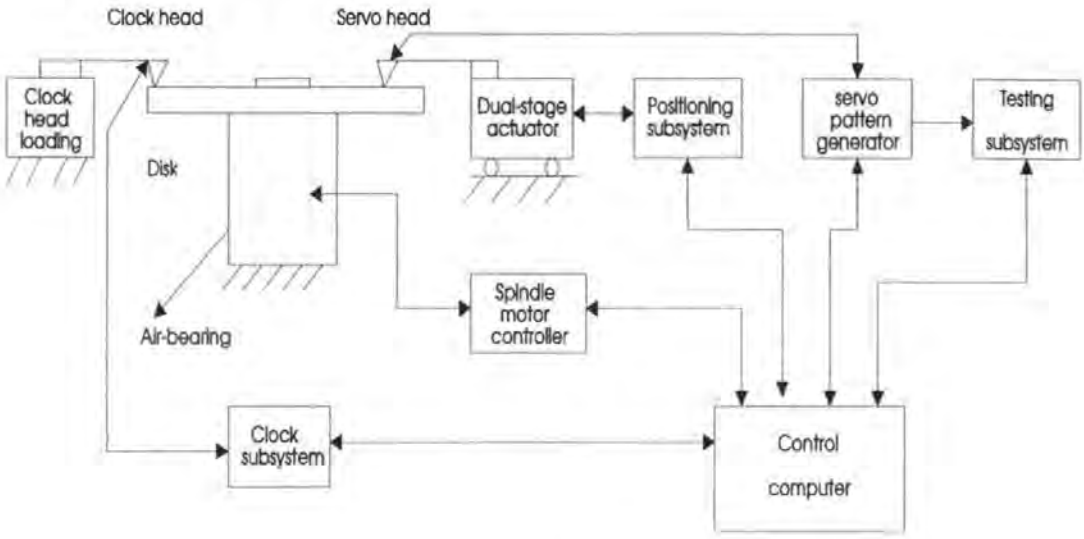

Figure 3.2 Block diagram of the submicron servo track writer system.

3.1.2.1 A head positioning subsystem for servowriter

In the servo track writer, the magnetic head must be positioned in any position on a disk. A two-dimension (x-y) is required. The positioning system used in the servo track writer is one which was developed by Dr. Darragh for his project [Darragh, 1994]. In the positioning system, two closed-loop digital servo feedback systems with x-y plane normal to the spindle is employed to move the head position to the target position with a error within a hundred nanometers. The head positioning subsystem comprises two optical diffraction sensors, two stepper motors and computer control system. The resolution of the positioning system in the x and y axes is 0.1 μm over a region of 45 mm. Its relative accuracy per 2 mm is greater than ± 0.05 μm [Darragh, 1994] [Speake, 1985]. In order to increase the positioning resolution, a PZ actuator (NLA-1.4×3×9 made by Tokin Ltd. in the Japan) was added in the positioning system as writing/reading submicron servo patterns in the experiment. It is possible to increase the accuracy to 0.01 μm and the resolution to 0.001 μm by using a laser interferometer measuring position.

3.1.2.2 The basic system of circumferential position

In this investigation, the angular position of the head on the disk is required when writing a servo pattern on the disk to line up every adjacent servo pattern radially. The basic circumferential position control system for a disk, or angular clock system, can employ an optical grating to achieve an angular output signal. But its accuracy (e.g. 0.0025°) is much lower than what is needed for this project (e.g. 0.00002°).

For this task, a sensor is used to supply fine resolution clock pulses that are synchronised to the angular position of the disk. This sensor is typically a stationary R/W head called a clock head (See Figure 3.3 and Figure 3.3 (a)). The special clock R/W head is placed at the outer diameter of the disk. After the R/W head writes the clock data on a round track called the clock track on the disk, the clock head can reproduce a series of highly accurate clock pulses. As the spindle motor speed varies due to random disturbances, the clock pulse follows the speed changes accordingly.

After writing the clock track, two tests immediately check clock track accuracy. One determines if the correct numbers of pulses have been produced and the other measures the timing gap between the last and first pulses on the clock track. If the clock track is perfect, this gap will equal the bit period. In this case of which the clock track is no perfect but acceptable, a condition called closure is achieved when the correct number of pulses has been written and the measured gap equals the bit period to within a specified accuracy, typically ± 10 - 15 ns. At a drive spindle of speed of 3600 rpm, the hard disk revolution period is 1/60 s and the required clock pulse position accuracy is ± 0.9×10^{-6} revolutions. Along the circumference of the disk, this corresponds to 0.26 μm at a radius of 45 mm.

An index mark is encoded in the clock track to indicate the start of the clock track. This index is used to synchronize the pattern generators at the start of each servo

track. This clock system's hardware and software can be seen in Appendix Hardware (J-1), (J-2) and (J-3) and Appendix Software A, respectively.

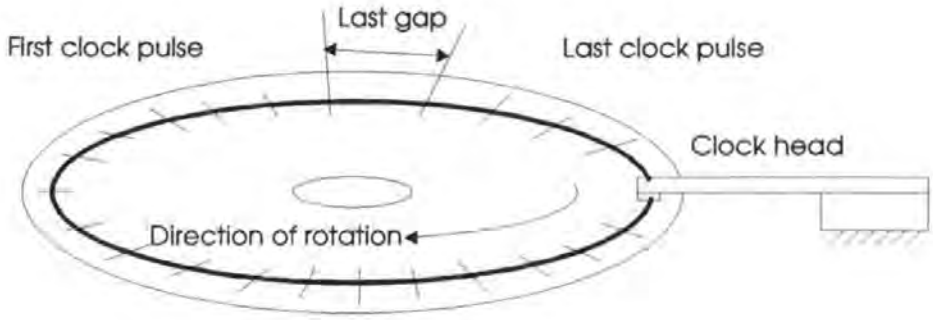

Figure 3.3 Schematic diagram of the angular clock subsystem.

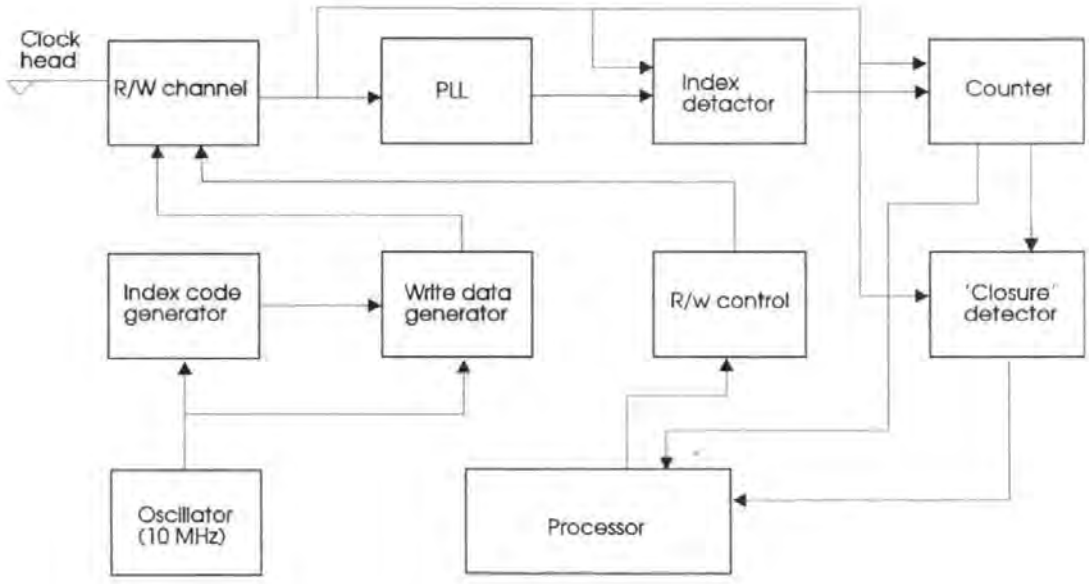

Figure 3.3 (a) Diagram of the circuit for the angular clock subsystem.

Clock track writing is difficult because spindle motors have a typical accuracy of only ± 0.1% of the specified spindle speed. At 3600 ± 3.6 rpm, for example, this amounts to a bit period tolerance of ± 16.6 μs, i.e. more than 1,000 times the required tolerance of ± 15 ns. This problem will be further discussed in Section 4.3.10.

3.1.2.3 Servo pattern generator

The pattern generator is usually programmable, but for servowriters with simple servo patterns it can be hardwired to write a limited number of servo codes. The pattern generator is a clock track counter that begins counting the 40-MHz PLL output clocks when the clock track index is received. At certain pre-programmed counts, the output of the pattern generator changes states to reverse the write current in the servo head. It is this sequence of transitions that makes up the servo codes. In the submicron servo track writer, the servo pattern generator triggered by the clock pulses and the index signal consists of a TMS320C50 DSP Starter Kit (DSK). The writing or editing of servo track and disk pattern is executed using the TMS32C50. Its software can be seen in Appendix Software B. A normal servo patterns waveform produced by the servo pattern generator is shown in Figure 3.4.

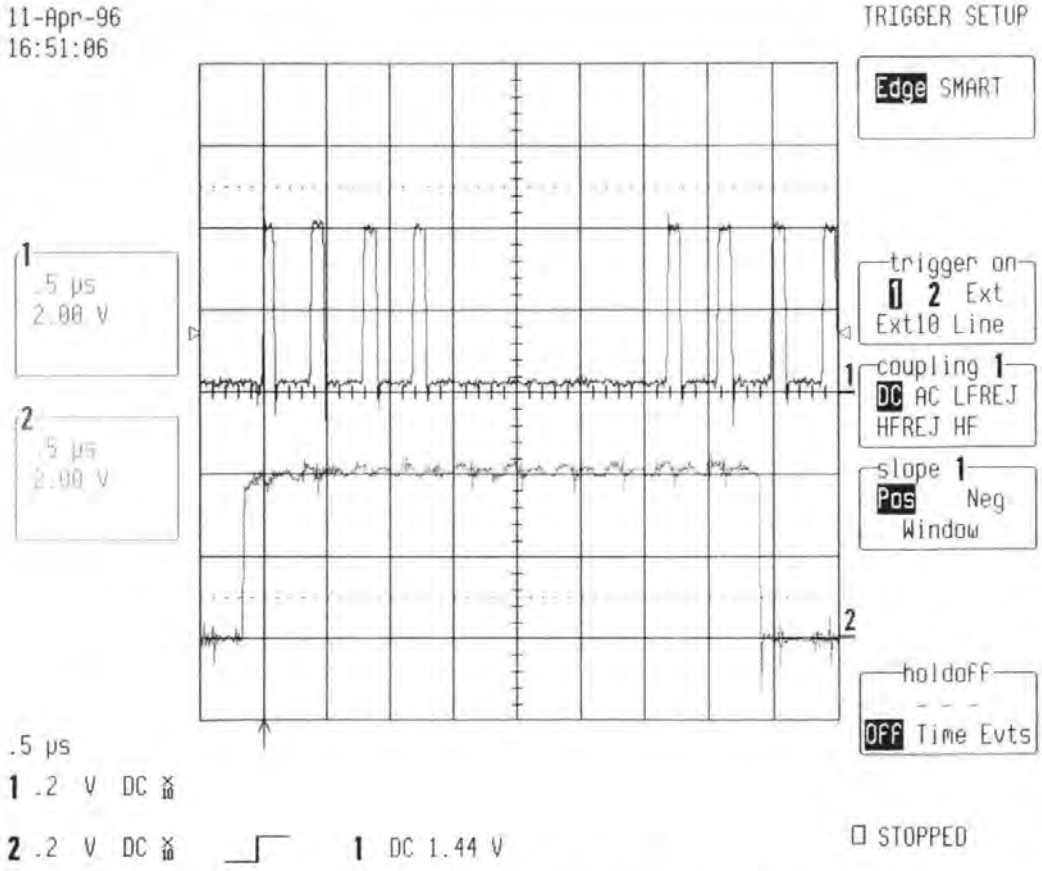

Figure 3.4 Waveform of the servo code signal generated by the DSK generator.

3.1.2.4 Servo pattern test

Writing servo patterns on a disk at exactly the correct locations does not guarantee a correctly-written disk. Because there are some defects on disks, the servo information was not recorded at those points. This becomes more serious, when the trackwidth is reduced to submicron size. The recording head may have been broken a shorted turn or other defect that prevented the servo pattern from being written on the disk.

Therefore the servowriter must check that each servo pattern bit has the correct amplitude and timing. Thus immediately after writing the information for a track, the servowriter's read/write head remains on track, reads back the information just written to the track and identifies incorrect, missing, or extra bits. This process of on-track verification is important to the high quality servo writing. After all servo patterns are written and passed, it is necessary to test: (a) servo pattern alignment in radial direction, (b) servo track width and (c) all servo pattern bits [Tan et al., 1991]. In the servo track writer, the test is simple and incorrect, missing, or extra bits are identified. Its circuit can be seen in the Appendix Hardware A.

3.1.2.5 Spindle motor speed control

The servo track writer is designed to write as circular a servo track as possible. The non-repeatable radial runout has to be as small as possible. The spindle system of the "Spin Stand" was used for this purpose. For the servo track writer, the disk is mounted on a spindle with an air bearing and the non-repeatable radial runout of the spindle and the disk is less than 0.1 μm. The spindle is driven by a 3 phase brushless motor and digitally-controlled electronic drive and can operate at speeds between 160 and 5400 rpm (160 rpm was set by adjusted the resistor at the PCB board of the spindle control

box in the experiment), and the resolution (Δv) and accuracy of the rotating speed are 0.01 rpm and ± 0.1 %. The disk is clamped firmly in place by a sprung rod which pulls the clamp face against the disk surface and down onto the spindle [Darragh, 1994] & [Speake, 1985].

The speed control of the disk is very important during clock writing and clock readback. If the speed varies too much during clock writing, the correct number of the clock pulse and good closure (there is an exact integral number of clock bits making up 1 circumference of the clock track) will not be obtained. The PLL that generates the system time base will go out of lock during read-back, if the speed varies too much. This will make the writing of good servo patterns impossible. The speed of the disk is controlled by comparing the motor Hall-effect sensors to the stable reference clock. For the servowriter, the reference is derived from a high-precision (six to seven significant digits) frequency source. The ± 0.1% accuracy of the speed is achieved.

The ± 0.1% accuracy of the speed is suitable during clock readback but not suitable during writing of the clock track without using a new clock-writing method as described in Section 4.3.10.

3.1.2.6 Adjustable skew angle unit

In this project, it is necessary to adjust both the skew of the head pole/gap with respect to a recorded track and the loading force. The head mounting unit developed by N. Darragh shown in page 35 of his Ph. D thesis [Darragh, 1994] is used to adjust the skew of head of the servo track writer. The head mounting unit provides z-height adjustment in the plane perpendicular to the disk to adjust the loading force and therefore, the flying height of the head. The dial gauge allows z-height adjustment to an accuracy of ± 12.7 μm. The bed onto which the head is attached can be rotated through

± 360° [Darragh, 1994]. In order to increase the rigidity of the head mounting unit, the vertical angle of the head is fixed in the experiment.

3.2 Read/Write Channel

3.2.1 Read/write channel for data

Figure 3.5 shows a schematic diagram of the data read/write channel developed by author, which is similar to one developed by N. Darragh [Darragh, 1994]. Recording data is generated in an 8165A programmable signal source. For an inductive write/read head a SSI 521R-6H read/write device was employed. In our design, the magnitude of write current is set externally using the adjustable resistor. The write drive and data generator are triggered by the "index pulse" created by clock angular system, so that it produces a write data enable signal that only writes a round. Drawings of the circuit and PCB board are in Appendix Hardware B.

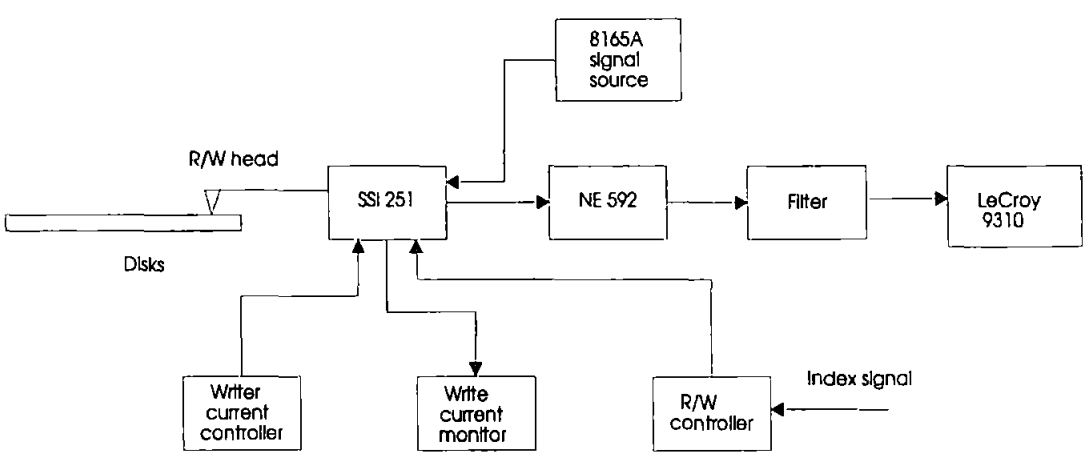

Figure 3.5 Schematic diagram of the data read/write channel.

Noise from the preamplifier is key since this noise will dominate the noise of following amplifiers. To minimize the noise, the technology in the design and development was used as following:

1. A special read amplifier (32R521R-6H specially designed as a preamplifier for HDD) with an input noise figure of only 0.5 nV/√Hz.

2. Mounting the amplifier as closely as possible to the read head (such as 20 mm in the design) to reduce external pick up and transmission line effect in the interconnection.

3. Substantial grounding for every part to reduce ground noise and transmission line effect in the interconnection.

4. Connection of a 10 pF capacitor between the outputs of the preamplifier to reduce high frequency noise.

Following the read amplifier a video amplifier, NE592, was employed as a second amplification stage, NE592 provides wide-band gain up to 50 MHz.

The output of the read amplifier of NE592 is observed at a digital storage oscilloscope (LeCroy 9310). The oscilloscope can sample at up to 1 G Sample/sec and store up to 50,000 consecutive samples. The output is also connected to a HP 4195A network/spectrum analyzer to measure spectrum of the readout.

3.2.2 The MR head read/write channel for servo

The MR head Read/Write Channel is similar to read/write channel for data (Drawings of the circuit and PCB board are in Appendix Hardware C, D and E). However, there are some differences between them, e.g.

1) A Read/Write device (type SSI32R1510R made by the Silicon Systems Ltd in USA) for MR head replaces the SSI 521;

2) The servo pattern generator in the servo track writer replaces the 8165A signal source.

3) The servo pattern generator has the function of controlling read/write operation of the MR head.

4) The cut-off frequency (designed at 200 kHz) of the low-pass fitter in the servo channel is much lower than that in the data channel. This is because the servo frequency is lower than the data frequency.

It should be noted that electrostatic protection must be used during operating a MR head because the electrostatic can easily break the MR head.

3.3 Other experiments

3.3.1 A measuring dynamic micron movement system

In order to measure the dynamic movement of the head or actuator, a micron movement measuring system was developed as shown in Figure 3.6 (a), (b) and (c). Figure 3.6 (a) is a photograph of the measuring system. In Figure 3.6 (b), the optical to electrical transducer was an integrated photo sensor. This transducer, known as a TSL214, consists of 64 charge-mode pixels arranged in a 64×1 linear array [Texas, 1991]. The mirror A was an adjustable plane mirror and the mirror B was a low mass mirror weighing less than 2 mg (a range of mirrors was used with weights between 1.0 mg and 2.0 mg). The laser was a He-Ne laser.

If the rotary bar is rigid and can freely rotate, referring to Figure 3.6 (b), $L_1 / L_2 = S / x_b$, so the movement, x_b, of the head at the b point on the mirror B is

$$x_b = \frac{S \cdot L_2}{L_1}. \tag{3-1}$$

where, S is the distance that the laser spot moves on the photo detector, L_1 is the distance between the reflecting light point b on the mirror B and the photo detectors, L_2 is the distance between the point b and the fixed end of the bar.

It should be noted that Eq. (3-1) is not correct when the rotary bar is a PZ bimorph and the end of the bimorph is fixed. In this case the bimorph bar is not rigid but bends. According to reference [Riley et al., 1989], we have the final angle (θ) between the end of the bar and the original bar axis position is,

$$\theta = \frac{QL_2^3}{6EJ} \tag{3-1a}$$

where Q is the distributed force, L_2 is the bar length, E is the Young's modulus of elasticity and J is the moment of inertia of the cross section.

In Figure 3.6 (b), the deflection (x_b),

$$x_b = \frac{QL_2^4}{8EJ} \tag{3-1b}$$

On the other hand, we have $$\sin\alpha = \frac{x_b}{L_2} \tag{3-1c}$$

When $\alpha \approx 0$, $$\alpha \approx \frac{x_b}{L_2} \tag{3-1d}$$

According to Eq. (3-1a), (3-1b) and (3-1d), we have, $\frac{\theta}{\alpha} = \frac{4}{3}$.

That is, Eq. (3-1) becomes,

$$x_b = \frac{3SL_2}{4L_1} \tag{3-1e}$$

In the 64 photo sensors of the TSL 214 detector, each pixel measures 120 μm × 70 μm with a 125 μm centre-to-centre spacing. The operation is simplified by internal logic requiring only clock-pulse and start-integration-pulse signals. On completion of the integration period, the change contained in each pixel is transferred in turn to the sense node under the control of the clock (CLK) and serial-input signals. The output-signal is serial. Each output period occupies 64 clock bits which correlate with the 64 photo

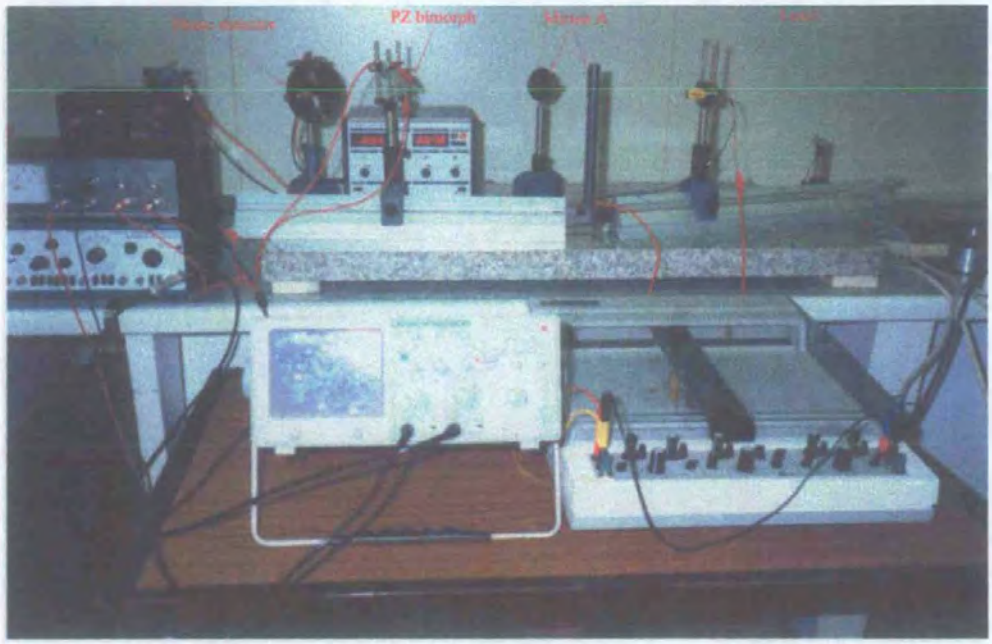

Figure 3.6(a) A photograph of the movement measuring system.

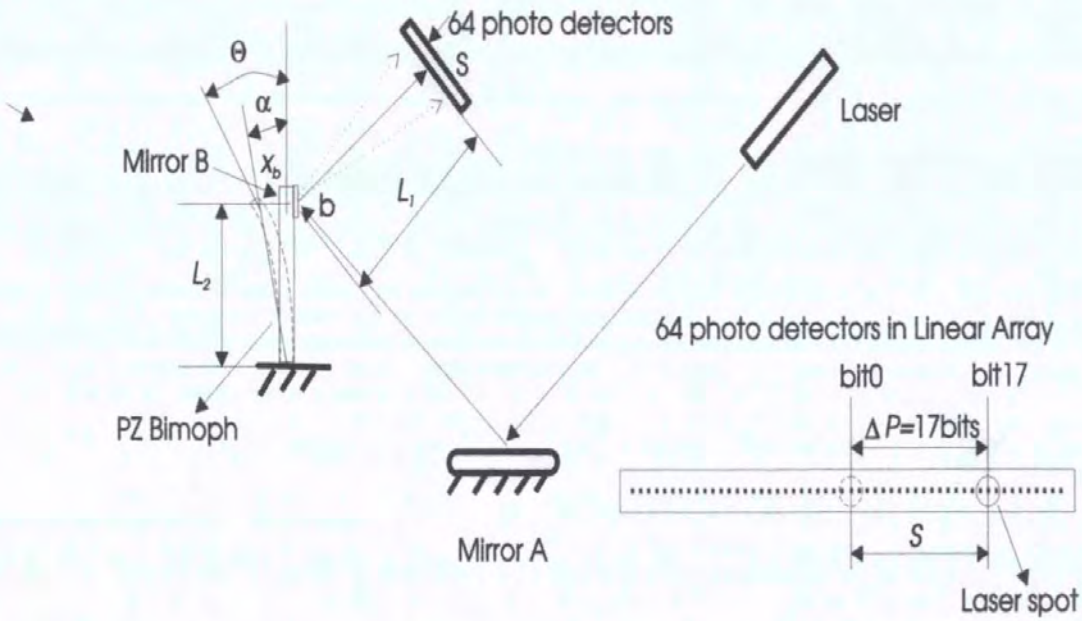

Figure 3.6 (b) Diagram of the measuring system (not to scale).

sensors. High-level voltage, '1' bits, in the output signal means that the spot of the laser is on the corresponding photo sensors. Deflection of the bimorph causes the laser beam to be reflected by a different angle and indicated by a change of position of '1' bit pattern in the output of the 64 bit photo detector, which is shown in the Figure 3. 6 (b).

Therefore, we have

$$S = \Delta P \ 125 \ \mu m \tag{3-2}$$

$$x_b = 125 \times \frac{3}{4} \Delta P \times \frac{L_2}{L_1} \tag{3-3}$$

$$V_b = \frac{3 \Delta P L_2}{4 T_s L_1} \tag{3-4}$$

where, V_b is the velocity of the point b on the mirror B, T_s is sampling time or 64 T_c (T_c is the clock period) and ΔP is the number of '1' bits moved.

This measuring system was tested by comparison with the value measured by the system and the value measured by the BH-Z microscope with calibrated television image when the PZ actuator was supplied with a stable voltage. The result is 15% error when measured small movement (less than 250 μm). It should be noted that the system is suitable for measuring small movement(less than 250 μm).

Figure 3.6 (c) shows the measuring circuit of the equipment.

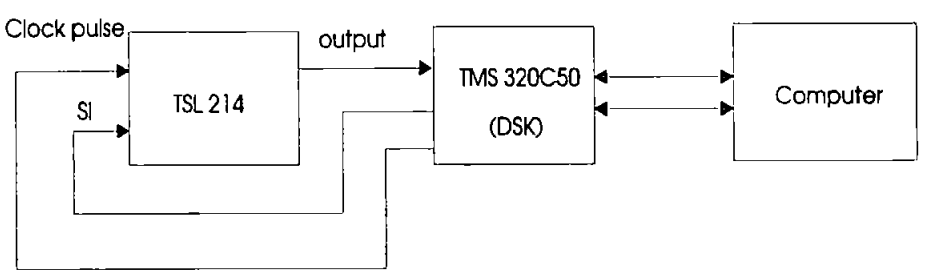

Figure 3.6 (c) The circuit for measuring the head movement system.

Its software can be seen in Appendix Software C.

The substrate of the mirror *B* is a silicon disk of thickness 150 μm. The reflection layer is a sputtered thin film of chromium with thickness of 1 μm. A 40 nm gold film is used as a protection layer on the top of the mirror. When the size of this mirror is 1.5 × 2 mm, the weight of the mirror is only 1.0 mg, and can therefore assure the measuring system of the desired accuracy.

Figure 3.7 shows the real-time movement curve of a PZ bimorph actuator (dimension 45×3×1 mm, the drive voltage 0 – 215 V) measured by the above measuring system. This shows the time constant of the actuator to be approximately 3.4` ms.

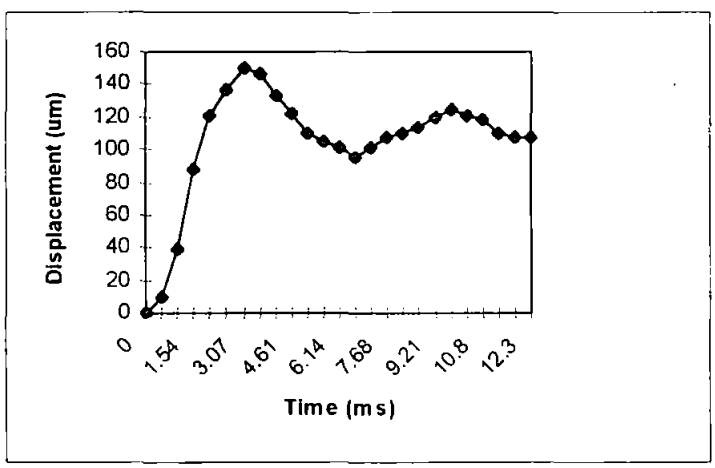

Figure 3.7 A real-time movement curve of a PZ actuator

3.3.2. Piezoelectric drive source

The block diagram and the circuit of the close-loop analogue voltage-drive circuit developed for a PZ actuator is given in Figure 3.8. The voltage on the actuator is compared with an input servo signal in the regulator stage of the amplifier. The actuator is then charged or discharged by variable amounts as required.

The PZ actuator is essentially a capacitive device, and therefore discharge time is long when the actuator is operated at a high frequency. In order to reduce the discharge

time, a pull down circuit is employed. This will be described and discussed in more detail in Chapter Five.

The electronic circuit can be seen in Appendix Hardware F.

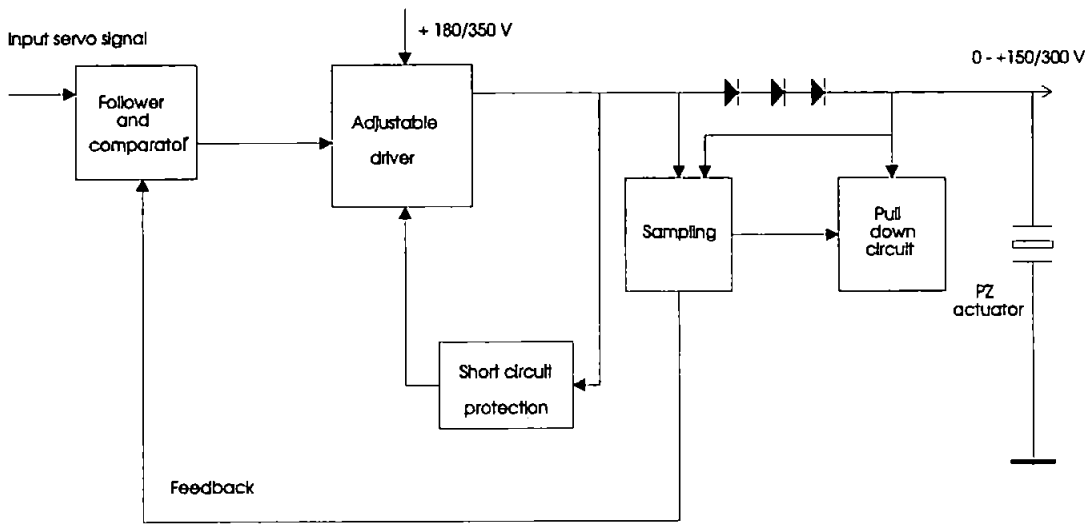

Figure 3.8 Diagram of the driver circuit for PZ actuator.

3.3.3 DSK development system

A TMS320C50 DSP Starter Kit (DSK) made by Texas Instruments, Figure 3.9, is used to design and develop the Hardware and Software of the above application systems. The DSK is a simple and effective developing tool for TMS320C50 DSP. The DSK has a TMS320C50 on board to allow full-speed verification of the TMS320C50 code. The DSK also provides the freedom to create dedicated software to run on the DSK board, allows the building of new boards, or to expand the system in many ways for different application systems.

The DSK software mainly consists of a powerful assembler and debugger. The DSK's assembler and debugger are software interfaces that help to develop, test, and refine DSK assembly language programs. The supplied debugger is Windows-oriented, which simplifies code development and debugging capabilities. The debugging is capable

of loading and executing code with single-step, breakpoint, and run-time halt capabilities [User's Guide, 1994].

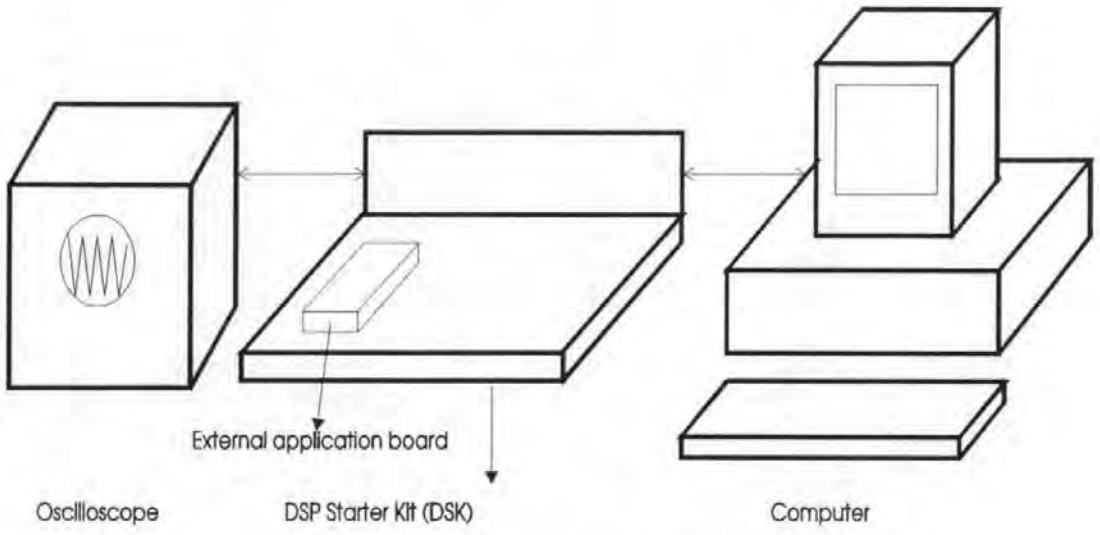

Figure 3.9 Schematic diagram of the DSK development system.

3.4 Main measuring techniques and methods

3.4.1 Magnetic force microscopy

Measurements of magnetic features, including the servo pattern, become increasingly difficult as the track densities of storage media increase. As a result, extremely high-resolution magnetic imaging is becoming a requirement for the magnetic recording research [Bond, 1993].

Magnetic force microscopes (MFM) bring the power of scanning probe microscopy (SPM) [Rugar, 1990] [Sarid, 1991] to a convenient and cost-effective imaging tool. Figure 3.10 is a schematic diagram of a magnetic force microscope. In the Figure 3.10, the magnetic tip scans across the surface of the sample and is ten or hundreds of nanometers above the sample. To experience a spatially varying force from the magnetic field produced by the recorded media. The magnetic gradients exert a force on the tip's magnetic moment, and monitoring the tip/cantilever response gives a

magnetic-force image. The magnetic-force image of sample's surface in x, y can be obtained when the piezoelectric scanner move in x, y direction. The magnetic tip is very small (a typical diameter of 50 nm) is magnetically sensitised by sputter coating with a ferromagnetic material.

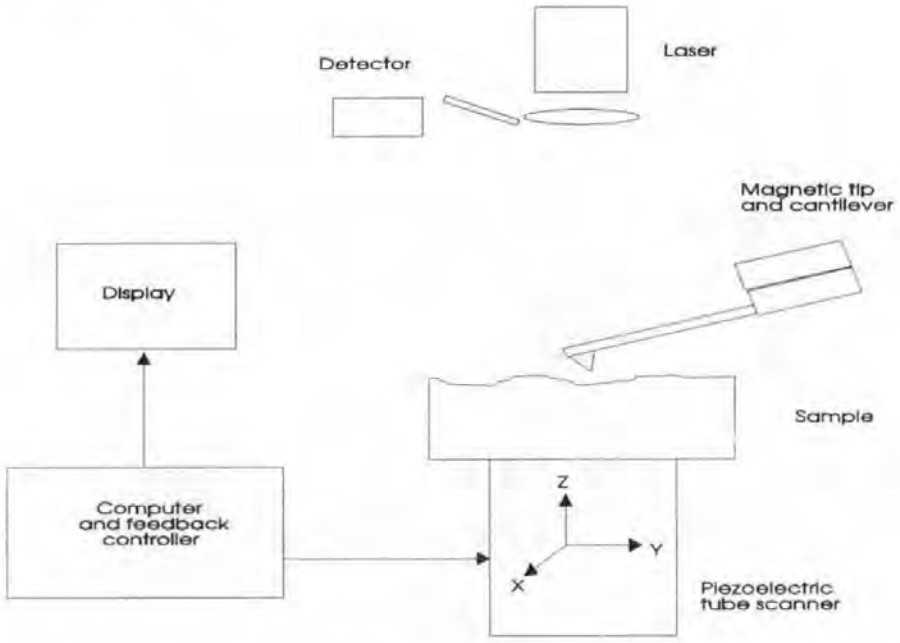

Figure 3.10 Schematic diagram of a magnetic force microscope [Bond, 1993].

Figure 2.10 is a MFM image of servo patterns recorded in the new mode on the rigid disk (the image was produced by Prof. Clegg and the servo patterns were recorded on the disk by the author).

3.4.2 Observation of servo pattern based on Bitter pattern techniques

In the Bitter pattern method, magnetised media are coated with a suspension of very fine magnetic particles which are attracted to regions of nonuniform field produced by the magnetisation pattern in the medium. The resulting patterns of particles are then viewed under a microscope. This technique was first used to observe domain walls in ferromagnetic metals [Bitter, 1931] and recorded transition on disk [Mee, 1989]. Both dimension and relative position of servo patterns on a disk can also be viewed.

Bitter methods are widely used because of their convenience. Although they give a useful qualitative picture of magnetization patterns, quantitative information is lacking. Water based ferrofluid (EMC 308) was used in this project experiment, to observe the size and position of the servo patterns. The average particle size, saturation magnetisation and resolution of EMC 308 are about 10 nm, 60 gauss and 0.05 μm respectively. EMC 308 used undiluted then diluted with zero, one, two, three times etc. of equal volume of distilled water. The solution was applied to the specimen by means of a Q-tip. At some dilution, depending upon the servo pattern, the best resolution will be achieved. In order to accelerate drying a heat lamp may be used. A microscope or SEM with sufficient magnification was used to observe the servo patterns. In the project, a BH-Z microscope with magnified television image was used to observe the bit patterns on various disks with Ferrofluid. The Ferrofluid was type EMC 308 diluted three times. Photograph of the servo patterns is shown in Figure 3.11 made by author at the Electron Microscopy Centre in University of Plymouth. It can be clearly seen the servo patterns on the disk.

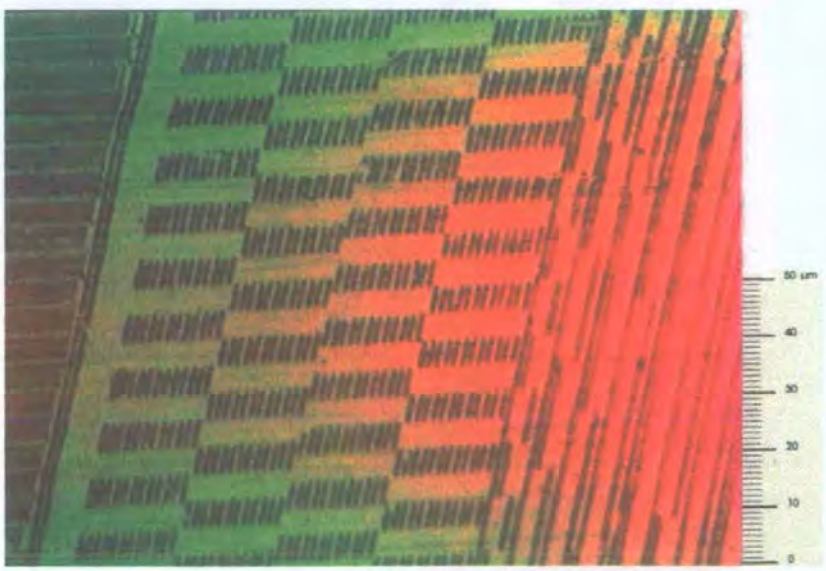

→Track direction

Figure 3.11 A servo pattern image based on Bitter pattern techniques.

3.4.3 Ultra-high speed microscope

An ultra-high speed microscope consists of two main subsystems: an ultra-high speed colour video camera with signal processing unit (type Kodak HS) loaned by the EPSRC Ruthersord Lab. and a BH-Z microscope given a resolution up to 0.5 μm (see Fig. 3.12). In the system shown in Figure 3.12, the ultra-high speed video camera was fixed in the normal microscope eye piece position using a C-mount adapter. Optical adjusting is needed, to ensure good quality pictures are obtained. For the ultra-high speed colour video camera with signal processing unit, several settings cover the range from 200 frames per second (f.p.s.) to 4500 f.p.s. with a full size picture, and up to 40,000 f.p.s. with a reduced size picture. The pictures are sampled and stored in the RAM of the system, then stored (recorded) on a magnetic tape if necessary. The amount of RAM allows a continuous series of 3000 pictures to be stored. These cameras are supplied complete with lighting and the facility to download pictures to VHS video and the RAM of the system [Kodak, 1991].

In the project, the system was employed to measure real-time movement of the magnetic head and the actuator using the position change of the head in a series of pictures. Figure 3.13 is a series of pictures of a moving head, in which the sample rate was 1000 f.p.s. In the figure 3.13, the real-time movement of the head is indicated by the movement of point (x, y) on the head in a series of pictures. According to the values of x and y, the curve of the movement can be drawn and the movement can be calculated.

3.4.4 Thin film deposition by sputtering

C/CoCrTa/Cr/CoCrTa/Cr multilayer films with different thickness were deposited on disks by rf-planar diode sputtering or rf-planar magnetron sputtering in a Nordiko

Figure 3.12 A photograph of the ultra-high speed microscope.

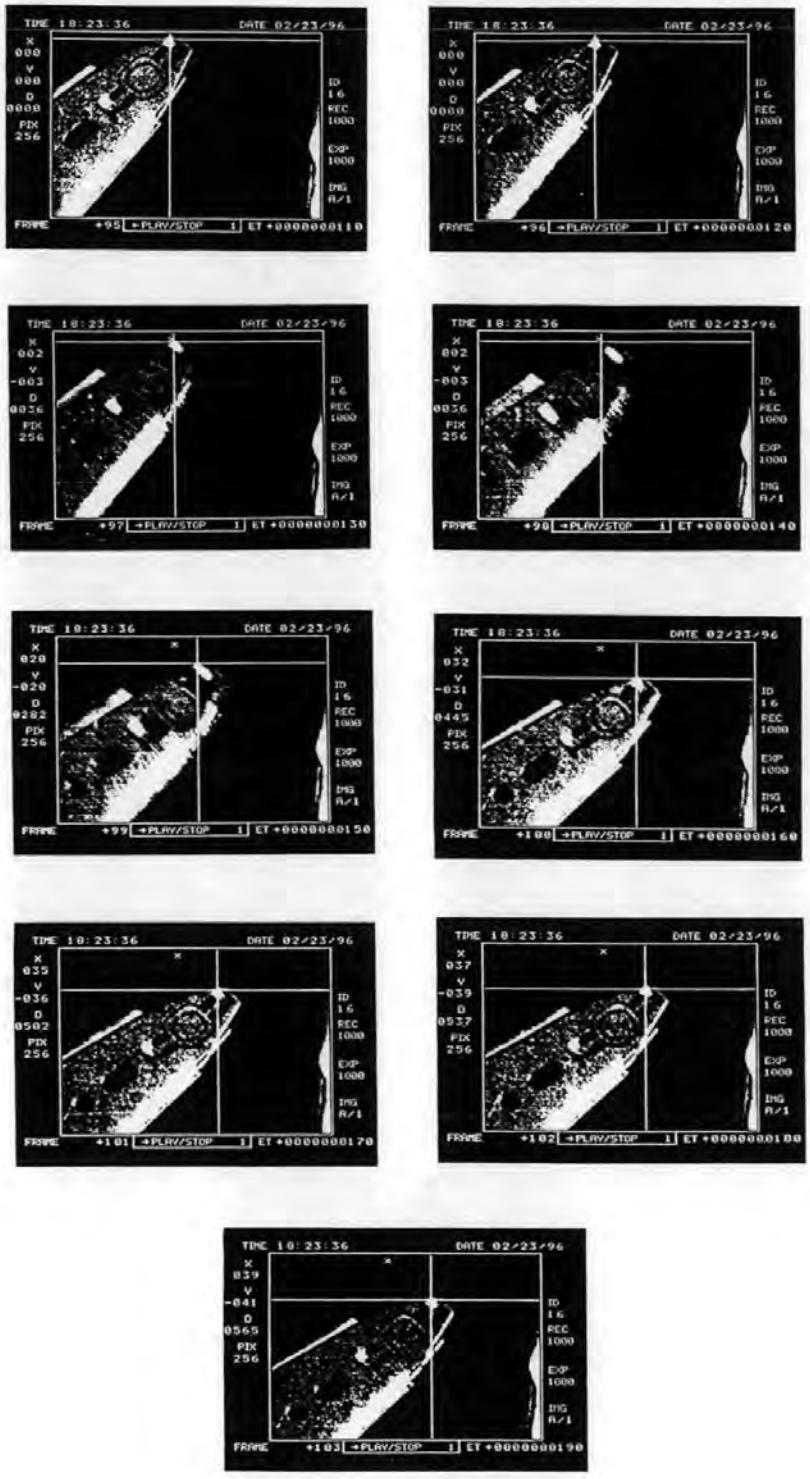

Figure 3.13 A continuous series of pictures showing a head moving.

NM2000 rf-sputtering unit to make the disk with data and servo layer for the study of the buried servo used in the project. This sputtering unit consists of a vacuum chamber, target and substrate electrode, a vacuum pump system and an rf power supply as well as its impedance matching network [Nordiko, 1987]. In rf-sputtering, the materials of the target are passed into the vapour phase by ion bombardment. These ions are provided by the inert gas (such as argon in the range of about 10×10^{-3} Torr), which is introduced to the sputtering chamber to form a plasma with the aid of an r.f power supply, once the chamber is pumped down to a pressures as low as 10^{-7} Torr. The power supply maintains the target at a negative potential (1500~2500V) relative to the plasma. The argon ions are accelerated with sufficient energy resulting in the ejection of target materials from the target surface. The substrate is suitably positioned to intercept these atoms. The films, which have similar composition with target material, are formed on the substrate surface. During the rf-sputtering, A substrate bias can be applied and the magnetron sputtering can be used to increase deposition rate of thin films [Mee, 1989] [Nordiko, 1987].

3.4.5 Vibrating Sample Magnetometer

The Vibrating Sample Magnetometer (VSM) is a commonly used instrument for the measurement of M-H loops and the magnetic properties of recording media, e.g. magnetization curves and remanence curves of recording media. Figure 3.14 is a schematic drawing of the VSM used in this work. It is a commercial instrument (Type is the V.S.M. 2001 made by Aerosonic Ltd.)

A magnetic field of up to 7,000 Oe is produced by an electromagnet and is applied to the sample. The sample is suspended on a nonmagnetic rod which vibrates perpendicular to the magnetic field at 60 Hz. When the sample vibrates, the pick-up coils

produce a voltage which is proportional to the magnetization of the sample. The voltage is amplified by a programmable amplifier. The computer samples the signal (A/D) and calculates the results [Aerosonic, 1985].

The VSM was employed to measure the magnetic performances of the disk which was made for the project (i.e. M-H loops, H_c and M_r).

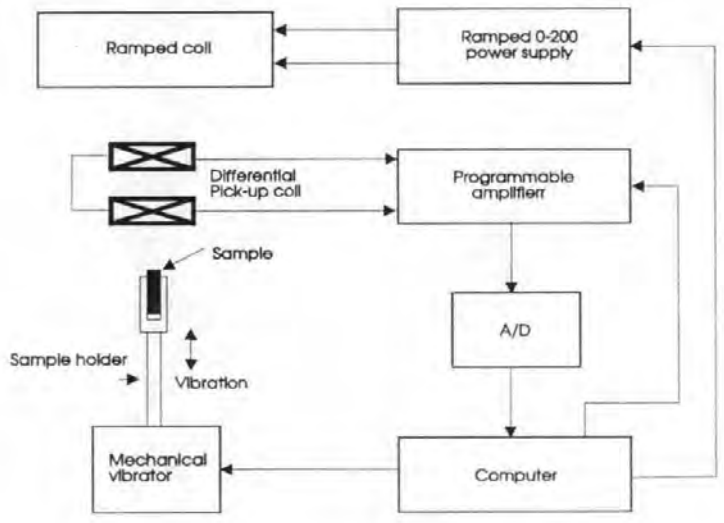

Figure 3.14 Schematic diagram of a vibrating sample magnetometer.

Chapter Four

Position Sensor System

4.1 Introduction

IBM demonstrated the technology of a magnetic recording density of 1 Gb/in^2 in 1989. They achieved a high signal to noise ratio (S/N) of about 20 dB including head, media and electronics in the data channel. Thereafter, a S/N ratio of 20 dB has been regarded as a basic requirement for high density magnetic recording, even for ultra high density magnetic recording up to 10 Gb/In^2 or beyond.

It is well known that the Equation for calculating the S/N is

$$S/N = \frac{A}{\sqrt{N_0 f}} \tag{4-1}$$

where, A is the 0 - peak value N_0 is the noise-frequency density, and f is the signal frequency.

Assuming that the f_d (frequency of data) is five times of the f_s (frequency of servo), then $(S/N)_s = \sqrt{5}(S/N)_d = 27dB$. However, the S/N of 27 dB which is used in the current embedded servo method for almost all HDD products, is not adequate. This is because the S/N of 27 dB which is the resolution of the servo (position) signal is equal to or less than 4.5%, thus the allowable servo error is less than 5 - 10 % [Mee, 1989]. It is clear that the quality of a servo signal with S/N of 27 dB is not good enough, even though other factors that may affect the quality of servo signal are not considered here.

Furthermore, Mee has indicated that the positioning of the head on the track for trackwidths of a few μm will require improvement. First, due to poor recording uniformity across very narrow track heads, the positioning accuracy requirements will exceed those just due to scaling. Second, asymmetries in MR heads will deteriorate the accuracy of the position error signals (PES) [Mee, 1996].

On longitudinally-magnetised magnetic rigid disks, the asymmetrical off-track response of the longitudinal read MR head is well-known. The asymmetrical off-track readout of an MR head on a longitudinal disk is shown in Figure 4.1 [Tsang et al., 1990 [1]]. Similar readouts for a perpendicular rigid disk, which were experimentally measured, are shown in Figure 4.2. The data and servo patterns are magnetized along the circumferential direction in a conventional rigid disk. When data trackwidth is reduced, the effective servo head width and the S/N of the servo signal are reduced. Therefore conventional servo heads suffer from low S/N and poor linearity of the PES for longitudinal and perpendicular rigid disks, as the trackwidth is reduced to submicron size.

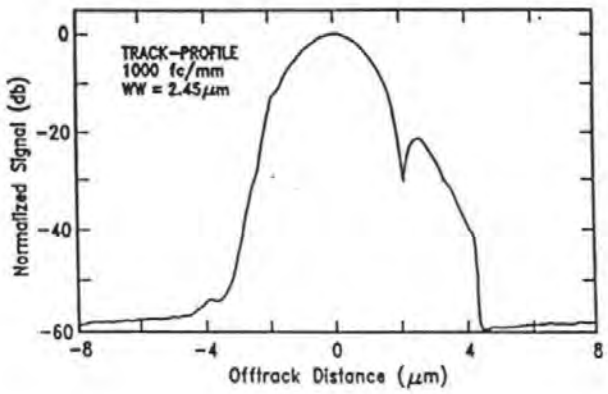

Figure 4.1 Off-track readout by the MR head in the IBM gigabit experiment.

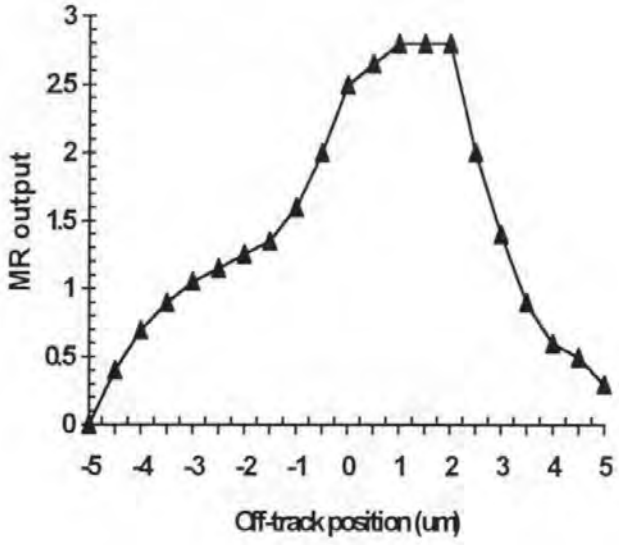

Figure 4.2 Off-track readout by an MR head on a perpendicular rigid disk.

According to the factors stated above, it is, however, difficult to use the conventional magnetic servo methods in a submicron-track servo for magnetic disks.

Two new servo methods will be discussed in more detail in the following sections, including the principles, the designs and the experimental results as well as some further discussions.

4.2. Principle of the new servo method

4.2.1 New servo methods for longitudinal media and perpendicular media

When trackwidth is reduced to submicron size, the main problems in the conventional servo method are (1) the readout will be reduced and (2) the asymmetries in MR heads will reduce the accuracy of the position error signals. For these reasons, the

key factor is the servo head width, which has to be reduced to submicron size when the track width is reduced to submicron size.

In order to overcome the above problems, two new servo methods are designed by using the new recording modes which are presented in Chapter Two. These new methods are shown in Figure 4.3 for longitudinal media and in Figure 4.4 for perpendicular media. The servo patterns in these new position sensors are magnetized along the radial direction by a transverse writing head which is aligned at a right angle to the normal data head. Servo signals are reproduced by a MR head which is also at a right angle to the data head.

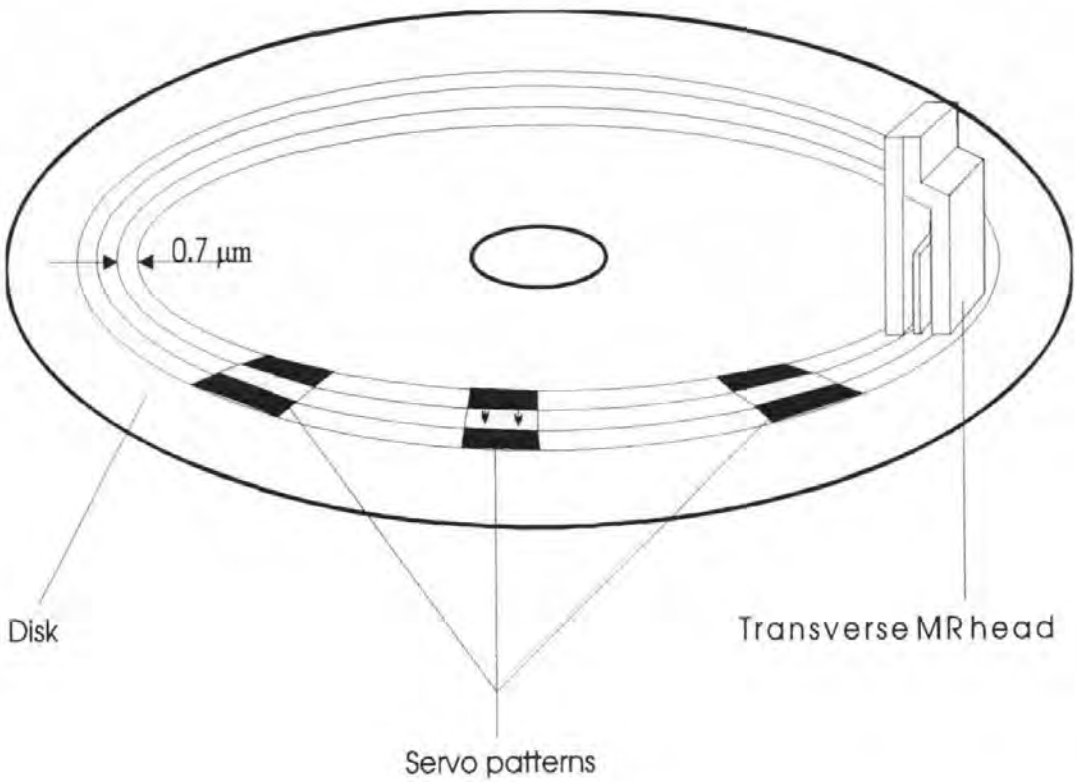

Figure 4.3 Schematic diagram of the new method using transverse MR head on longitudinal rigid disk.

4.2.1.1 Formatting or writing the servo pattern

In the recording method the data track pitch is equal to the servo pattern bit width (w_s) measured in the radial direction. The w_s is defined by the gap width (g_w) of the transverse write head and the position difference of the servowriting head between the adjacent writes in the radial direction ($\Delta R = R_t - R_{t-1}$) as contacting recording. It is found that

$$w_s = g_w \qquad g_w < \Delta R$$

$$w_s = \Delta R \qquad g_w > \Delta R \tag{4-2}$$

The bit length (L_s) of a servo pattern in the circumferential direction is defined as:

$$L_s = V_s \times t \tag{4-3}$$

where V_s is the speed of moving media and t is the pulse width of writing current.

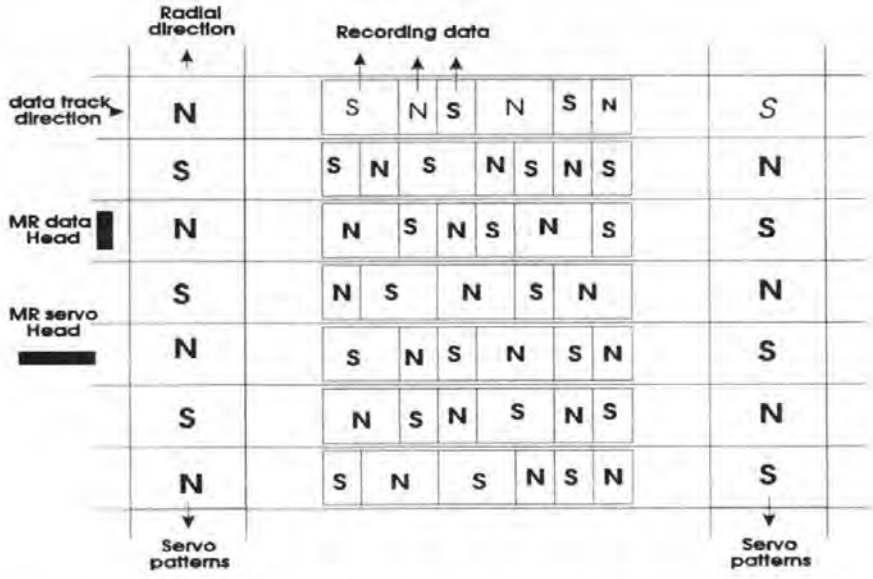

Figure 4.4 Schematic diagram of the new servo method on perpendicular rigid disks

Here, side writing phenomena is along the circumference of the circle. Hence it has no effect on the quality of the servo pattern in the radial direction in this new method for the detected head position.

4.2.1.2 Reproduced PES signal

Figure 4.5 (a), (b) and (c) shows a simplified model of the reproducing process using the transverse read MR head on the longitudinal media. If the magnetization distribution in a servo pattern is assumed to be uniform, the side writing phenomena is negligible and the MR head is uniform and symmetrical, the output (V) of the MR head when passing over a single servo pattern at different points can be approximated by equation (4-4).

$$V = V_{p,\max}\frac{z}{L_{MR}}\left(\frac{2x}{W_s}-1\right) \qquad \text{when } 0 < z < L_{MR},\ 0 < x < w_s$$

$$V = V_{p,\max}\left(\frac{2x}{w_s}-1\right) \qquad \text{when } L_{MR} < z < L_s,\ 0 < x < w_s$$

$$V = V_{p,\max}\left(1-\frac{z-L_s}{L_{MR}}\right)\left(\frac{2x}{w_s}-1\right) \qquad \text{when } L_s < z < (L_s + L_{MR}),\ 0 < x < w_s \qquad (4\text{-}4)$$

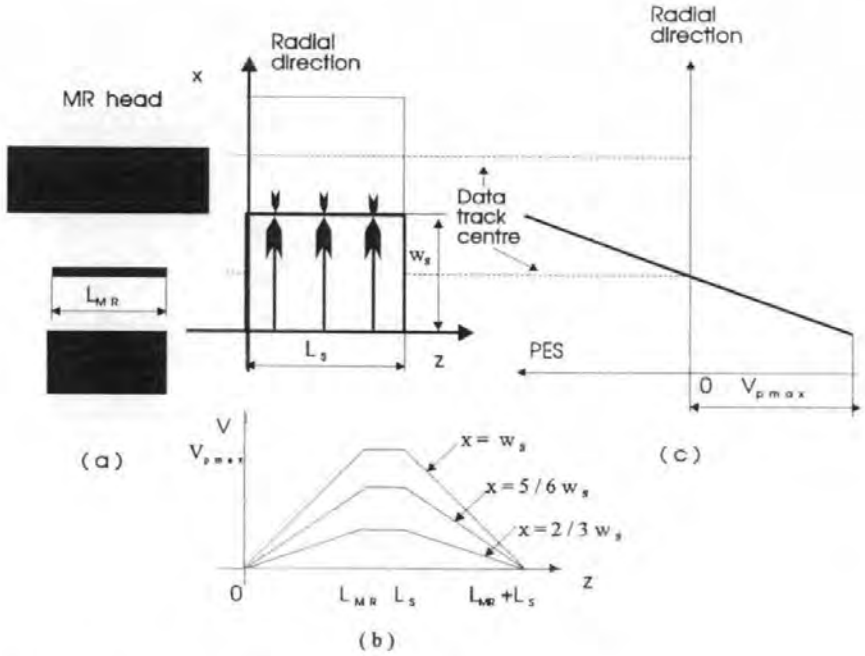

Figure 4.5 A simplified model for the reproducing process using transverse read MR head on longitudinal rigid disks.

where $V_{p,\max}$ is the maximum peak voltage reproduced by the MR head when it aligns with the track edge of a servo pattern, L_{MR} is the trackwidth of the MR head, w_s is the servo pattern bit width, L_s is the servo pattern bit length, x and z are the position coordinates of the MR head with reference to the right tip of the MR stripe. The origin of the coordinate system, as shown in Figure 4.5 (a), is located at the lower left corner of a servo pattern.

The output of the MR head calculated by Equation (4-3) when the MR head is crossing a servo pattern along the longitudinal direction at different off-track displacement is shown in Figure 4.5 (b), which also shows the output of the transverse MR head reaches a maximum V_p when the whole MR head is on the top of a servo pattern. Such a maximum output depends on the off-track displacement of the MR head. Therefore, the envelope curve of V_p at different x, which is shown in Figure 4.5 (c), can be used as a position error signal (PES).

Figure 4.6 (a), (b) and (c) show a simplified model of the reproducing process using the transverse read MR head on the perpendicular media in the new method. In the ideal case, the readout of the MR head may be expressed by equation (4-5).

$$V = V_{p,\max}\frac{z}{L_{MR}}\left(\frac{2(x-nw_s)}{w_s}-1\right), \qquad \text{when} \quad 0 < z < L_{MR},\ 2(n-1) < \frac{x}{w_s} < 2n-1$$

$$V = V_{p,\max}\left(\frac{2(x-nw_s)}{w_s}-1\right), \qquad \text{when } L_{MR} < z < L_s,\ 2(n-1) < \frac{x}{w_s} < 2n-1$$

$$V = V_{p,\max}\left(1-\frac{z-L_s}{L_{MR}}\right)\left(\frac{2(x-nw_s)}{w_s}-1\right), \qquad \text{when } L_s < z < L_{MR}+L_s,\ 2(n-1) < \frac{x}{w_s} < 2n-1$$

$$V = V_{p,\max}\frac{z}{L_{MR}}\left(1-\frac{2(x-(n+1)w_s)}{w_s}\right), \qquad \text{when} < \frac{x}{w_s} < 2n.$$

$$V = V_{p,\max}\left(1-\frac{2(x-(n+1)w_s)}{w_s}\right), \qquad \text{when } L_{MR} < z < L_s,\ 2n-1 < \frac{x}{w_s} < 2n$$

$$V = V_{p.\max}\left(1-\frac{z-L_s}{L_{MR}}\right)\left(1-\frac{2(x-(n+1)w_s)}{w_s}\right), \qquad \text{when } L_C<x<W_{MR}+L_C,\ 2n-1<\frac{z}{L_R}<2n \tag{4-5}$$

where $V_{p,max}$ is the maximum peak voltage reproduced by the MR head when it passes the centre of a servo pattern, L_{MR} is the length of the MR head, w_s is the servo pattern bit width, L_s is the servo pattern bit length, n is data track number and x direction is along the radius of the disk. The right tip of the MR head is the reference point of (x, z).

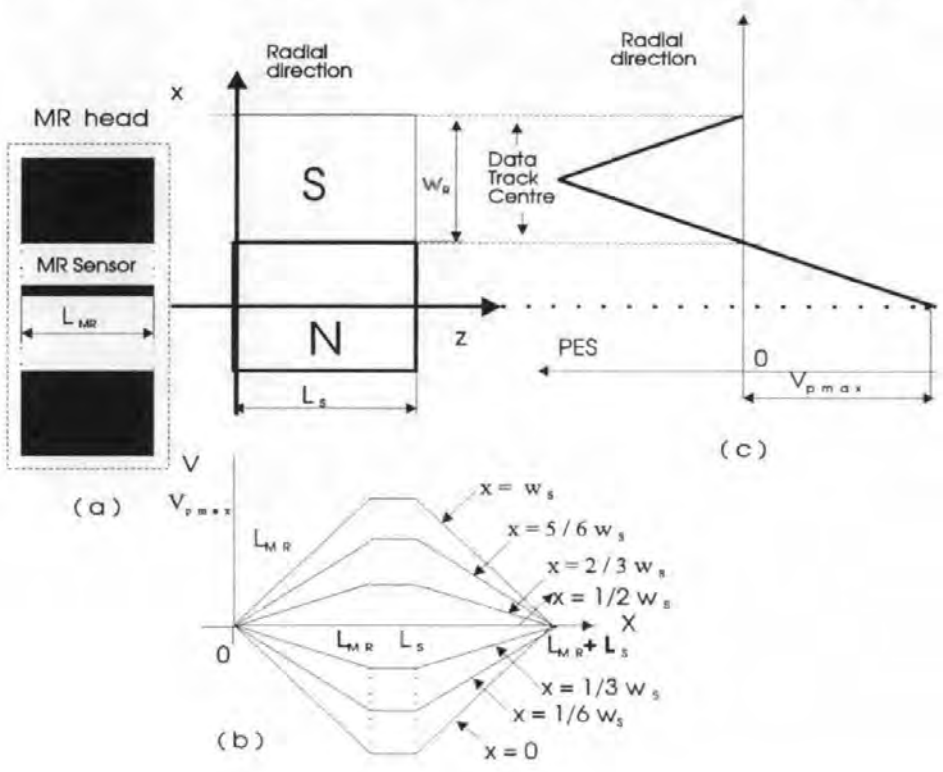

Figure 4.6 A simplified model for the reproducing process using a transverse read MR head on perpendicular rigid disks.

The readout of the MR head calculated by equation (4-5) as the MR head crosses a servo pattern along the z axis direction at different off track displacements in the x direction is shown in Figure 4.6 (b). It shows the readout of the transverse MR head reaches a maximum V_p in the centre of a servo pattern measured along the x axis

direction. Such a maximum depends on the off-track displacement of the MR head. Therefore, the envelope curve of V_p at different x, which is shown in Figure 4.6 (c), can be used as the PES. The points where the PES is equal to zero are used to indicate the data track centre.

4.2.1.3 Advantages of the new servo method

The obvious advantage of these new servo methods is that the desired output of the servo head is no longer affected by the data trackwidth. Furthermore, the asymmetrical off-track response, which is typical for longitudinal read MR heads [Yen, 1982], has no effect on the accuracy of the PES signal (for more detail see section 4.3.3). Therefore, such a transverse read MR servo head can reproduce high quality PES for a submicron track servo in longitudinal and perpendicular media recording.

4.2.2 New servo method based on the servo layer

In the above methods, the servo signal is no longer continuous. Therefore, for small disks (i.e. 1.3") these servo systems may have narrower bandwidth, poorer transient response, and may be highly sensitive to variations and the medium defects as the trackwidth is reduced to submicron size.

[Haynes, 1981] used a "buried servo" to obtain a positioning system on 50 μm trackwidth, in which servo and data can share a media surface area by using the surface for data only and deeper positions for servo only. In our studies, the medium of the disk consists of a top data layer, a middle 'isolation' layer and a bottom servo layer as shown in Figure 4.7. The data layer is exclusively for data bits and magnetized along the circumferential direction. The servo layer is exclusively for servo bits and magnetized

along the radial direction by a transverse writing head that is aligned at right angles with the normal data head. The isolation layer is used to reduce the effect of the servo layer in reproducing data bits in the data layer and to guard against the data head re-writing servo information in the servo layer. The servo signals are reproduced by a transverse MR head with its stripe and pole gap tangential to the circumferential direction. The data signals are reproduced by a conventional MR head. The major advantages of this servo method are that the servo signal is continuous, its quality has low sensitivity to the medium defects and it is no longer limited by the data trackwidth.

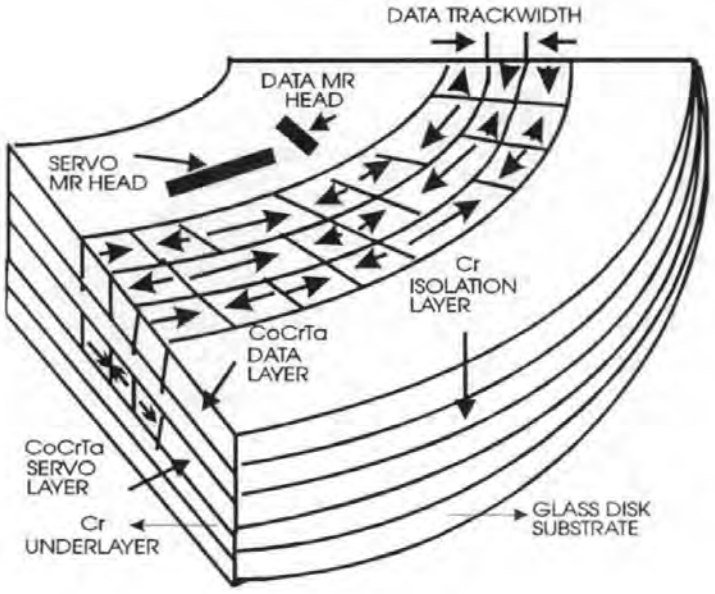

Figure 4.7 Schematic diagram of the new servo method using a buried servo layer and a transverse MR head.

4.2.2.1 Servo pattern

In order to reduce high frequency components, any harmonics and peak shift of the servo signal, the servo pattern was designed as shown in Figure 4.8 (a), so that servo signals reproduced by the servo head have low frequency and are near sinusoidal.

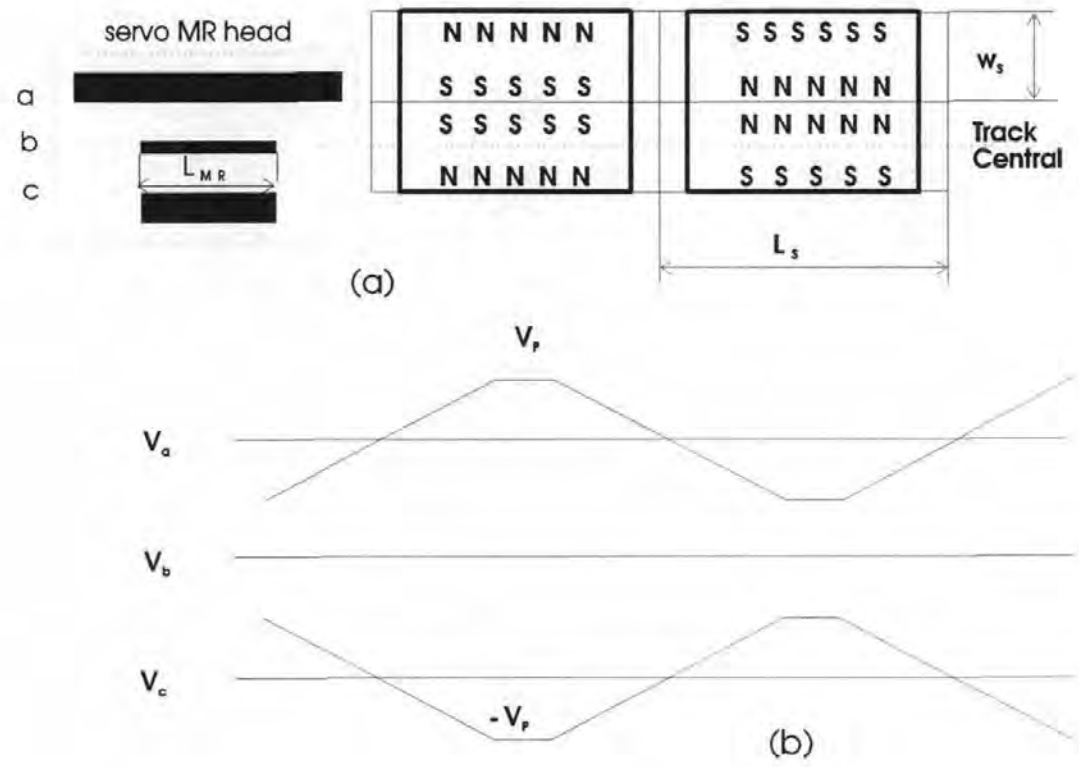

Figure 4.8 (a) The MR head footprint for detecting transverse magnetised servo patterns; (b) Output voltages of the MR head.

The total number (N) of servo patterns per track and servo signal frequency (f) are defined by:

$$N = \pi R / L_s, \tag{4-6}$$

$$f = N \times V_s \tag{4-7}$$

where N must be an integer number, R is the radius of the central line of the data magnetic track and V_s is the rotating speed of the disk.

When $L_s > L_{MR}$, the asymmetrical off-track response and the side writing phenomenon have no effect on the accuracy of the detected head position. In Figure 4.8 (b), V_a, V_b and V_c are waveforms when the MR head crosses the servo pattern along the circumferential direction at points *a*, *b* and *c*. Peak value V_p of the position signal can be used to indicate off-track displacement. The envelope curve of V_p can therefore be used as a position error signal (PES).

4.2.2.2 Servo detection

In this new servo detective system, the servo signal is about 200 kHz for a 2.5″ disk and the servo pattern width (W_s) is 15 μm for a disk rotating at 3600 rpm. The frequency of the data signal is usually over 10 MHz. This is over 50 times that of the frequency of the servo signal. Therefore the data and servo signal occupy high and low frequency parts of the spectrum. Noise between servo and data signal can therefore be filtered out using high and low pass filters.

4.2.2.3 Sputtering multilayer thin films on disks

In our experiments, servo layer, data layer, isolation layer and underlayer were deposited onto 2.5″ glass disks by rf-sputtering. The background pressure was approximately 2×10^{-7} Torr and the sputtering pressure (Ar) was 10 mTorr. A substrate bias (-100V) was applied during the process of sputtering CoCrTa thin film. Magnetron sputtering was used to increase deposition rate of the Cr thin film. The thickness of each layer was controlled by deposition time and using a movable shutter. The temperature of the substrate was controlled upto 300°C in order to achieve different coercivities for servo and data layers, e.g. 180°C for the data layer with 1300 Oe and 270°C for the servo layer with 1900 Oe. The Cr layer was grown with a deposition rate of 1000 Å/min

using a sputtering power of 600 W, whilst the CoCrTa layer was 200 Å/minute using a sputtering power of 400 W. The structure of the multilayer thin films is shown in Figure 4.7.

4.3 Results and discussion

4.3.1 The relationship between geometrical shape of the MR gap and the PES performance

The space between the shielded poles of the head is defined as the gap width (g_w,) the length of the smallest pole in the track direction is called the gap length (g_L) when the transverse head is placed as shown in Figure 4.1. The length of servo pattern in the track direction is called the servo (position) pattern length L_s, and the width of servo pattern in the track transverse direction is called the track width of the servo pattern or servo track (w_s). It should be noted that the width of the data track is about 75% of the track pitch, but the width of the servo track is equal to the track pitch or the servo track pitch.

The relationship between the shape of the MR gap and the performance of the PES signal is studied and discussed, by investigating the variation of the readout, linearity and S/N using a different shapes of head gap and servo pattern size. The study shows how the gap length and the width of servo pattern affect the quality of servo (position) signal and how the gap width and length of servo pattern affect the quality of the servo signal.

4.3.1.1 Simulation

A two-dimensional version of the well-known reciprocity integral was used to simulate (model) the readback response of the MR servo head. Suppose that the length of the servo pattern is much greater than the width of the MR servo head and the gap

length of the head. Suppose that the recording media has been written with a perfect, undistorted sine wave of longitudinal magnetisation along the transverse track direction, which has the same magnitude and phase angle throughout the coating depth (as shown in Figure 4.9). Then,

$$M = M_0 \sin kx \tag{4-8}$$

the PES voltage is [Mallinson, 1993]

$$V(t) \propto \frac{I \cdot \Delta pw}{tD} \cdot M_0 \left(\frac{1 - e^{-k\delta}}{k} \right) e^{-kd} \cdot \frac{\sin\left(kg_w / 2\right)}{kg_w / 2} \cdot \cos kx \cdot 2 \sin \frac{k(g+t)}{2} \tag{4-9}$$

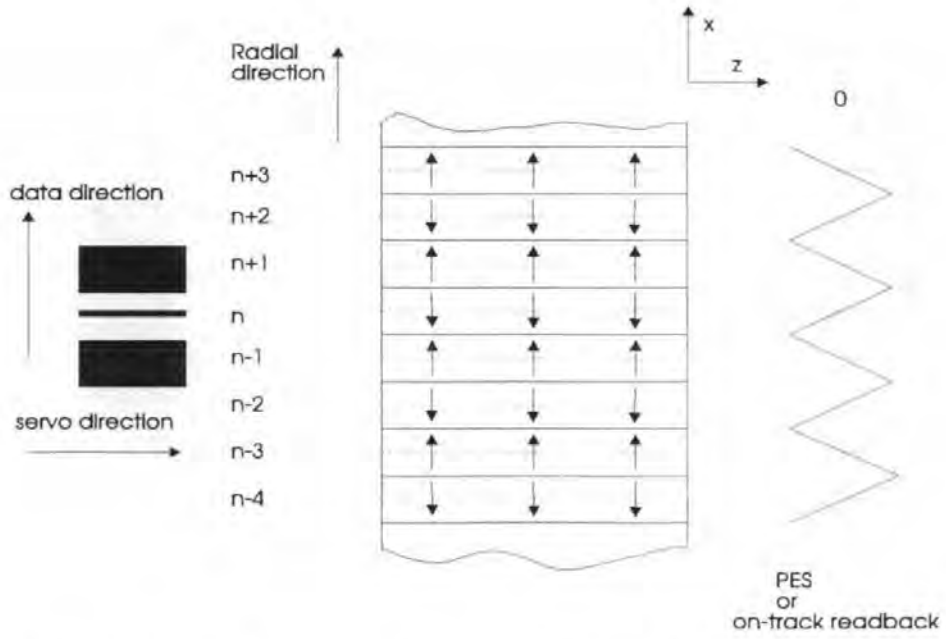

Figure 4.9 Showing reading signal in the radial and the circumferential direction.

Note that the PES is the envelope curve of the peak value of the readback signal reproduced by the MR servo head. The simulation results show that *V(t)* has maximum value when gap length is equal to 0.459λ (0.92 bit length).

4.3.1.2 Sensitivity of the PES

In order to optimise the magnitude of the PES, an experiment was undertaken using a disk on which one hundred transverse servo tracks, with various trackwidths

ranging from 0.40 μm to 8.2 μm, were written by the Submicron Servo Track Writer. The PES was reproduced by the shielded head, which was made by IBM and was maintained at 90° degree (transverse) with the normal data head position. (So it is 'in contact' recording). Other experimental conditions are the same as Section 2.2.4. The experimental results are shown in Figure 4.10 and Figure 4.11.

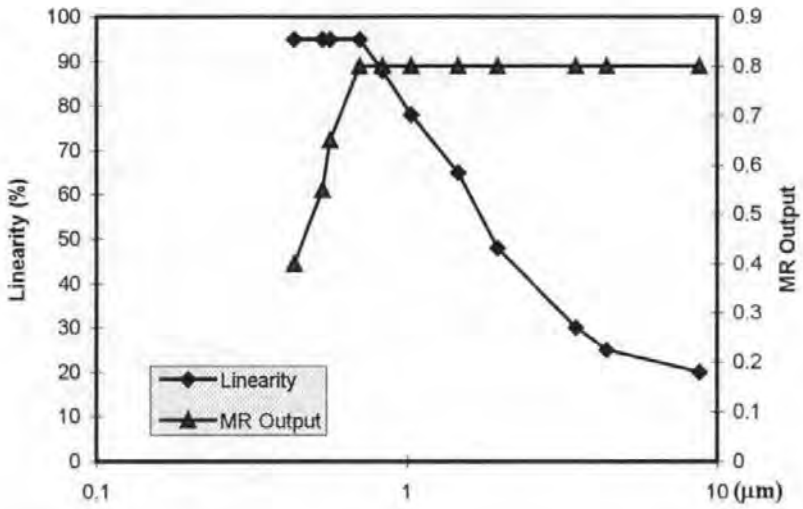

Figure 4.10 Readout and linearity of the PES signal vs. servo pattern bit length on longitudinal media.

It can be seen from Figure 4.10 and Figure 4.11 that the maximum PES level (MR output) is constant for a bit length equal to or greater than the gap length of the MR head, and the best linearity is constant for the bit length equal to or less than the gap length of the head. As a result, optimum quality of the PES was obtained when servo pattern bit width is equal to the MR head inter-shield spacing in contact recording.

The simulated result matches well with the experimental result, but the value of the experimental result is about g_w of 0.08 greater than the simulated result. There are two possible reasons for such a difference, one is the gap loss and another is the distribution of M. The real distribution of M is not an undistorted sine wave, rather it is

more like a stepped wave as the width of the servo pattern is much greater than the transition region, so the simulated result is slightly smaller than the experimental result.

In the experiment, the side read and the side write are removed by increasing the length of the servo pattern. The maximum signal level of the MR head is obtained when $g_w \leq w_s$. This may be explained as follows:

(i) When $g_w \leq w_s$, only a part of the magnetic field produced by the servo pattern could be introduced to the MR film because the shielded layers shield part of the magnetic field. However, the maximum combined field is not reduced. For this reason, the maximum combined field can be measured by the MR film when $g_w \leq w_s$.

(ii) When $g_w > w_s$, the maximum leave out field will be reduced by the fields of the adjacent servo patterns between the shielded poles. So the maximum signal level of the head will be reduced.

4.3.1.3 Linearity of the PES

The linearity of the PES signal is very important. The definition of the linearity can be found in section 1.2.3.3.(2).(c). This section investigates how the width and length of the gap of the MR servo head and the servo pattern affect the PES linearity. The experimental condition is the same as Section 4.3.1.2.

1. Size in the radial direction

In this study, a few hundreds servo tracks with widths ranging from 0.3 μm to 8.3 μm were magnetised along the transverse track direction on the disk. A MR shielded head, used as a reproduce head, was turned 90° degree with respect to a normal data head. A typical PES signal (or the envelope curve of the peak of the reproduced signal of the MR head) is shown in Figure 4.9. In this case, the gap width is equal to the width of

the servo pattern. The relationships of the linearity and w_s/g_w are shown in Figure 4.10 for the longitudinal media and in Figure 4.11 for the perpendicular media. Several results can be observed in Figure 4.10 and Figure 4.11:

(a). the linearity of the PES decreases as the w_s/g_w value increases when $w_s > g_w$.

(b). the linearity of the PES is slightly increased as the w_s/g_w value increases when $w_s \leq g_w$. This is because the peak of the PES increases as w_s/g_w value increases.

(c). the maximum linearity is obtained at the point of $w_s = g_w$.

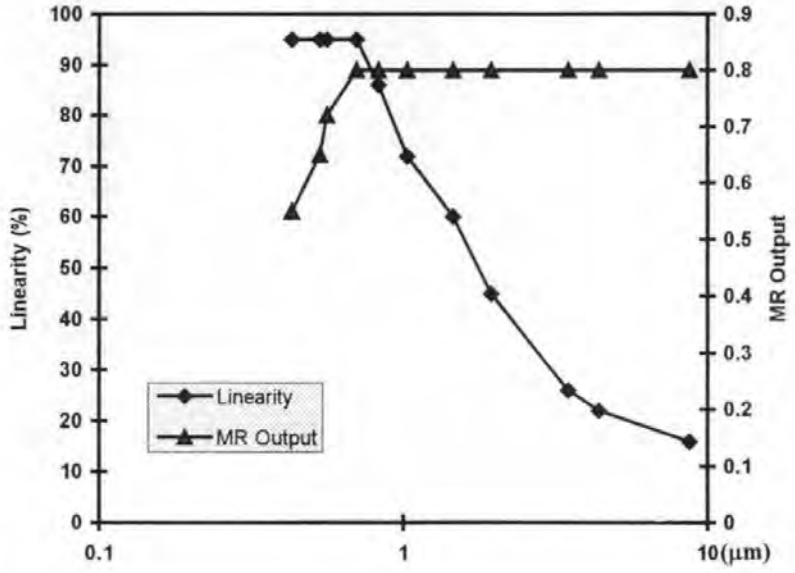

Figure 4.11 Readout and linearity of the PES signal vs. servo pattern bit length on perpendicular media.

2. The size in the track direction

In each of these studies, the same heads and disks are employed. The Submicron Servo Track Writer (SSTW) writes the servo patterns on the disk tracks. The clock signal supported by the SSTW was used as the write signal for the servo write head. The frequency of the clock signal can be adjusted by the SSTW to meet the need for writing the widths of the servo pattern. The widths of the servo pattern range from 0.1 g_L (the

gap width) to 10 g_L. The servo patterns with the same width and with an alternating 180° phase shift on each adjacent track were written on 11 tracks. The experiment was made on the mid-track (6th track) in order to negate the affect of the adjacent tracks.

Figure 4.12 is showing the relationship between the linearity of the PES and the width of the servo pattern.

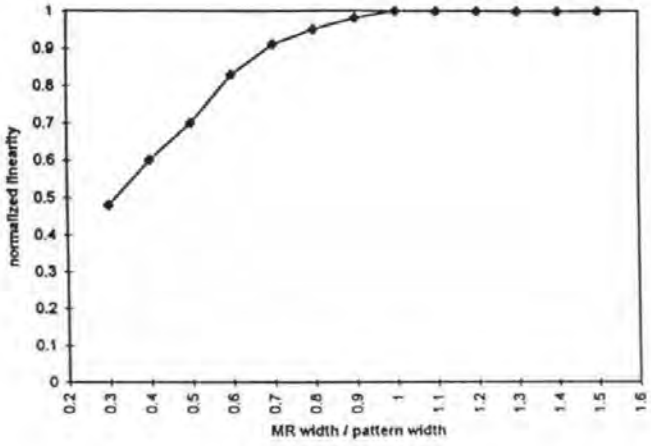

Figure 4.12 The relationship between the linearity of the PES with the width of MR servo head and the servo pattern

As seen in Figure 4.12, the linearity is almost a constant when $L_s/g_L > 1$, but it approaches zero when g_L/L_s is close to n, and n is an integral even number 2, 4, 6,..... This is because the reproduced signal is near zero when $n \approx g_L/L_s$.

4.3.1.4 The signal-to-noise (S/N) of the PES signal

Measuring the signal-to-noise of a PES signal is more complex than that of the data signal in Hard Disk Driver (HDD). This is because the noise of the data signal is only considered from one source, whilst the noise of the PES signal is determined from two sources, on-track and off-track.

The total S/N of the PES consists of two parts, one is the S/N of the disk and the another is the S/N of the 'non-disk'. The disk noise includes the media noise and the transition noise. The non-disk noise includes the head noise and the electronics noise. More details about the media noise and the head noise for narrow tracks can be found in the study of the data channel [Tsang et al., 1990[1]] [Tsang et al., 1990[2]].

In this project, two kinds of the PES S/N, the **on-track** S/N and the **off-track** S/N, are defined. The on-track S/N is the output signal reproduced by the servo head when it is positioning or following at the centre of track or very near the centre of servo track. The off-track S/N is the output signal reproduced by the servo head when it is off the track centre of servo track by a distance x.

1. Measuring the S/N of the PES

(1). The On-track S/N of the PES

When the MR servo head is in the centre of a track, S/N of the output of the servo head is the on-track noise. Its measuring method is similar to that of data channel, which is presented a method of measuring in data channel by Darragh [Darragh, 1994].

(2). The off-track S/N of the PES

Measuring the off-track S/N of the PES is more difficult than measuring the on-track S/N of the PES, because the off-track S/N of the PES is a function of the off-track distance x. In our experiment the method used to measure the signal to noise ratio of the servo channel is illustrated in Figure 4.13. The circuit is shown in part of the Appendix Hardware G. In the experiment, each servo pattern or servo track is written with equal width. At this track density the replay waveform is approximately sinusoidal. The PES signal is passed through a zero crossover detector which detects the cross-zero location of the PES signal. The outputs of the cross-zero detector are fed to a timer. The timer produces m timing pulses to trigger the A/D converter when sampling the PES signal.

This means that any one of $V_1 \cdots V_m$ is of equal sample space and is sampled from every track. At every point of $V_{11} \cdots V_{nm}$, the variance (ΔV_{nm}) of the samples and the signal amplitude (V_{nm}) over the sample space are stored and calculated by the microprocessor (n is the number of tracks over the sample space, m is the number of position offset the track centre). Then the signal to noise ratio at the point from 1 to m over the sample space can be calculated by

$$S/N_m = \frac{\frac{1}{n}\sum_{i=1}^{n} V_{im}}{\sqrt{\frac{1}{n}\sum_{i=1}^{n} \Delta V_{im}^2}} \qquad (4\text{-}10)$$

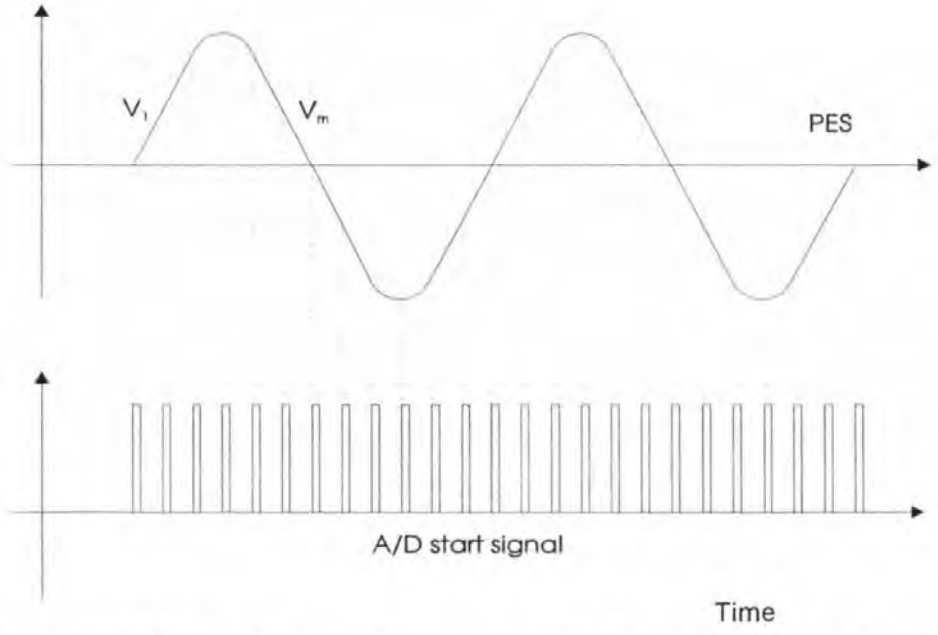

Figure 4.13 The method used to measure the S/N of the servo channel.

2. Calculation of the S/N of the PES signals

In a longitudinal magnetic recording system, the noise (V_s) produced by the transition region is proportional to the length (ΔL) of the transition region or the area (S_T) of the transition region [see Eq. (1-22)].

To help calculate the S/N of the PES, a new variable S_d is introduced to describe the number of the transition regions per unit area. For a conventional recording system, the S and S_d in an area of $W \times L$ are given by

$$S = \frac{2L \bullet W \bullet \Delta L}{\lambda_d} \tag{4-11}$$

and

$$S_d = \frac{2\Delta L}{\lambda_d} \tag{4-12}$$

where S is the number of the transition, λ_d is the recording wavelength, W is the trackwidth, L is a length in the track direction which is greater than W.

The S' and S_d' for the new position measuring system are given by

$$S' = \frac{2L \bullet W \bullet \Delta L}{\lambda_s} + L \bullet \Delta L = LW\left(\frac{2\Delta L}{\lambda_s} + \frac{\Delta L}{W}\right) \tag{4-13}$$

and

$$S_d' = \left(\frac{2\Delta L}{\lambda_s} + \frac{\Delta L}{W}\right) \tag{4-14}$$

To compare these two systems, we have

$$\frac{S_d}{S_d'} = \frac{2\Delta L / \lambda_d}{\frac{2\Delta L}{\lambda_s} + \frac{\Delta L}{W}} = \frac{W \bullet \lambda_s}{\lambda_d (W + \lambda_s)} \tag{4-15}$$

Suppose $\lambda_d = \frac{\lambda_s}{10}$, according to the fact that the width of the MR head is 10 times of the gap length of the MR head, then Eq. (4-15) becomes

$$\frac{S_d}{S_d'} = \frac{10W}{W + \lambda_s/2} = \frac{10}{1 + \lambda_s/2W} \tag{4-16}$$

If $\lambda = 2W$, then $\frac{S_d}{S_d'} = \frac{10}{1+1} = 5$

Therefore, theory shows that the transition noise in the PES signal in the new method is less than 0.5 n times that of the data signal when the data frequency is greater than n times that of the on-track servo signal.

3. Results and discussion

Using the above measuring method, the results of the off-track S/N of the PES signal versus the servo trackwidth and the length of gap of the servo MR head on longitudinal media are shown in Figure 4.14. The experimental condition is the same as Section 4.3.1.2. The S/N measuring method in Section 4.3.1.4 is used.

Note that the measuring method of the off-track S/N of the PES cannot be used to measure the value of PES near zero, but the value of the PES near zero can be obtained from the measurement of the on-track S/N of PES.

It is seen in Figure 4.14, that the maximum S/N of the PES signal occurs when $x = 0$ or when the servo MR head is aligned with the track centre. This is because only at the track centre can the MR film sense the weakest field produced by the transverse transition region at the track edges. Secondly the minimum S/N of the PES signal occurs at $x = W/2$ or when the MR head is aligned with the track edge. This is because at this point, the MR head senses not only the strongest field produced by a transverse transition at the track edges, but also the transition region between the bits in the track direction. Thirdly, the S/N of the PES signal increases as the g of the MR head reduces. Therefore, the greater the ratio of g and W, the smaller the difference between the maximum and minimum values of the S/N of the PES signal.

4.3.2 The skew angle

The use of a rotary actuator in present-day magnetic disk drives causes read/write heads to be skewed with respect to the track direction over most of the disk

surface. The skew angle can also introduce an offset from the track centre affecting the readout performance of the head according to the normal recording model [Wiesen et al., 1993] & [Liu et al., 1996].

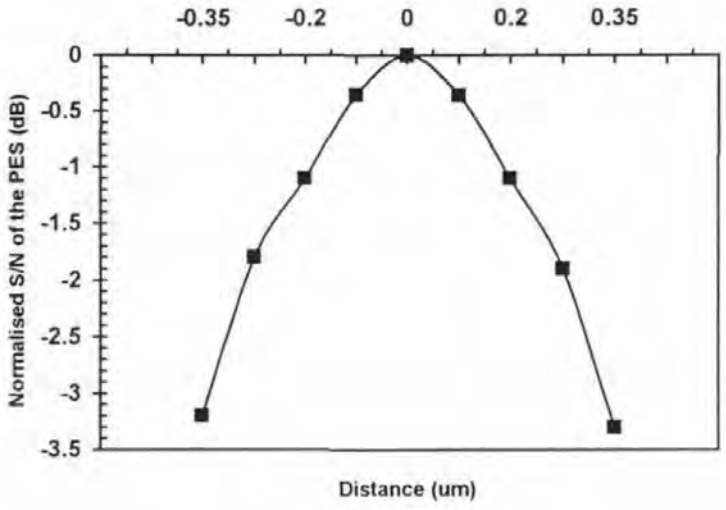

Figure 4 .14 The variation of the off-track S/N with the servo trackwidth and length of the gap of a servo MR head on longitudinal media.

Therefore, understanding the relationship between the skew angle and the recording performance in the new recording model and the new position sensor is very important for this project.

4.3.2.1 Analysis of producing the skew angle

Two methods may be used to write the servo pattern on a disk. One is using the data head of the HDD to write directly the servo pattern on disks, then the skew angle of the servo pattern will exist over the whole disk surface when a rotary VCM is used. The servo pattern written this way is shown in Figure 4.15.

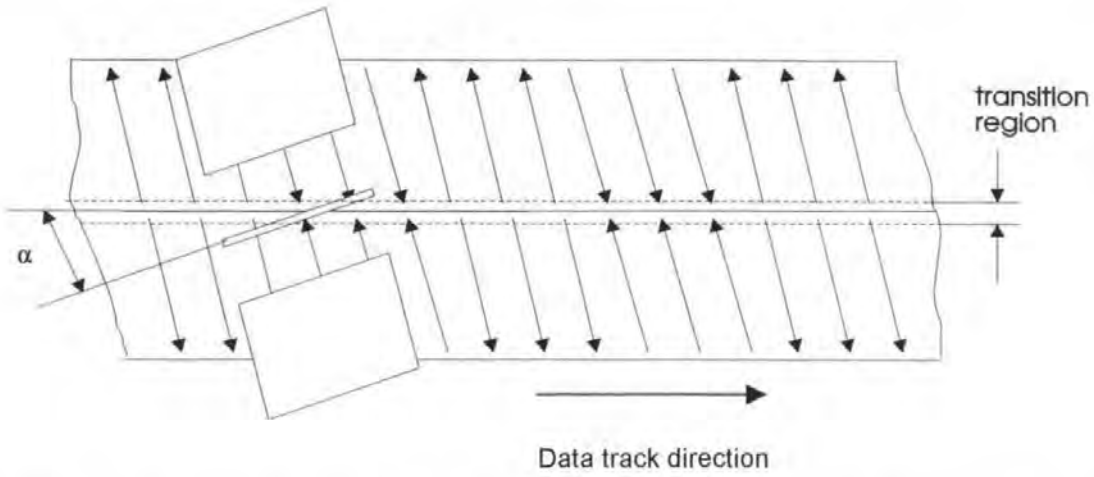

Figure 4.15 Showing the written servo pattern with a skew angle when using a rotary voice coil motor (VCM).

Another way is to use an extra head for writing the servo pattern. No written skew angle will exist in this way since usually the head of the servo track writer is moved straight along the radial direction of the disk. However, the read skew angles will still exist since the read head is driven by a rotary voice coil motor as shown in Figure 4.16.

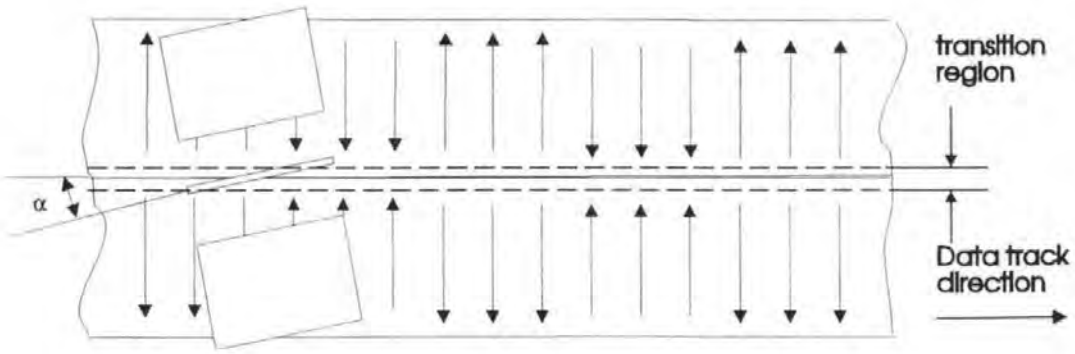

Figure 4.16 Showing the reading servo pattern with a skew angle when using a rotary voice coil motor (VCM).

4.3.2.2 The effect of skew angle on the read and write heads

When a head writes and reads a servo pattern, with a skew angle α in the new models, it can be seen that the readout of the MR servo head is inversely proportional to skew angle. The readout is zero when $\alpha = \alpha_0$. The α_0 can be expanded by

$$\alpha_0 = \sin^{-1} \frac{w_s}{g_L} \tag{4.21}$$

It is clear that α has to be less than α_0 in the new application.

1. Write with the skew angle

Eq. (4-2) defines the trackwidth of the servo pattern when the write head has no a skew angle. Including a skew angle, Eq. (4-2) becomes,

$$w_s = g_w + g_L \cdot \sin\alpha \qquad g_w < \Delta R \tag{4-22}$$

$$= \Delta R \qquad g_w > \Delta R$$

where, $\Delta R = R_i - R_{i-1}$

2. Experimental results

In order to understand further the relationship between skew angles (from 0° to α_0) and the readout of the MR servo head, experiments were carried out using a specially developed submicron servo track writer (SSTW). The servo trackwidth, the length and width of gap of the servo MR head are 0.7 μm, 4 μm and 0.7 μm respectively. The selected range of skew angle adjustment is -20° to +20°. The skew angle was adjusted on the submicron servo track writer (see section 3.1.2.6). The experimental conditions are the same as Section 4.3.1.2.

Figure 4.17 shows the relationship between the skew angle and the readout of the MR servo head.

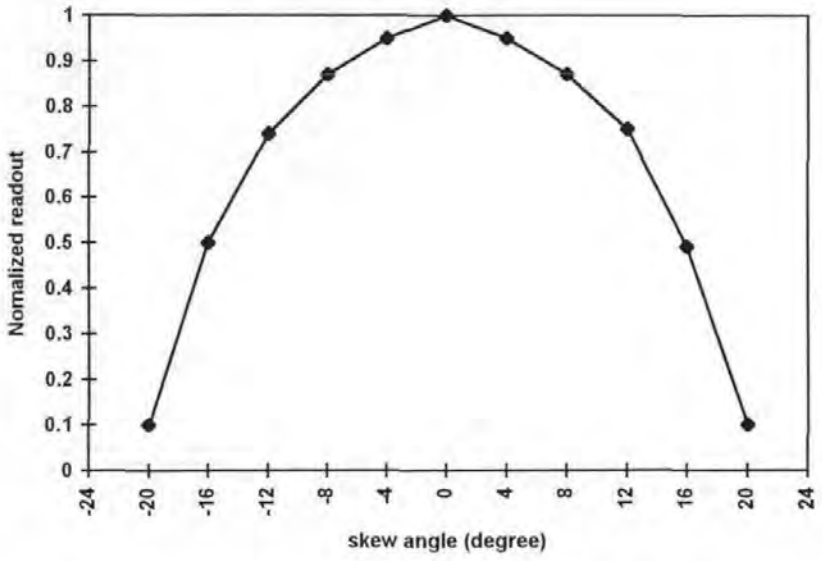

Figure 4.17 Readout of the servo head via the skew angle.

The following conclusions can be made from Figure 4.17.

(1) The maximum readout of the MR servo head is obtained at the point at which the skew angle is zero. The readout will be near zero when the skew angles are near ±20°.

(2) The readout of the MR servo head reduces as the skew angle increases.

(3) The decrease of the readout is small in the region where the skew angle is from -10° to +10°, i.e. less than 20%. This is because the two ends of the MR servo head are at the two opposite edges of the servo track respectively when $\alpha \approx \pm 10°$. Once the edges of the MR head cross over the edges of the servo track, reverse magnetization will reduce the readout of the MR servo head. For this reason, the readout of the servo MR head will be quickly reduced.

(4) It is seen that the curves of skew angle versus the readout of the MR servo head are near symmetrical about the zero point of the skew angle.

(5) Compared with the current embedded servo method, this position sensor system is more sensitive to skew angle variations.

3. Summary

In summary, the variation of the skew angle affects the readout of the MR servo head. This is not a serious problem for recording systems with a linear or even a rotary voice coil motor. This is because the skew angle variation throughout the data area is a function of the actuator arm length, (measured between the actuator pivot and the spindle motor centre). Accordingly, the head skew angle variation of a HDD could be limited within ±1° with a long-arm rotary actuator. This has been reported by Yoshikawa [Yoshikawa et al., 1996].

4.3.3 The asymmetry effect of the MR head

For longitudinally recorded magnetic rigid disks, it is well known that the off-track response for a MR read head on narrow track is asymmetrical [Tsang et al., 1990[1]]. For a perpendicularly recorded rigid disk this effect is more serious than for the longitudinal rigid disk. Figure 4.2 shows experimental results showing an asymmetrical off-track readout produced by an MR head on a perpendicular rigid disk. The asymmetrical phenomenon of the MR head has been studied and analysed by Yen [Yen 1982]. The component of the MR stripe magnetization along the stripe axis (x-direction) results in the asymmetrical off-track response. In theory, the phenomenon can not be removed in either disk. However, as is discussed below, this phenomenon does not affect the quality of servo signal in those position sensors.

When the MR servo head moves along the track or z coordinate direction, the waveform of the readout of the head may be asymmetric due to the component field in the z coordinate. The magnitude of the peak of the readout will indicate the off-track distance in a direction at 90° to this, i.e. the x-direction. After the head and the servo pattern have been selected, the asymmetry effect on the magnitude and position of the peak is to be fixed. Since the envelope curve of the peaks at different x points will be used as the PES signal, it will correspond to the readback waveform produced by the MR head in a similar way to its output when used as a normal data head. The PES signal, therefore, is symmetrical at the peak point, and at the zero point [Tsang et al., 1990[2]].

From these experiments, it seems that the asymmetry effect of the MR head could be neglected for the PES signal in this method.

4.3.4 The MR servo head

4.3.4.1 Consideration of the MR servo head

Another main advantage of these new methods is to enable optimisation of the designs of the data head and the servo head, as well as their channels by using an independent MR head as a servo head. Therefore, the function of each head can be optimised individually.

The optimisation of the MR data/servo composite head in the new servo method is as follows:

(1) The data head can be reduced to 70 % of the track pitch for effective data reading. The gap width of the servo head can be equal to the track pitch.

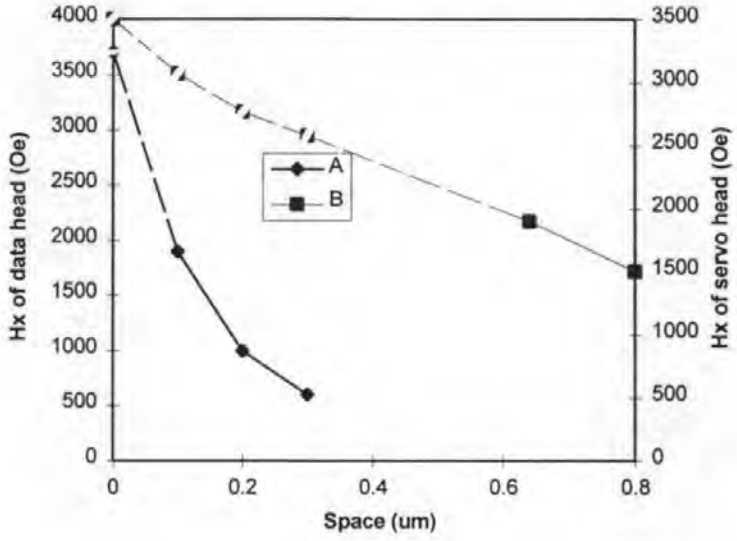

Figure 4.19 The decay of the writing field of the data head (Curve A) and the servo head (Curve B) with space

4.3.7 The S/N ratio of both signals

The experimental results for the S/N ratio of servo and data signals show that the S/N of the servo signal is increased as the coercivity of the data layer or the thickness of isolation layer is reduced or as the coercivity of the servo layer is increased. It also shows that the S/N of the data signal is increased as the coercivity of the data layer is reduced or the thickness of isolation layer or the coercivity of data layer are increased.

It was also found that when the data frequency to the servo frequency ratio increases, the S/N of both data and servo signals increase, which is certainly helpful to a recording system with a high longitudinal packing density.

It is found that the S/N of the PES signal is increased if the data layer is erased (AC or DC erase) by the data head after writing the servo pattern. The reason for this increase is that the data head can rewrite data bits on which the servo pattern has been

(2) The servo reproduced signal can be designed to be independent of the data signal. For example, the frequency of the servo reproduced signal can be optimised by using the method of Patapoutian [Patapoutian et al., 1996] and it is not limited by the bandwidth of the data channel. In his method, this optimal frequency of servo signal depends on the estimation scheme used, that is whether we estimate the amount of signal from peak rectified area or matched filter estimator.

(3) The servo signal can be detected at the same time as the data head writes data on a data track. This is impossible for current embedded servo methods because a single head is used for both tasks.

4.3.4.2 Effects of a different position between data head and servo head

In this study, since the data head and the servo head have to work on different tracks, the temperature and the skew angle of the heads may affects the position accuracy. The error produced by the skew can be compensated for by accurate calculation. Thus the temperature effect is small in this case. For example, if there is a temperature change of 40°C or a temperature difference of 10°C between the disk with sodalime glass and the composite head, the position error will be about 16 nm and 12.8 nm respectively.

4.3.5 Variation of a servo readout with isolation layer thickness, coercivity and trackwidth of the servo head

For the new servo method with separate servo under layer, the data track was written all "1"s and the data layer had H_c = 1300 Oe. The thickness of isolation between the servo and data layers was 0.2 μm. The coercivity of the servo layer is 1900 Oe. The widths of servo pattern in radial and circumferential directions were 0.7 and 15 μm respectively. The curve in Figure 4.18 shows that the servo signal output is reduced as the thickness of the isolation layer is increased. The thickness of isolation layer is adjusted by depositing time. Other experimental conditions are the same as Section 4.3.1.2.

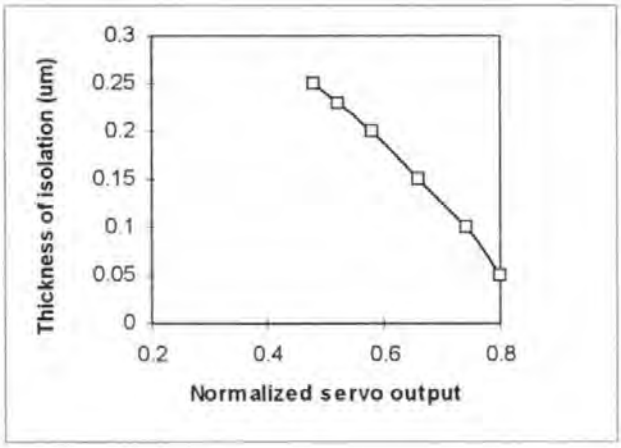

Figure 4.18 Servo MR output vs. isolation layer thickness on the disk.

Therefore, it can be concluded that the readout of the servo MR head increases as the MR trackwidth of the servo head increases or the thickness of the isolation layer reduces.

4.3.6 Writing the servo pattern and data bits

From Eq. (1-12) and Figure 1.8, it can be seen that the magnitude and gradients of the writing field of a head are dependent on its gap length (g), the space between the gap, the position near the gap and the magnitude of the write current. Therefore the servo pattern and the data bit can be written independently by carefully selecting the gap length and the magnitude of the write current.

In this study, a servo write head with a large gap (0.7 μm) was used to write the servo pattern, so that a gradual reduction of the writing field with depth can be produced. To keep the integrity of servo patterns, a data head with a smaller gap (0.25 μm) was used to write the data bits. The relationship between the write magnetic field for data and servo heads and the space between head and medium can be estimated by measuring output of the MR, which is shown in Figure 4.19. Curve A is for the write head with 0.7 μm gap. Curve B is for the data head with 0.25 μm gap. Write Current is 50 mA for both.

Further experimental results of reading and writing on the disk show that the recording magnetic field H_{xd}, produced by the data write head, must be less than 0.5 H_{cs} (H_{cs} is the coercivity of the servo layer) at the upper boundary of servo layer, to keep the integrity of the servo layer. In addition, the H_{xd} should be twice more than the coercive field at the bottom boundary of the data layer. The servo recording field H_{xs} produced by a servo write head must be one and half times greater than the H_{cs} of the bottom boundary of the servo layer. In the experiment, in fact, the fringing field of the magnetic head was controlled by adjusting the current through the head.

increase is not really clear. It is fact that the data head can rewrite data bits on which the servo pattern has been written on the data layer, but the remnant servo pattern in the guard band between two data tracks will form a new noise source for the servo MR head. Thus results in a reduction of the S/N of the PES. In other words, the S/N of the PES signal is increased if the remnant servo pattern on the data is erased.

To optimise the above system it is necessary to establish the S/N of the data signal by choosing H_{cd} (data) and then adjusting the isolation layer thickness, H_{cs} (servo) and the trackwidth of the servo head to increase the S/N of the servo signal.

4.3.8 Multilayer media with servo layer

The dependence of the coercivity of Cr-CoCrTa media for longitudinal magnetic recording on the substrate temperature has been studied by a few researchers [Maeda & Takei, 1991] and [Cord, 1993]. This phenomenon was also observed in our initial experiments. The experimental results of coercivity vs substrate temperature is shown in Figure 4. 22. This indicates that the desired coercivity can be obtained by controlling the substrate temperature during film deposition.

It was reported that the thickness of the Cr separation layer (in the range 0 to 30 nm) in a double-magnetic-layer film also can affect coercivity and squareness [Min et al., 1991]. Similar effect has been experimentally found in this project when Cr layer thickness changed from 0.1 μm to 0.3 μm.

The effect of overall thickness of multilayer films on disk was observed by atomic force microscope before and after deposition with a total film thickness of about 0.25 μm. Results show that the surface roughness increases slightly after deposition as seen Fig 4.20 and Fig 4.21.

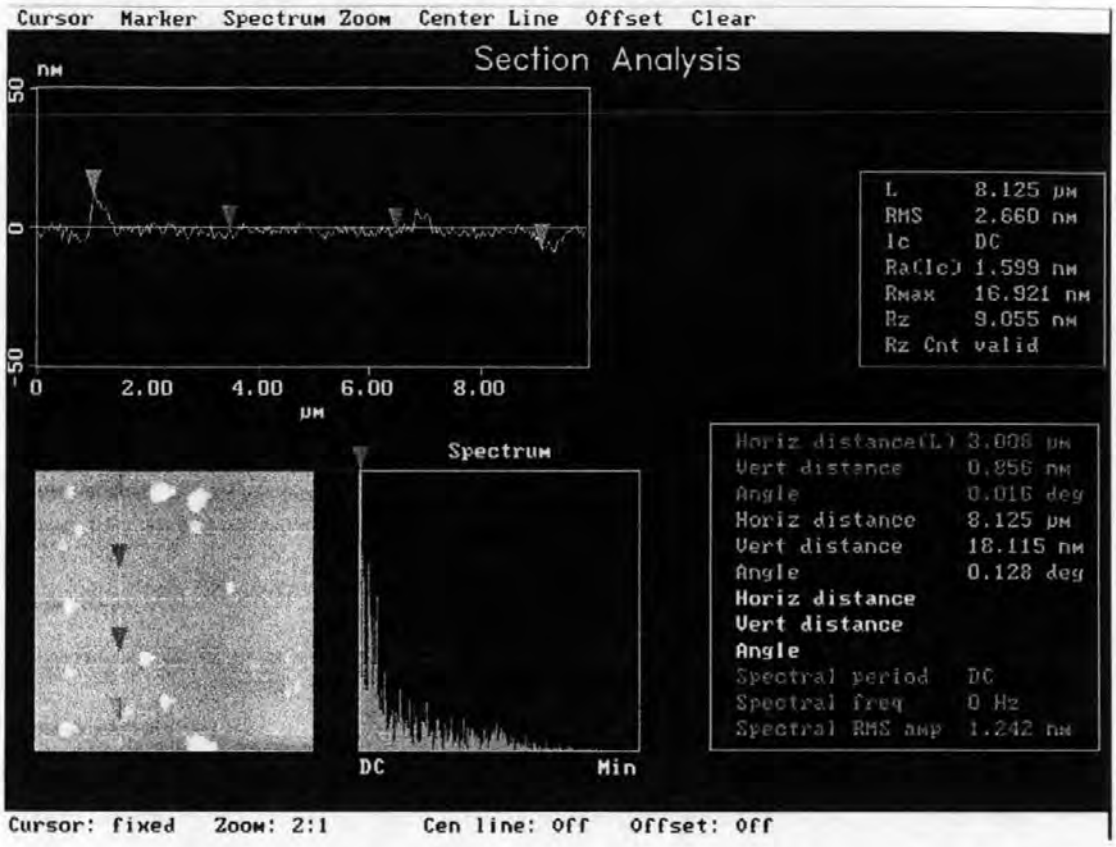

Figure 4.20 The surface roughness image of the glass disk before the deposition.

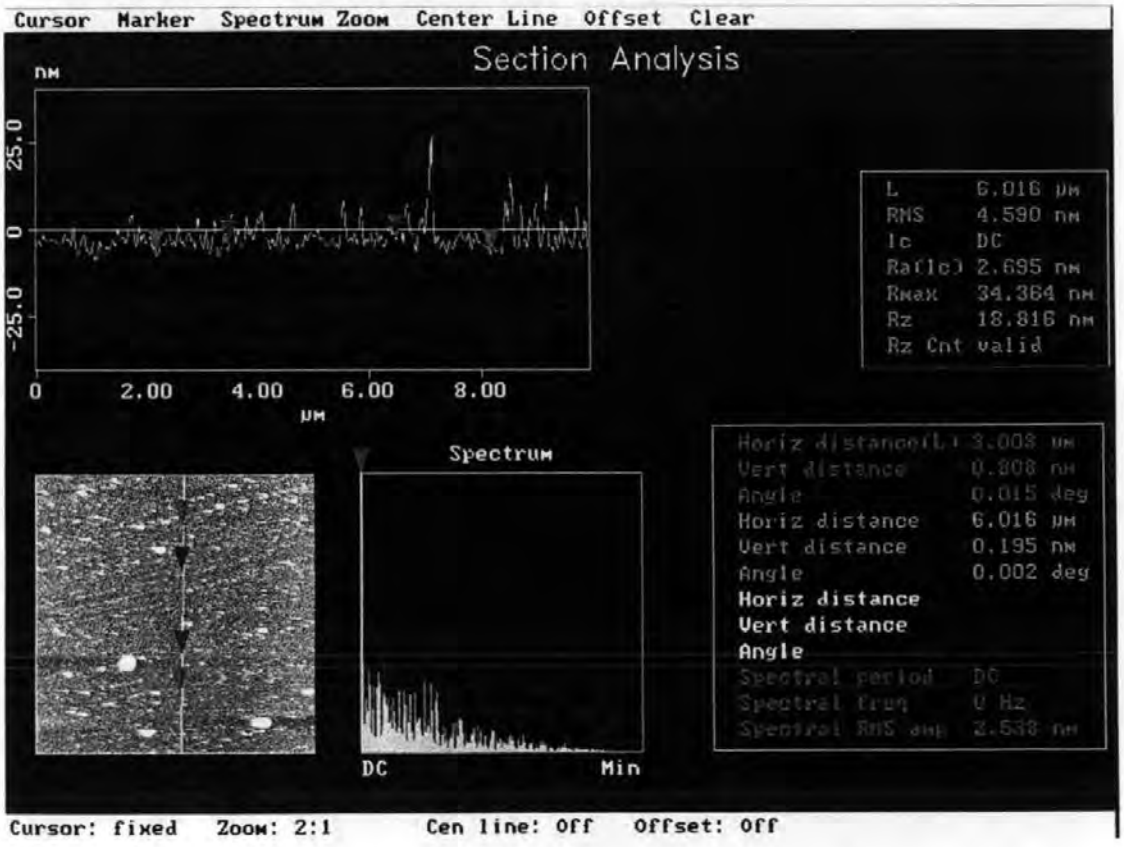

Figure 4.21 The surface roughness image of the glass disk after the deposition.

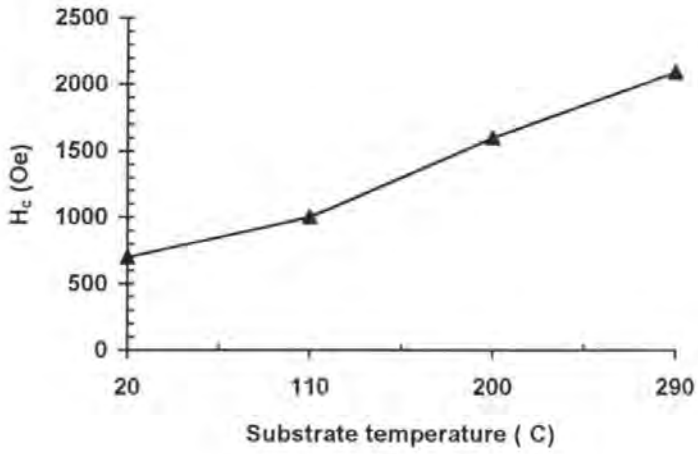

Figure 4.22 The coercivity H_c versus substrate temperature.

The experimental results indicate that the coercivities of servo layer and data layer can be changed by elevated substrate. Experimental result also shown that the added film thickness does not significantly effect the surface roughness of the disk the wear performance.

4.3.9. Design Implementation

4.3.9.1 The position sensor system for longitudinal and perpendicular recording

The transverse head for writing the servo pattern is a thin film inductive head with a gap length of 0.7 μm and a trackwidth 6.0 μm. The transverse MR servo head is a commercial shielded MR head with a gap length of 0.7 μm and a trackwidth of 4 μm. A 3.5" rigid disk with longitudinal recording media of coercivity 1800 Oe, which made by IBM, was used for the longitudinal recording position sensor system. A 3.5" glass disk coated with CoCrTa single layered perpendicular media was also used for the perpendicular recording position sensor system. The CoCrTa media was deposited on a Ti underlayer, with coercivity of 2000 Oe and thickness of 0.2 μm [Mapps et al.,

1993]. The servo pattern was written by a newly developed submicron servo track writer. 98304 clock pluses were written on the clock track by a 5 MHz source at the speed of 3051.76 rpm (on how to write the clock track see Section 4.3.10). A servo written signal was formed by the clock signal divided by 64. 1536 servo patterns with 0.7 μm trackwidth were formatted on a series of circles on the disks at the disk speed of 300 rpm. Each servo pattern bit length is about 6 μm. They occupy about 6.8 % of the data area.

A PES signal is produced by the demodulation of the position signal and this is shown in Appendix Hardware K.

In fact the demodulator is a sample-and-hold chip triggered by the delayed angular clock signal with a fixed delay to ensure that the output peak of the servo MR head was held.

The overall experiment's hardware and software are shown in Appendices Hardware G and Software D. In the Appendix Hardware G, the SH-ADA board was supplied by San Huan Electrons Ltd. [San Huan, 1992]. In this board, the A/D is a TLC08220 with a transfer rate of 2.5 μs and resolution of 8 bits, the D/A is a DAC0801 with transfer rate of 1 μs. ICES-G3 board is a Intel 8032 simulating board which was supplied by Wei Fu Ltd. [Wei Fu, 1993]. Technical details of other boards can be found in Appendix Hardware B, C, D, F, H and K. The sampling rate of the system was at 768 Hz, because the digital filter is used to reduce PES noise and the sampling rate. The digital PID (proportional integral differential) was used as a regulator in the system.

The dual-stage actuator consists of a coarse actuator (voice coil motor-VCM) and a fine piezo-actuator (PZ). The VCM was taken from a commercial hard disk drive made by Seagate. The PZ bimorph is supplied by KNT Co. and has been used by the author as a fine actuator having a dimensions of 15 × 1.5 × 0.6mm (free length 8.2 mm),

a maximum piezo deflection $L_{p\text{-}max}$ = 4 μm, the resonant frequency $f_{p\text{-}r}$ = 2.7 kHz. The VCM has $L_{v\text{-}max}$ = 50 mm, $f_{v\text{-}r}$ = 350, the motor torque constant K_i = 0.05 N-m/rad Their details can be seen in Chapter Five. The circuit of driving VCM can be seen in Appendix Hardware H.

The 0.7 μm track following experiments using longitudinal and perpendicular recording media were undertaken on the SSTW with air bearing spindle. Because the MR head was turned 90° to its normal operation condition and so can only be running at very low speed, the experimental disks were running at slow speed (300 rpm) and so the head and the disk were running in contact.

A PES waveform reproduced from longitudinal media when seeking track was shown in Figure 4.23. The first part of the curve shows an accelerating period for the servo head. The S/N, linearity and servo gain of the PES are sufficient for the track following. Figure 4.24 (a) and (b) show the PES signals when the servo head seeking track across 45 tracks and 22 track respectively. Figure 4.25 (a) shows two PES waveforms with and without track following for a disk mounted on an ordinary rigid disk drive. *A* and *B* on waveform (i) are the points where the crossing direction of the head changes. The waveform (ii) in Figure 4.25 (a) shows the residual following error on 0.7 μm tracks is less than 0.07 μm (rms). Figure 4.25 (b) shows two PES waveforms with and without track following for a disk mounted on the spindle of SSTW.

The servo MR head accesses 22 tracks on perpendicular media in Figure 4.24 (b). The S/N and linearity of the accessing waveform are sufficient for reliable operation and optimal seek performance. A degree of eccentricity always exists because the centre of the disk as written on an air bearing system, and the centre of rotation of the spindle motor in a disk drive are bound to differ. The left half of waveform (i) of Figure 4.26 shows that servo MR head crosses 8 tracks towards the inner; its right half means that

the MR head crosses 8 tracks towards the outside. The points *A* and *B* are points at cross direction change and points of maximum offset. The waveform (ii) in Figure 4.26 shows the residual following error on a 0.7 μm disk track with air bearing spindle using closed loop servo control. The error is less than 0.07 μm (rms).

The disk running speed in this experiment was low since the heads were not specifically designed for transverse writing and reading. Nonetheless, sufficient information has been obtained to prove the principle of this method for submicron track following at normal disk operating speeds (e.g. 3600 rpm).

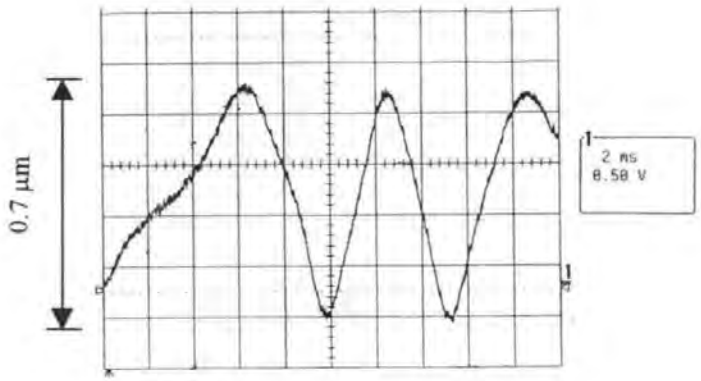

Figure 4.23 A PES waveform of seeking track

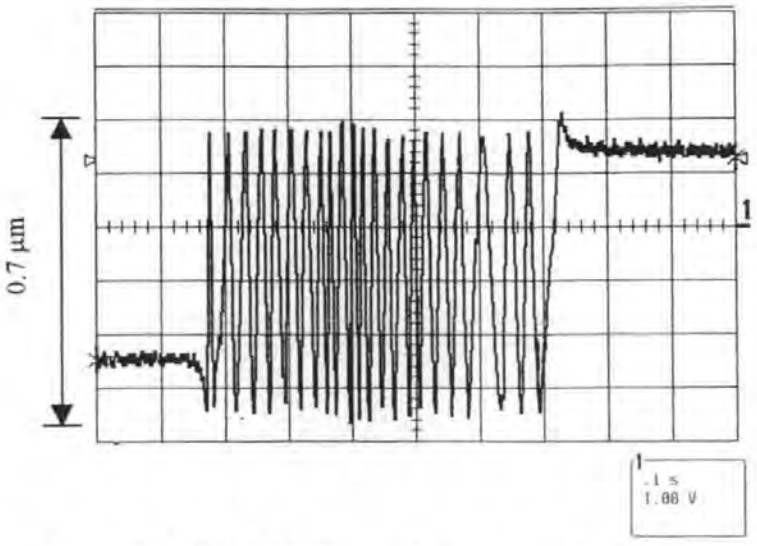

Figure 4.24 (a) A PES waveform accessing 45 tracks

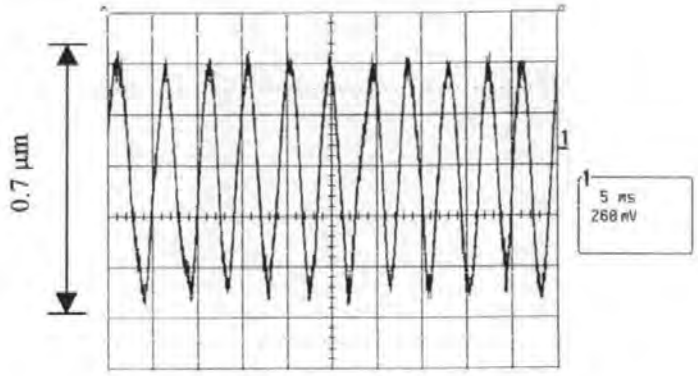

Figure 4.24 (b) A PES waveform accessing 22 tracks

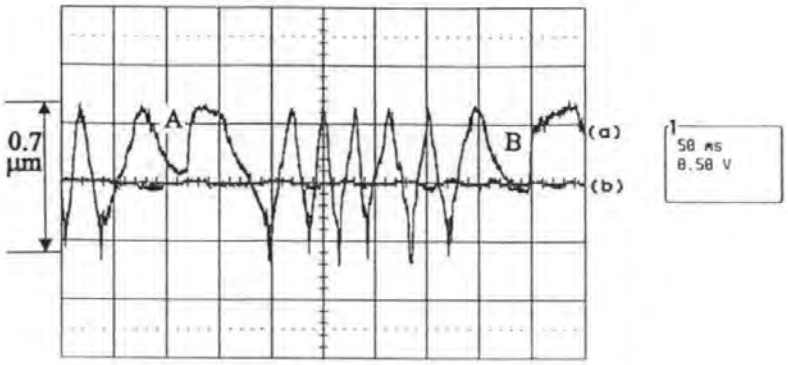

Figure 4.25 (a) PES waveforms without following (i) and with track following (ii).

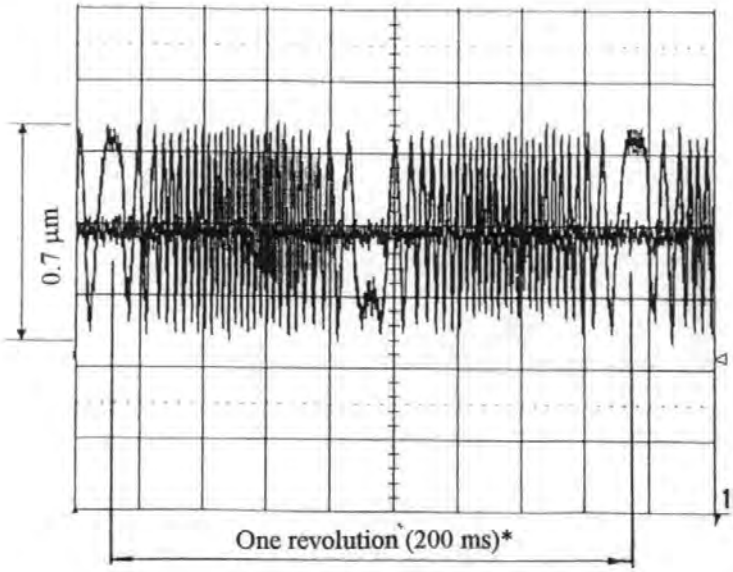

* The fine adjustment of the time base was used in order to achieve clear picture showing a revolution.

Figure 4.25 (b) PES waveforms without following (i) and with track following (ii).

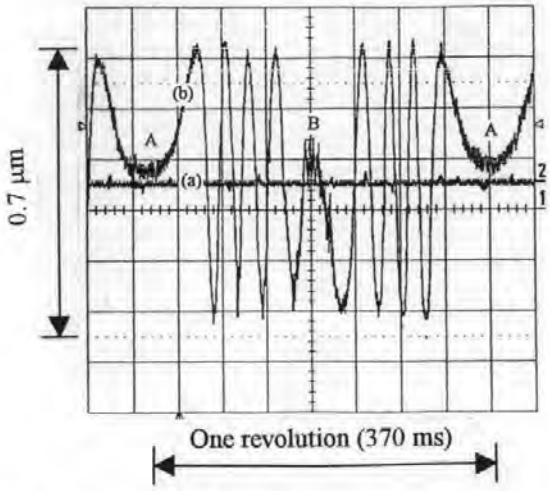

Figure 4.26 (i) A PES waveform without track following;

(ii) A PES waveform with track following (the speed was at 160 rpm).

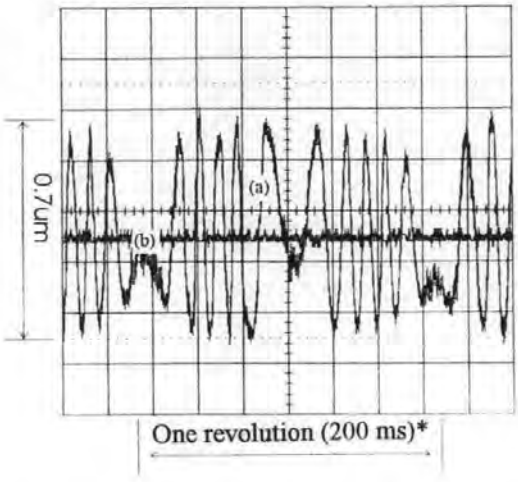

* The fine adjustment of the time base was used in order to achieve clear picture showing a revolution.

Figure 4.27 (i) A PES waveform without track following (ii) A PES waveform with track following.

4.3.9.2 Position servo system with separate servo layer

The 2.5" glass disk for servo experiment was made by the author. It has a 40 nm-thick CoCrTa film servo layer of coercivity 1900 Oe and B-H loop squareness $S^* = 0.78$, the CoCrTa data layer had a coercivity of 1300 Oe, thickness 35 nm and $S^* = 0.81$, isolation layer was 200 nm thick and carbon overcoat 25 nm thick. The servo bits in the

servo layer were written by a thin film inductive transverse head with trackwidth 6 μm and gap length 0.7 μm. The servo signal was reproduced by a shielded transverse MR head of trackwidth 4 μm and an inter-shield gap length 0.7 μm. A data write head with shorter gap length (0.25 μm) was used, so that it did not rewrite servo bits. After the servo patterns were recorded, the data layer was D.C. or A.C. erased with a magnetic field whose strength was less than the servo write field. Then data tracks on the data layer were written with an all "1" 's pattern. A dual-stage actuator with piezo-electric bimorph was used in the track-following servo experiment. The servo was tested on 0.7 μm servo trackwidth, as the disk was running at a speed of 300 rpm with the servo head running "in contact" with the disk. The waveform (i) in Figure 4.27 shows the PES waveform without track following and with a degree of eccentricity to test the track following properties. The waveform (ii) shows that the residual following error on 0.7 μm track is less than 0.1 μm.

4.3.10 A new method for writing the clock track

In order to format equally all servo patterns on a circular path on a disk and to line up every adjacent servo pattern radially, the clock pulses are synchronised to the angular position of the disk for the servo writing head [Tan et al, 1991] and a new method of writing the clock track with low rotary accuracy of the spindle was studied and developed. The following four subsections give details of this new method, including the theory, derivation, results and conclusion.

4.3.10.1 Theory

Clock track writing is difficult because spindle motors have a typical accuracy of only ± 0.1 percent of the specified spindle speed. If the spindle speed is at 3600 ± 3.6

rpm, for example, this amounts to a bit period tolerance of ± 16.6 μs, which is 1,000 times more than the required tolerance of ± 15 ns.

The new method of writing a clock track is given by

$$N = f \cdot t = \frac{2\pi \cdot f}{\omega} \tag{4-19}$$

where f is the frequency of the writing clock, ω is the angle speed of the disk, and N is the total number of clock cycles per track.

In theory, an integral number of complete clock cycles around a particular clock track can easily be achieved by adjusting f or ω. However, in practice, the variable f and ω are not constants and are changing with time.

It was found experimentally that variables f and ω follow a normal distribution (see Figure 4.28 and Figure 4.29). Thus a random variable x may be defined as the time of one revolution and a random variable y as the time of counting N writing clock pulses, so that their probability density can be given by

$$p(x) = \frac{1}{\sqrt{2\pi} \bullet \sigma_x} \bullet e^{\frac{-(x-\sigma_x)^2}{2\sigma_x^2}} \tag{4-20}$$

and

$$p(y) = \frac{1}{\sqrt{2\pi} \bullet \sigma_y} \bullet e^{\frac{-(x-\sigma_y)^2}{2\sigma_y^2}} \tag{4-21}$$

It can be seen that writing N clock pulses per revolution is met in the case when $x = y$. Assuming that a variable z is defined by

$$z = x - y \tag{4-22}$$

then, the distribution function of z is

$$f_z(z) = p\{Z \le z\} = \iint f(x,y)dxdy \quad (x\text{-}y \le Z) \tag{4-23}$$

Choosing the integrating area of the line $z = x\text{-}y$ for Eq. (4-23), so that

$$f_z(z) = \int_{-\infty}^{\infty}\int_{-\infty}^{z+y} f(x,y)dxdy \tag{4-24}$$

From Eq. (4-23), differentiation of $f_z(z)$ yields

$$f_z(z) = \int_{-\infty}^{\infty}\frac{d}{dz}\int_{-\infty}^{z+y} f(z+y,y)d(z+y)dy = \int_{-\infty}^{\infty} f(z+y,y)dy \tag{4-25}$$

As x and y are independent of each other, it can be written

$$f(x,y) = f_x(x) \bullet f_y(y), \tag{4-26}$$

which, in view of Eq. (4-24), leads to

$$f_z(z) = \int_{-\infty}^{\infty} f_x(z+y) f_y(y)dy \tag{4-27}$$

$f_x(z+y)$ and $f_y(y)$ are given by Eq. (4-20) and (4-21). On substituting Eq. (4-20) and (4-21) into Eq. (4-27), it follows that

$$f_z(z) = \frac{1}{\sqrt{2\pi\left(\sigma_x^2+\sigma_y^2\right)}} \bullet e^{\frac{-\left(z-a_x+a_y\right)^2}{2\left(\sigma_x^2+\sigma_y^2\right)}} \tag{4-28}$$

which implies that is also following the probability density of z the normal distribution.

In what follows, some special cases of Eq. (4-28) are discussed:

(1). When $z=0$ $(x = y)$, Eq. (4-28) reduces to

$$f_z(z) = \frac{1}{\sqrt{2\pi\left(\sigma_x^2+\sigma_y^2\right)}} \bullet e^{\frac{-\left(a_x-a_y\right)^2}{2\left(\sigma_x^2+\sigma_y^2\right)}} \tag{4-29}$$

which is the probability density of writing N clock pulses round a track.

(2). When $a_x = a_y$, Eq. (4-28) reduces to

$$f_z(0) = \frac{1}{\sqrt{2\pi\left(\sigma_x^2+\sigma_y^2\right)}} \tag{4-30}$$

which stands for the maximum value of writing N clocks around the track.

It is shown from Eq. (4-29) that the probability of writing N integral clocks around the track is maximum when the central frequency of the writing clock is equal to the central frequency of the speed of disk.

The values of σ_x and σ_y are the steady properties of the disk speed and writing frequency, which are constant for the given system. The probability of writing N integral clocks around a track also depends on these values.

4.3.10.2 Calculation

Supposing that x and y are independent, the probability (P) of writing N integral clock pulses per track in a different case can be given by

$$P(x = y) = \sum_{i=-\infty}^{\infty} P(x = n_i, y = n_i) \tag{4-31}$$

As an example, when distributions are given by Figure 4.28 and Figure 4.29 with $a_x - a_y = 0$, we have $P(x = y) = 20.9$ %. For the same distribution as above but with $|a_x - a_y| = 20$, we have $P(x = y) = 5.3$ %.

4.3.10.3 Experimental Results

In order to measure accurately the angular speed of the disk, the period per revolution is counted by a standard source. The index pulse is produced by a Hall element, which is mounted on the spindle. The period is measured by the TF830 1.3 Ghz Universal Counter. The curve of probability distribution of the rotating speed period is obtained as shown in Figure 4.28, which is approximately the normal distribution. From Figure 4.28, it was found that $a_x = 165,832$ and $\sigma_x = 93$, which are estimated by the number of pulses source of 10 MHz. The pulse width *(T)* consisting of 165,888 pulses with a 10 MHz writing clock is also measured in the same manner and its probability

distribution is shown in Figure 4.29, which is also approximately the normal distribution and with $a_y = 165{,}842$ and $\sigma_y = 2$.

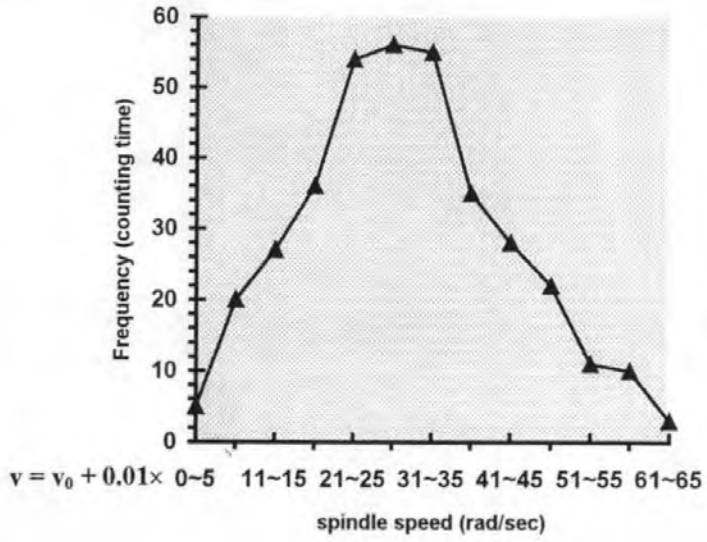

Figure 4.28 The probability distribution of the spindle speed (v_0 = 378.57 rad/s).

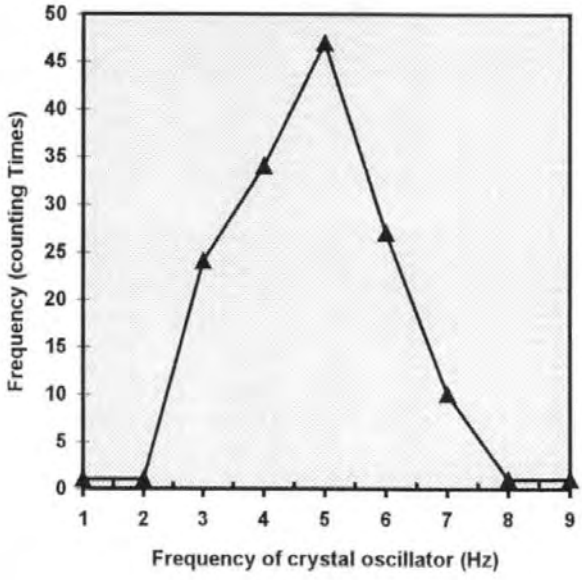

Figure 4.29 The probability distribution of the frequency of the crystal oscillator ($T = a_y - 5$).

Further, the measurement of each period was carried out and the results listed in Table 4.1. It can be seen that the experimental results agree well with the theoretical ones.

Table 4.1 Experimental results from writing N clock pulse around

Period	Experimental times 1	2	3	4	5	6	7	8	9	10	average time (s)	$\sigma_x-\sigma_y$	calculating results
1	5	4	6	5	3	3	7	2	4	5	4.2 s	0	20.9%
2	34	18	25	30	33	40	36	22	23	25	28.6 s	20	5.3%

Two waveforms (taken from experimental results) of the clock pulse with good closure (there is an exact integral number of clock bits making up 1 circumference of the clock track) and without closure respectively are shown in the Figure 4.30 and Figure 4.31. The closure means that the gap between the first clock bit and the written last clock is equal to the normal gap in the clock track.

It should be noted that it is not necessary to rewrite clock track every time both to turn on power of STW and to change speeds of the spindle. The clock system could work if the performace of the clock channel is suitable. After clock track on the disk which was running at high speed (e.g. 3600 rpm) is written, a MR head can be used as the clock head during reproduced the clock signal, if the disk is running at low speed (e.g. 300 rpm).

4.3.10.4 Conclusion

(1) $P(x = y)$ increases with reducing $|a_x - a_y|$, when $x = y$, which can be obtained by adjusting the speed of the spindle.

(2) When $a_x = a_y$, the higher stability of the spindle speed, the smaller $|\sigma_x|$, and the higher $P(x = y)$.

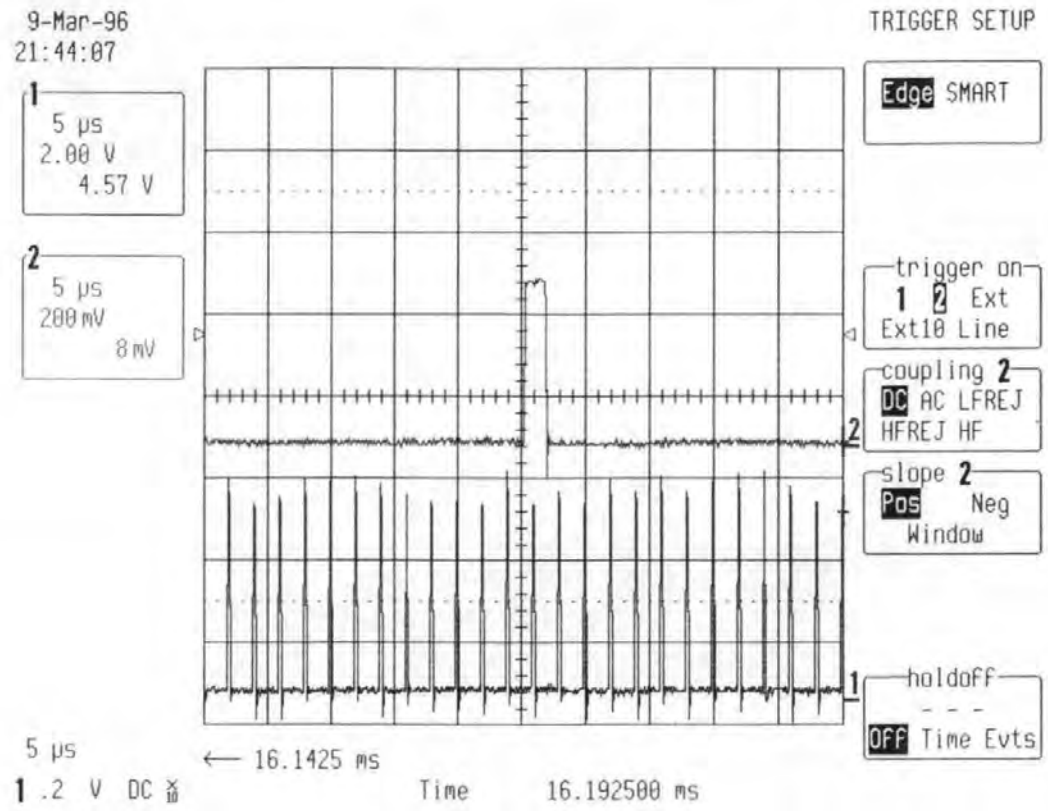

Figure 4.30 A waveform of the clock pulse with good closure.

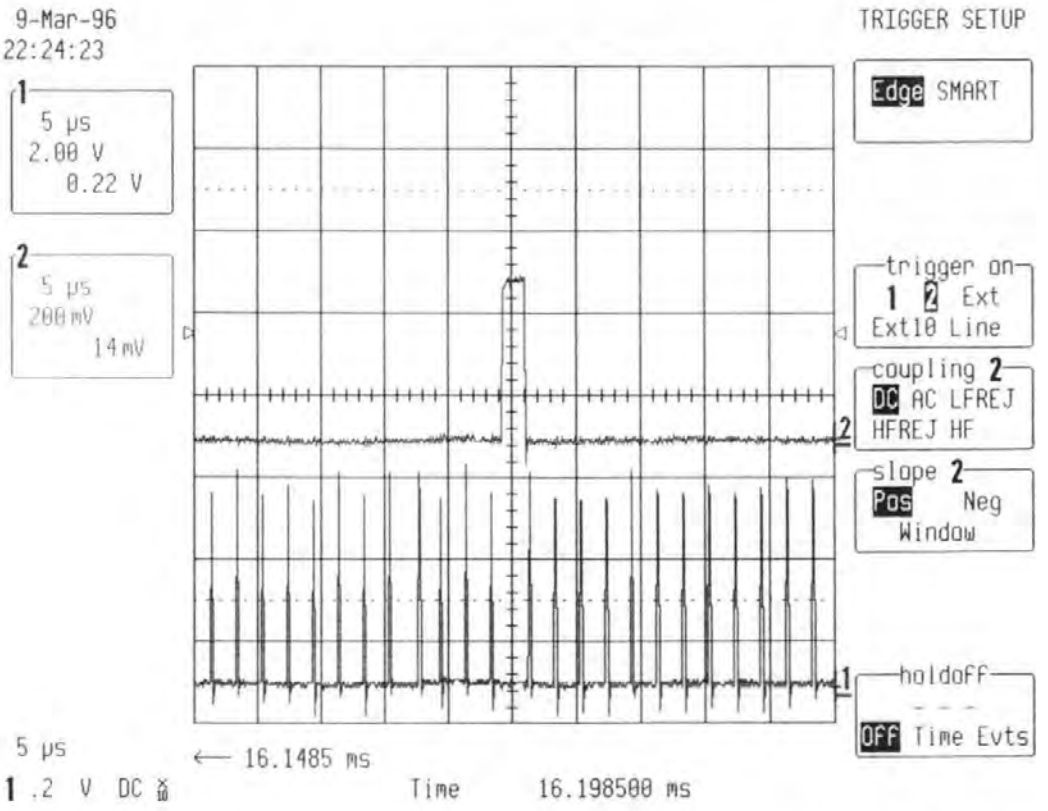

Figure 4.31 A waveform of the clock pulse without good closure

(3) Accordingly $p(\mu - 3\sigma < x < \mu + 3\sigma) = 1$, if $a_y - 3\sigma \le a_x \le a_y + 3\sigma$, then $P(x = y) = 1$, and $P(x = y)$ increases with reducing in $|\sigma_x - \sigma_y|$.

4.3.11 Comparison of the magnetic servo method with an optical servo method used on a hard disk drive

There are increasing interest in using optical servo method on HDD, however, there are very few publications concerning the fundamental magnetic performance of these methods. The application limits are not yet known. Such limits will depend on some factors such as the optical spot diameter and the height of the bump (pits, lands and grooves). For example the minimum track pitch on the disks is determined by the diameter of the spot. When the light wavelength is approximately 0.8 μm, the minimum theoretical diameter of the spot is about 0.5 μm, using a conventional lens system [Mallinson, 1993] & [Knight, 1997]. In this case, servoing on a track pitch of 0.74 μm on a digital versatile disk (DVD) has been achieved by using a red laser (0.65 μm), which has a minimum spot size of ~0.4 μm. It was recently reported that the minimum theoretical diameter limits has been improved by the use of a "solid immersion lens" (SIL) as used in liquid immersion microscopy. The resulting spot is approximately half the size of the spot obtained by a conventional system which uses only an objective lens, giving a spot size of 0.26 μm for a red laser [Knight, 1997]. Therefore the optical servo method could theoretically work on a submicron track servo on a hard disk drive.

Secondly, most optical disk drive servo signals (position signal) come from permanent physical features (pits, grooves and lands) on disks. The bump height of $\lambda/4$ (such as 130 nm for a red laser) is much more than the flying height of 20 nm [Mutoh et al., 1996]. In this case, the pits, grooves and lands used to indicate position on the disk would reduce the stability of the flying height for near-contact recording and producing a

disturbing force on the slider. The disturbing force changes with the position on the disk [Hua, 1990]. Consequently, the pits, grooves and lands may also increase the wear of the head in the case of contact recording.

Finally, if an optical servo method to be used for a magnetic disk, which means adding an additional optical head system to the disk, something should to be keep in mind, such as the need for optical head alignment and increased cost.

In our new servo method, the width of a servo MR head is not limited by data track pitch and the width of the head can be a designed value. Mori et al. found that the S/N ratio of an isolated servo signal of an optical head is about 2.5 times more than that of the MR head in a normal servo method (both of 2 μm trackwidth) [Mori et al, 1991]. However, it is well known that the S/N ratio of MR heads is proportional to its trackwidth, which means that if an MR head with a trackwidth of more than 5 μm is used for a 2 μm track servo in the new method, the S/N ratio of an isolated servo signal of the MR head should be near that of the laser diode (LD) head. In our experiment, a high quality servo signal on the track of trackwidth 0.7 μm has been obtained using an MR head of trackwidth 4 μm (see Fig. 4.23) and this servo signal quality is sufficient to servo the head within 5%~10 % error of the data track width of a HDD.

Finally, in our new servo methods, MR servo head can be integrated with data head and the cost of making the integrated data/servo head may slightly increase, but this new servo methods do not require special disk with bumps. The new method uses a rigid disk which is totally featureless i.e. with smooth surfaces. Such disks can easily be manufactured.

4.3.12 Comparison of the new servo method with embedded servo method

All currently available commercial hard disk drives employ the embedded servo for head positioning and following. The demodulation of the readback signal in the embedded servo method to obtain a position estimate can be described by

$$PES = \overline{A} - \overline{B} \tag{4-32}$$

where $\overline{A}$ and $\overline{B}$ are the amplitudes of the peaks of pulse A and B respectively.

For the new servo method

$$PES = \overline{A} \tag{4-33}$$

Note that the point with $PES = 0$ in both methods corresponds to a data track centre.

In what follows the new servo method is compared to the embedded servo method, using for example the sensitivity, linearity, and the S/N of the signal.

4.3.12.1 Sensitivity

Assume that the value of head sensitivity is K for both heads, the trackwidth of the MR head is W_e for the embedded method and W_n for new servo method and W is the servo trackwidth. The readback for the embedded servo method is given by,

$$V_e = K \bullet W_e \tag{4-34}$$

and its sensitivity is,

$$K_e = K \bullet \frac{W_e}{W} \tag{4-35}$$

Similarly, the readback V_n for the new servo method is

$$V_n = KW_n \tag{4-36}$$

And its sensitivity is,

$$K_n = K \bullet \frac{W_n}{W} \tag{4-37}$$

The substitution of Eq. (4-37) into (4-35) leads to

$$\frac{K_e}{K_n} = \frac{W_e}{W_n} \tag{4-38}$$

Note that, W_e is limited by W, but W_n is not limited and can be adjusted by the designer. Therefore the sensitivity of the new servo method is W_n/W_e times than that of the embedded servo method.

4.3.12.2 Linearity

Comparison of the linearity of the new method with the that of the embedded servo method is similar to that of the on-track readback of the MR data head with a crosswalk curve of the MR head. The linearity of the new servo method is much better than that of the embedded servo method, which can be seen in more detail in section 4.3.1.3.

4.3.12.3 S/N of the PES signal

In general, the *S/N* ratio is defined by,

$$S/N = S/N_{total} \tag{4-39}$$

in which,
$$N_{total} = \sqrt{N_{non-disk}^2 + N_{disk}^2 + N_{transition}^2} \tag{4-40}$$

For the embedded servo method, $(S/N)_e$ is given by

$$(S/N)_e = \frac{K \bullet W_e}{\sqrt{N_{(non-disk)e}^2 + N_{(disk)e}^2 + N_{(transition)e}^2}} \tag{4-41}$$

and for the new servo method, $(S/N)_n$ is given by

$$(S/N)_n = \frac{K \bullet W_n}{\sqrt{N_{(non-disk)n}^2 + N_{(disk)n}^2 + N_{(transition)n}^2}} \tag{4-42}$$

where W_e is servo head width in embedded servo method, and W_n is in the new servo method, $N_{(disk)}$ is the noise of disk media, excluding the noise of the transition range.

On substituting Eq. (4-42) into (4-41), we have

$$\frac{(S/N)_e}{(S/N)_n} = \frac{W_e\sqrt{N^2_{(non-disk)_n} + N^2_{(disk)_n} + N^2_{(transition)_n}}}{W_n\sqrt{N^2_{(non-disk)_e} + N^2_{(disk)_e} + N^2_{(transition)_e}}} \tag{4-43}$$

Due to using the same disk $N_{(disk)e} = N_{(disk)n}$ and it is assumed that $N_{(non-disk)n} = N_{(non-disk)e}$ and $N_{(transition)e} = N_{(transition)n}$, which yields

$$\frac{(S/N)_e}{(S/N)_n} = \frac{W_e}{W_n} \tag{4-44}$$

From previous argument (see section 4.3.1.4), the maximum value of $(\frac{N_{(transition)e}}{N_{(transition)n}} \le 2)$, now consider the situation when the value of $(N_{transition})$ is the worst case, $N_{(transition)}$ ≅ $N_{(non\text{-}disk)}$ and $N_{(transition)}$ ≅ $N_{(disk)}$. Then Eq (4-43), reduces to

$$\frac{(S/N)_e}{(S/N)_n} = \frac{2W_e}{W_n} \tag{4-45}$$

Therefore, the S/N ratio of the new servo method will be higher than that of the embedded servo method when taken $W_n > 2W_e$.

4.3.13 Comparing the new servo method with the discrete servo method

In Section 1.2.3.1 (1) (c), the discrete servo methods including the Graph Head Positioning (GHP) and the Pre-Embossed Rigid Magnetic (PERM) methods have been reviewed. It is well known that the advantage of the discrete servo method is the reduction of the distribution of the data track. However, a recent study shows that a guard band of 0.1 μm is enough for a continuous media in a hard disk drive with a track pitch of 1.3 μm [Mutoh et al., 1996]. This leads to a reconsideration of the necessity of etching a guard band. From the servo point of view, the main advantage of the PERM method is that it is not necessary to use special equipment for writing the servo pattern

(e.g. conventional STW). However, to get very high quality servo (position) signals, it seems that the PERM method is not better than other traditional servo methods in its sensitivity, linearity and the S/N of the servo (position) signal. Similar problems exist in the GHP method too.

On the other hand, both the above methods use etch or stamp technology to make marks, grooves, and lands on the surface of the disk for recording servo patterns. Thus these marks, grooves and lands may reduce the stability of the flying height of the head in near-contact recording [Hua, 1990].

Another problem of the GHP method concerns servo writing. As a personal opinion, lower relative accuracy of the head positioning is needed when writing a servo pattern in the GHP method, but higher absolute accuracy of the head positioning is needed, because the position of every discrete etched block of the magnetic material is absolutely fixed. It should be noted that it is only necessary to have high relative accuracy of the head positioning when writing the servo patterns using a general servo track writer; absolute accuracy is not necessary. When the trackwidth reduces to submicron size, writing servo patterns using the GHP method is more difficult than using conventional methods. Therefore, both the GHP and PERM methods may be not ideally suited for submicron track positioning and following.

4.4 Summary

In section one, the reasons why current servo methods are not suitable for a submicron track servo were given. The key problems are low S/N ratio of the PES signal and asymmetries in the MR head.

In the second section, a new servo method based on a new magnetic recording model for servo patterns was proposed. In the new method, the servo patterns are

magnetised along the radial direction by a transverse writing head that is aligned at right angles with the normal data head. The servo signals are reproduced by a transverse MR head with its stripe and pole gap tangential to the circumferential direction. Expressions for the PES signals on longitudinal and perpendicular media were developed. As a further development, a new buried servo method has been proposed and it is shown that by using a servo layer underneath the data layer, a continuous servo signal can be obtained.

In section 4.3, experimental results and discussion of the new method were given. In section 4.3.1, the effect of the length of the MR sensor and the distance between the shields of the head on the servo signal amplitude and linearity were investigated. Parameters such as the spacing and length of the servo-pattern elements have been optimised so as to achieve minimum jitter and maximum utilisation of the surface of the disk. The factors affecting the S/N of the position sensor have been analysed and demonstrated.

In section 4.3.2, the reason why the skew angle in the new servo method has to be less than $\alpha_0 = \sin^{-1}\frac{w_s}{g_L}$ was given. The linear and rotary voice coil motor with small skew angle are suitable for this application.

In section 4.3.3, experimental results and theoretical analysis show that the asymmetry effect of the MR head can be negligible for the PES signal in the new servo method.

From section 4.3.5 to 4.3.8, the new buried servo method was discussed and demonstrated. This included investigation of the servo signal amplitude, linearity and the S/N ratio of the PES signal as affected by media layer thickness and coercivity. The

desired performance of the data servo and isolation layers can be achieved by controlling the depositing conditions such as elevated substrate.

In section 4.3.9, the design of the position servo system is discussed and the track following results of three new types of position servo system are given. A new method of writing the clock track, which can be used to obtain a high quality clock signal for writing the servo pattern, was developed and given in the following section. Finally, comparison of the new servo method with an optical servo, embedded servo and discrete servo indicates that the new servo method may be the best candidate for a submicron track servo system (from a practical point of view).

Following discussion of the new position measuring system, a new dual-stage actuator for the project will be discussed in the next chapter.

Chapter Five

Actuator

5.1 Introduction

Actuators are the part of a servo control system used to control the movement of multiple head-arm assemblies across the disk surface in order to maintain the heads on-track and to minimize track misregistration during the processing of a recording. The voice-coil motor (VCM) is used as an actuator in almost all hard disk drives.

A linear voice-coil actuator prime mover has a voice-coil motor consisting of a permanent magnet structure and a movable bobbin or coil attached, through a T plate, to the comb of arms carrying the read/write heads. The movable assembly is supported on bearings that move on hardened flat surfaces called ways. Voice-coil motors have antecedents in the motors used in loudspeaker system.

The IBM 3380 disk drive actuator is a linear VCM. Another type of voice-coil actuator, the rotary actuator, has found wide usage in small-size (e.g. 3.5 inches) hard disk drives. Rotary actuators with dynamic balance may be less susceptible than linear actuators to vibrations that cause the heads to be forced off track. With linear actuators, radial forces can result in radial motion of the heads, particularly if the frequency of the excitation is outside the bandwidth of the servo system. However, the modes of vibration of the suspensions and arms in a rotary actuator have greater effects on servo

performance than in the case with linear actuators. However, the resonant frequency of both actuators is below 600 Hz. This limits the allowable servo bandwidth. Thus the bandwidth of the servo system for submicron trackwidth has to be higher than 3 - 5 kHz. One method of increasing the actuator bandwidth is to mount a fine actuator on top of a coarse one. This is called a dual-stage actuator. The positioning range of the actuator for 3.5, 2.5 and 1.8 inch disks are respectively about 1, 0.7 and 0.4 inches. The positioning range for the fine actuator is only a few microns, and its bandwidth is more than 3 kHz. This is similar to the actuator of an optical disk.

The VCM has been extensively studied by other researchers, as described in section 1.3.1.3 of Chapter One. More details can also be found in the book by Mee [Mee, 1989]. Therefore, the discussion here will be focused on the fine actuator and the dual-stage actuator.

5.2 Mathematical Model for a Dual-stage Actuator

The dual-stage actuator developed for this project is shown in Figure 5.1. It consists of a high bandwidth fine actuator mounted on top of a large VCM actuator. A simple model of the dual-stage actuator is developed. It consists of two moments of inertia that are actuated by ideal torque inputs and are coupled by a spring-damper system. Figure 5.2 shows a diagram of the model, where y_1 is the absolute angle, y_2 is the relative actuator angle, u_1 is the coarse actuator torque input and u_2 is the fine actuator torque input. J_1 is the coarse actuator moment of inertia, J_2 is the fine actuator moment of inertia, k is the fine actuator coupling spring constant and B is the fine actuator coupling damping coefficient.

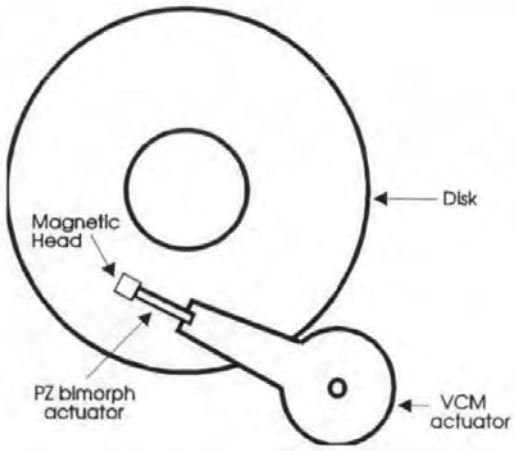

Figure 5.1 A dual-stage actuator.

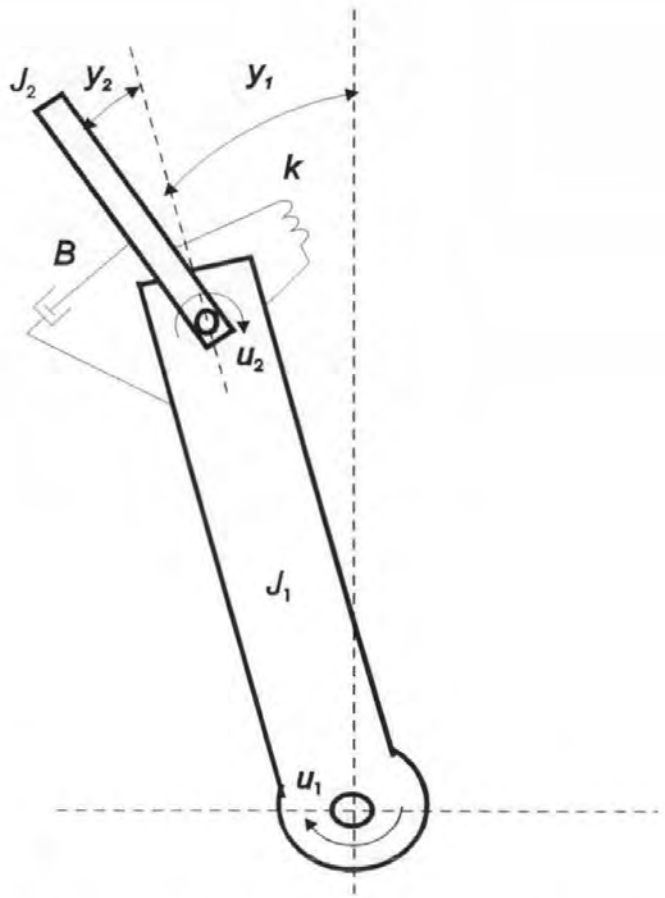

Figure 5.2 Diagram of the model of a rotary dual-stage actuator.

A state-space model for the actuator in Figure 5.2 is given in Eq. (5-1).

$$\begin{bmatrix} \dot{x}_1 \\ \dot{x}_2 \\ \dot{x}_3 \\ \dot{x}_4 \end{bmatrix} = \begin{bmatrix} 0 & 1 & 0 & 0 \\ \frac{-k}{J_e} & \frac{-B}{J_e} & 0 & 0 \\ 0 & 0 & 0 & 1 \\ \frac{k}{J_2} & \frac{B}{J_2} & 0 & 0 \end{bmatrix} \begin{bmatrix} x_1 \\ x_2 \\ x_3 \\ x_4 \end{bmatrix} + \begin{bmatrix} 0 & 0 \\ \frac{1}{J_1} & \frac{-1}{J_e} \\ 0 & 0 \\ 0 & \frac{1}{J_2} \end{bmatrix} \begin{bmatrix} u_1 \\ u_2 \end{bmatrix}$$

$$y = [1010] \begin{bmatrix} x_1 \\ x_2 \\ x_3 \\ x_4 \end{bmatrix} \qquad (5\text{-}1)$$

where the equivalent moment of inertia J_e, is defined as $(J_1 \cdot J_2)/(J_1+J_2)$; and

$x_1 = y_1$, is the absolute angle of the coarse actuator;

$x_3 = y_2$, is the relative angle between the coarse and fine actuator;

$x_2 = \dot{x}_1$, is the angular velocity of the coarse actuator;

$x_4 = \dot{x}_3$, is the angular velocity of the fine actuator;

$\dot{x}_2$ is the angular acceleration of the coarse actuator;

$\dot{x}_4$ is the angular acceleration of the fine actuator.

To help visualise the actuator dynamics, a block diagram for the actuator, (based on equation 5.1), is shown in Figure 5.3 (a). Note that Figure 5.3 (b) is a block diagram of a single VCM actuator, illustrating the standard transfer function of

$$\frac{y_1}{u_1} = \frac{k_f}{Js^2 + Bs + k} \qquad (5\text{-}1a)$$

where K_f is the torque constant, J is the moment of inertia of the moving part of VCM, B is the viscous damping coefficient of the bearing, k is the return spring constant.

According to the above requirements, it is necessary to design a dual-stage actuator consisting of a PZ bimorph as the fine actuator and a VCM as the coarse

actuator (see Figure 5.4). In the dual-stage actuator, PZ bimorph and VCM are supplied by NTK Co. and Seagate Co. respectively.

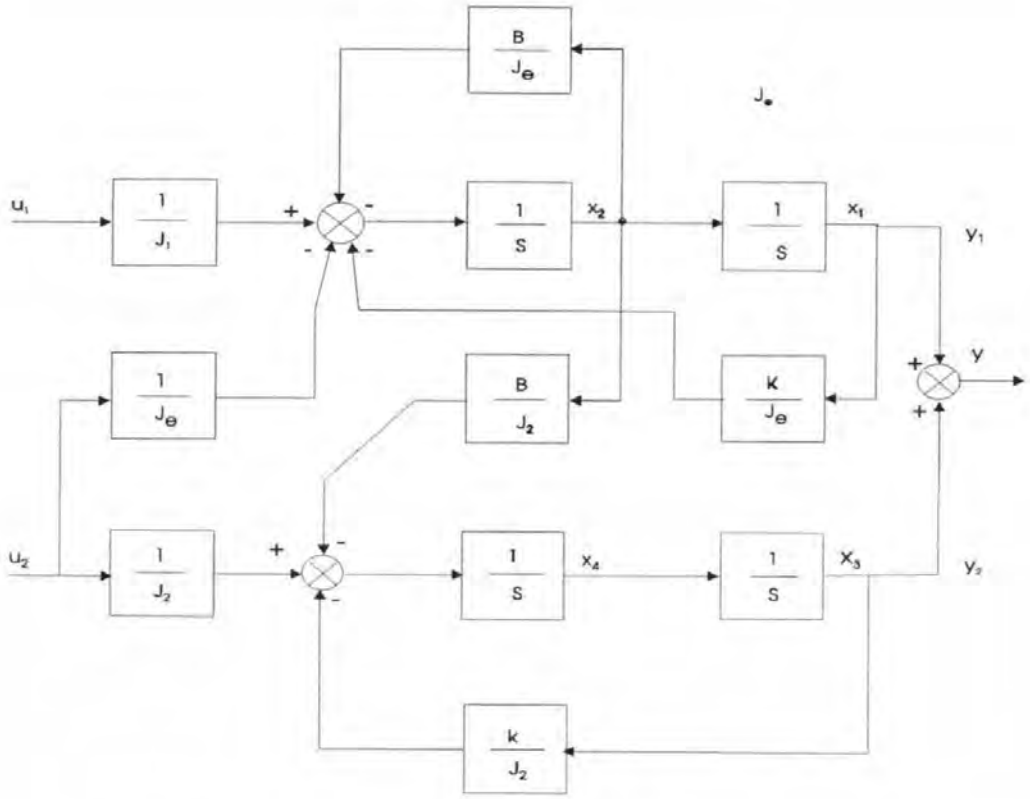

Figure 5.3 (a) Block diagram of a rotary dual-stage actuator.

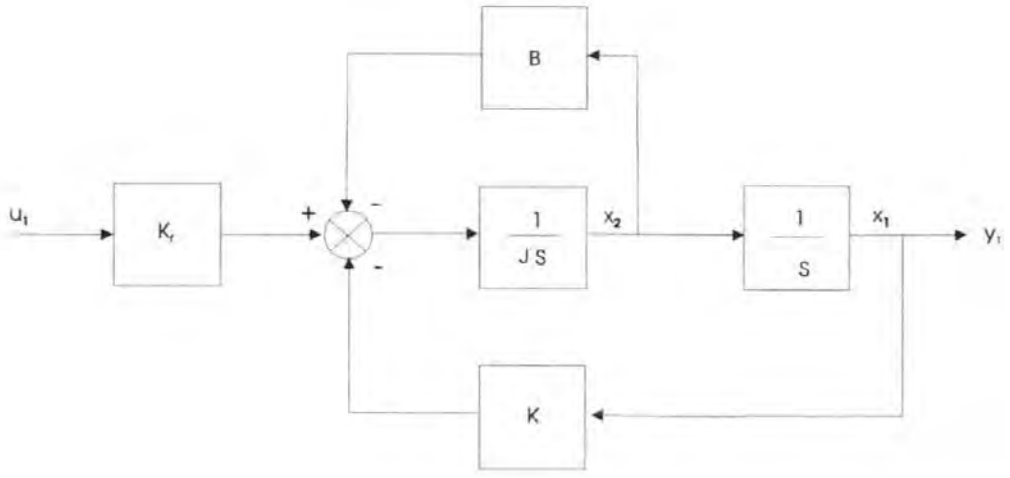

Figure 5.3 (b) Block diagram of a single voice coil motor actuator.

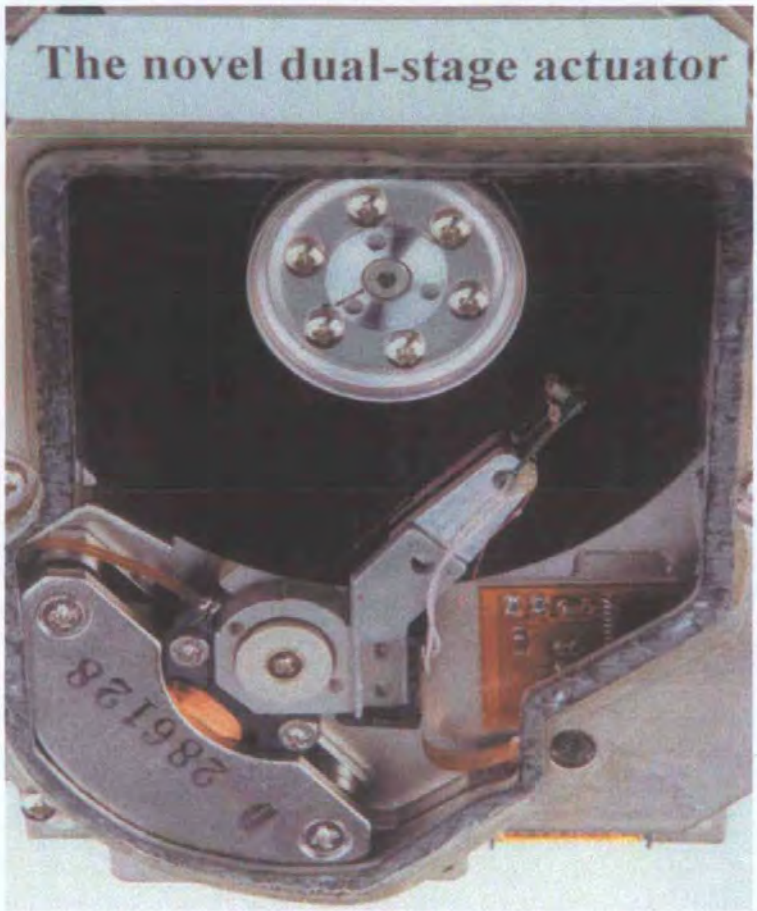

Figure 5.4 A photograph of the rotary dual-stage actuator.

5.3 Piezoelectric Bimorph Fine Actuator

Optical disk drives (CD-ROM or magneto-optical drives) use microactuators for precise positioning. However, there are different forms of microactuators for hard disk drives.

The magnetic head in a hard disk drive is much smaller than an optical head. An optical disk drive has one head generally, but a hard disk drive has more than two heads. In order to incorporate many microactuators in one drive, each microactuator for the hard disk drive should have a very small volume and be lightweight (e.g. few mg).

The fine actuator may operate on electrostatic, electromagnetic, or piezoelectric principles.

An electrostatic micro-actuator consists of a rotational plate connected to the substrate by spring flexures. The plate is driven by interdigitated electrodes that are electrostatically activated to produce rotary motion. It yields a high bandwidth due to its low inertia. However fabrication is very difficult because of the many lithographic processes required.

The piezoelectric effect and the inverse piezoelectric effect were discovered by Jacques and Pierre Curie in 1880. These effects have been applied extensively in almost all kinds of electromechanical transducers, such as generators, sonic and ultrasonic transducer sensors, and actuator for micron and nenometer movement [Clegg et al., 1997].

Piezoelectric actuators include both composite actuators and flexure (or bimorph) actuators. The advantage of the composite actuators is its very high resonant frequency of over 20 kHz. The disadvantages include starting-up, high drive voltages, larger volume, smaller displacement and high cost. In the case of piezoelectric (PZ) ceramics flexure actuators, high deflections are possible, but the blocking forces and resonant frequency are relatively low.

5.3.1 Design and optimisation of the PZ actuator

The operation principle of the bimorph (flexure) actuator, which is used in this project, is shown in Figure 5.5. A voltage is applied to the plates in such a way that one plate contracts while the other expands and since the plates are glued together, they bend.

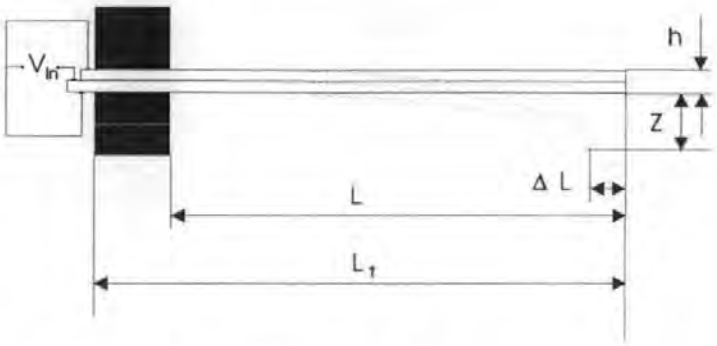

Figure 5.5 The operation principle of a PZ bimorph actuator.

Both plates are polarised in the same direction and can be connected in parallel. This offers higher sensitivity and the possibility of applying a bias voltage to generate an electric field parallel to the direction of polarisation, thus eliminating the risk of depolarisation.

As described previously (page 161), the deflections possible with this actuator are high (up to a few hundreds μm) but blocking forces are relatively low. The elements are generally thin, long and compliant. Stiffness is low and so is the resonant frequency. The main characteristics of interest are defined as [Waander, 1991]:

Deflection (Z) = $(K_z \times L^2 \times V)/h^2$ (m/V)

Blocking force (F) = $(K_f \times h \times W \times V)/L$ (Newtons/V)

Resonant frequency (f_r) = $(K_f \times h)/L^2$ (Hertz)

Capacitance (C) = $K_c \times L_t \times W)/h$ (Farads)

where, h = thickness, L_t = total length, L = free length, W = width and Z is deflection. K_z, K_f and K_c are constants which are dependent on the material of bimorph.

When used as a fine actuator in a disk drive, it is necessary to optimize the possible combination of deflection, resonant frequency and blocking force in advance. Multiplying the Z and f_r above and inserting $V = Eh/2$, gives:

$$Zf_r = 0.18 \times 10^{-6} E \qquad \text{mHz/V} \qquad (5\text{-}2)$$

This means that the product of deflection and resonant frequency is a constant for a given field strength. In practical applications this field strength is limited by the effects of depolarisation and flashover or breakdown. The DC field opposing the direction of polarisation is limited by the PZ material, e.g. the alternating fields for PXE 5 can be up to 500 V/mm, and if a bias field is used, the practical limit (in air) increases to 1 kV/mm. Therefore for an alternating voltage of 500 V/mm, the resulting relation is $Zf_r = 90\times10^{-3}$ Hz m/V. For this actuator any combination of Z and f_r may be chosen by varying dimension (e.g. the free length and thickness) of the bimorph element and drive voltage, as well as material of the bimorph element.

According to the above discussion, any combination of Z and f_r for the actuator designed for this project may be chosen by varying the free length and thickness, as well as material of the bimorph element.

5.3.2 Results and discussions

5.3.2.1 Results

The size of the PZ fine actuator, used in this project and shown in Figure 5.4, is 15×1.5×0.6 mm (free length 8.2 mm). Its type number is EB-T-320 made by NTK Co. in Japan. The characteristic properties were measured as: maximum deflection of 4 μm, f_r = 2.7 kHz, F_{max} = 0.3 N, $C = 2 \bullet 10^{-9}$ F, when drive voltages are 60 V and the MR head and the small spring mass is 11 mg. Curve A is obtained when the drive voltage increases from 0 to 60 volts. Curve B is obtained when the drive voltage reduces from 60 to 0 volts. The displacement is observed on a TV monitor of a BH-Z microscope with supported the resolution which is that 1 cm length on the TV screen (21″) is equal to 3.15 μm (of course light wavelength limits the resolution). The relationship of the fine

actuator's displacement in the radial direction of the disk and the voltage applied to the bimorph is shown in Figure 5.6. Hysteresis and creep phenomena of the piezoelectric bimorph plate ensure that the two curves do not overlap.

The relationship of load and resonant frequency of a fine actuator with PZ bimorph of dimensions 15×1.0×0.6 mm (free length 8.2 mm) is shown in Figure 5.7. In this experiment, the effective mass of the bimorph is 70 mg and the mass of the slider and small load spring is 11 mg (the load). Then the resonant frequency of the fine actuator is about 2.7 kHz, which was measured by using the method described as follows: in the measurement, the PZ bimorph is used as a sensor of measuring the mechanical vibration when a shock force is applied to the end of the bimorph. The resulting waveform of resonant frequency of the actuator can be seen and measured on a scope.

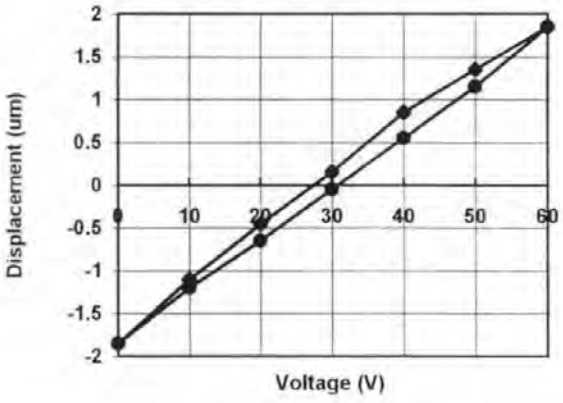

Figure 5.6 Displacement versus voltage of the fine actuator.

Figure 5. 8 shows the response of the bimorph to a step input. This shows the time constant of the actuator to be approximately 0.35 ms, which was measured by an ultra-high speed microscope described in the section 3.4.4.

Since charge constants d_{33} of PZ material (d_{33} is the induced strain per unit electric field in direction 3) and d_{31} of PZ material (d_{31} is the mechanical strain induced in

positive temperature coefficients [Waander, 1991], the displacement of a PZ actuator increases with increasing temperature. A similar result was found by experiment in the PZ fine actuator.

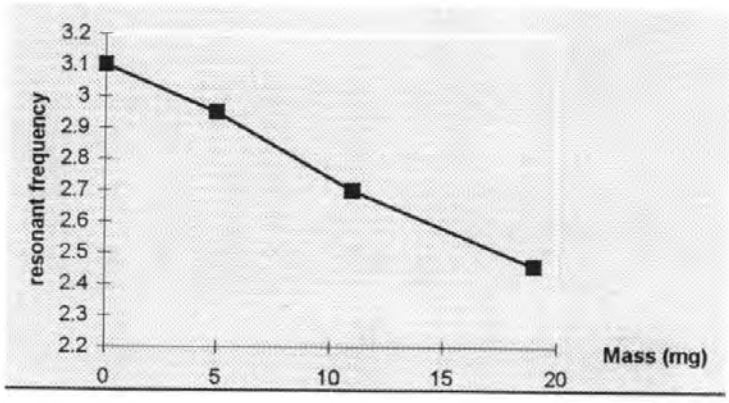

Figure 5.7 The relationship of load and resonant frequency of the PZ actuator.

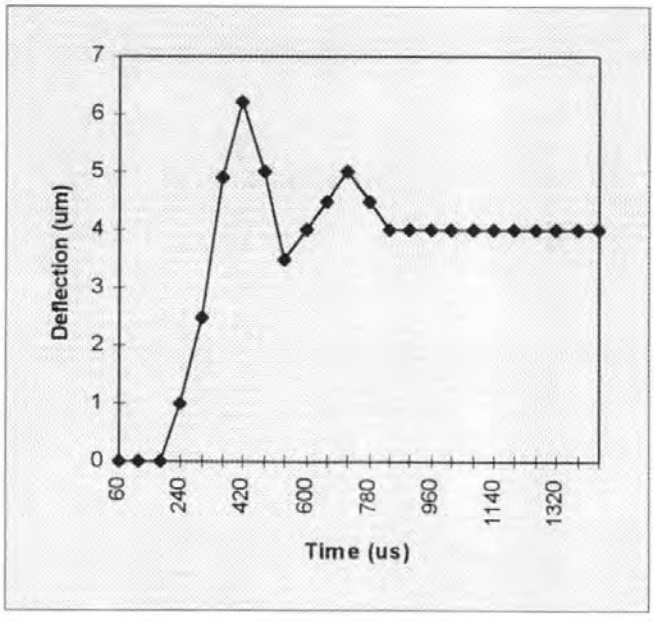

Figure 5.8 A step response of the PZ actuator.

If the operating voltage on the PZ microactuator is set to a new value, it can be seen, after the actual expansion, that a slow drift occurs in the same direction as shown in Figure 5.9. In the experiment, the dimension (45×3×1.0mm) of PZ was used rather than the dimension (15×10×0.6mm) of the PZ fine actuator, because the drift for the PZ fine actuator with dimension (15×10×0.6mm) is difficult to see by the BH-Z microscope. In the experiment (step drive voltage is 0 to 280 V), this drift is closely associated with the hysteresis behaviour and is caused by a follow-up polarisation of the ceramic. The drift is very small (3%~4 %) and decreases logarithmically in time, so that a certain percentage of the path is slowly moved every time cycle. However, closed loop control can overcome the drift.

Multilayer PZ bimorph actuators can be produced with the layer thicknesses as low as 20 or 40 μm. The elongation per unit length or height is roughly the same as for "classical" actuators. The difference is that the effect is reached for a much lower voltage. The lower drive voltage (e.g. 12 V) means simpler hard disk drive circuits. Figure 5.10 shows the performance of a typical multilayer flexure mode actuator [Waander, 1991]. This performance could be used as the next generation of PZ actuator. This will be further discussed in the Section 5.5.

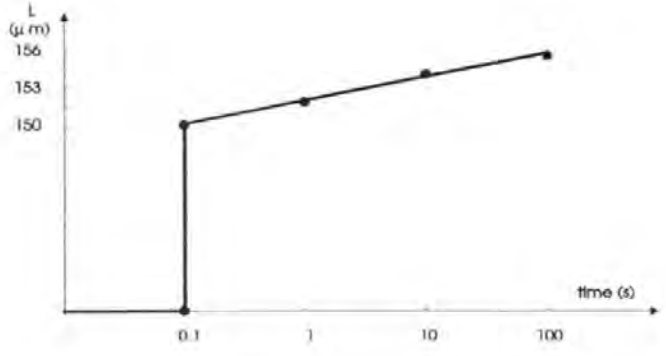

Figure 5.9 Drift phenomenon of the PZ fine actuator.

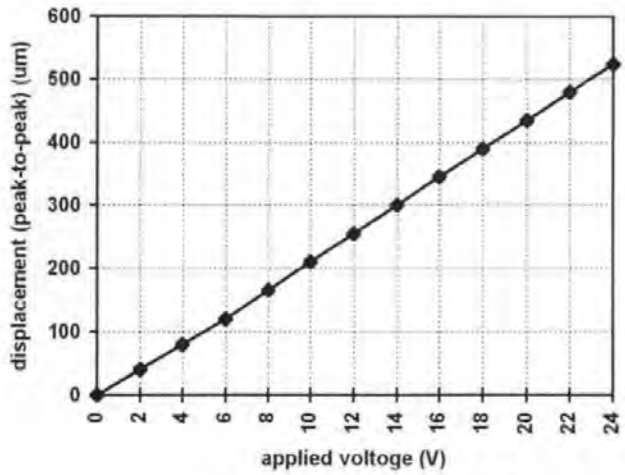

Figure 5.10 Applied voltage vs. deflection for a multilayer bimorph actuator

In general, the PZ bimorph fine actuator has 4 μm deflection when the drive voltage is 60 V, resonant frequency of 2.7 kHz with load of 11 mg. The time constant is about 0.3 ms. These characteristics are suitable for the application in this project. Even though it has positive temperature coefficients and a drift of 3-4 %, closed loop control can overcome them. The fine actuator with VCM actuator has successfully driven the servo head following 0.7 μm tracks at low rotating speed, because the servo head can not fly on disk. According to performance of the fine actuator, it could be used at high rotating speed (e.g. 3600 rpm).

5.3.2.2 Comparing single actuator and dual-stage actuator

When recorded trackwidth is reduced, the servo system bandwidth has to be increased because positioning accuracy of the system must be increased. It is clear that

the dual-stage actuator has to be used if the trackwidth is reduced to submicron size in a HDD because of the power required and the stiction/friction of the VCM actuator.

To increase the servo bandwidth one must increase the servo loop gain to be able to respond quickly enough to keep below the allowable track misregistration (TMR) values. For the VCM actuator this can only be done by increasing the power. The power required by the actuator to follow a given frequency is proportional to the fourth power of the frequency (see Eq. (1-27)). For example, consider a disk drive at fixed track density. Increasing the spindle speed in this drive from 3600 rpm to 5400 rpm will require a one and half of the bandwidth and a 5-fold increase in actuator driver power to maintain the same TMR specifications when other conditions are similar. This solution to increase servo bandwidth does not meet the objectives of tomorrow's HDD's.

It is well known that for rotary mechanical actuators, the ratio of torque constant (K_t) to inertia (J) increases as the force factor decreases. This suggests the use of a dual-stage actuator, in which a fine actuator rides on the VCM (coarse) actuator. In such a system if the ratio (K_t/J) could be increased by a factor of 5 over the coarse actuator, then the track-following bandwidth over a few track pitches could be increased by a factor of 1.5. The power required to achieve this bandwidth with a two-stage actuator would be reduced by a factor about 5×5 when compared to the coarse actuator [Fan et al., 1995].

On the other hand, very low angular velocity in the VCM actuator increases the stiction/friction hysteresis in the actuator bearing, causing the servo system to go into a small but troublesome limit cycle behaviour due to the hysteresis [Koizumi & Kuroda, 1990]. This hysteresis may change irregularly with temperature and humidity, and may vary across the disk drive population. Thus, hysteresis is difficult to predict, and has a

considerable effect on system performance. It especially affects actuator positioning for submicron-meter displacement. The maximum hysteresis in the fine PZ actuator was approximately 5 volts (Fig. 5.6), which indicates the possibility of limit cycle behaviour. However, practical observations of the system under normal operating conditions did not show any sign of limit cycle oscillations. From this it is concluded that limit cycles do not seriously affect the operation of the designed dual-stage actuator. It is therefore suggested to use a dual-stage actuator.

5.3.2.3 Comparing PZ bimorph actuator and electrostatic microactuator

1. Driving force

The magnitude of the driving force of a microactuator is very important. The electrostatic driving force is expressed by [Fan, 1996].

$$F_x = \frac{\varepsilon_0 t}{2g} V^2 \tag{5-3}$$

where, ε_0 is the electric (space) constant, V, g and x are the voltage, gap and overlap between two electrodes respectively, and t is the thickness of the electrodes. The driving force for PZ actuator is

$$F_x = \frac{d_{31}}{K_{pz}} \bullet V \tag{5-4}$$

It should be seen that the driving force of the PZ actuator and the electrostatic actuator are proportional to $\frac{d_{31}}{K_{pz}}$ and $\frac{\varepsilon_0 t}{2g}$ respectively and $\frac{d_{31}}{K_{pz}}$ (i.e. 4×10^{-3}) is much greater than $\frac{\varepsilon_0 t}{2g}$ (i.e. 3×10^{-6}). Therefore, achieving a lower driving voltage for an electrostatic microactuator is more difficult than that for PZ actuator if a large driving

force is needed, even though the driving force of an electrostatic actuator is proportional to the square of the applied voltages.

2. Resonant frequency

An accurate analytical expression [Tang, 1989] for the fundamental lateral resonance frequency, f_r, is:

$$f_r = \frac{1}{2\pi}\left(\frac{2Eh\left(w/L\right)^3}{M_p + 0.3714M}\right)^{1/2} \tag{5-5}$$

where, M_p and M are the masses of the plate and the supporting beam; h, w and L are the thickness, width and length of each beam respectively.

Eq. (5-5) does not consider the mass of the load. In the case of a microactuator, f_r is as high as 9 kHz for a very light movable mass of 45 μg [Fan et al., 1995].

In [Fan et al., 1995], the curve of load via f_r has not been reported. However, in general the resonant frequency of a system capable of oscillating is dependent on its elastic properties and system mass. The resonant frequency of an electrostatic microactuator or PZ microactuator is also subject to this law, whereby the effective mass is a function of both the mounting of the element and of any other masses which are attached to it. An external mass that is attached to the actuator causes a reduction in the resonant frequency f_r. The resonant frequency of an installed actuator can always be compared to the resonant frequencies of actuators which are restrained only on one side and have no load.

In the case of a PZ actuator, we have

$$f_r' = f_r\sqrt{\frac{m}{m+2M}} \tag{5-6}$$

where, m is the mass of PZ microactuator on its own; M is an external mass; f_r is the resonant frequency without the load and f_r is the resonant frequency with the load.

As can be seen, equation (5-6) is suitable for an electrostatic microactuator. Generally the mass of a PZ actuator is much greater than the load (such as the slider of a magnetic head). Results in Figure 5.7 agree with Eq. (5-6). The higher resonant frequency (f_r) of an electrostatic microactuator can be obtained when the MR head is only very light, however, the external mass slightly reduces the f_r of the PZ actuator because its mass is much greater than the mass of electrostatic actuator.

3. Mass of actuator

The magnitude of the mass of the microactuator is also important for the bandwidth of the actuator. New terms F_p (driving force per unit mass) and M_p (driving moment per unit mass) are defined here. For example, in Ottesen's work [Ottesen, 1994], the mass of the rotary microactuator is 10 mg. In this project, the PZ microactuator has a mass of about 70 mg. Because Ottesen did not describe the magnitude of the force moment, the M_p of the electrostatic microactuator cannot be directly compared with the M_p of the PZ microactuator.

In general the driving force of the PZ microactuator (0.3 N) is about a thousand times greater than that of electrostatic microactuator (0.3 mN) [Horowitz, 1995]. Therefore, the equivalent mass of a PZ actuator for the same driving force is much smaller than that of an electrostatic microactuator, even if the mass of the PZ actuator is greater than that of electrostatic one.

4. Non-linearity

Non-linearities exist in all actuators. The non-linearity of the electrostatic actuator is also dependent upon the finite size of electrodes [Fan, 1996]. This means

that $\frac{\partial C}{\partial x} \neq a$, where a = constant, C = capacitance, x = x-axis distance. At the drive part, the static displacement x as a function of drive voltage is given by

$$x = \frac{\partial C / \partial x}{2K_{sys}} \bullet V^2 \tag{5-7}$$

where K_{sys} is the system spring constant and V is the drive voltage.

For a PZ microactuator, $x = K_{pz} \bullet V$ (5-8)

It can be seen that the relationship between x and V is linear for the PZ actuator and quadratic for the electrostatic one. Strictly speaking, the relationship for the PZ actuator is not absolutely linear because of the dielectric hysteresis of the PZ material (see Figure 5.7). In general, the linearity of the PZ microactuator is much better than the electrostatic one.

5.Temperature effects

The properties of PZ actuator are more temperature dependant than those of the electrostatic actuator. Using adaptive control for the head servo system can help eliminate this effect.

6. Cost

The electrostatic microactuator is built by silicon surface micromachining technology. The fabrication process is complex and expensive and fabrication technology is still developing. The classical fabricating process for the PZ bimorph actuator (called the screen printing process) has been developed for many years and it is much easier and cheaper than that for the electrostatic microactuator.

5.3.2.4 Comparing PZ bimorph actuator and PZ axial actuator

At the beginning of section 5.3, a PZ axial actuator has been compared with a PZ bimorph actuator. Here are some further discussions.

The bonded layer between the PZ rings increases the hysteresis because the PZ axial actuator is stacked by many PZ rings and the bond is not rigid. So the glue lines cannot be so thin as that of a PZ bimorph actuator (see Figure 5.6 and [Mori et al., 1991]), even though both actuators are built up using the same PZ material.

A large drive force is a great advantage for a PZ axial actuator, but it is not necessary in this application since the mass of head is smaller than 10 mg. Normally, the equivalent capacitance of a PZ axial actuator (e.g. 130 nF in [Mori et al., 1991]), is a few hundreds of times greater than that of a PZ bimorph actuator (e.g. 720 pF in Figure 5.4, which is used as the fine actuator in a hard disk drive [Mori et al., 1991].) So the actual resonance frequency is lower than that defined in theory, because the bandwidth of the drive source is limited. However, a similar effect has not been seen in the PZ bimorph actuator, due to its smaller equivalent capacitance.

5.3.2.5 Improving the PZ bimorph dynamic behaviour by modifying the drive circuit

Figure 5.11 shows details of the circuit of a PZ actuator. Suppose that the charge and discharge resistances of the drive circuit are R_c *(f)* and R_d *(f)* respectively. R_c *(f)* and R_d *(f)* are proportional to the frequency, and under normal operating conditions R_d *(f)* is greater than R_c *(f)*. Therefore the rising voltage $V_c(t)$ and decaying voltage $V_d(t)$ on the PZ actuator (as a function of time) are respectively

$$V_c(t) = V\left(1 - e^{\frac{t}{R_c(f)C}}\right) \tag{5-9}$$

$$V_d(t) = V \bullet e^{-\frac{t}{R_d(f)C}} \tag{5-10}$$

where C is an equivalent capacity of the PZ bimorph and V is the target voltage. The voltage rises or drops exponentially with the time constant $R_c\ (f)C$, or $R_d\ (f)C$.

The ideal dynamic behaviour can be obtained when $RC < \frac{T_r}{10}$, where T_r is the periodic time at the resonance of the PZ bimorph actuator. Once the bimorph is selected, the magnitude of C will be fixed, so it is only possible to reduce RC by reducing R (R is $R_c\ (f)$ or $R_d\ (f)$).

In order to ensure the close loop stability of the drive circuit for PZ bimorph, the bandwidth of the system is limited. When the frequency increases, $R_c\ (f)$ increases and in particular $Rd\ (f)$ will be increased very quickly.

Figure 5.11 displays a part of circuit shown in Figure 3.8. The PZ actuator dynamic behaviour has been improved by using this design of drive circuit.

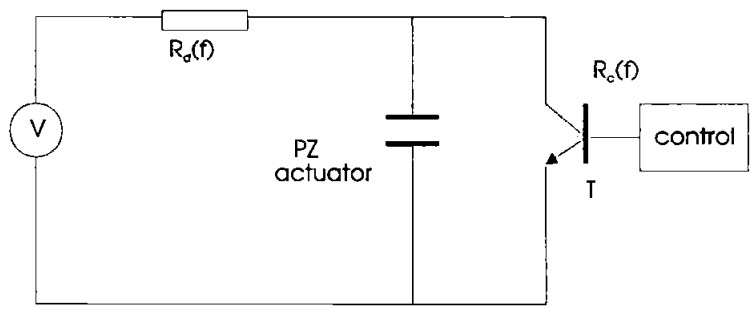

Figure 5.11 Diagram of the pull down circuit.

In this circuit, when the voltage has to be reduced, the power field effect transistor T is switched on. The voltage is directly discharged by T. $R_d\ (f)$ is the on-resistance of T (such as 0.2 Ω at f = 1 MHz). The output capacity of the transistor can be neglected if it is a high frequency transistor (such as a few tens pF at f = 1 MHz).

Therefore, by optimising the design of drive circuit, the dynamic behaviour has been improved and successfully used in the project.

5.3.2.6 Higher operating frequency

The bimorph actuator used in a hard disk drive is operating at higher frequency when track following. Three factors should be kept in mind.

First the hysteresis losses in the materials heat up the actuator and can increase the maximum displacement. Second, the construction between the head and bimorph should be as compact as possible to avoid spurious resonance below the main resonance of the actuator. Third, inserting a notch filter at this frequency which is the main mechanical resonance of the bimorph actuator, should be effective in reducing the resonance and increasing servo stability, i.e. the phase margin.

5.4. New structure between head and actuator

Usually the slider of a head is connected to the actuator by the head suspension which support provides the loading forces between the head and disk. In the study by Naruse et al. [Naruse et al., 1983], it was shown that the suspension resulted in an output from the position channel for a rotary actuator. In the design for this project (see Figure 5.12), using a PZ bimorph to replace the suspension does not produce the adverse affects on servo performance. The very small load spring offers a loading force of 0.1mg. The spring has almost no vibration in the radial direction. In the Fig. 5.12, the slide with MR sensor and the small spring is taken from a commercial MR head. The spring is fixed at end of a PZ bimorph and turned 90° to the normal direction. There is no data MR sensor on the slide. The drawn data MR sensor indicates relative position between the data and servo MR sensors.

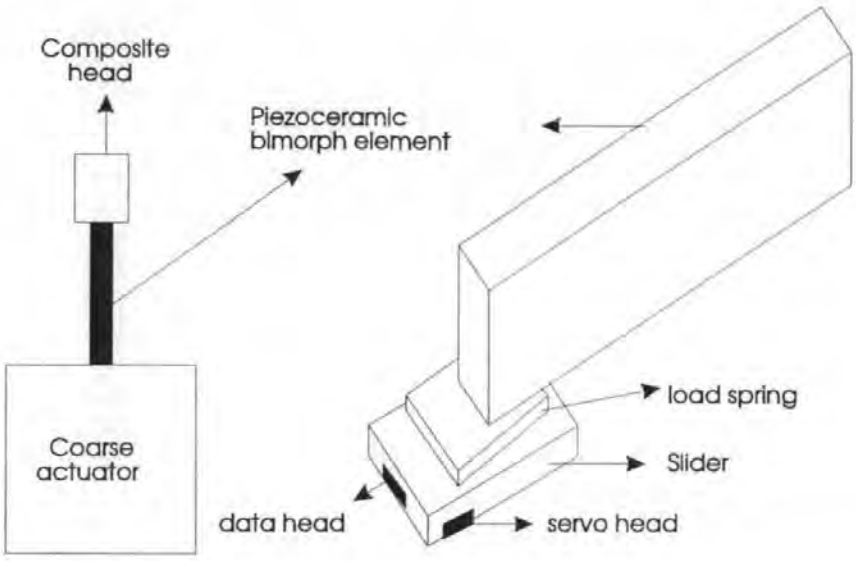

Figure 5.12 The structure of the data/servo MR composite head.

Figure 5.13 shows a frequency response of the head/suspension/actuator measured by HP 4195 Network/spectrum Analyzer. In the measurement, the PZ bimorph is used as a sensor measuring the mechanical vibration when a shock force is applied to the end of the bimorph. The resulting spectrum waveform of resonant frequency of the actuator can be seen and measured. The above dual-stage actuator has successfully driven the head with the new structure following 0.7 μm tracks. The first peak is the resonance frequency of the PZ bimorph. The second and third peaks are produced by the load spring and are much smaller (-60 dB) than the first peak.

It is important in the small disk drive that the fine actuator is a part of the structure of the data/servo MR composite head. Further discussion of this point is provided in the next section.

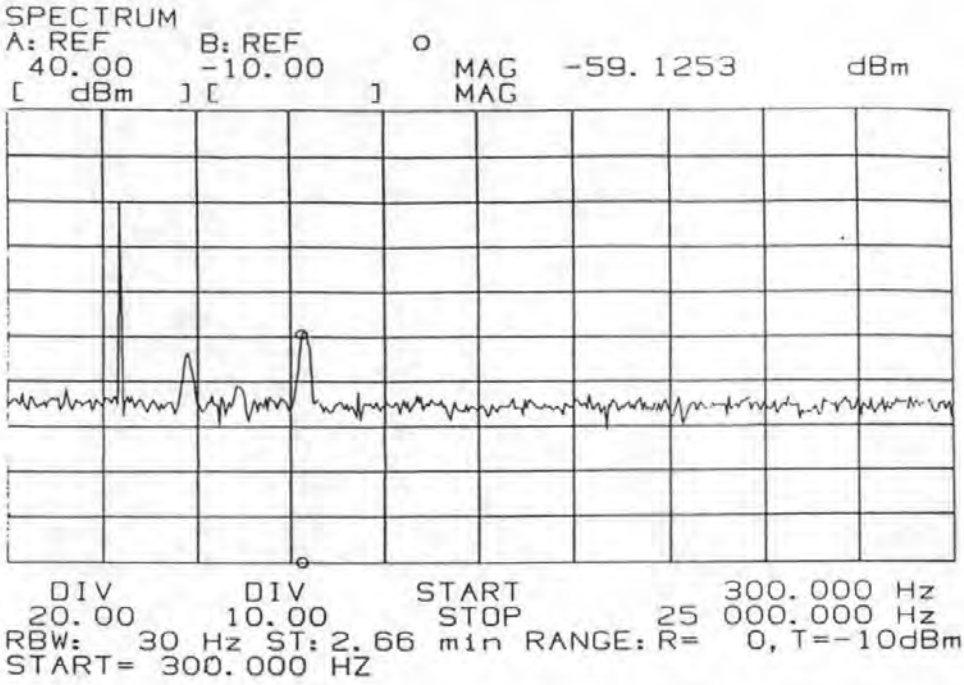

Figure 5.13 A spectrum of the head/suspension/actuator.

5.5 Consideration of an integrated fine actuator

Servo systems with 100 kTPI, necessary for recording density of 100 Gb/in^2, may need a fine actuator with a moving region about 1 μm and a resonant frequency over 3 kHz [Miu & Tai, 1995]. In such an application, construction of the magnetic head may employ a magnetoresistive integrated slide/suspension head such as the Censtor's integrated head [Hamilton, 1991]. The actuator of PZ thin film for positioning with micron and nenometre precision have be developed by Jenkins and Clegg et al. [Jenkins & Clegg et al., 1996] & [Jenkins & Clegg et al., 1998]

In order to meet the need for ultra-high track recording density, the multilayer piezoelectric film in the new design will be deposited on one or two of the sides of the suspension of the integrated head, as shown in Figure 5.14. In this case, the form of parallel bimorph would be employed. Figure 5.15 shows the mechanical model of the new integrated fine PZ actuator.

Figure 5.14 (a) A new Idea of integrated fine actuator.

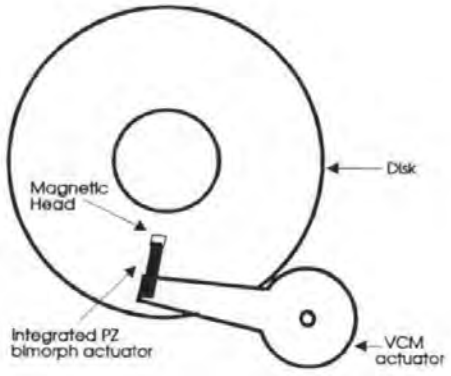

Figure 5.14 (b) A new structure of the integrated fine actuator and a VCM.

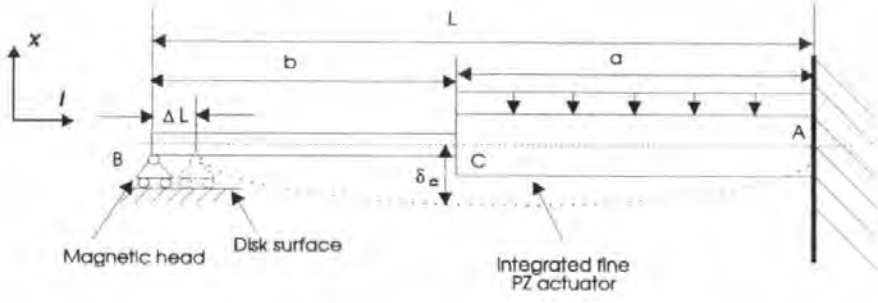

Figure 5.15 The mechanics model of the new integrated fine PZ actuator.

According to the model, the deflection δ_c at point C can be calculated as follows.

(1) The deflection at the point $x = B$, is $\delta_x = \dfrac{qa^4}{8E_aI_a} + \dfrac{qa^4}{6E_aI_a} = \dfrac{7qa^4}{24E_aI_a}$ (5-11)

where, q is the uniform load intensity generated by the integrated PZ multilayer; E_a and E_b are Young's module for the beams a and b.

(2) The deflection at the point $x = B$ produced by the reaction P at the point A is

$$\delta_x^{'} = \frac{8Pa^3}{24}\left(\frac{7}{E_aI_a} + \frac{1}{E_bI_b}\right) = \frac{Pa^3}{3}\left(\frac{7}{E_aI_a} + \frac{1}{E_bI_b}\right) \tag{5-12}$$

(3) The deflection at the point B is equal to zero, that is $\delta'_x = \delta_x$, as the loading force of a magnetic head is

$$P = \frac{7qaE_aI_aE_bI_b}{8E_aI_a\left(7E_bI_b + E_aI_a\right)} \tag{5-13}$$

(4) The deflection at the point $l = c$ produced by q is

$$\delta_{xc} = \frac{qa^4}{8E_aI_a} \tag{5-14}$$

(5) The deflection at the point C produced by P is

$$\delta_{xc} = \frac{Pa^3}{3E_aI_a} + \frac{P \bullet a \bullet a^2}{2E_aI_a} = \frac{5Pa^3}{6E_aI_a} \tag{5-15}$$

So the total deflection at the point C is

$$\delta_c = \frac{qa^4}{8E_aI_a} - \frac{5}{6} \bullet \frac{a^3}{E_aI_a} \bullet \frac{7qaE_bI_b}{8\left(7E_bI_b + E_aI_a\right)} = \frac{qa^4}{8\left(E_aI_a\right)}\left(1 - \frac{5}{6} \bullet \frac{7E_bI_b}{7E_bI_b + E_aI_a}\right) \tag{5-16}$$

Suppose that the deflection curve for the composite beam is a circular arc of constant curvature, then

$$\frac{1-\cos\alpha}{\alpha} = \frac{\delta_c}{a} \tag{5-17}$$

and

$$\Delta L = L\left(1 - \frac{\sin\alpha}{\alpha}\right) \tag{5-18}$$

that is

$$\Delta L = f(V, K_F, E_a, E_b, I_a, I_b, a, b) \tag{5-19}$$

where α is half of the angle subtended by this arc.

Therefore, a linear relationship between ΔL and V may be obtained by careful choice of the parameters of Eq. (5-19).

Comparing with other fine actuators, the new design has many advantages.

1. very low drive voltages such as + 12 V can be achieved by using a very thin piezoelectric multilayer.

2. high resonance frequency because of the low mass resulting from the integrated construction.

3. much easier to fabricate than the electrostatic microactuator.

4. the loading force of the head can be easily controlled (see Eq. 5-13), which is very important for contact recording. As indicated in Eq. (5-13) and Eq. (5-18), ΔL and P can be controlled by the applied voltage on the PZ actuator. A desired loading force could be produced by applying a fixed drive voltage to the actuator. At this point, small changes of drive voltage, around the fixed drive voltage, could be insensitive for the loading force but could still produce the desired displacement in the radial direction (see Fig.5.14 (b)) as the required displacement is very small (i.e.1 μm). Therefore by optimising the design of the actuator through selecting various parameters in Eq. (5-19), the required relationship between ΔL and P for a specific application can be achieved. Since the loading force of the head can be controlled easily, it is possible to apply a bigger load force when reading and writing, and a smaller load force in other cases to reduce the head wear.

5. has the potential of improving linearity by selecting low dielectric hysteresis.

6. the low drive voltage reduces the temperature sensitivity of the bimorph.

5.6 Summary

The reasons for using a dual-stage actuator are discussed in section one. A single voice coil motor actuator with low resonant frequency (such as 600 Hz) limits the servo

bandwidth. A dual stage actuator with a bandwidth higher than 2 kHz can meet the needs of the positioning and following servo system for submicron trackwidth.

In section 5.2, a mathematical model for a rotary dual-stage actuator is developed and a block diagram of this model is given.

The overall performances of a fine actuator (PZ bimorph actuator) is described in section 5.3. Experimental results are presented and discussed, such as the spectrum of the resonant frequency f_r, the drift of deflection with temperature, step response and the relationships between the deflection and the applied voltage, load and resonant frequency.

Comparison of a PZ bimorph actuator with an electrostatic microactuator have shown that the PZ actuator may be much better than the electrostatic microactuator. Specific improvement includes a lower driving force, increased linearity, and increased resonance frequency with a load as well as lower cost. The comparison between a PZ bimorph and an axial PZ actuator was also made. The drive circuit has been optimised and used for improving the dynamic behaviour of the PZ bimorph. The operating performance of PZ actuator at high frequency is analysed.

In section 5.4, the development of a new structure between head and actuator is described. It is shown that the mechanical resonant frequency of the microactuator can be improved by using this new design.

In section 5.5, a new consideration of integrated fine actuator is presented. The ideal performance of the actuator could be obtained by optimising related parameters. The main advantages of the new design, such as high resonance frequency, easier fabrication, very low drive voltages and controllability of the loading force of the head are discussed.

Chapter Six

Servo Controller

6.1 Introduction

The objective with a high-performance storage device actuator's servo control is to move the recording head from one track to another track, in the shortest possible time, within a specified off-track error limit. After the head has settled on the track, the servo must be able to keep the head on the track within the specified off-track error limits. Many controllers for HDD have been researched [Workman, 1987] [Jayantha et al., 1991] [Miu & Bhat, 1991] [Stich et al., 1987] with the aim of achieving higher track density. But until now the maximum TPI in these studies is still lower than 6000 and digital servo control has never been studied in HDD servo systems using dual-stage actuators. In order to demonstrate submicron track following and validate the new position sensor system and the new actuators, appropriate controllers for them are developed. The design of the controllers for the dual-stage actuator is discussed. The systematic design of a controller for single PZ actuator is also discussed. In this project, the MR head was turned 90° in non-normal operation condition and could only be run at very low speed resulting in a low sample rate because the number of servo pattern on the disk is fixed. Therefore simulation was used to investigate the characteristics of a full speed system.

6.2 Design of the servo controller for dual-stage actuator

6.2.1 Specification of the servo controller

In digital servo control, the values of the system parameters are represented by numbers which do not change with age or temperature unless programmed to do so. Digital control is inherently much more flexible than traditional analogue servo control [Franklin et al., 1990]. For this reason, digital servo control is employed for both the following mode and for seeking mode of the new controller.

The head positioning servo control system for 0.7 μm track (36 kTPI) consists of the position sensor subsystem, described in Chapter Four, the dual-stage actuator (shown in Figure 5.4) of Chapter Five and the controller in this section. The servo pattern of width of 0.7 μm on the disk for the position sensor was formatted by a submicron servo track writer (SSTW). 1535 servo patterns were written on each servo track of the disk. The servo pattern's bit length is about 6 μm and occupies about 6.8 % of the data area. The servo head is a shielded MR head with gap length 0.7 μm and track width of 4 μm.

The characteristic properties of the fine actuator in the dual-stage actuator are as follows:

1) Maximum displacement: 4 μm (drive voltage 60 V)

2) Resonant frequency: 2.7 kHz

3) Drive force torque (max): 0.53 Nm (drive voltage 60 V)

4) Return spring constant: 30 Nm/rad

5) Viscous damping coefficient: 0.0038 Nm/(rad/sec)

6) Inertia of moving mass 0.0011 kgm^2.

For the Voice coil motor,

1) Viscous damping coefficient: 0.0042 Nm/(rad/sec)

2) Resonant frequency	350 Hz
3) Actuator torque constant:	0.05 Nm/rad
4) Inertia of moving mass	0.013 kgm^2
5) Return spring constant:	10 Nm/rad
6) Demodulator gain	1 Volt/track
7) Track Pitch (TP)	0.7 μm

Takaishi (1996) used the system shown in Figure 6.1 to control a dual stage actuator [Takaishi et al., 1996]. A similar system was developed by Mori et al. in 1991 [Mori et al., 1991]. In Figure 6.1, it is acceptable to neglect the piezoelectric (PZ) microactuator's force to the voice coil motor (VCM) because the PZ actuator is lightweight (e.g. 50 mg) and its primary resonance frequency is high. In order to prevent the PZ actuator from going to the end of its stroke, the VCM controller C_{vcm} (s) must follow the movement of the PZ actuator. The open-loop transfer function of this servo system is calculated as follows,

$$C_{PZ}(s)\{P_{PZ}(s) + P'_{PZ}(s)C_{VCM}(s)P_{VCM}(s)\} \tag{6-1}$$

If the estimator of the microactuator, $P'_{pz}(s)$ estimates the movement of the microactuator completely, then, the above open-loop transfer function becomes

$$C_{pz}(s)P_{pz}[1 + C_{VCM}(s)P_{VCM}(s)] \tag{6-2}$$

Therefore, the VCM controller and piezoelectric actuator controller can be designed separately [Takaishi et al., 1996].

The difference between Takaishi's dual-stage actuator and this one is that in this system a PZ bimorph replaces the PZ axial actuator. A comparison of a PZ bimorph actuator and a PZ axial actuator can be seen in Section 5.3.2.4. From the controller design point of view, many characteristics are similar. However, in this project, the time

constant of the VCM actuator is about 10 times more than that of the PZ actuator. Consequently the VCM actuator works in a relatively low frequency region compared to the PZ actuator. This enables the VCM controller and piezoelectric (PZ) actuator controller to be designed separately.

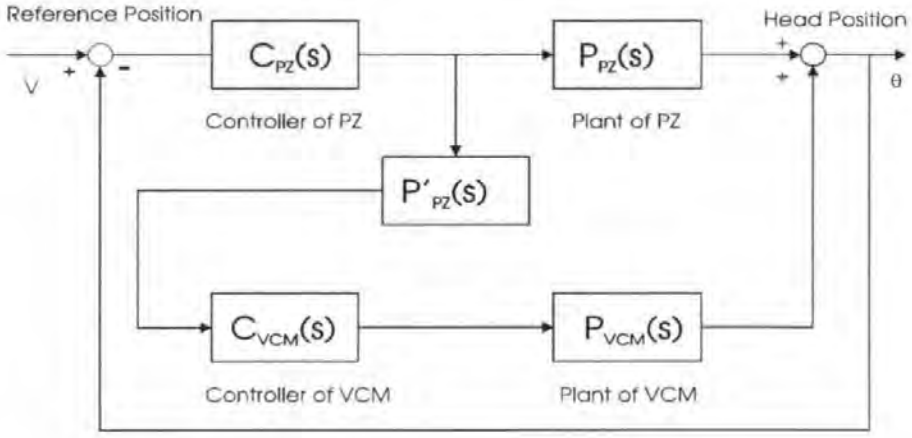

Figure 6.1 A controller for the dual-stage actuator [Takaishi et al., 1996]

6.2.2 MATLAB simulation of the VCM actuator and the PZ microactuator

Using Newton's law, the simplest open-loop plant transfer function is given as [Mee, 1989],

$$J\frac{d^2\Theta}{d^2t} + C\frac{d\Theta}{dt} + K\Theta = K_v V \tag{6-3}$$

where J is the inertia of the moving part of the actuator, C is the viscous damping coefficient of the system, K is the return spring constant, K_v is the motor torque constant, θ is the angular of the head and V is the input voltage.

Taking the Laplace transform of Eq.(6-3) and rearranging gives the transfer function

$$\frac{\Theta(s)}{V(s)} = \frac{K_v}{Js^2 + Cs + K} \tag{6-4}$$

Using the above characteristic properties of the VCM actuator and the PZ actuator, Eq. (6-4) becomes, respectively ($\Theta \approx \Theta_1 + \Theta_2$, and $\Theta_1 \gg \Theta_2$)

$$\frac{\Theta_1(s)}{V(s)} = \frac{0.049}{0.013S^2 + 0.0042S + 10} \tag{6-5}$$

$$\frac{\Theta_2(s)}{V(s)} = \frac{0.53}{0.0011S^2 + 0.0038S + 30} \tag{6-6}$$

It is necessary to transform Eq.(6-5) & Eq.(6-6) to the Z domain as a digital controller is to be designed. The equations can respectively be discretized as follows:

$$\frac{\Theta_1(z)}{V(z)} = \frac{(4.797z + 4.795)10^{-5}}{z^2 - 1.979 + 0.9984} \qquad (T_1 = 0.005\ S) \tag{6-7}$$

$$\frac{\Theta_2(z)}{V(z)} = \frac{(6.015z + 6.012)10^{-5}}{z^2 - 1.991z + +0.9981} \qquad (T_2 = 0.0005\ S) \tag{6-8}$$

Please note that in practice a single high speed A/D converter would be used. The low speed sampler T_1 is applied by software in the VCM controller.

6.2.3 Implementation of the compensator for the PZ microactuator

To analyze the model using the software in the Appendix Software E, it can be seen that the poles of Eq. (6-7) are very lightly damped and near the unit circle. Therefore, it is necessary to add a compensator to increase the damping of the system. A simple lead compensator [Franklin et al., 1990] will suffice, i.e.:

$$D(z) = k(z-a)/z \tag{6-9}$$

In order to study the design of the compensator, the software is developed using MATLAB as shown in Appendix E.

Simulation gives values for k and a of 7340 and 0.85 respectively in order to produce less than the specified 30% overshoot in response to a step input shown in Figure 6.3. Also the robustness of the design can be observed using the software. The values of k and a were varied by approximately 6% and the controller held the system within specification.

Figure 6.2 shows the Bode magnitude and phase plots of the open-loop frequency response.

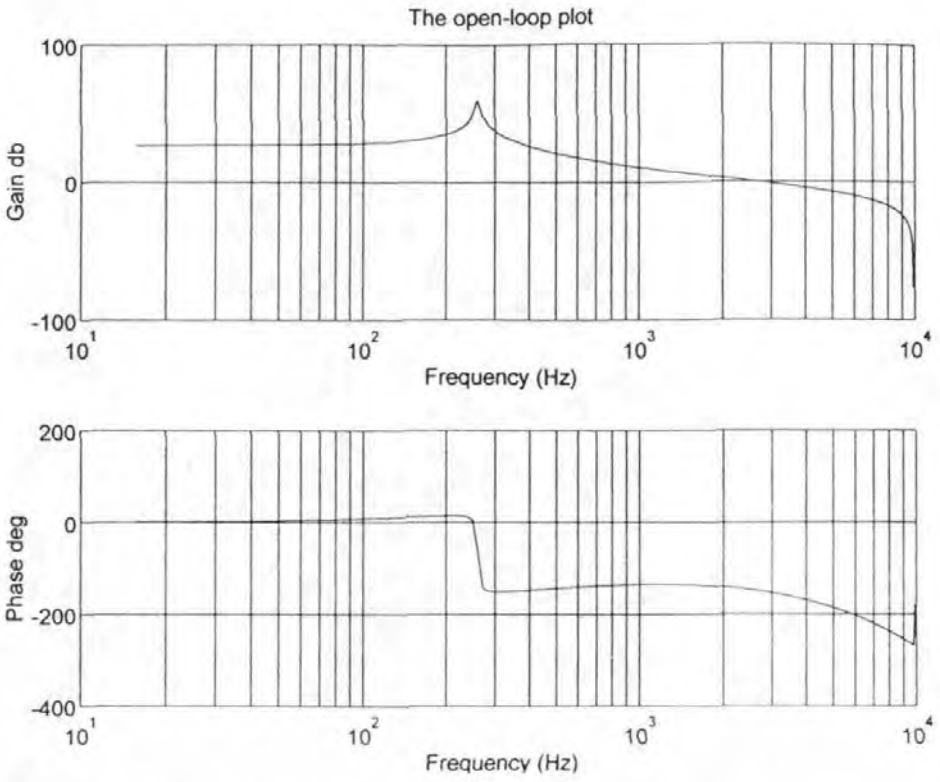

Figure 6.2 Open-loop frequency response of the PZ servo system.

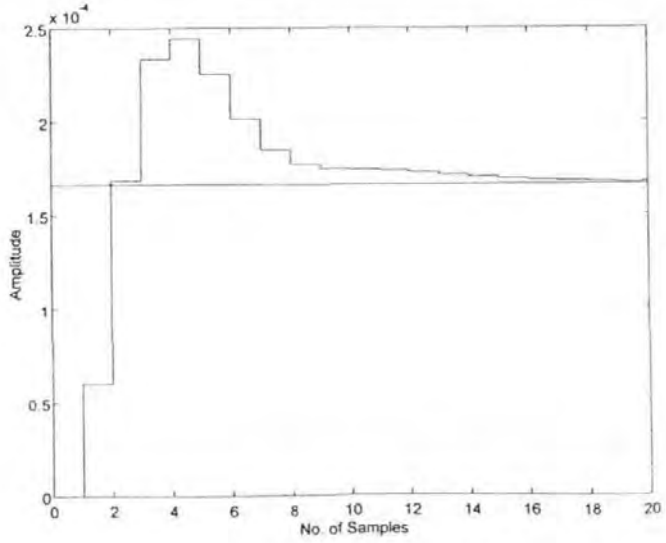

Figure 6.3 Step response of the compensated PZ servo system (T_2 = 0.5 ms)

Note that the design has a phase margin (PM) of 40° and a gain margin (GM) of 11 dB which are close to the required specifications. The bandwidth is about 2.4 kHz.

Figure 6.3 shows the closed loop step response. It is clear that the seek time (<3 ms) and the overshoot (<30 %) requirements have been met for the step response from the reference input.

6.2.4 Implementation of the compensator for the VCM actuator

The design of the controller for VCM actuator using MATLAB is similar to that of the PZ actuator. Figure 6.4 shows the corresponding Bode magnitude and phase plots of the open-loop frequency response, respectively. Simulation gives values for k and a of 4120 and 0.86 respectively for a step response, in order to produce less than the specified 30 % overshoot in Figure 6.5.

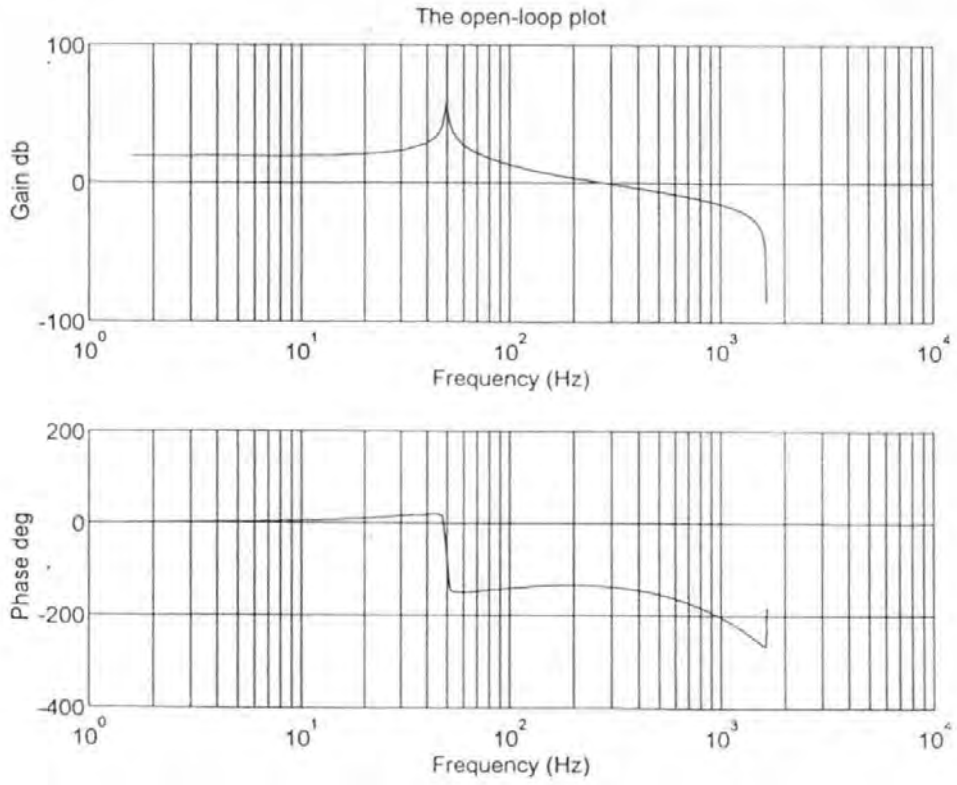

Figure 6.4 Open-loop frequency response of the VCM system.

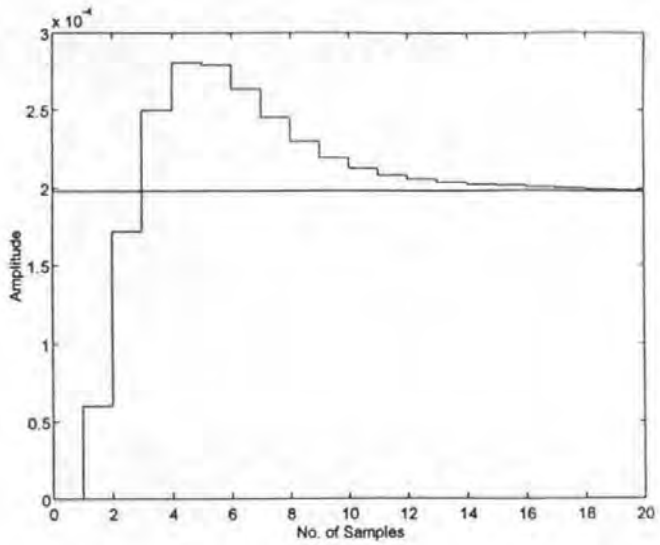

Figure 6.5 Step response for the VCM system (T_1 = 5 ms)

6.3 Design of a servo controller for a single PZ actuator

6.3.1 Specification of the servo controller

For the 10 Gb/in^2 project of the C.R.I.S.T. [Mapps, 1995] TPI and BPI will be 25.4 k tracks (trackwidth 1 μm) and 400 k bits respectively. The glass disk, of 1.8 inches in diameter, is coated with CoCrTa media and will be running at fixed speeds of 3600 rpm (± 0.1 %). An integrated read/write head can consist of a hundred MR/inductive heads with trackwidths of 1 μm [Mapps, 1995]. There is a gap of 100 μm between each of the MR / inductive heads, that is, there only are 100 data tracks between two these heads. It is necessary that these heads accurately position and follow 1 μm tracks with only 0.1 μm error when the disk is running at 3600 rpm.

The main requirements for the very accurate and very fast head servo control system for a single PZ actuator are:

1. Seek time : 1 ms track- track, max. < 18 ms any track

2. Servo bandwidth: 3000 Hz

3. Positioning and following error: 0.1 μm

4. Resolution: 0.04 μm

5. Magnetic trackwidth: 1 μm (TPI = 25, 400 tracks)

6. Positioning range: ± 75 μm

7. Disk rotating speed: 3600 rpm

Note that the positioning range includes the 100 μm between each of the heads and some eccentricity at the centre of the disk as the written servo pattern and the centre of rotation of the spindle motor are bound to differ. This difference was measured and found to be, in all cases, less than 25 μm.

6.3.2 Design of the controller hardware

Figure 6.6 shows a block diagram of a digital servo control of the disk drive designed to meet the desired specification.

In the Figure 6.6, the A/D is a TLC0820CLV with a transfer rate of 2.5 μs and resolution of 8 bits. The D/A is a DAC1208LCJ with transfer rate of 1 μs and resolution of 12 bits. The microprocessor is a DSP (32TMS50C) with 35 ns single-cycle fixed-point instruction execution time (28.6 MIPS). Sample rate in the servo system is 24 kHz. The period is 42 μs. In that time, the 32TMS50C is capable of executing 1142 fixed-point operations.

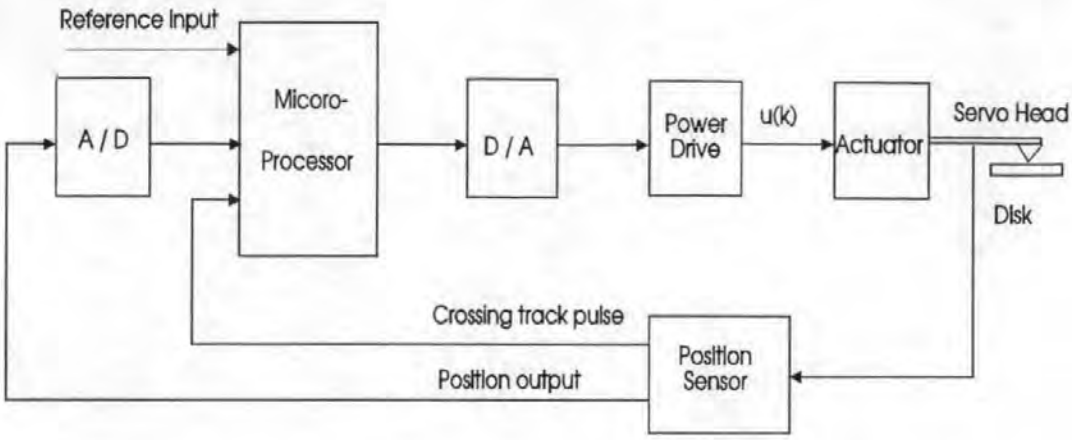

Figure 6.6 Block diagram of the digital servo control system.

6.3.3 Design of control algorithm

There are two basic modes of operation: track follow and track access mode. In the track follow mode, a Type 1 system is implemented with a three-state feedback: position, velocity (derived from an estimator), and integrated position.

The seek mode is implemented by causing the actuator velocity to follow a profile, stored in a look up table, which is pre-computed off-line and is a function of the distance to the target track.

Since only the position is available as a measurement both modes of operation use a 'reduced order estimator' to produce the estimated velocity and bias. An extra state is included in both the control algorithm and estimator to account for the time delay in computing the control effort. A parameter Γ_1 is used to achieve an adaptive control for the servo system. Figure 6.7 shows a design of block diagram of the overall software for this servo system, according to Eq. (6-13) to Eq. (6-17).

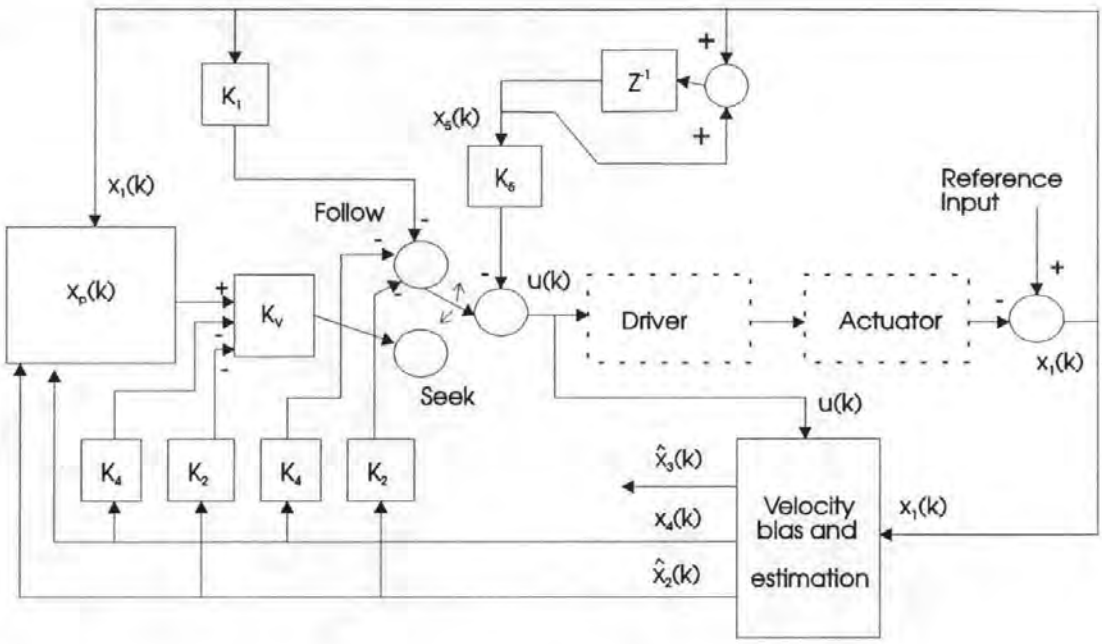

Figure 6.7 Block diagram of the overall software system

6.3.3.1 Mathematical model of the actuator

A model, preferably with a minimum number of states, that captures the relevant features of the dynamics is essential for practical realisation of real-time control algorithms. The state space description in discrete time [Ottesen, 1987] is give by:

$$\mathbf{x}(k+1) = \Phi\mathbf{x}(k) + \Gamma u(k) \qquad (6\text{-}10)$$

$$\mathbf{y}(k) = \mathbf{H}\mathbf{x}(k),$$

where

$$\Phi = \begin{bmatrix} 1 & 1 & \Gamma_1 & \Gamma_{11} \\ 0 & 1 & \Gamma_2 & \Gamma_{21} \\ 0 & 0 & 1 & 0 \\ 0 & 0 & 0 & 0 \end{bmatrix} \qquad \Gamma = \begin{bmatrix} \Gamma_{12} \\ \Gamma_{22} \\ 0 \\ 1 \end{bmatrix} \qquad \mathbf{H} = [1\ 0\ 0\ 0]$$

Note that the state variables x_1, x_2, x_3 and x_4 have been normalised in the description.

The above variable parameters are defined as following:

Defined	Unit
x_1 = position	track number
x_2 = velocity	tracks/second
x_3 = bias force	volts (equivalent drive input)
x_4 = delayed driver input	volts
x_5 = integrated position	track number
u = driver input	volts

Systems constants are:

Defined		Unit
K_m - driver constant	60	V/V
K_f - actuator force constant	0.004	N/V
m - delay time	50	μs
T_{pm} - trackpitch	10^6	tracks/metre
M - actuator moving mass	0.002	kg
K_d - demodulator gain	1	Volt/track
T - sample time	130	μs

These values represent realistic values for practical PZ actuators and are in agreement with published work.

Elements of plant control effort input matrix is

$$\Gamma_{11} = \Gamma_1[2m/T - (m/T)^2] = 0.3$$

$$\Gamma_{12} = \Gamma_1[1 - (m/T)^2] = 1.72$$

$$\Gamma_{21} = 2\Gamma_1 m/T = 1.55$$

$$\Gamma_{22} = 2\Gamma_1(1 - m/T) = 2.48 \qquad (6\text{-}11)$$

where $$2\Gamma_1 = \Gamma_2 = (K_m K_f T^2 T_{pm} K_d) / M \qquad (6\text{-}12)$$

6.3.3.2 Estimator algorithm

States of position, velocity and bias are required in high-precision position servo systems. But in this position sensor, there are no outputs of state velocity and bias. However the DSP (Digital Signal Processor) containing an approximate dynamic model of the electromechanical system can calculate the values of estimated velocity and bias. The digital estimator algorithm based upon Franklin's method is shown as follows [Franklin et al., 1990]:

$$\hat{x}_2(k+1) = \hat{x}_2(k) + \Gamma_2 \hat{x}_3(k) + \Gamma_{21} x_4(k) + \Gamma_{22} u(k) + L_2 P_s;$$

$$\hat{x}_3(k+1) = \hat{x}_3(k) + L_3 P_s; \qquad (6\text{-}13)$$

$$P_s = x_1(k+1) - x_1(k) - \hat{x}_2(k) - \Gamma_1 \hat{x}_3(k) - \Gamma_{11} x_4(k) - \Gamma_{12} u(k) \qquad (6\text{-}14)$$

Where $\hat{x}_2(k+1)$ is the estimated velocity, $\hat{x}_3(k+1)$ is the estimated bias force and P_s is the measured position error signal. L_2 and L_3 are filter coefficients which determine the filtering properties of the estimator and how fast its response is. It will be further discussed below in Section 6.3.4.1.

6.3.3.3 Track following control algorithm

In head positioning there are two models, track following and track seeking. The purpose of the track following model is to keep the head on track and overcome the effect of disturbances such as bias forces, external vibrations, disk spindle bearing run-out and imbalance, and noise in the position measurement. The four states $x_1(k+1)$, $\hat{x}_2(k+1)$, $x_4(k+1)$ and $x_5(k+1)$ are used in the track following control algorithm. $x_5(k+1)$ is calculated as follows:

$$x_5(k+1) = x_5(k) + x_1(k) \qquad (6\text{-}15)$$

$x_5(k+1)$ is used to reduce the following error.

The track following control algorithm designed for the system [Franklin et al., 1990] is as follows:

$$u(k)=-K_1x_1(k)- K_2\hat{x}_2(k+1) -K_4x_4(k) -K_5x_5(k) \quad (6\text{-}16)$$

The constants K_1, K_2, K_4 and K_5 are determined by pole placement methods and by frequency response criteria. These will be discussed below Section 6.3.4.2.

6.3.3.4 Track seek control algorithm

The purpose of the seek mode is to move the head from one track to another desired track in the quickest possible manner. This is the fastest procedure for time control. The seek control algorithm procedure is the same as the track following algorithm design with, of course, a new scaling matrix. The seek mode is designed to follow the optimised profile in Figure 6.8. In the seeking mode, the equation for the input of the PZ bimorph is

$$u(k) = +K_v[x_p(k)-(K_2\hat{x}_2(k)+ \Gamma_{21}x_4(k))]- K_5x_5(k) \quad (6\text{-}17)$$

where the first term is the expected velocity. The second term is the resulting velocity. $K_5x_5(k)$ is the bias error correction. The delayed input (x_4) terms are added to the position and velocity as in the track follow control law in order to change smoothly from the seek mode to the following mode. K_v is the velocity profile control gain and is set equal to K_2 when switching from track seek to track follow mode in order to minimise transient change-over effects.

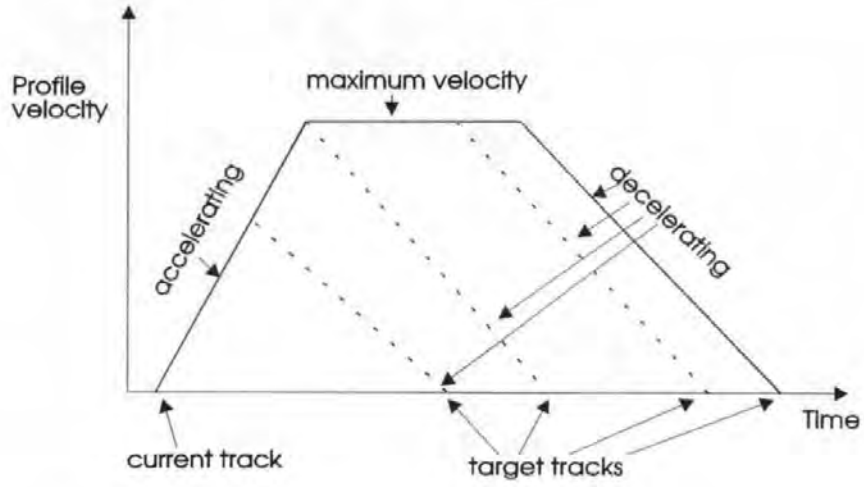

Figure 6.8 Velocity profile of the track seeking mode.

6.3.4 Discussion and simulation

6.3.4.1 Estimator constants L_2 & L_3

In this Section, the calculation of L_2 & L_3, using Chen's method [Chen, 1984], is discussed.

To investigate an estimator for the unmeasured part of the state, the state vector is divided into two parts: x_a is the portion directly measured, which is y, and $\mathbf{x}_b$ is the remaining portion to be estimated. The complete system description becomes

$$\begin{bmatrix} x_a(k+1) \\ \mathbf{x}_b(k+1) \end{bmatrix} = \begin{bmatrix} \Phi_{aa} \Phi_{ab} \\ \Phi_{ba} \Phi_{bb} \end{bmatrix} \begin{bmatrix} x_a(k) \\ \mathbf{x}_b(k) \end{bmatrix} + \begin{bmatrix} \Gamma_a \\ \Gamma_b \end{bmatrix} u(k)$$

$$y(k) = [1 \quad 0] \begin{bmatrix} x_a(k) \\ \mathbf{x}_b(k) \end{bmatrix} \tag{6-18}$$

Thus the reduced-order estimator equations are [Franklin et al., 1990]

$$\hat{\mathbf{x}}_b(k+1) = \Phi_{bb}\hat{\mathbf{x}}_b(k) + \Phi_{ba}x_a(k) + \Gamma_b u(k) + \mathbf{L}_r\left[x_a(k+1) - \Phi_{aa}x_a(k) - \Gamma_a u(k) - \Phi_{ab}\hat{\mathbf{x}}_b(k)\right] \tag{6-19}$$

Choosing arbitrary eigenvalues for the estimator of -3 and -3 + 2j, we have to find a **L** such that the eigenvalues of Φ_{bb} - **L**•Φ_{ab} are -3 and -3 ± 2j. Suppose that **L** = $\{L_1, L_2, L_3\}$, then we have

$$\Phi_{bb} = \begin{bmatrix} 1 & 4.6 & 1.55 \\ 0 & 1 & 0 \\ 0 & 0 & 0 \end{bmatrix}; \qquad \Phi_{ab} = \begin{bmatrix} 1 & 2.03 & 0.3 \end{bmatrix}$$

and

$$\begin{aligned} &\det(sI - \Theta_{bb} + L\Theta_{ab}) = \\ &s^3 + (L_1 + 2.03L_2 + 0.3L_3 - 1)s^2 + (-L_1 + 2.03L_2 - 0.95L_3 + 1)s - 1.25L_3 \end{aligned} \tag{6-20}$$

Equating coefficients with those of

$$(S+3)\ (S+3+2j)(S+3-2j) = S^3 + 9S^2 + 31S + 39;$$

gives:

$$L_2 = 4.9 \text{ and } L_3 = -31.2.$$

Therefore Equations (6-13) and (6-14) are complete.

Note that it is difficult to determine which are the best eigenvalues because the larger the magnitudes of the negative real parts of these eigenvalues, the faster $\hat{x}_b(k)$ approaches $x_b(k)$. However, these will cause large gains in **L** and generate larger magnitudes in transient behaviour, as in the state feedback case. Large gains and large transients will also cause the estimator to saturate. A simple and reasonable guideline is, the magnitudes of the negative real parts of the eigenvalues of Φ - **LH** be two or three times those of $\Phi + \Gamma\mathbf{K}$ [Chen, 1984].

6.3.4.2 K_1, K_2 K_4 and K_5 in the track following control algorithm

The selection of K_1, K_2, K_4 and K_5 were determined by pole placement methods and by frequency response criteria.

One way to select suitable values of K_1, K_2, K_4, and K_5 is by means of comparing the coefficients of det ($s\mathbf{I} - \Phi' - \Gamma'\mathbf{K}$) and $\bar{\Delta}(S)$ [Chen, 1984].

Another way is to employ the MATLAB command:

$$\mathbf{K} = \text{place (a, b, c, d)} \tag{6-21}$$

Once the matrices **L** and **K** have been determined, the performance of the total system can be investigated in both the frequency and time domains. By means of continuing this design process, it is possible to find an **L** and **K**, which can meet the necessary design criteria.

In order to study the design of the **K** and **L**, the software is developed using MATLAB as shown in Appendix Software F.

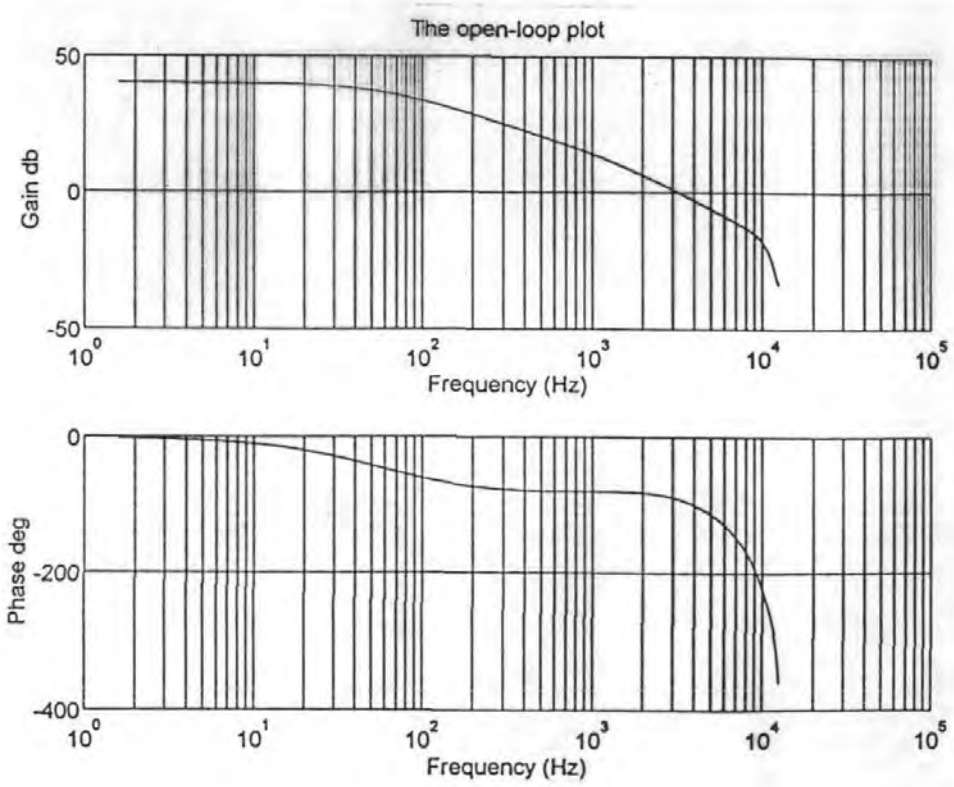

Figure 6.9 The open-loop frequency response of the servo system.

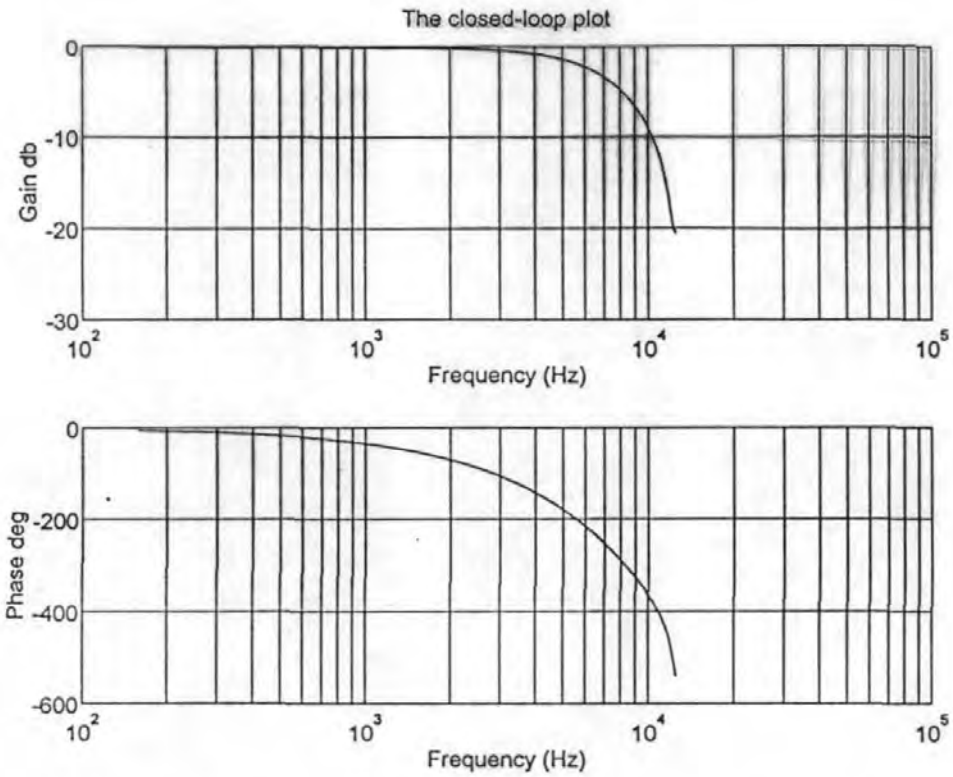

Figure 6.10 The closed-loop frequency response of the servo system.

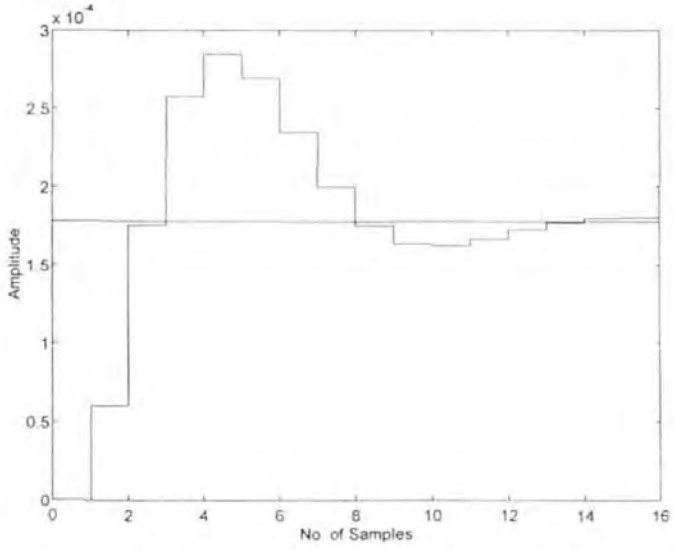

Figure 6.11 A step response of the servo system (T = 0.13 ms).

Simulation gives values for **K** = [0.8458, 0.5381, 0.3629, 0.2299] for a step response in order to meet the specification. Figure 6.9 shows the open-loop frequency response of the servo system. Figure 6.10 shows the closed-loop frequency response of the servo system. Figure 6.11 shows the step response. Also the robustness of the design can be observed using the software. The values of **K** were varied by approximately 5 % and the controller held the system within specification.

6.3.4.3 The profile in seeking control algorithm

The profile velocity $x_p(k)$, corrected for delay, is given by

$$x_p(k) = \text{profile}[x_1(k) + \Gamma_{11}x_4(k)] \qquad (6\text{-}22)$$

The profile is a table of values in the DSP that represent a desired velocity at a given distance from the target track. The nominal velocity profile is generated using a scaled and discretized model of the actuator. Missing velocity data inbetween two sampled values are obtained using linear interpolation with respect to position. The acceleration and deceleration phases are determined by choosing the maximum desired voltage. The profile is improved by experiments. Many of the properties (e.g. seeking time) can be controlled through the design of the profile.

6.3.4.4 Adaptation scheme

Typically, the above actuator's servo performance changes with time, environmental conditions and error between average and practical values of composites. The parameter Γ_1 indicates these change. Hence, it is necessary to adapt Γ_1 on-line [Ottesen, 1987].

In order to make estimating Γ_1 on-line as easy as possible, suppose that a special seek is executed under special conditions as follows:

1. By doing two seeks, one in each direction, and then averaging the Γ's that result, the bias force can be removed from the measurement.
2. The measurement is taken during the acceleration phase of a seek with a constant, non-saturating drive, the effect of the computation delay (the state x_4) is also removed. The Γ_{12} and Γ_{22} multiplying u(k) in equation (6-10) become equal to Γ_1 and Γ_2, respectively.
3. A non-saturating drive must be applied to the PZ actuator driver so that the voltage is known.
4. The position is then measured at each sample position of the acceleration.

Then, the estimate of Γ_1 can be derived using equation (6-10) as follows [Ottesen, 1987]:

$$\Gamma_1 = [x_1(k+1) - 2x_1(k) + x_1(k-1)]/[u(k) + u(k-1)] \qquad (6\text{-}23)$$

Once Γ_1 is calculated, it can be used to modify the gain from the track seeking and following output equations for more optimal performance to adapt to the change in Γ_1 and Γ_2 ($\Gamma_2 = 2\Gamma_1$).

Thus the system may be considered to be adaptive taking into account changes in physical characteristics.

6.4 Summary

In section 6.2 a servo controller for a dual stage VCM/PZ actuator has been designed, which employs digital servo control for both following mode and seeking

mode. Simulated results using MATLAB have indicated a performance which satisfies stated technical requirements of overshoot, seek time and robustness.

In Section 6.3, an advanced digital, two modes controller (seek and follow), suitable for a single PZ actuator was designed. The estimator algorithm, track following control algorithm and track seek control algorithm are discussed. The selection of filter coefficients **L** of the estimator and gains **K** of the controller in the track seek and track following control algorithms are described and discussed. It was shown how the two mode digital controller could be made adaptive by automatic adjustments designed to compensate for physical changes caused by environmental features and wear, etc. Simulated results for the advanced two mode controller again demonstrated a performance meeting the specified design criteria.

In summary two controllers have been designed and simulated using MATLAB. In each case the simulated results were consistent with the required performance criteria.

Chapter Seven
Conclusions and Future Work

7.1 Conclusion

For a magnetic rigid disk, it is important not only to increase bit density, but also to increase track density. The increase in track density is dictated by the track width of read and write heads and the accuracy with which the heads can be positioned. The aim of this work was to demonstrate and understand a servo measuring system, actuator and controller for ultra-high track-density recording rigid disks.

7.1.1. New recording model for the servo pattern

In the study of the position sensor system, it was found that the problems in using current servo methods are the low S/N ratio of the PES signal and asymmetries in the MR head as trackwidth is reduced to submicron.

A new recording model for a magnetic servo pattern is proposed and it was found that is suitable for ultra-high track density (e.g. 50 kTPI). The recorded track width in the new mode was mainly dependent on the gap length of the write head, the magnitude of the write current, H_c of the medium and the space between the head and

the medium. It was observed that there is a transition region because of the component of the head field in the track direction. The arc shape of the transition region must be symmetrical about the centre of the track. For its reproduced process, it was also found that the MR head output was maximum or zero respectively when the length of the MR equals to one or half of the recording wavelength. It was observed that the S/N of the output of the MR head may independent of the trackwidth of the recording track, but may proportional to the MR length, due to the L and g of the MR head are less than recording bit length and trackwidth respectively. This is of great interest for reading and writing servo pattern on submicron tracks, because the readout of the MR head is proportional to the length of MR in the track direction and is no longer limited by the trackwidth of the recording track, even though the number of BPI may limited by the length of the MR head.

7.1.2 Position sensor system

A study of the relationship between geometrical shape of the MR gap and the position error signal performance in the new method shows that the maximum sensitivity, the best linearity and PES can be obtained when the gap length of the servo MR head is equal to the servo track pitch (servo pattern width) and the gap width is equal to the servo pattern length. The maximum sensitivity was proportional to the gap width of the MR head when the gap width was less than the servo pattern length. The S/N of PES increases as the gap width increases.

In the study of the new servo method with buried servo layer under the data layer, it was observed that the readout of the MR servo head increases with the thickness of the separation layer reduces. The experimental results on the S/N of servo and data

signals show that the S/N of the servo signal was effected by some factors such as the coercivity of the data layer or the thickness of isolation layer and the coercivity of the servo layer. It also shows that the S/N of the data signal may also effected by the coercivity of the servo layer or the thickness of isolation layer or the coercivity of data layer. It was also found that when the data frequency to the servo frequency ratio increases, the S/N of both data and servo signals increase, which may be of great interest and help for the high BPI recording system.

The experimental results and theory analysis show that the asymmetry effect of the MR can be negligible for the PES signal in the new servo method, and the skew angle of the servo head has to be less than $\alpha_0 = sin^{-1}(2W/L)$. The linear voice coil motor and rotary voice coil motor with small skew angle in this case are suitable for the method.

The experiments at lower disk rotation speed are achieved for track following at 36 kTPI (0.7 μm track-width) with a 10 % (rms) track runout, using this method. The track following results of three new types of position servo system show that the S/N ratio, the linearity and output level can be suitable for a submicron track servo. Study of writing clock track for STW shows that the probability (P) of writing N integral clock pulses around track on disks is dependent on the frequency of writing clock pulses and the speed of the disk. It is clear that (a) the probability (P) increases with reducing the difference of two the central frequencies of the spindle speed and the clock pulse and the P has maximum value when the difference is equal to zero, (b) when the difference is equal to zero, the higher stability of the spindle speed, the higher the probability.

Finally, the comparison of the new servo method with the optical servo, embedded servo and discrete servo indicates that the new servo method may be one of the best candidates for a submicron track servo system.

7.1.3 Actuator

The dynamic performance of dual-stage actuators was investigated for submicron track positioning and following. Results of a comparison of single and dual-stage actuator show that dual-stage actuator has excellent performance in terms of resonant frequency and power consumption. Employing a dual-stage actuator in the case of a high bandwidth servo system was suggested. The study of the PZ bimorph actuator as a fine actuator shows that its displacement is proportional to the applied voltage. Its resonant frequency is dependent on the dimensions and properties of PZ material and is reduced when the mass of the slider increases. It is found that hysteresis and creep phenomena of the piezoelectric bimorph plate ensure that the two curves do not overlap. This result suggests that the major effect on the performance of the PZ actuator was mainly due to the properties of PZ material and hence it was necessary to develop new PZ material. Comparing a PZ bimorph actuator with an electrostatic microactuator shows that the PZ actuator is much better in many respects, such as its driving force, its linearity, the resonance frequency with a load as well as its cost. The comparison between a PZ bimorph and an axial PZ actuator shows that the drive voltage and equivalent capacity of a PZ actuator are lower than that of an axial PZ actuator. The mechanical resonance frequency of the actuator assembly can be raised by a new structural design between the head and the actuator. A new integrated fine PZ bimorph actuator was investigated in our design. An approximately linear relationship between the displacement and the applied voltage could be obtained by optimising relative parameters. At the same time, the loading force of the head in contact recording can be easily controlled by the integrated PZ actuator.

7.1.4 Controller

The two-stage controller design was discussed for submicron track positioning and following. It was found the VCM controller and the PZ controller can be designed separately because the time constant of the VCM actuator is a few orders of magnitude greater than that of the PZ actuator, It was found that a compensator [k(z-a)/z] can increase the damping of the PZ and VCM system and improve the robustness of the systems. Optimum values for k and a can be obtained using the software developed by the author. Simulated results using MATLAB have indicated that the performance of this system which satisfies stated technical requirements of overshoot, seek time and robustness.

Using state space method, a controller of single PZ actuator for 1 μm trackwidth HDD is designed including hardware and software. A mathematical model of the PZ actuator can be described by four states, position, velocity, bias force and delayed driver input. Using the dynamic model, the values of estimated velocity and bias force have been calculated in the estimator algorithm. L_2 and L_3 of filter coefficients determine the filtering properties of the estimator and its speed of response and they can be obtained from det ($sI-\Phi_{bb} + L\Phi$). For the track following control algorithm, the equation $u(k) = -K_1x1 - K_2x_2 - K_4x_4 - K_5x_5$ is employed. The selection of constants K_1, K_2, K_4 and K_5 can be determined both by pole placement methods and by frequency response criteria. In the track seek control algorithm, the seek mode is designed to follow the optimised profile and the K_v was set equal to the K_2, which can be of help to minimise transient motion during settling. Experimental results show how the two mode digital controller could be made adaptive by automatic adjustments designed to compensate for physical changes caused by environmental features and wear, etc. Simulated results for the advanced two

mode controllers also provide the values of performance, which may meet the need of specified design criteria.

In summary two controllers have be designed and simulated using MATLAB. In each case results were consistent with the required performance criteria.

7.2 Future Work

The research carried out for this project has generated a substantial amount of potential further work, as described below.

The position sensor system developed in this investigation needs to be further improved. First, this kind of servo head has not yet been developed. The data presented in this thesis was obtained in the case of the MR data head (which was turned an angle of 90° degree) was used as the servo head. The basic design for the servo head in section 4.3.4 was not good enough. It is necessary to develop a new servo head. Second, it is necessary to obtain more insight information and understanding about the transition region between the servo bits in track direction, particularly in the four tips of the square servo bit. The task could be accomplished using micromagnetic modelling and computation. Third, the time used in writing all the servo patterns on a disk was taken n times more than that of current product (n is the ratio of TPI in this investigation and TPI in current product). The method of self-servo writing of a submicron servo track should to be further studied. How to make the head positioning system within the HDD work without a conventional servo pattern should to be taken in account when writing the servo pattern.

The actuator in this investigation has only demonstrated in the case of the dual-stage actuator with a resonant frequency was less than 5 kHz, and the response

performance of the dual-stage actuator has not been demonstrated with the disk rotating at 3600 rpm. In fact, all of the disks in the disk drive are rotating at 3600 rpm or greater than 3600 rpm. For this reason, it is ideal to repeat the experiments at 3600 rpm. The hysteresis of the bimorph may give some problems.

Digital control for the servo control system has been simulated by using 'MALAB' software. Limited simulation results have shown that there was a significant difficulty due to the friction between the head and disk in contact recording. Further experimental study is needed to understand such an effect and to study new control algorithms.

Appendix Software (A)

```
Page   1

Addr  Code  Source Line

            ;     This is the program for the clock system of the
submicron
            ;     servo track writer. The microprocessor is Intel
8032. The
            ;     program was developed by Baolin Tan in 1994.

                  ORG   0000H

0000 020028       LJMP  START
0003 020098       LJMP  INT0
0006 FF           MOV   R7,   A
0007 08           INC   R0
0008 FF           MOV   R7,   A
0009 F3           MOVX  @R1,  A
000A FF           MOV   R7,   A
000B 7FFF         MOV   R7,   #0FFH
000D 02010C       LJMP  L010B
0010 FF           MOV   R7,   A
0011 96           SUBB  A,    @R0
0012 FF           MOV   R7,   A
0013 DB06         DJNZ  R3,   L001A
0015 C9           XCH   A,    R1
0016 FF           MOV   R7,   A
0017 5E           ANL   A,    R6
0018 FF           MOV   R7,   A
0019 C4           SWAP  A
001A FF           MOV   R7,   A
001B B4FF13 L001A:      CJNE  A,    #0FFH,      LFFF7
001E FF           MOV   R7,   A
001F E9     L0027:      MOV   A,    R1
0020 FF           MOV   R7,   A
0021 3B           ADDC  A,    R3
0022 FF           MOV   R7,   A
0023 FB           MOV   R3,   A
0024 FF           MOV   R7,   A
0025 BFFFF7       CJNE  R7,   #0FFH, L0027
0028 749B   START:      MOV   A,    #9BH
002A 759000       MOV   P1,   #00H
002D 901003       MOV   DPTR, #1003H
0030 F0           MOVX  @DPTR,      A
0031 75A8E0 LFFF7:      MOV   IE,   #0E0H
0034 75B8E4       MOV   IP,   #0E4H
0037 7EFF         MOV   R6,   #0FFH
0039 7FFF         MOV   R7,   #0FFH
003B 7804         MOV   R0,   #04H
003D 752A00       MOV   2AH,  #00H
0040 75F000       MOV   B,    #00H
0043 7D00         MOV   R5,   #00H
0045 7C00         MOV   R4,   #00H
0047 75F000       MOV   B,    #00H

C:\MCS51\WORK\ASM\CLOCK.ASM
```

```
Addr  Code  Source Line

004A 7D00          MOV   R5,   #00H
004C 7C00          MOV   R4,   #00H
004E 7930          MOV   R1,   #30H
0050 D290   L0051: SETB  P1.   0
0052 120104        LCALL L0103
0055 C290          CLR   P1.0
0057 120104        LCALL L0103
005A D290          SETB  P1.0
005C 120104        LCALL L0103
005F C290          CLR   P1.0
0061 7EFF          MOV   R6,   #0FFH
0063 7FFF          MOV   R7,   #0FFH
0065 53908F        ANL   P1,   #8FH
0068 C290          CLR   P1.   0
006A E8            MOV   A,    R0
006B C4            SWAP  A
006C 4290          ORL   P1,   A
006E 205606        JB    56H,  L0078
0071 C291          CLR   P1.1
0073 D291          SETB  P1.1
0075 8002          SJMP  L007A
0077 D293   L0078: SETB  P1.3
0079 D2A8   L007A: SETB  IE.0
007B 1F     L007C: DEC   R7
007C EF            MOV   A,    R7
007D 7006          JNZ   L0086
007F EE            MOV   A,    R6
0080 600B          JZ    L008E
0082 1E            DEC   R6
0083 80F6          SJMP  L007C
0085 00     L0086: NOP
0086 00            NOP
0087 205513        JB    55H,  L009E
008A 02007B        LJMP  L007C
008D C2A8   L008E: CLR   IE.0
008F C293          CLR   P1.3
0091 C291          CLR   P1.1
0093 D297          SETB  P1.7
0095 020050        LJMP  L0051

0098 D255   INT0: SETB  55H
009A C2A8         CLR   IE.0
009C 32           RETI
            ;
009D 7EFF   L009E: MOV   R6,   #0FFH
009F 7FFF         MOV   R7,   #0FFH
00A1 C255         CLR   55H
00A3 C291         CLR   P1.1
```

C:\MCS51\WORK\ASM\CLOCK.ASM

```
Addr  Code  Source Line

00A5 C293          CLR   P1.3
00A7 120104        LCALL L0103
00AA 901002        MOV   DPTR, #1002H
00AD E0            MOVX  A,    @DPTR
00AE F8            MOV   R0,   A
00AF C3            CLR   C
00B0 9401          SUBB  A,    #01H
00B2 70D9          JNZ   L008E
00B4 901001        MOV   DPTR, #1001H
00B7 E0            MOVX  A,    @DPTR
00B8 F9            MOV   R1,   A
00B9 C3            CLR   C
00BA 943B          SUBB  A,    #3BH
00BC 70CF          JNZ   L008E
00BE 901000        MOV   DPTR, #1000H
00C1 E0            MOVX  A,    @DPTR
00C2 C3            CLR   C
00C3 9400          SUBB  A,    #00H
00C5 70C6          JNZ   L008E
00C7 C297          CLR   P1.7
00C9 205614        JB    56H,  L00DF
00CC 902000        MOV   DPTR, #2000H
00CF E0            MOVX  A,    @DPTR
00D0 F5F0          MOV   B,    A
00D2 C3            CLR   C
00D3 9427          SUBB  A,    #27H
00D5 40B6          JC    L008E
00D7 7429          MOV   A,    #29H
00D9 95F0          SUBB  A,    B
00DB 40B0          JC    L008E
00DD 305603        JNB   56H,  L00E2
00E0 020050 L00DF: LJMP  L0051
00E3 D256   L00E2: SETB  56H
00E5 D291          SETB  P1.1
00E7 7AFF          MOV   R2,   #0FFH
00E9 7BFF          MOV   R3,   #0FFH
00EB 020050        LJMP  L0051
00EE 759000        MOV   P1,   #00H
00F1 120104        LCALL L0103
00F4 D290          SETB  P1.0
00F6 120104        LCALL L0103
00F9 C290          CLR   P1.0
00FB C256          CLR   56H
00FD D291          SETB  P1.1
00FF 00     L00FE: NOP
0100 00            NOP
0101 00            NOP
0102 80FB          SJMP  L00FE


C:\MCS51\WORK\ASM\CLOCK.ASM
```

```
Page   4

Addr  Code  Source Line

0104 740F   L0103:      MOV   A,    #0FH
0106 00     L0105:      NOP
0107 00           NOP
0108 D5E0FB L0107:      DJNZ  ACC,  L0105
010B 22           RET
             ;
010C 32     L010B:      RETI
010D FE           MOV   R6,   A
010E D9FE   L0109:      DJNZ  R1,   L0109
0110 D8F6         DJNZ  R0,   L0107
0112 D002         POP   02H
0114 D001         POP   01H
0116 D000         POP   00H
0118 22           RET
             ;
0119 FF     L0110A:     MOV   R7,   A
011A DFFE   L0110B:     DJNZ  R7,   L0110B
011C 7FFF         MOV   R7,   #0FFH
011E DCFE   L0110E:     DJNZ  R4,   L0110E
0120 DBFE   L0110F:     DJNZ  R3,   L0110F
0122 22           RET


             END


             Symbol          Value  Type

             INT0          = 0098H
             L001A         = 001BH
             L0027         = 001FH
             L0051         = 0050H
             L0078         = 0077H
             L007A         = 0079H
             L007C         = 007BH
             L0086         = 0085H
             L008E         = 008DH
             L009E         = 009DH
             L00DF         = 00E0H
             L00E2         = 00E3H
             L00FE         = 00FFH
             L0103         = 0104H
             L0105         = 0106H
             L0107         = 0108H
             L0109         = 010EH
             L010B         = 010CH
             L0110A        = 0119H
             L0110B        = 011AH
             L0110E        = 011EH
             L0110F        = 0120H
             LFFF7         = 0031H
             START         = 0028H


             Public symbols:   24
             Local symbols :    0
```

Appendix Software (B)

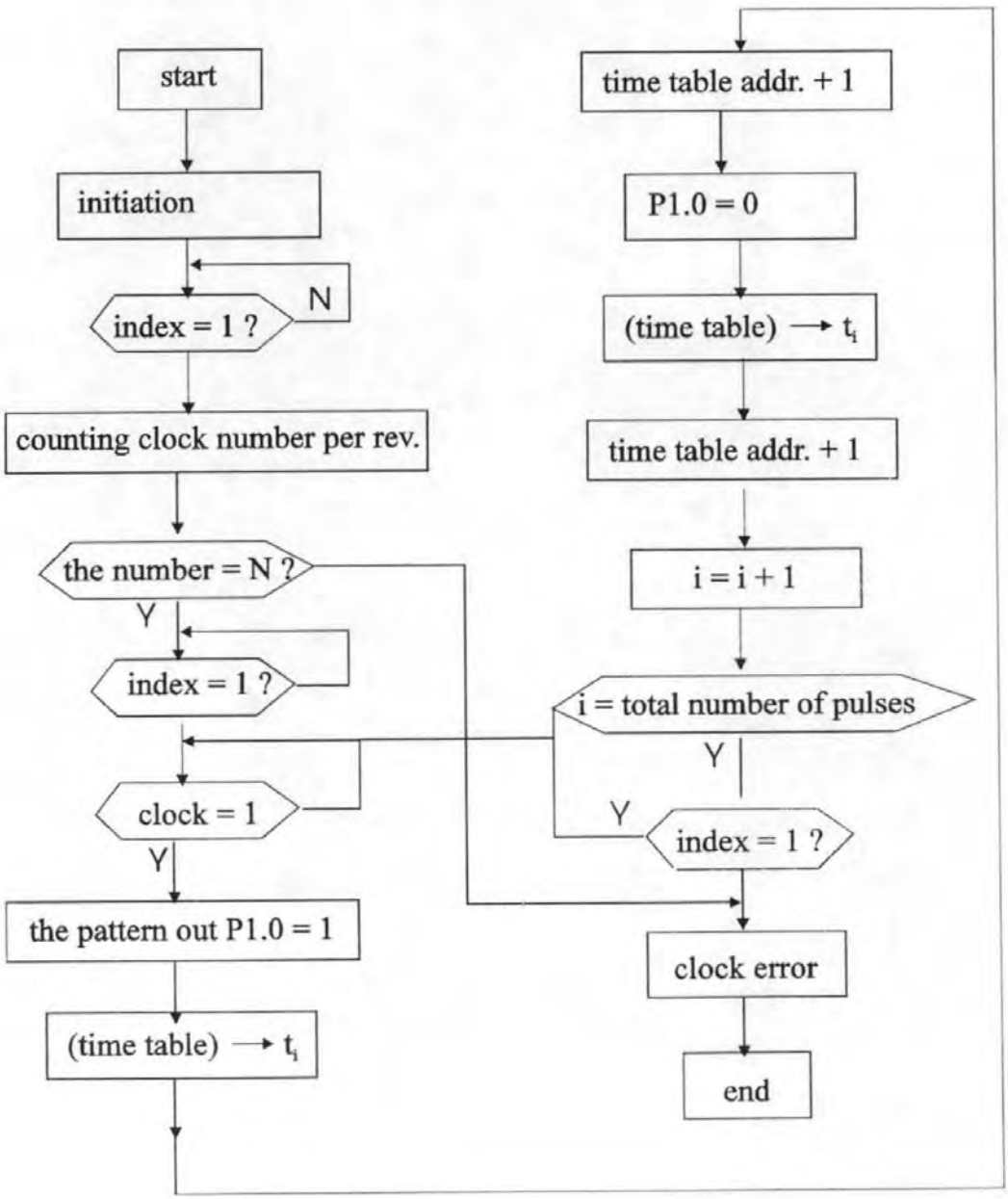

The block diagram for the servo pattern generator.

Appendix Software (C)

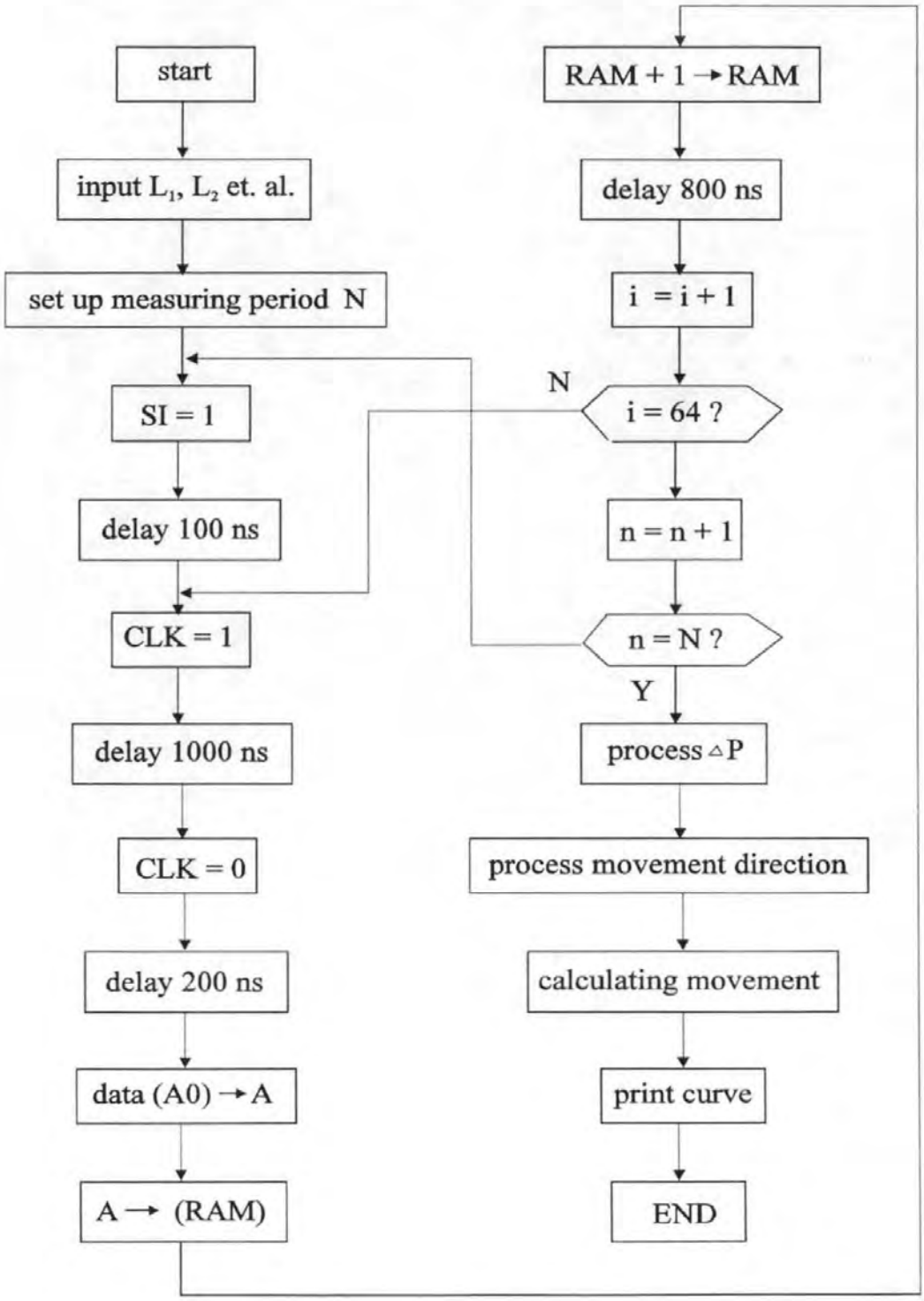

The block diagram for the measuring dynamic movement system.

Appendix Software (D)

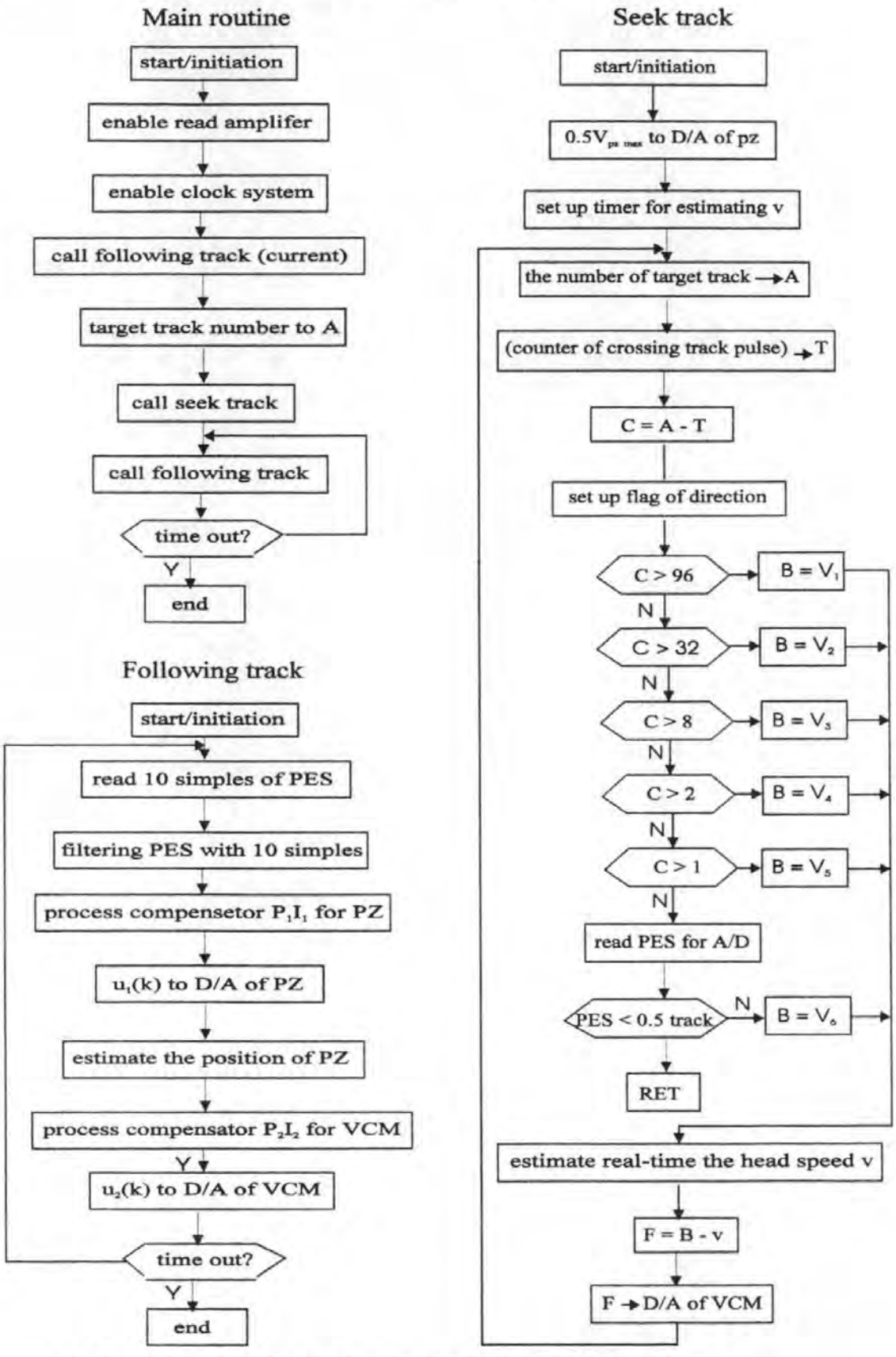

The block diagram for the head servo system on 0.7 μm tracks.

Appendix Software (E)

```
% ------------------------------------------------------------------
% This is a script file to design read/write head position controller
% with a dual-stage actuator for computer HARD DISK Drive.

% To execute, just type 'control'
% ------------------------------------------------------------------

%       Copyright (c) 1996 by Baolin Tan

% Using Newton's law, the simplest model for the read/write head has the
% following differential equation:
%
%  I*theta_ddot + C*theta_dot + K*theta = Ki * i
%

% Taking the laplace transform, the transfer function is:
%                Ki
%  H(s) = ----------------
%         I s^2 + C s + K
%
% Using the values I=.011 Kg m^2, C=.004 Nm/(rad/sed), K=10 Nm/rad,  and
% Ki=.05 Nm/rad form the transfer function description of this system

I = .0011; C = 0.0042; K = 50; Ki = .53;
NUM = [Ki];
DEN = [I C K];
printsys(NUM,DEN,'s');

pause % Press any key to continue ...

% Our task is to design a digital controller that can be used to provide accurate
% positioning of the read/write head. We will do the design in the digital domain.

% First we must discretize our plant since it is continuous.  Since our
% plant will have a digital-to-analog-converter (with a zero-order hold)
% connected to its input, use the 'zoh' discretization method
% of the function C2DM. Use sample time Ts = 0.005  (5 ms)

Ts = 0.0005;
w = logspace(0,4);
[mag,phase] = bode(NUM,DEN,w);
[num,den] = c2dm(NUM,DEN,Ts,'zoh');
[mzoh,pzoh,wzoh] = dbode(num,den,Ts);

% Now plot the results as a comparison.  Press any key after the plot ...
```

```
echo off
subplot(211)
semilogx(w/2*pi,20*log10(mag),wzoh,20*log10(mzoh))
xlabel('Frequency (Hz)'), ylabel('Gain db')
title('c2d comparison plot')

subplot(212)
semilogx(w/2*pi,phase,wzoh,pzoh)
xlabel('Frequency (Hz)'), ylabel('Phase deg')
pause % Press any key to continue ...
echo on

pause % Press any key to continue ...

% Now analyze the discrete system.
disp('Discrete system');
printsys(num,den,'z');

% Plot step response
subplot(111)
dstep(num,den); pause % Press any key after the plot ...

% The system oscillates quite a bit.  This is probably due to very light
% damping.  We can check this by computing the open loop eigenvalues.

disp('Open loop discrete eigenvalues'); ddamp(den,Ts);
zgrid('new'), pzmap(1,den); pause % Press any key after the plot ...

% Note that the poles are very lightly damped and near the unit circle.
% We need to design a compensator that increases the damping of this system.

% Let's try to design a compensator.  The simplest compensator is a simple gain.
rlocus(num,den), hold off; pause % Press any key after the plot ...
% As shown in the root locus, the poles quickly leave the unit circle and go
% unstable.  We need to introduce some lead or a compensator with some zeros.
% Try the compensator:       K(z + a)
%                      D(z) = --------  where a < b
%                             (z + b)

pause % Press any key to continue ...

% Form compensator and connect in series with our plant
% Use a = -.85 and b = 0.
[numc,denc] = zp2tf([.85 ]',[0]',1);
[num2,den2] = series(numc,denc,num,den);

% Lets see how the frequency response has changed.
[mag,phase,w] = dbode(num,den,1);  % Use normalized frequency
```

```
[mag2,phase2] = dbode(num2,den2,1,w);

% Now plot a comparison plot.  Press any key after the plot ...
echo off
subplot(211), semilogx(w,20*log10(mag),w,20*log10(mag2))
xlabel('Frequency (rad/sec)'), ylabel('Gain dB')
subplot(212), semilogx(w,phase,w,phase2)
xlabel('Frequency (rad/sec)'), ylabel('Phase deg')
% Plot -180 degree line
hold on; semilogx([min(w(:)),max(w(:))],[-180,-180],'w--'); hold off;
pause % Press any key to continue ...
echo on

% So our compensator has indeed added lead.

% Now let's try the root locus again with our compensator
subplot(111);
zgrid('new'); rlocus(num2,den2); hold off; pause % Press any key after plot ...

% This time the poles stay within the unit circle for some time.
% Now its your turn, Using RLOCFIND chose the poles with greatest damping
% ratio.  (The lines drawn by ZGRID show the damping ratios from z=0 to 1
% in steps of .1)

pause % Press any key and then choose a point on the plot
[k,poles] = rlocfind(num2,den2);

disp(['You chose gain: ',num2str(k)]); ddamp(poles,Ts);

% Let's form the closed loop system so that we can analyze the design.
[numc,denc] = feedback(num2,den2,k,1);

% These eigenvalues should match the ones you chose.
disp('Closed loop eigenvalues'); ddamp(denc,Ts);

pause % Press any key to continue ...

% Closed loop time response
dstep(numc,denc); pause % Press any key after the plot ...

% So the response looks pretty good and settles in about 14 samples
% which is 14*Ts secs.

disp(['Our disc drive will have a seek time > ',num2str(14*Ts),' seconds.'])

pause % Press any key to continue ...

% Let's now look at the robustness of our design.  The most common classical
```

```
% robustness criteria is the gain and phase margin. The criteria is determined
% by forming a unity feedback system, calculating the Bode response and looking
% for the phase and gain crossovers. MATLAB contains a function MARGIN that
% determines the phase and gain margin given the Bode response.

% Form unity feedback system by connecting our design system with the gain
% we chose. Leave the loop open so we can compute the open loop Bode response.
[num2,den2] = series(num2,den2,k,1);

% Compute Bode response and margins
[mag,phase,w] = dbode(num2,den2,Ts);
[Gm,Pm,Wcg,Wcp] = margin(mag,phase,w); pause % Press any key after the plot ...
% Plot Bode plot with margins
margin(mag,phase,w); pause % Press any key after the plot ...

echo off
subplot(211)
semilogx(w/2*pi,20*log10(mag))
xlabel('Frequency (Hz)'), ylabel('Gain db')
grid on
title('The open-loop plot')

subplot(212)
semilogx(w/2*pi,phase)
xlabel('Frequency (Hz)'), ylabel('Phase deg')
grid on
pause % Press any key to continue ...

% Gain margin db, @ frequency, Phase margin, @ frequency
Margins = [20*log10(Gm),Wcg,Pm,Wcp]
pause %press ang key to continue...


% Our design is robust and can tolerate a 10 db gain increase and a 40 degree
% phase lag without going unstable. By continuing this design process we may
% be able to find a compensator that will stabilize the open loop system and
% allow us to reduce the seek time (more damping would allow us to reduce the
% settling time in the step response).

echo off
```

Appendix Software (F)

```
% ------------------------------------------------------------
% This is a script file to design magnetic head servo controller
% with a single PZ actuator for computer hard disk drive.
% ------------------------------------------------------------

% Copyright (c) 1997 by Baolin Tan

pause% press any key to continue

% Input parameter array of the plant;
a = [1,1,0,0.3; 0,1,0,1.55; 1,0,1,0; 0,0,0,0];
b = [1.72; 4.48; 0; 1];
c = [0,0,0.99,0];
d = [0];
Ts = 0.00013;
w = logspace(2,5);
% [ad,bd,cd,dd] = c2dt(a,b,c,Ts,0);
% disp(ad); disp(bd); disp(cd); disp(dd);
% pause;
[num,den] = ss2tf(a,b,c,d);
printsys(num,den,'z');
pause;

% dbode(num,den,Ts,w);
pause;
den1 = den+num;
num1 = num;
printsys(num1,den1,'z');
% dbode(num1,den1,Ts);
pause;
p = [-0.01+0.1j -0.01-0.1j -0.2+0.2j -0.35-0.2j];
K = place(a,b,p);

disp(K);
pause;
% K = [332 59348];
G = a-b*K;
b = K(3)*b
disp(G);
a = G;
pause;
[num,den] = ss2tf(a,b,c,d);
printsys(num,den,'z');
pause;
% w=logspace(2,5);
```

```
dstep(num,den);
pause;
dbode(num,den,Ts,w);
pause;
[mag,phase,w]=dbode(num,den,Ts);
subplot(211);
semilogx(w/(2*pi),20*log10(mag));
% w=logspace(0,5);
grid on;
xlabel('Frequency (Hz)'), ylabel('Gain db');
grid on;
title('The closed-loop plot');
subplot(212);
% w=logspace(0,5);
semilogx(w/(2*pi),phase);
grid on;
xlabel('Frequency (Hz)'), ylabel('Phase deg');
grid on;
% Margins = [20*log10(Gm),Wcg,Pm,Wcp];
pause;
pause;
den1 = den-num;
num1 = num;
printsys(num1,den1,'z');
w = logspace(2,5);
[mag,phase,w] = dbode(num1,den1,Ts);
[Gm,Pm,Wcg,Wcp] = margin(mag,phase,w); pause % Press any key after the plot ...
% Plot Bode plot with margins
margin(mag,phase,w); pause % Press any key after the plot ...

echo off
subplot(211)
semilogx(w/(2*pi),20*log10(mag))
xlabel('Frequency (Hz)'), ylabel('Gain db')
title('The open-loop plot')

subplot(212)
semilogx(w/(2*pi),phase)
xlabel('Frequency (Hz)'), ylabel('Phase deg')
pause % Press any key to continue ...

% Gain margin db, @ frequency, Phase margin, @ frequency
Margins = [20*log10(Gm),Wcg,Pm,Wcp]
pause %press ang key to continue...

[mag,phase,w]=dbode(num1,den1,Ts);
[Gm,Pm,Wcg,Wcp] = margin(mag,phase,w);
Margins = [20*log10(Gm),Wcg,Pm,Wcp];
```

```
pause;
subplot(211);

semilogx(w/(2*pi),20*log10(mag));
% w=logspace(0,8);
grid on;
xlabel('Frequency (Hz)'), ylabel('Gain db');
grid on;
title('The open-loop plot');
subplot(212);
% w=logspace(0,6);
semilogx(w/(2*pi),phase);
grid on;
xlabel('Frequency (Hz)'), ylabel('Phase deg');
grid on;
Margins = [20*log10(Gm),Wcg,Pm,Wcp];
pause;
end
```

Appendix Hardware (A)

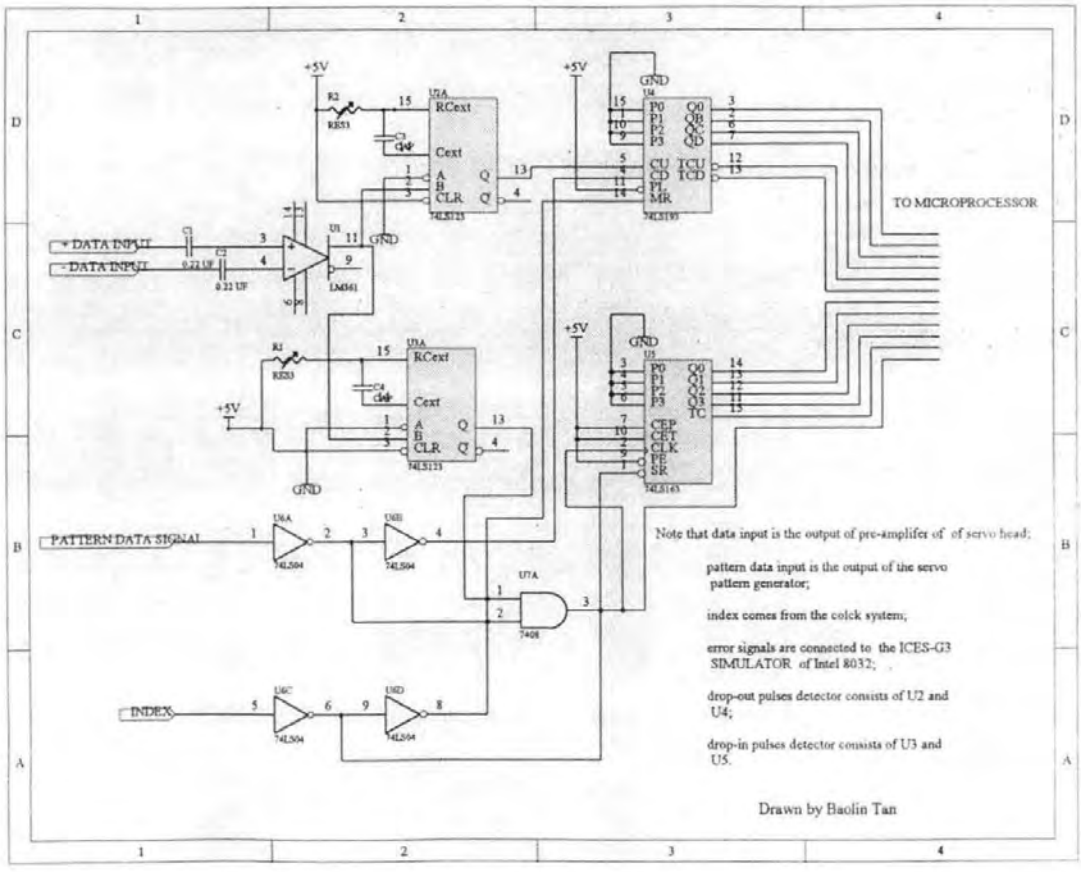

Appendix Hardware (A) is the test circuit of the STW.

Appendix Hardware (B)

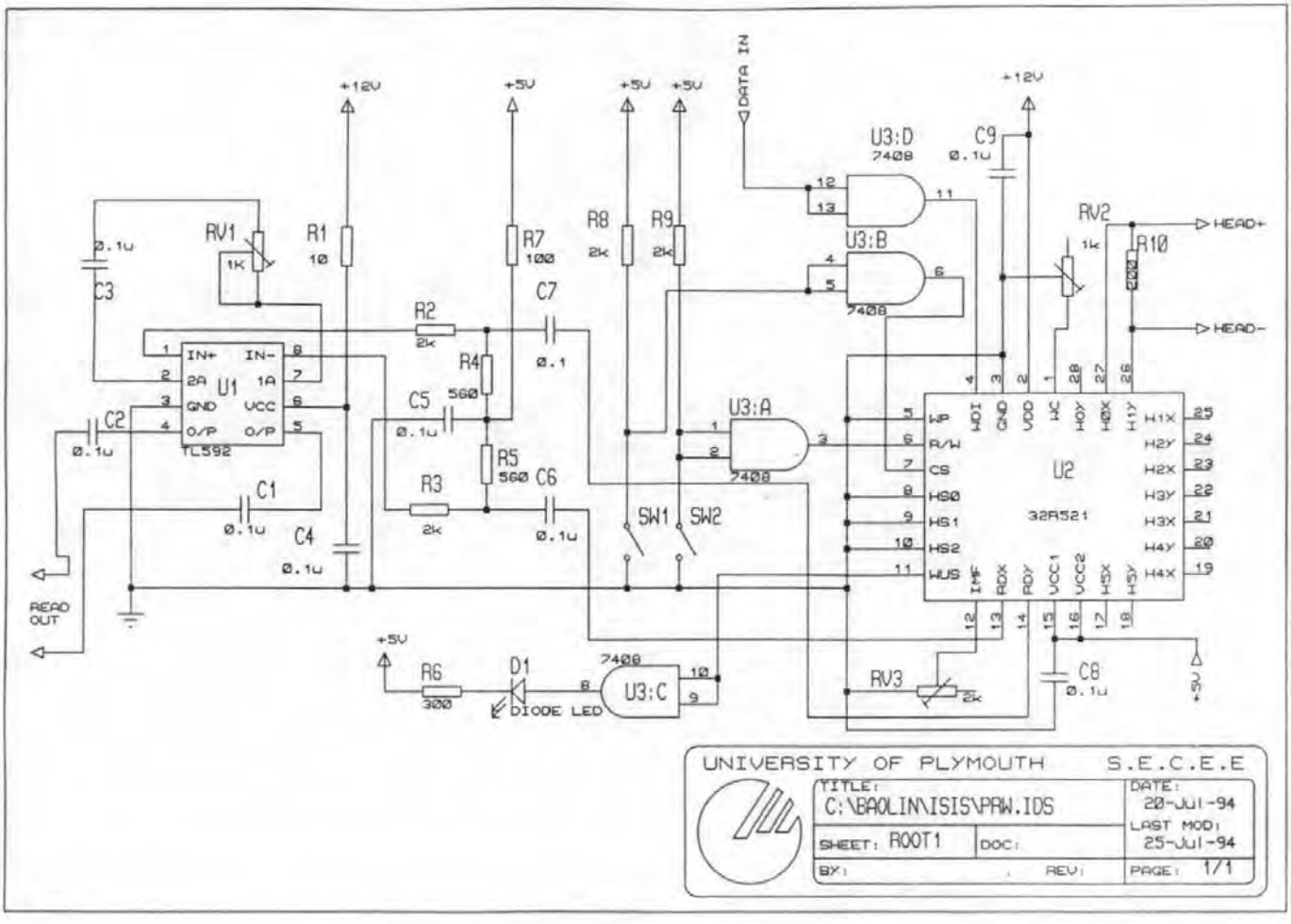

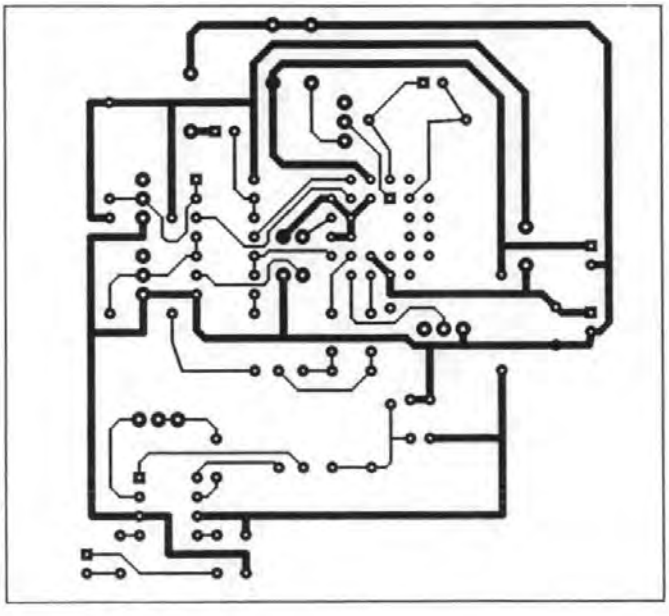

Appendix Hardware (B) is the Read/ Write circuit and its PCB board of the thin film head.

Appendix Hardware (C)

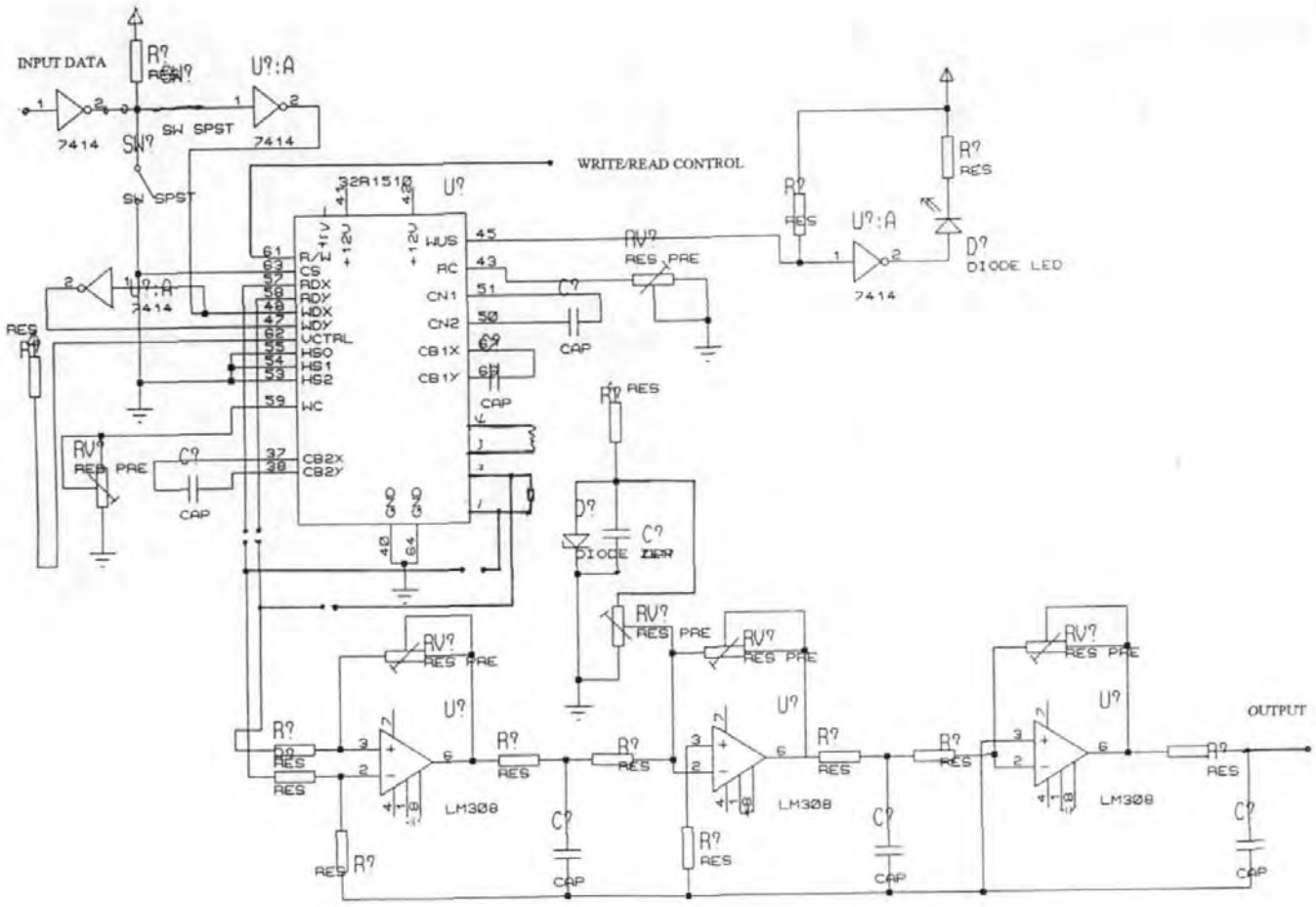

Appendix Hardware (C) is the read/write circuit of the MR head.

Appendix Hardware (D)

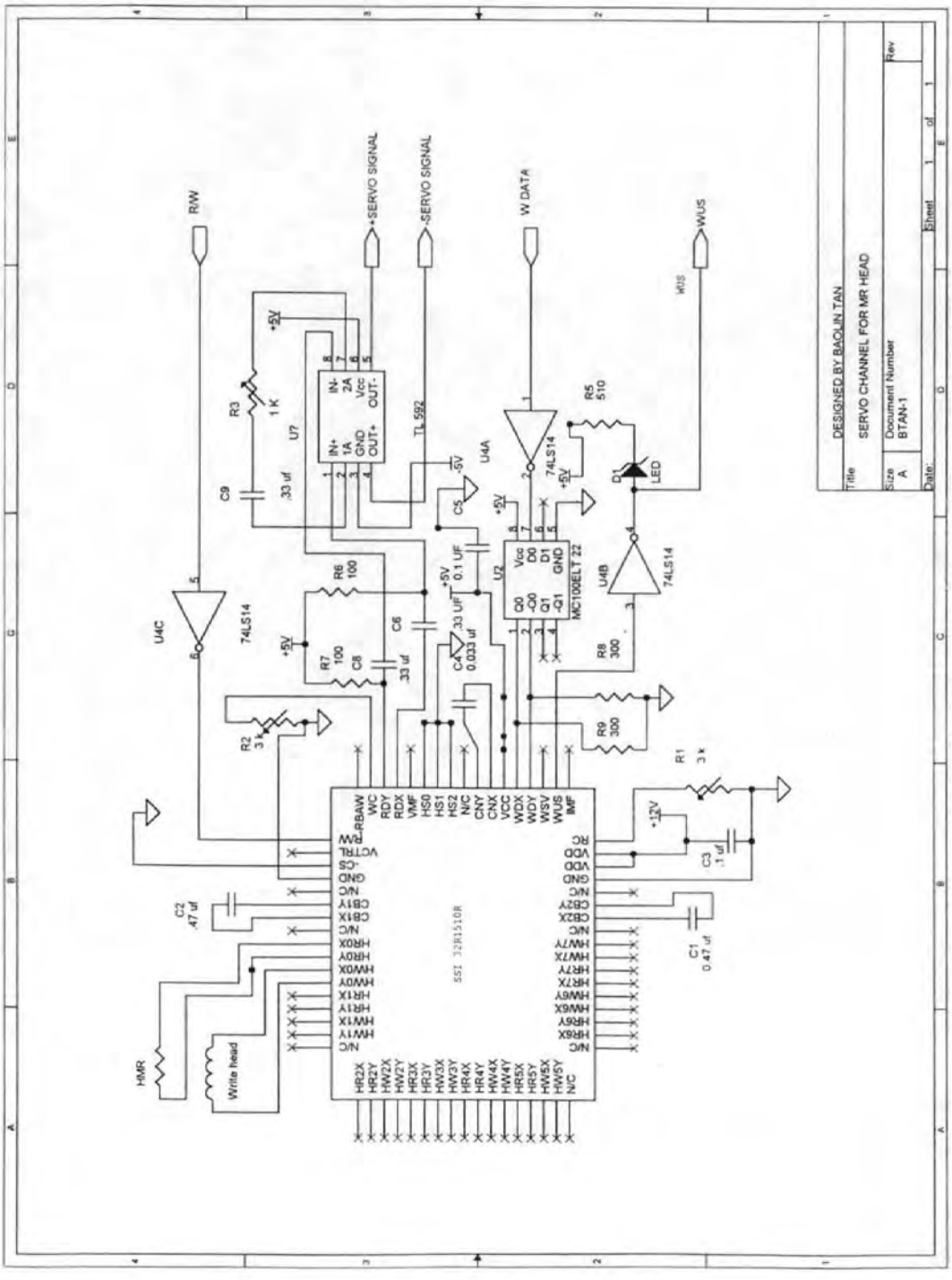

Appendix Hardware (D) is the read/write circuit of the MR head.

Appendix Hardware (E)

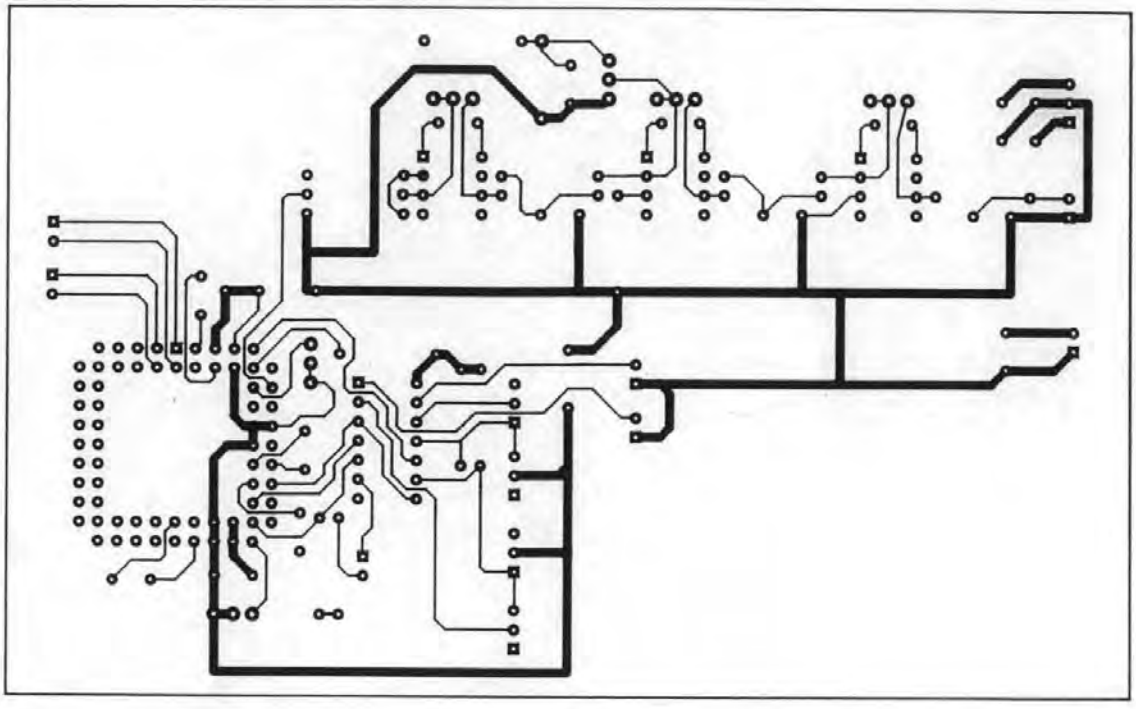

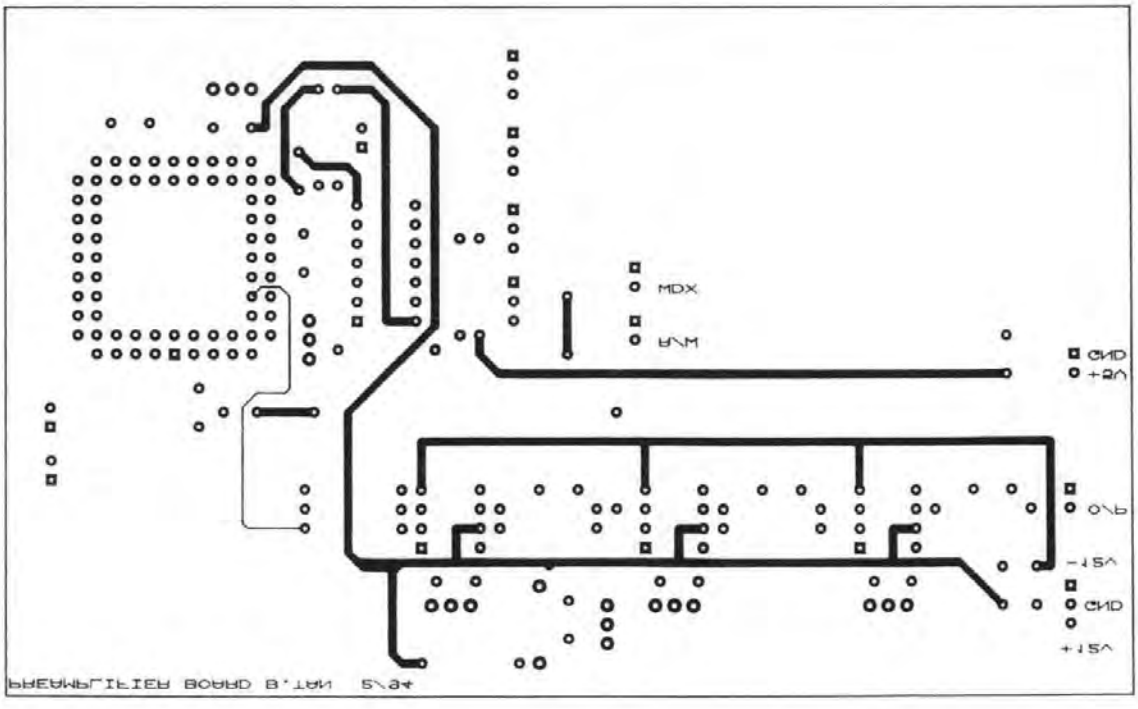

Appendix Hardware (E) is the PCB board drawn of read/write circuit of MR head.

Appendix Hardware (F)

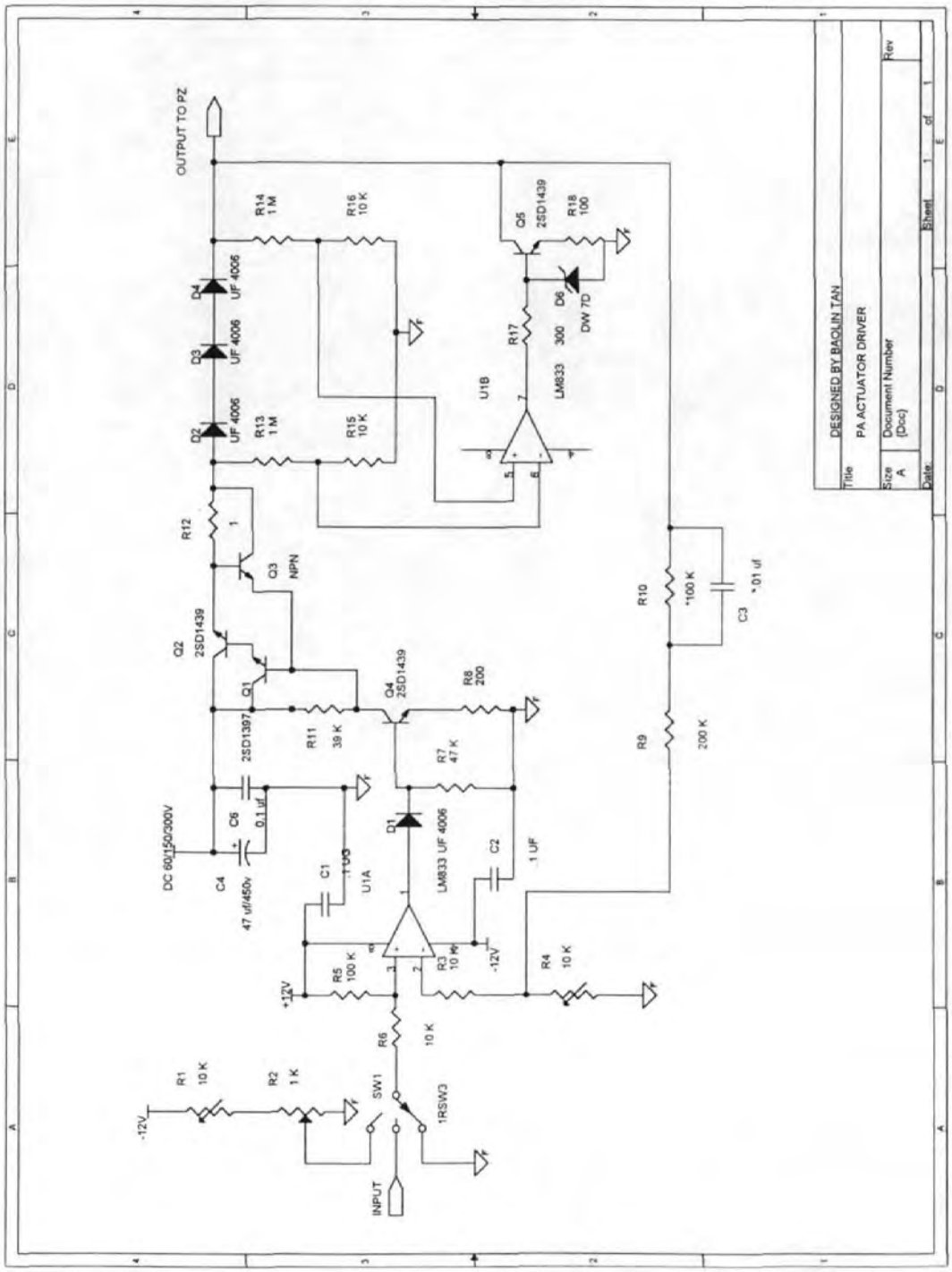

Appendix Hardware (F) is the circuit drawn of PZ actuator drive.

Appendix Hardware (G)

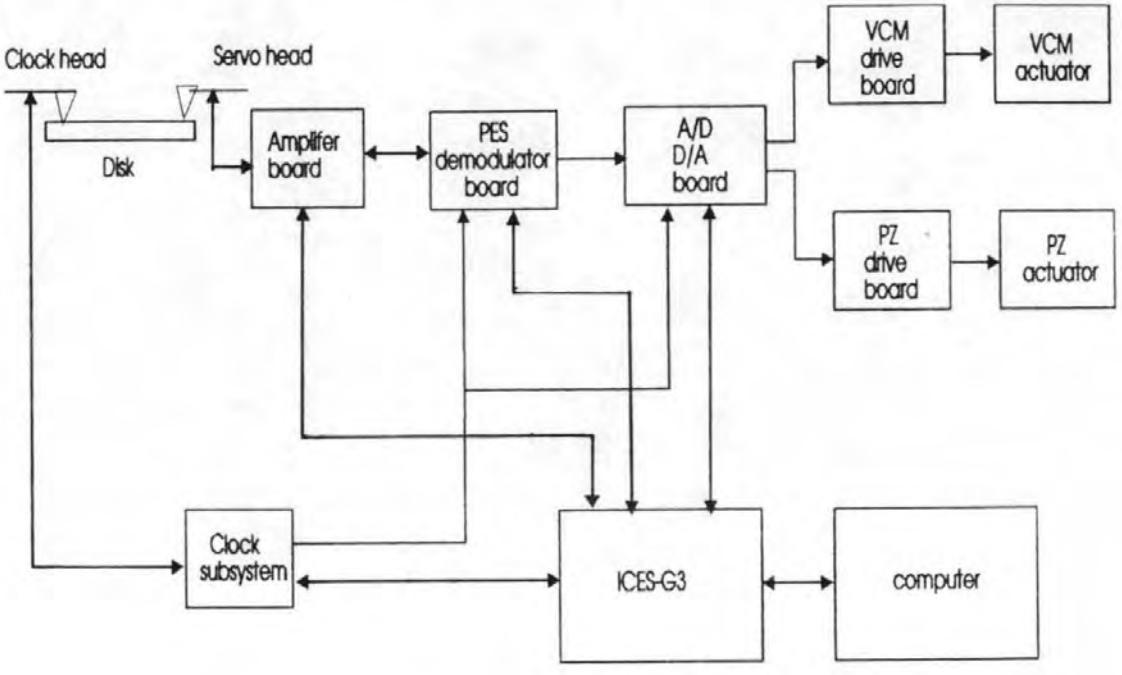

Appendix Hardware (G) is the connection diagram of the overall system for servo on 0.7 μm tracks.

Appendix Hardware (H)

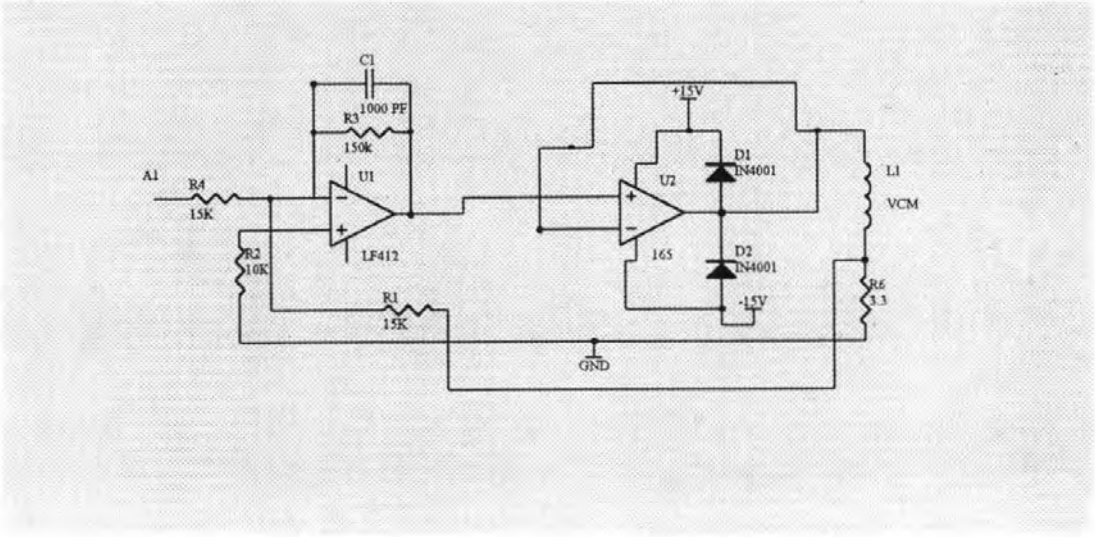

Appendix Hardware (H) is the power drive circuit for VCM

Appendix Hardware (J-1)

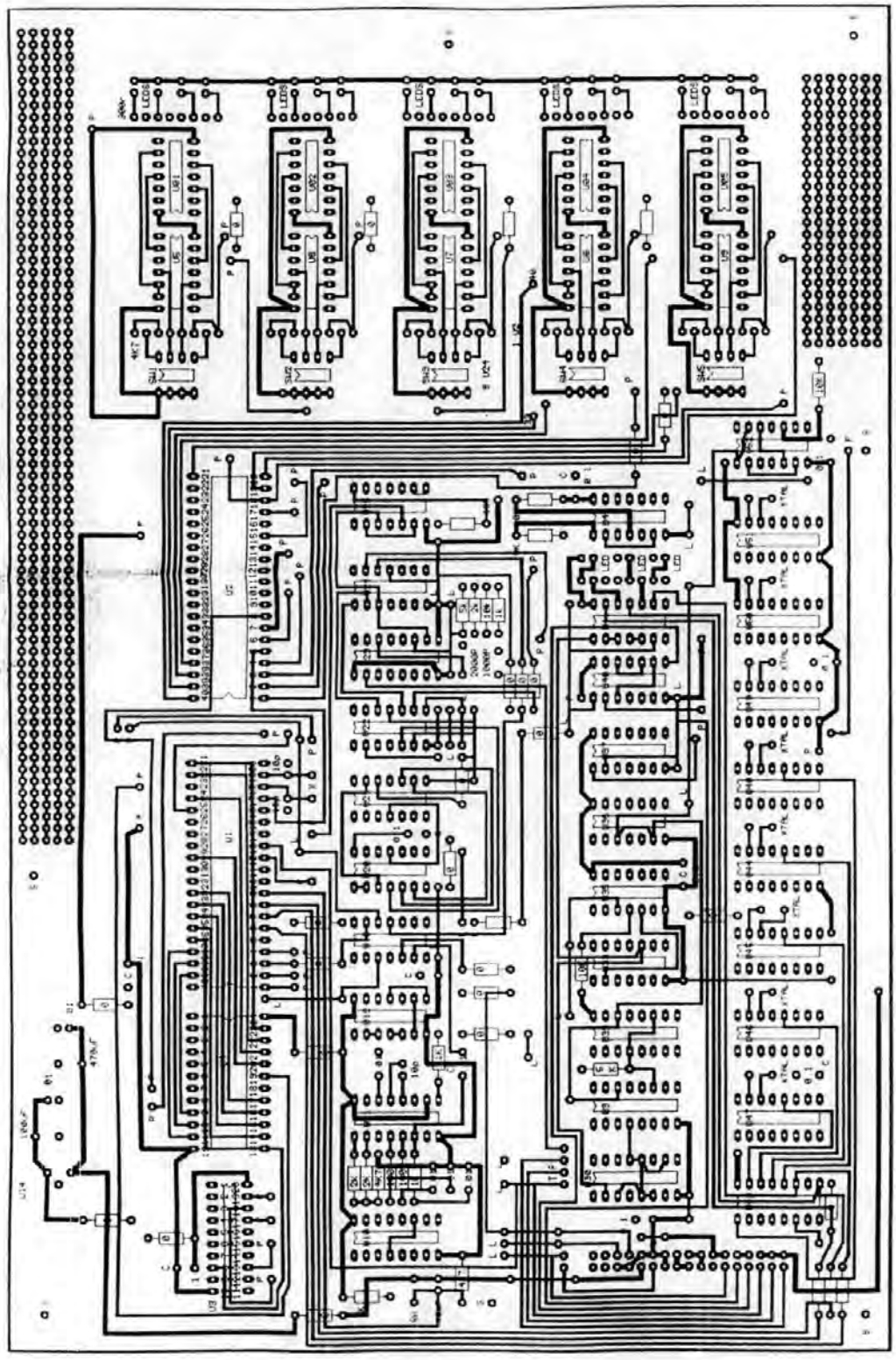

Appendix Hardware (J-1) is main PCB board drawn (A) of the clock system of STW.

(For its circuit please contact The Research Centre in Information Storage Technology at Plymouth University.)

Appendix Hardware (J-2)

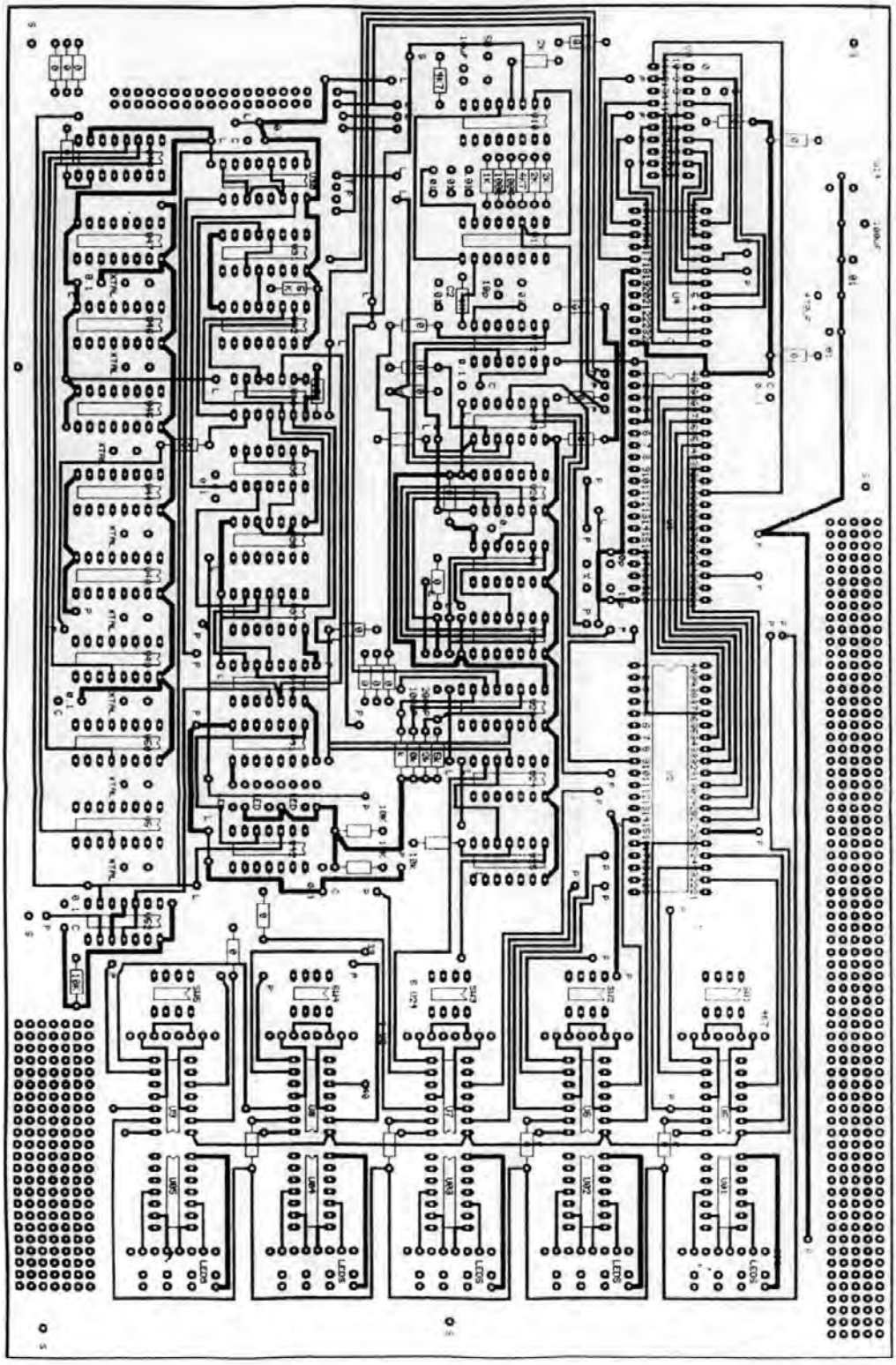

Appendix Hardware (J-2) is PCB board drawn (side B) of clock system of STW.

(For its circuit please contact The Research Centre in Information Storage Technology at Plymouth University.)

Appendix Hardware (K)

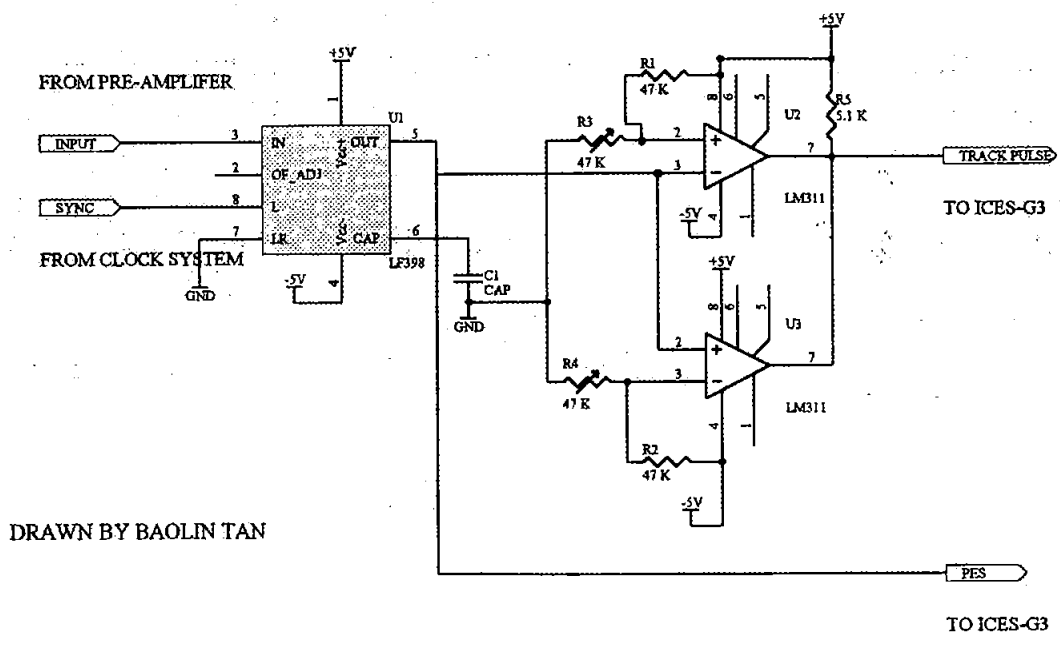

Appendix Hardware (K) is the demodulator circuit of PES.

Bibliography

[Aerosonic, 1985] Aerosonic Ltd. UK, "Handbook of V. S. M. 2001", 1985

[Akagi et al., 1991] Akagi K., Nakao T., Miyamura Y., "High Density Magnetic Recording Tracking Method Using A Laser Diode", IEEE Trans. on Magn., Vol. 27, No. 6, p5301, 1991.

[Beardsley & Zhu, 1991] Beardsley I. A. & Zhu J. G., "Significance of δM Measurements in Thin Film Media", IEEE Trans. on Magn., Vol. 27, No. 6, p5037, 1991.

[Bertram & Mapps et al., 1994] Bertram H. & Mapps D. et al., "Applied Magnetism", ISBN 0-7923-2622-9, Kluwer Academic Publishers, 1994.

[Bitter, 1931] Bitter F., "On Inhomogeneities in the Magnetisation of Ferromagnetic materials", Phys. Rev., 38, p1903, 1931.

[Bond, 1993] Bond J., "The Incredible Shrinking Disk Drive", Solid State Technology, p39, Sept. 1993.

[Chandrasekhar. & Mapps, 1996] Chandrasekhar R. & Mapps D. J., "The effects of samarium addition on CoCrTa-based thin films for magnetic recording", J. of Magnetism and Magnetic Materials, Vol. 155, p202, 1996.

[Chapman, 1963] Chapman D. W., "Theoretical Limit on Digital Magnetic Recording Density", Proc. IEEE, 51,394 (1956).

[Chen, 1984] Chen C. T., "Linear System Theory and Design" ISBN 0-03-060289-0, CBS College Publishing, 1984.

[Clegg et al., 1997] Clegg W. W., Jenkins D. F. L. and Cunningham M. J., "The preparation of 0-3 piezoceramic-polymer thick films and their application

as micro-mechanical actuators", Sensors and Actuators A, A58, p173-177, 1997.

[Chou & Krauss, 1996] Chou S. Y. & Krauss P. R., "Quantum Magnetic Disk", J. of Magnetism and Magnetic Materials, Vol. 155, p151, 1996.

[Commander and Taylor, 1980] Commander R. D. & Taylor J. R., "Servo Design for an Eight-Inch Disk File", Disk File Technology, No. GA 26-1665-0, p90, 1980.

[Cord et al., 1993] Cord B., Schuller K. H. et al., "Sputtering of High Coercivity/Low noise CoCrTa Bilayered Hard Disks in a Manufacturing System", IEEE Trans. on Magn., Vol. 29, No. 6, p3694, 1993.

[Darragh, 1994] Darragh N., "An Adaptive Partial Response Data Channel for Hard Disk Magnetic Recording", PhD. Thesis, University of Plymouth, 1994.

[Deserre, 1985] Deserre J. R., "Transversal Recording on Radially Anisotropic Disc", IEEE Trans. on Magn., Vol. 21, No. 5, 1985.

[Doerner et al., 1991] Doerner M. F., Wang P. W. et al., "Cr Underlayer Effects in Longitudinal Magnetic Recording", Mat. Res. Soc. Proc., Vol. 232, p27, 1991.

[Dong, 1983] Dong C., "Dual-Path Electromagnetic Actuator for A High Performance Magnetic Disk Drive", IEEE Trans. on Magn., Vol. 19, No. 5, p1689, 1983.

[Fan et al., 1994] Fan L. S., Ottesen H. H. and Reiley T. C., "Shock-Resistant Rotary Microactuator for Fine Positioning of Recording Heads", IBM Technical Disclosure Bulletin, Vol. 37, No. 08, p401, 1994.

[Fan et al., 1995] Fan L. S. & Ottesen H. H., "Magnetic Recording Head Positioning at Very High Track Densitied Using a Microactuator-Based Two-stage Servo System", IEEE Trans. Ind. Elec. Vol. 42, No. 3, p223, 1995.

[Fan, 1996] Fan L. S., "Design and Fabrication of Microactuators for High Density Data Storage", IEEE Trans. on Magn., Vol. 32, No. 3, p1855, 1996.

[Fazzio et al., 1993] Fazzio D. P., Moser M. A. et al., "Head actuator dynamics of an IBM 5 1/4-inch disk drive", IBM J. Res. Develop., Vol. 37, No. 4, p479, 1993.

[Franklin et al., 1990] Franklin G. F., Powell J. D. & Workman M. L., "Digital control of Dynamic Systems", ISBN 0-201-51884-8, Addison-Wesley Publishing Company Inc. 1990.

[Futamoto et al., 1991] Futamoto M., Kugiya F. et al., "Investigation of 2 Gb/in^2 Magnetic Recording at a Track Density of 17 kTPI", IEEE Trans. on Magn., Vol. 27, p5280, 1991.

[Hamilton, 1991] Hamilton H., "Contact Recording on Perpendicular Rigid Media", J. of the Magnetics Society of Japan, Vol. 15 Supplement, No. S2, p483, 1991.

[Hansen, 1981] Hansen N. H., "A Head-Positioning System Using Buried Servos", IEEE Trans. on Magn., Vol. 17, No. 6, p2735, 1981.

[Harker et al., 1981] Harker J. M. et al., "Quarter Century of Disk File Innovation", IBM J. Res. Develop, Vol. 25, No. 5, p677, 1981.

[Haynes, 1981] Haynes M. K., "Magnetic Recording Techniques for Buried Servos", IEEE Trans. on Magn., Vol. 17, No. 6, p2730, Nov. 1981.

[Herk, 1977] Herk A. V., "Side fringing fields and write and read crosstalk of narrow magnetic recording heads," IEEE Trans. Magn., Vol. MAG-13, p1021-1-28, July 1977

[Herk & Bijl, 1980] Herk A. V. & Bijl H., "Measurement of side-write Erase, and Read Behaviour of Conventional Narrow Track Disk Heads", IEEE Trans,

on Masnetics. Vol. 16, No. 1, p114, 1980

[Hiyane et al., 1972] Hiyane M. & Inoue Y. et al., "Development of Linear Motion Actuator", Fujitsu Scientific and Technical Journal, p59, June 1972.

[Honda et al., 1996] Honda N., Ouchi S., Iwasaki S., "Extremely High Linear density Recording by Perpendicular Magnetizaton", IEEE Trans. on Magn., Vol. 31, No. 5, p3815, 1996.

[Horowitz & McCormick, 1991] Horowitz R. & McCormick J., "A Self-Tuning Control Scheme for Disk File Servos", IEEE Trans. on Magn., Vol. 27, No. 6, Nov. 1991.

[Horowitz, 1995] Horowitz R. et al., "Position Sensing and Control of Electrostatically-Driven Polysilicon Microactuators", Presented at TMRC'95, in Pittsburgh, p1, 1995.

[Howard, 1994] Howard J. K., "Present and Future of Ultra-High Density Magnetic Recording", J. Magn., Soc. Japan, Vol. 18, No. S1, p59, 1994.

[Hua, 1990] Hua C., PhD. Thesis, "Investigation into Etched Magnetic disk and servo system for HDD", University of Sci. & Tech. China, 1991.

[Hua & Zhang, 1989] Hua C. & Zhang J., "A Novel Servo Disk for High Track Density and High Speed Seeking", 34th Annual Conference on Magnetism and Materials, 1989.

[Hunt, 1971] Hunt R., "A magentoresistive readout transducer", IEEE Trans. on Magn., Vol. 7, p150, 1971.

[Inada et al., 1983] Inada H., Nomura T. and et al., "Two Stage Tracking Servo System for Optical Disk File", NEC Research and Development, No. 71, p33, 1983.

[Inoue et al., 1974] Inoue Y. & Sata et al., "New Linear Motion Actuator for head Positioning", Fujitsu Scientific and Technical Journal, p95, 1974.

[Ishida et al., 1993] Ishida T. & Morita O. et al., "Discrete-Track magnetic Disk Using Embossed Substrate", IEICE Trans. Fundamentals, Vol. E76-A, No. 7, p1161, 1993.

[Ishii & Mizukami, 1987] Ishii K. & Mizukami M., "High Density Servo Signal Detection for Accurate Head Positioning", IEEE Trans. on Magn., Vol. 23, No. 5, p3684, 1987.

[Iwasaki & Takemura, 1975] Iwasaki S. & Takemura K., "An Analysis for the Circular Mode of Magnetization is Short Wavelength Recording", IEEE Trans. on Magn., Vol. 11, No.5, p1173, 1975.

[Iwasaki & Nakamura, 1977] Iwasaki S. & Nakamura Y., "An Analysis for the Magnetization Made for High Density Magnetic Recording", IEEE Trans. on Magn., Vol. 13, No. 5, p1272, 1977.

[Jackson et al., 1988] Jackson B, Knowles V. & Wilcox R., "A Novel Way of Formatting to Accommodate Variations in Heads and Media", IEEE Trans. on Magn., Vol. 24, No. 6, p2958, 1988.

[Jayantha et al., 1991] Jayantha M. S., Chainer T. J. & Brown D. H., "Digital Servo Control of a Novel Disk Actuator", IEEE Trans. on Magn., Vol. 27, p4476, 1991.

[Jeffers, 1986] Jeffers F., "High Density Magnetic Recording Heads", Proc. IEEE 74, p1540, 1986.

[Jenkins et al., 1996] Jenkins D.F.L., Cunninghamm M.J., Clegg W. W., Velu G. and Remiens D., "The use of sputtered PZT films for moving micro-mechanical structures with nanometric precision", Presented at ECAPD-3, Bled, Slovenia, August 1996.

[Jenkins et al., 1998] Jenkins D. F. L., Clegg W. W, Velu. G., Cattan E. and Remiens D., "The characterisation of PZT films of differing orientations for MEMS applications", Presented at ECAPD-IV, Montreux, Switzerland, August 1998.

[Jones, 1978] Jones R. E., "Analysis for the magnetisation mode for high design magnetic recording heads", IEEE Trans. on Magn., Vol. 14, p509, 1978.

[Jones & Mee, 1986] Jones R. E. & Mee C. D., Magnetic recording handbook, Part 1, chapter 4, "Recording Heads", 2nd Ed., McGraw-Hill 1986.

[Karlquist, 1954] Karlquist O., "Calculation of the magnetic field in ferromagnetic layer of a magnetic drum", Trans. Roy. Inst. Tech. (Stockholm) 86, p3, 1954.

[knight,1997] Knight G., "Near field recording", Terastor Ltd., www.idema.org/insight/novdec97/terastor.html, 1997.

[Kobayashi & Tang, 1970] Kobayashi & Tang, "Application of Partial-response Channel Coding to Magnetic Recording System", IBM J. Res. & Dev., Jan. 1970.

[Kobayashi & Tang, 1971] Kobayashi & Tang, "Application of Probabilistic Decoding to Digital Magnetic Recording", IBM J. Res. & Dev., Vol. 15, p64, Jan. 1971.

[Kodak, 1991] Kodak Ltd., "Handbook of ultra-high speed camera (Kodak HS)", 1991.

[Koizumi & Kuroda, 1990] Koizumi T. and Kuroda O., "Analysis of Damped Vibration of a System with Rolling Friction-Rolling Friction Depends on the Displacement-," J. Of Japanese Society of Tribologists, Vol. 35, No. 6, p435-439, 1990.

[Koshino & Ogawa, 1980] Koshino N. & Ogawa S., "Optical Method of the Head Positioning in Magnetic Disk Systems", IEEE Trans. on Magn., Vol. 16, No. 5, p631, 1980.

[Koster & Arnoldussen, 1989] Koster E. & Arnoldussen T., "Magnetic Recording Handbook", Edited by Mee D. & Daniel E., Part One; Chapter 3 "Recording Media", McGraw-Hill, ISBM 0-07-041274-X, 1989.

[Lambert et al., 1987] Lambert S. et al., "Recording Characteristics of Submicron Discrete Magnetic Track", IEEE Trans. on Magn., Vol. 23, No. 5, Sept. 1987.

[Lambert et al., 1991] Lambert S. et al., "Beyond Discrete Tracks: Other Aspects of patterned Media", J. Appl. Phys., 69 (8), p4724, 1991.

[Lee et al., 1991] Lee J., Wallash A. & Poon A., "Effect of Read/ Write Misalignment and Asymmetric Side Reading on Magnetoresistive Head Off-track Performance", J. Appl. Phys. 69(8), p5399, 1991.

[Lee et al., 1993] Lee T. H. & Low T. S. et al., "DSP-based Seek Controller for Disk Drive Servo mechanism", IEEE Trans. on Magn., Vol. 29, No. 6, p4071, 1993.

[Lee et al., 1995] Lee T. H., "Internal Model Control (IMC) Approach for Designing Disk Drive Servo-controller", IEEE Trans. Magn., Vol. 42, No. 3, June 1995.

[Lindholm, 1977] Lindholm D. A., "Magnetic Fields of finite track width heads" IEEE Trans on Magn., Vol. 13, p1460, 1977.

[Liu et al., 1996] Liu B & Hu S B et al., "Skew Angle and Its Effects on Gb/in^2 Density Magnetic Recording" IEEE Trans on Magn., Vol. 32, No 3, p1743, 1996.

[Machinski, 1967] Machinski E., U.S. Pat. No. 3,313,899, 11/04/1967.

[Maeda & Takei, 1991] Maeda Y. & Takei K., "Compositional Inhomogeneities in Co-Cr-Ta/Cr Films for Longitudinal Magnetic Recording", IEEE Trans. on Magn., Vol. 27, No. 6, p4721, 1991.

[Mallinson, 1993] Mallinson J. C., "The Foundations of Magnetic Recording" Academic Press Inc., London, 1993.

[Mapps & Pan, 1993] Mapps D. J. & Pan G., "New Materials for Perpendicular Magnetic Disk Recording", Proc. of the International Conference on Materials, Ikebukuru, Tokyo, Japan, Sept. 1993.

[Mapps et al., 1993] Mapps D. J., Pan G., Akhter M. A., Onodera S. and Okabe A., "In-contact magnetic recording performance of Pt / CoCrTa thin films on glass computer disks", J. of Magn., and Magn., Mat., 120, p305, 1993.

[Mapps, 1994] Mapps D. J., "Magnetoresistance" Chapter in "Applied Magnetism", ISBN 0-7923-2622-9, Kluwer Academic Publishers, 1994.

[Mapps, 1995] Mapps D. J., "Magnetics-Based Computer Memories Towards and Beyond the End of the Century", Faculty Lecture, University of Plymouth, U.K., 1995.

[Mastsuoka et al., 1982] Mastsuoka, Iioshi Y. and et al., "Formation of Ba-Ferrite Films with Perpendicular Magnetization by Targets-Facing Type of Sputtering", IEEE Trans. on Magn., Vol. 18, p625, 1982.

[Maury, 1981] Maury C., "High Track Density For Magnetic Disk Drives With an 'Embedded Servo' Positioning System", IEEE Trans. on Magn., Vol. 17, No. 4, p1396, 1981.

[Mee, 1989] Mee C. D. & Daniel E. D., "Magnetic Recording Handbook", ISBN 0-07-041274-X, McGraw-Hill Book Company, New York, NY 10020, 1989.

[Mee, 1996] Mee C. D., "MRM'95 Forward", J. of Magnetism and Magnetic Materials, 155, p1, 1996.

[Menon, 1996] Menon A. K., "Towards 100 Gb/in^2 Recording Systems: The Evolution of High Density Magnetic Storage Systems", Invited Ewing Lecture, The Royal Society, London, 1996.

[Middleton & Wright, 1982] Middleton B. & Wright C., "Perpendicular Recording", IERE Conf. Proc., Vol. 54, p181, 1982.

[Miles & Middleton, 1991] Miles J. J. & Middleton B. K., "Micronmagnetic Simulations of Transverse Recording", IEEE Trans. on Magn., Vol. 27, No. 6, p4969, 1991.

[Min et al., 1991] Min T. & Zhu J. G. et al., "Effects of Inter-layer Magnetic Interactions in Multilayered CoCrTa/Cr Thin Film Media", IEEE Trans. on Magn., Vol. 27, No. 6, p5058, 1991.

[Miu & Bhat, 1991] Miu D. K. & Bhat S. P., "Minimum Power and Minimum Jerk Position Control and its Applications in Computer Disk Drives", IEEE Trans. on Magn., Vol. 27, p5304 1991.

[Miu & Tai, 1995] Miu D. K. & Tai Y. C., "Silicon Micromachined SCALED Technology", IEEE Trans. Ind. Elec., Vol. 42, No. 3, p234, 1995.

[Mori et al., 1991] Mori K. & Munemoto T. et al., "A Dual-Stage Magnetic Disk Drive Actuator Using a Piezoelectric Device for a High Track Density", IEEE Trans. on Magn., Vol. 27, No. 6, p5298, 1991.

[Murdock et al., 1992] Murdock E. S., Simmons R. F. and et al., "Roadmap for 10 Gbit/in^2 Media: challenges", IEEE Trans. on Magn., Vol. 28, No. 5, p3078, 1992.

[Mutoh et al., 1996] Mutoh H. & Kanai H. et al., "5 Gb/in^2 Recording

Demonstration with NiFe/$Co_{90}Fe_{10}$ Spin-Valve Heads and Low-Noise Thin-Film Disks", IEEE Trans. Magn., Vol. 32, No. 5, p3914, 1996.

[Nagata et al., 1987] Nagata N., Fukazawa T. and et al., "Yoke Type Magnetoresistive Heads with Suppresses Barkhousen Noise", IEEE Trans. on Magn., Vol. 23, No. 5, p2500, 1987.

[Nakamura, 1991] Nakamura Y., "Theoretical and Experimental Prospects of perpendicular magnetic recording", J. Magn. Soc. Japan, Vol. 15, No. S2, p497, 1991.

[Nakamura et al., 1994] Nakamura Y. & Muraoka H. et al., "submicron Trackwidth Recording Utilising a Novel Single Pole Head", J. Magn. Soc. Japan, Vol.18, No. S2, p583, 1994.

[Nakanishi et al., 1983] Nakanishi et al., "High Track Density Head Positioning Using Sector Servos", IEEE Trans. on Magn., Vol. 19, No. 5, Sept. 1983.

[Naruse et al., 1983] Naruse J., Tsutsumi M. & Tamura T., "Design of a Large capacity Disk Drive with Two Actuator", IEEE Trans. on Magn., Vol. 19, p1695, 1983.

[Nishiyama et al., 1987] Nishiyama T. et al., "Recording characteristics of metal-in-gap mini composite head", IEEE Trans. on Magn., Vol. 23, p2931, 1987.

[Nordiko, 1987] Nordiko Ltd., "Handbook on RF sputtering with the NM 2000 sputtering modules and the Nordiko N6-1400 Pumping System", 1987.

[Ogatak, 1990] Ogatak, "Modern Control Engineering" Prentice-Hall, Inc., 1990.

[Oswald, 1974] Oswald R. K., "Design of a Disk-file Head-positioning Servo",

IBM J. Res. Dev., Vol. 18, p506, 1974.

[Ottesen, 1987] Ottesen H. H., "Proceedings of Conference on Applied Motion Control'87", Minneapolis MN, p35-41, 1987.

[Ottesen, 1994] Ottesen H. H., "Future Servo Technologies for Hard Disk Drives", J. Magn. Soc. Japan, Vol. 18, No. S1, p31, 1994.

[Pan, 1993] Pan G. H., PhD. Thesis, University of Plymouth, 1993.

[Pan & Mapps, 1996] Pan G. & Mapps D. J., "A New Fabrication Method for Submicron Trackwidth Thin Film Head", Presented in Intermag'96, BB-09, 1996.

[Parker et al., 1993] Parker M. et al., "Crystallographic Structure of CoPtCr/CrV Thin Films at Revealed by Cross Section TEM and X-ray Pole-Figure Analysis", J. Appl. Phys., Vol. 73, p5560, 1993.

[Patapoutian et al., 1996] Patapoutian A., "Optimal Burst Frequency Derivation for Head Positioning", IEEE Trans. on Magn., Vol. 32, No. 5, p3899, 1996.

[Patel, 1977] Patel T. R., "Multi-Actuator System Using Single Magnetic Circuit", Pat. No. 4,136,293, 1977.

[Richter & Talke, 1988] Richter W. O. & Talke F. E., "Nonrepeatable Radial and Axial Runout of 5 1/4" disk Drive Spindles", IEEE Trans. on Magn., Vol. 24, No. 6, Nov. 1988.

[Riley, 1989] Riley. W. and Zachary. L., "Introduction to Mechanics of Materials", John Wiley & Sons Inc., TA405.R54, 1989.

[Romankiw et al., 1970] Romankiw I.T. et al., "Batch Fabricated Thin-Film Magnetic Recording Heads", IEEE Trans. Magn., MAG-6, p597, 1970.

[Rugar, 1990] Rugar D., "Atomic Force Microscopy", Physics Today, Vol. 43,

p23, 1990.

[Sarid, 1991] Sarid D., "Scanning Force Microscopy", Oxford Univ. Press, New York, 1991.

[San Huan, 1992] San Huan Ltd., "Handbook of SH-ADA board", 1992.

[Sauter, 1971] Sauter G. F., United States Patent No. 3,611,417, 5/10/1971.

[Sauter et al., 1972] Sauter G. F., Paul and et al., "Transverse Recording Using Thin Film Recording Heads", IEEE Trans. Magn., Vol. 8, p192, 1972.

[Sauter & Paul, 1972] Sauter G. F. & Paul M. C., "Transverse Recording Using Thin Film Recording Heads", IEEE Trans. on Magn., Vol. 8, No. 2, June 1972.

[Scranton et al., 1983] Scranton R. A. et al., "A Novel High Performance, Low Mass Disk Head Actuator", IEEE Trans. on Magn., Vol. 19, No. 5, p1692, 1983.

[Sebestyen, 1973] Sebestyen L. E., Digital Magnetic Tape Recording for computer Application, Chapman and Hall, London, 1973.

[Seko & Takeda, 1994] Seko S. & Takeda T., "A Study on Double Gap Magnetic Head Positioning System for Hard Disk Drive", J. Magn. Soc. Japan, Vol. 18, No. S1, p41, 1994.

[Shishida et al., 1993] Shishida K. et al., "Fast Head Positioning Method of Magnetic Disk Drives", IEEE Trans. on Magn., Vol. 29, No. 6, p4045, 1993.

[Simulink, 1993] The Math Works Inc. "Simulink Handbook", 1993.

[Speake, 1985] Speake Co. Ltd., "Handbook for disk test station", 1985.

[Sri-Jayantha et al., 1991] Sri-Jayantha M. & Chainer T. J. et al., "Digital Servo Control of a Novel Disk Actuator", IEEE Trans. on Magn., Vol. 27, No. 6,

Nov. 1991.

[Stephens & Workman, 1986] Stephens H. C. and Workman L., "Position Error Signal Modulator/Demodulator", U. S. Patent No. 4,575,776, 1986.

[Stich et al., 1987] Stich M. C. & Resman J. B. et al., USA Patent No. 4,697,127, 29/09/87.

[Sui & Kryder, 1993] Sui X. & Kryder M., "Magnetic Easy Axis Randomly In-plane Oriented Barium Hexaferrite Thin Film Media", Appl. Phys. Lett., Vol. 63, p1582, 1993.

[Sui & Kryder, 1994] Sui X. & Kryder M., "Effects of CoTi-Doping on Longitudinal Barium Ferrite Thin Film Media", IEEE Trans. on Magn., Vol. 30 No. 6, p4044, 1994.

[Susuki & Iwasaki, 1982] Susuki T. & Iwasaki Y., "Magnetization Transitions in Perpendicular Magnetic Recording", IEEE Trans. on Magn., Vol. 18, No. 2, p769, 1982.

[Takaishi et al., 1996] Takaishi K., Imamura T. et al., "Microactuator Control For Disk Drive", IEEE Trans. on Magn., Vol. 32, No. 3, p1863, 1996.

[Takano et al., 1991] Takano H., Fukuka H., Suzuki M., Shiiki K. and Kitada M., "Submicron-Trackwidth Inductive/MR Composite Head" IEEE Trans. on Magn., Vol. 27, No. 6, p4678, 1991.

[Tan et al., 1991] Tan B. et al., "A New Method of Testing Servo Writing Pattern", J. Magn. Soc. Japan, Vol. 15, No. S2, p331, 1991.

[Tang, 1989] Tang W. C. et al., "Laterally Driven Polysilicon Resonant Microstructures", J. of Sensor and Actuator, Vol. 20, p25-32, 1989.

[Tanaka et al., 1994] Tanaka S. et al., "Characterization of Magnetizing

Process for Pre-Embossed Servo Pattern of Plastic Hard Disks", IEEE Trans. on Magn., Vol. 30, No. 6, p4209, 1994.

[Texas, 1991] Data Sheet of TSL214 of the Texas Instruments Co., June 1991.

[The Math Works, 1992] The Math Works, Inc., "Control System Toolbox User's guide", 1992.

[Thornton, 1989] Thornton J. A., J. Vac. Sci. Tech. A4(6), p3059, 1989.

[Tsang et al., 1990 [1]] Tsang C. and Chen M. M. et al., "Gigabit Density Recording using Dual-Element MR/Inductive Heads on Thin Film Disks", IEEE Trans. on Magn., Vol. 26, No. 5, p1689-1693, 1990.

[Tsang et al., 1990 [2]] Tsang C. and Chen M. M. et al., "Performance Study & Analysis of Dual-Element Head on thin Film Disk For Gigabit-Density Recording", IEEE Trans. on Magn., Vol. 26, No. 6, p2948, 1990.

[Tsang et al., 1996] Tsang C. and Santini H. et al., "3 Gb/In^2 Recording Demonstration with Dual Element heads & Thin Film Disks", IEEE Trans. on Magn., Vol. 32, No. 1, p7, 1996.

[Ullah et al., 1994] Ullah M. & Parker M. et al., "Laser Annealing of Barium Ferrite Thin Films with Longitudinal Orientation", Paper GP-14, presented at 6th Joint MMM-Intermag Conference, Albuquerque, NM, June 1994.

[User's Guide, 1994] TMS320C50 DSP Starter Kit User's Guide, Texas Instruments, 1994.

[Van Herk, 1977] Van H. A., "Side Fringing fields and write and read crosswalk of narrow magnetic recording heads", IEEE Trans. on Magn., Vol. 13, p1021, 1977.

[Velu & Lambeth, 1991] Velu E. & Lambeth D., "CoSm Based High Coercivity Thin Films for Longitudinal Recording", J. Appl. Phys., Vol. 69, p5175, 1991.

[Velu & Lambeth, 1992] Velu E. & Lambeth D., "High Density Recording on SmCo/Cr Thin Film Media", IEEE Trans. on Magn., Vol. 28, No. 5, p3249, 1992.

[Waander, 1991] Waanders J. W., "Piezoelectric Ceramics Properties and Application", Philips Components, Marketing Communications, 1991.

[Wang et al., 1991] Wang Z. G. et al., "A New Concept of Discrete Magnetic Track Servoing", J. Magn. Soc. Japan, Vol. 15, No. S2, p327, 1991.

[Warner, 1974] Warner M., "Flying magnetic transducer having three rail", U.S. Patent No. 3,823,416, 1974.

[Watanbe et al., 1993] Watanabe K., Takeda T., Okada K. & Takino H., "Demonstration of Track Following Technique Based on Discrete Track Media", IEEE Trans. on Magn., Vol. 29, No. 6, p4030, 1993.

[Weerasooriya et al., 1994] Weerasooriya S. & Low T. S. et al., "Adaptive Time Optimal Control of a Disk Drive Actuator", IEEE Trans. on Magn., Vol. 30, No. 6, p4224, 1994.

[Weerasooriya & Phan, 1995] Weerasooriya S. and Phan D. T., "Discrete-time LQG/LTR Design and Modelling of a Disk Drive Actuator Tracking Servo System", IEEE Trans. on Industrial Electronics, Vol. 42, No. 3, p240, June 1995.

[Wei Fu, 1993] Wei Fu Ltd., "Handbook of ICES-G Board", 1993.

[Wiesen et al., 1993] Wiesen K. & Lansky R. M. et al., "Recording Asymmetries at large Skew Angles", IEEE Trans. On Magn., Vol. 29, No. 6, p4002, 1993.

[Williams & Comstock, 1972] Williams M. & Comstock R., "An analytical model of the write process in digital magnetic recording", AIP Conf. Proc. 5, p738, 1972.

[Wood, 1984] Wood R., Ahlgrim S., Hollarmask K. and Stenerson R., "An Experimental 8-Inch Disk Drive with 100 Megabytes per Surface", IEEE Trans. Magn., MAG-20, p698, 1984.

[Wood, 1994] Wood R., "The Magnetic Recording Channel: Challenges and Directions", IEEE Magnetic Society Distinguished Lecture for 1994, presented at CRIST, Plymouth, U.K., 1994.

[Workman, 1987] Workman M. L., "Adaptive Proximate Time Optimal Servomechanism", PhD. Thesis, Stanford University, 1987.

[Yamaguchi et al., 1992] Yamaguchi T. & Shishida K. et al., " Improvement of Servo Robustness for Digital Sector Servo System", IEEE Trans. on Magn., Vol. 28, No. 5, p2910, 1992.

[Yamamoto et al., 1987] Yamamoto S., et al., "Extremely high bit density recording with single pole perpendicular head", IEEE Trans. on Magn., Vol. 23, No. 5, p2070, 1987.

[Yen, 1982] Yen N. H., "Asymme Crosswalk of Magneoresistive Head", IEEE Trans. on Magn., Vol. 18, No. 6, p1155, 1982.

[Yen et al., 1990] Yen J. Y. & Hallamasek K. et al., "Track-following Controller Design for a Compound Disk Drive Actuator", ASME J. of Dynamic Systems, Measurement, and Control, Vol. 112, No. 3, p391, 1990.

[Yogi et al., 1990] Yogi T. & Tsang C., et al., "Longitudinal Media for 1 Gb/in^2 Areal Density", IEEE Trans. on Magn., Vol. 26, No. 5, Sept. 1990.

[Yogi & Nguyen, 1993] Yogi T. & Nguyen T. A., "Ultra High Density Media: Gigabit and Beyond", IEEE Trans. on Magn., Vol. 29, No. 1, Jan. 1993.

[Yoshikawa et al., 1996] Yoshikawa N. et al., "An Experiment for Head Positioning System Using Submicron Track-Width GMR head", IEEE Trans. on

Magn., Vol. 32, No. 5, p3905, 1996.

[Youngquist et al., 1961] Youngquist R. J. et al., "Magnetic Reader", U.S. Patent No. 3,013,206, 1961.

[Zhang et al., 1991] Zhang J. L. et al., "Analysis On The Readback Waveform Etched Magnetic Disk", J. Magn. Soc. Japan, Vol. 15, No. S2, 1991.

[Zhang et al., 1994] Zhang J. L. et al., "High Track Density Graphic Head Positioning Method", J. Magn. Soc. Japan, Vol. 18, No. S1, p37, 1994.

[Zhu & Bertram, 1991] Zhu J. & Bertram N., "Reversal Mechanisms and Domain Structures in Thin Film Recording Media", J. Appl. Phys., Vol. 69, p6084, April 1991.

[Zhu, et al., 1992] Zhu J. G., Arnoldussen T. C. et al., "Side Writhing Phenomena in Narrow Track Recording", Intermag'92, paper FA-07, 1992.

[Zhu & Ye, 1992] Zhu J. G., Ye X. G. and Arnoldussen T. C., "Side Writing Phenomena in Narrow Track Recording", IEEE Trans. on Magn., Vol. 28, p2716, No. 5, 1992

[Zhu, 1993] Zhu J. G., "Transition Noise Properties in Longitudinal Thin Film Media", IEEE Trans. on Magn., Vol. 29 (1), p195-200, 1993.

A New MR Head Track Following Method for Submicron Track Servo on Rigid Disks

Baolin Tan, Genhua Pan, Desmond J. Mapps
Centre for Research in Information Storage Technology
University of Plymouth, Plymouth, Devon, PL4 8AA, U.K.

Abstract—**An accurate head positioning system uses a magnetoresistive head to generate a servo signal from radially magnetised servo patterns on a rigid disk. The servo patterns are written by a thin film transverse write head and occupies about 6.8% of data area for submicron track servo. Track following on 0.7 μm tracks has been demonstrated using the new servo method on longitudinal rigid disks.**

I. Introduction

High areal recording density results when both linear density and track density are pushed to the limits of the respective technologies. One significant advantage of the optical recording system is that a track following accuracy of 0.1 μm is used on tracks of 1 μm wide. Magnetic recording systems have a much higher linear density but tracks are still much wider than for optical recording systems. Attempts to overcome this have been made in the recent past. For example, K. Akagi et al. [1] used a laser-diode optical system fixed to the side of a magnetic head to obtain a high quality servo signal via a piezoelectric actuator aimed at 17 kTPI (trackwidth 1.5μm). This led to a system reported by Futamoto et al. [2] to operate at 2 Gb/in^2. More recently, Watanabe et al.[3] described a MR head servo method based on an embossed glass disk. The track width and guard band were 3.6 μm and 1.6 μm respectively. In this paper, a new servo method is described using inductive thin film write and MR read heads mounted transverse to the usual data recording direction. This leads to a very sensitive servo system for submicron track following.

II. Principle of the Track Following Method

The data and servo pattern in a conventional rigid disk are magnetized along circumferential direction. When trackwidth is reduced, the servo head width has to be reduced and the S/N of the servo signal is consequently reduced. Therefore conventional servo heads suffer from low S/N and poor linearity of position error signal (PES) as the trackwidth is reduced to submicron size [1]. As shown in figure 1, the servo patterns in this new track following method are magnetized along the radial direction by a transverse writing head which is aligned at a right angle with the normal data head. Servo signals are reproduced by a MR head which is also at a right angle to the data head.

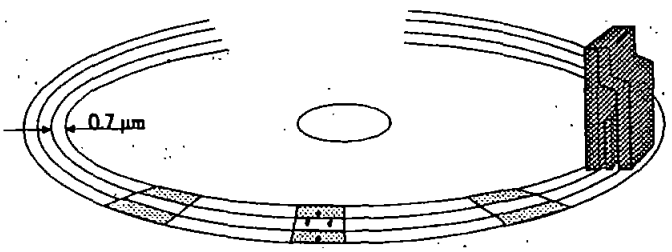

Fig. 1 Schematic diagram of the new servo method using transverse MR head.

The data track width in this new servo method is defined by the bit length of the servo patterns which is determined roughly by the gap length and the radial displacement of the servowriting head between the two adjacent writes.

The bit width of a servo pattern in this new method is apparently a function of the trackwidth of the servowriting head, the moving speed of the disk media and the pulse width of writing current.

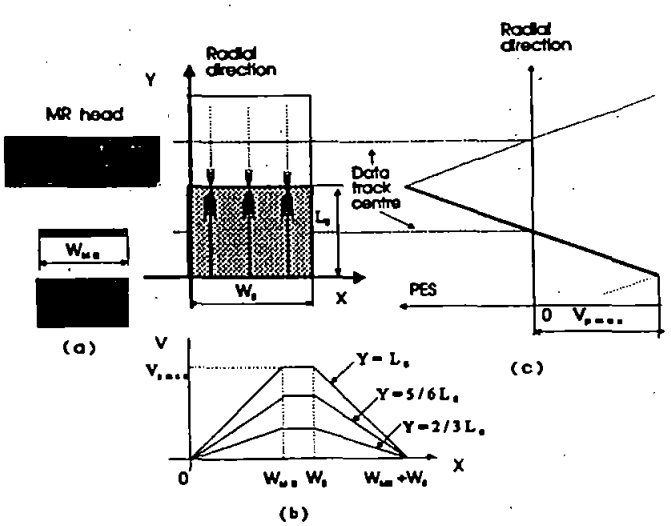

Fig. 2 A simplified model for the reproducing process using transverse read MR head

Manuscript received Apr. 6th 1994

Because of the transverse writing of the servo patterns, the side writing phenomenon from which the conventional servo writing method suffers[4] has no effect on the quality of the servo pattern in this new method.

Figure 2 (a), (b) and (c) shows a simplified model of the reproducing process using the transverse read MR head. If the magnetization distribution in a servo pattern is assumed to be uniform, the side writing phenomena is negligible and the MR head is uniform and symmetrical, the output (v) of the MR head when it passes over a single servo pattern could be roughly expressed by equation (1).

$$V=\begin{cases} v_{p,max}\, x/W_{MR}\,(2y/l_s-1), & \text{when } 0<x<W_{MR},\ 0<y<l_s \\ v_{p,max}\,(2y/l_s-1), & \text{when } W_{MR}<x<W_s,\ 0<y<l_s \\ v_{p,max}(1-(x-W_s)/W_{MR})(2y/l_s-1), & \text{when } W_s<x<(W_s+W_{MR}),\ 0<y<l_s \end{cases} \quad (1)$$

Where $V_{p,max}$ is the maximum peak voltage reproduced by the MR head when it aligns with the track edge of a servo pattern, W_{MR} is the trackwidth of the MR head, W_s is the servo pattern bit width, l_s is the servo pattern bit length, x and y are the position coordinates of the MR head with reference the right tip of the MR stripe. The origin of the coordinate system, as shown in figure 2(a), is located at the low left corner of a servo pattern.

The output of the MR head calculated by equation (1) when the MR head crossing a servo pattern along the longitudinal direction at different off-track displacement is shown in figure 2(b), which shows the output of the transverse MR head reaches a maximum v_p when the whole MR head is on the top of a servo pattern. Such a maximum output depends on the off-track displacement of the MR head. Therefore, the envelope curve of v_p at different y, which is shown in figure 2(c), can be used as position error signal (PES).

The obvious advantage of this new servo method is that the desired output of the servo head is no longer affected by the data trackwidth. Further more, the asymmetrical off-track response, which is typical for longitudinal read MR head[5],has no effect on the accuracy of the PES. Therefore, such a transverse read MR servo head could reproduce high quality PES for submicron track servo.

To realize submicron track following , a very accurate mechanical actuator is needed. Consequently a dual-stage actuator[6] must be used. As the track runout is of the order 100 μm, feed-forward head control is employed to minimize the runout in the new servo method.

III. Design Implementation

The transverse writing head is a thin film inductive head with gap length of 0.8 μm and trackwidth 6.0 μm. The transverse MR servo head is a shielded MR head with gap length of 0.7 μm and trackwidth of 4μm. A 3.5" rigid disk with longitudinal recording media of coercivity 1800 Oe were used. The writing of the servo patterns was undertaken on an air bearing disk spindle with nonrepeatable runout of less than 0.07 μm. An actuator with positioning accuracy of better than 0.05 μm was used to move the write head along the disk radial direction. When the disk running, the positioning actuator moves the write head to the first servo track position and servo pattern " 1 " was written into the track. The actuator then moves the write head to the next track position and servo pattern " 0 " was written into the track. The above process was repeated until the required number of servo tracks were all written. In order to optimise the quality of the PES, one hundred transverse servo tracks with various trackwidths ranging from 0.43 μm to 7.3 μm were written. The PES was then reproduced by using the shielded transverse MR head. The experimental results are show in figure 3.

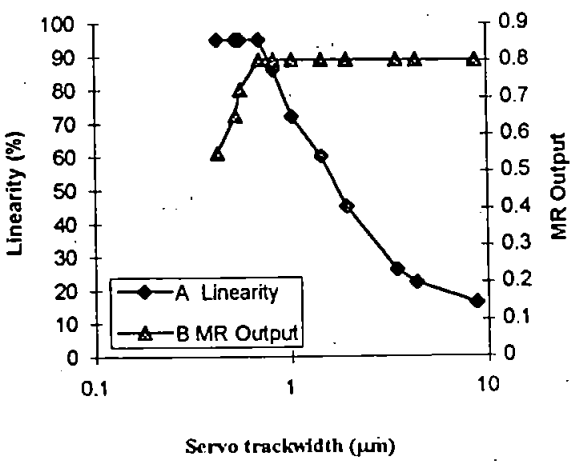

Fig. 3 readout, linearity of PES vs. servo trackwidth

Curve A in fig. 3 shows that the maximum PES level, which is produced when the MR head is aligned with the track edges, is independent of the servo trackwidth for trackwidth equal to or greater than the MR head inter-shield spacing. curve B in fig. 3 shows that the linearity [7] of PES improves as the servo trackwidth is reduced. As a result, the optimum quality of the PES was obtained when servo trackwidth is equal to the MR head inter-shield spacing, 0.7 μm in this experiment. Therefore track following on narrower tracks is possible if servo head with narrower gaps are used.

The submicron track following experiment was undertaken on an ordinary Winchester disk drive using the same kind of MR head and disks used in the above experiment. The servo patterns of the disk for track following experiment were pre-written using the air bearing spindle with low rotation speed. In order that the servo pattern is dispersed equally on a circular path, a clock head was used to supply clock pulses that are synchronized to the

angular position of the disk for the write head. 1536 servo patterns with trackwidth 0.7 μm were formatted on each single circular of the disk.[8] The servo patterns bit length is about 6μm. They occupy about 6.8 % of the data area.

The dual-stage actuator consists of a coarse actuator and a fine actuator in the experiment. The fine actuator has two piezoceramic bimorph elements, the structure of which is shown in Fig. 4. The dimensions of the element are 10 × 1.5 × 0.6 mm. The piezoceramic bimorph plate is simple and would become part of the structure of the head in future. The fine actuator has a 4 μm displacement when applied voltage is 50 v.

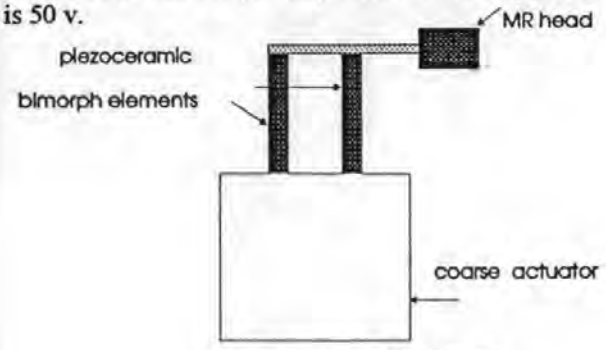

Fig. 4 Structure of a fine actuator.

A PES waveform reproduced by the servo MR head when it was seeking track is shown in Fig. 5. Its seeking speed on 0.7 μm track is about 10,000 tracks / S. The beginning part of the curve shows an accelerating period of the servo head. The S / N, linearity and servo gain of the PES is sufficient for the track following.

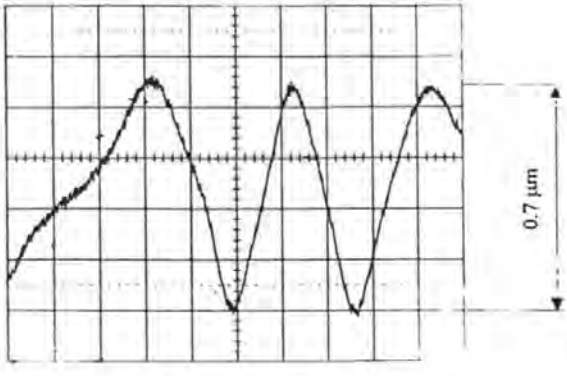

Fig. 5 A PES waveform obtained by transversing MR head as it crosses 5 tracks of 0.7μm.

Figure 6 shows two PES waveforms with or without track following for a disk mounted on an ordinary rigid disk drive. A and B on waveform (a) are the points where the crossing direction of the head changes. The waveform (b) in Fig. 6 shows the residual following error on 0.7 μm tracks is less than 0.07 μm (rms).

The disk running speed in this experiment was low since the heads were not specifically designed for transverse writing and reading. Nonetheless, sufficient information has been obtained to prove the principle of this method for submicron track following at normal disk operating speeds (e.g. 3600 rpm).

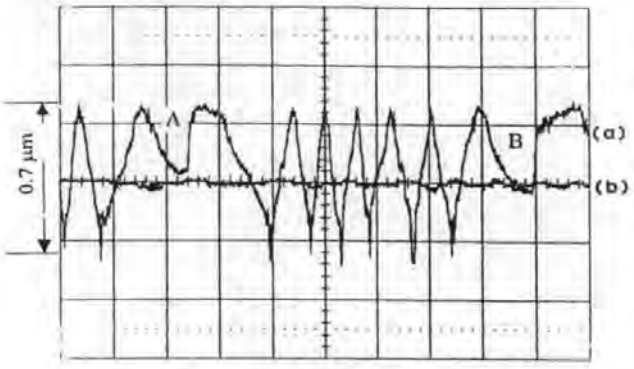

Fig. 6 (a) A PES waveform without track following, (b) A PES with track following

IV. Conclusion

A new servo system suitable for submicron track following has been reported in this paper. The experiments at lower disk rotation speed is achieved to track following at 36 k TPI (0.7μm trackwidth) with a 10 % track rms run-out, using this method.

Acknowledgment

The authors wish to thank Dr. N. Darragh for his helpful experiment and technical assistance. We also wish to thank Mr. S. C. Warner for his technical assistance. Special thanks are due to Prof. Ting Hua Liu from Hangzhou Computer Peripheral Equipment Research Institute of China for his encouragement.

References

[1] K. Akagi, T. Nakao, Y. Miyamura, "High Density Magnetic recording Tracking Method Using a Laser Diode" , *IEEE Trans. Magn.*, Vol. 27, PP5301-5303, Nov. 1991.

[2] M. Futamoto, F. Kugiya, M. Suzuki, H. Takano, Y. Matsuda, N. Inaba, Y. Miyamura, K. Akagi, T. Nakao and H. Sawaguchi, "Investigation of 2Gb/in^2 Magnetic Recording at a Track Density of 17 k TPI", *IEEE Trans. Magn.*, Vol. 27, P P5280-5285, Nov. 1991.

[3] K. Watanabe, T. Takeda, K. Okada and H. Takino, "Demonstration of Track Following Technique Based on Discrete Track Media", *IEEE Trans. Magn.*, Vol. 29, P P4030-4032,Nov. 1993.

[4] Jian-Gang Zhu, Xiao-Guang Ye and T.C. Arnoldussen,"Side Writing Phenomena in Narrow Track Recording", *IEEE Trans., Magn.*, Vol. 28, PP2716-2718, Sep. 1992.

[5] J. K. Lee, A. Wallash and A. L. Poon, " Effect of Read / Write Misalignment and Asymmetric Side Reading on Magnetoresistive Head Off-Track Performance", *J. Appl. Phys.* 69(8), PP5399-5401, April, 1991.

[6] K. Mori, T. Munemoto, H. Otsuki, Y. Yamaguchi and K. Akagi,"A Dual-stage Magnetic Disk Drive Actuator Using a Piezoelectric Device for High Track Density", *IEEE Trans. Magn.*, Vol. 27, PP5298-5300, 1991.

[7] K. Ishii and M. Mizukami,"High Density Servo Signal Detection for Accurate Head Positioning", *IEEE Trans. Magn.*, Vol. 23, PP3684-3686, Sep. 1987.

[8] Baolin Tan, Z.Yang, Y. Zhu and D. He,"A New Method of Testing Servowriting Pattern", *J. Magn. Soc. Japan*, Vol.15, No. S2, PP331-336, 1991 (PMRC'91).

Journal of The Magnetics Society of Japan Vol.18, Supplement, No.S1 (1994)

A New MR Head Track Following Method for Submicron Track Servo on Perpendicular Rigid Disks

Baolin TAN*, Genhua PAN, Desmond J. MAPPS

Centre for Research in Information Storage Technology
University of Plymouth, Plymouth, Devon, PL4 8AA, U.K.

Abstract—An extremely sensitive system detecting head position for submicron track following is achieved using a MR servo head which is at a right angle with the normal data head and radially magnetised servo patterns which are written by a thin film transverse write head. A dual-stage mechanical actuator system employing piezo-electric bimorph element as a fine actuator and as a bearing spring of the MR composite head is developed. On perpendicular rigid disks, track following on 0.7 μm track has been demonstrated using the new servo method.

I. INTRODUCTION

The minimum trackwidth in perpendicular magnetic recording rigid disks, as predicted by Nakamura [1], could be as small as 50 nm. The increase in track density is dictated by the head width and the accuracy with which the head can be positioned. K. Akagi et al. [2] developed an optical servo method on magnetic disk to obtain a high quality servo signal with a trackwidth 1.5 μm. A. Mori et al. [3] developed a dual-stage actuator used to 1.5 μm magnetic track following. K. Watanabe et al. [4] achieved 5.2 μm track following based on discrete track media using a servo signal reproduced by the data MR head. Recently, B. Tan et al. [5] has demonstrated track following on 0.7μm track on longitudinal rigid disks for longitudinal recording. However the submicron track following for perpendicular magnetic disk has never been studied.

The investigation reported in this paper is concerned with a new method of submicron track following on rigid disks with perpendicular recording media. Using such methods, a high quality of position error signal (PES) was obtained and 0.7 μm track following was demonstrated.

II. PRINCIPLE OF THE TRACK FOLLOWING METHOD

On longitudinal magnetic rigid disks, the asymmetrical off-track response for longitudinal read MR head is well-known. On perpendicular rigid disks it is more. An asymmetrical off-track readout by MR head on perpendicular rigid disks is shown in the Fig. 1. On the other hand, the data and servo pattern are magnetized along the circumferential direction in a conventional rigid disk. When data trackwidth is reduced, the effective servo head width and the S/N of the servo signal are reduced. Therefore conventional servo heads suffer from low S/N and poor linearity of PES for perpendicular rigid disks as the trackwidth is reduced to submicron size.

Baolin Tan is a visiting researcher in the C.R.I.S.T. Uni. of Plymouth U. K. now. He is with Hangzhou Computer Peripheral Equipment Research Institute of China.

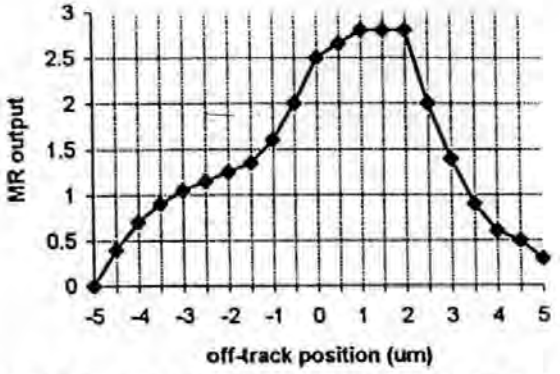

Fig. 1 Servo (off-track) curve reproduced by MR head on a perpendicular magnetic disk.

As shown in figure 2, the servo patterns in this new track following method are written along the radial direction by a transverse writing head that is aligned at a right angle with the normal data head. Servo signals are reproduced by a MR head with its stripe and pole gap tangential to the direction of the data track.

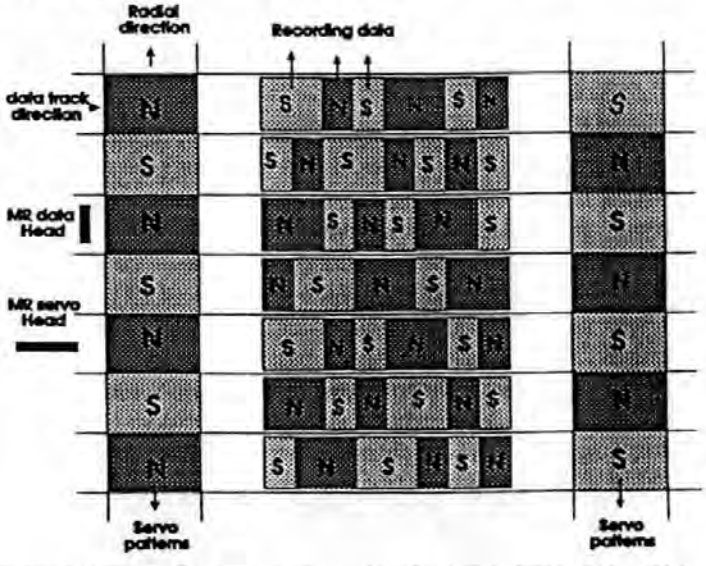

Fig. 2. Schematic diagram of new head position detection method

In the radial recording method the data trackwidth is equalled to the servo pattern bit length (L_R) in the radial direction. The L_R is defined by the gap length (g) of transverse write head and the position difference ($\Delta R = R_i - R_{i-1}$) of the servowrite head between the adjacent writes in the radial direction. It is found that

$$L_R = \begin{cases} g & g < \Delta R \\ \Delta R & g > \Delta R \end{cases} \quad \ldots\ldots (1)$$

The bit width (L_C) of a servo pattern in the circumferential direction is defined as following:

$$L_C = W_W + V\ t \quad \ldots\ldots (2)$$

W_W----the write head width, V----the speed of moved media
t----the pulse width of writing current

In this method, the side writing phenomena has no effect on the quality of the servo pattern for detecting head position because the side writing phenomena is not in the edge of data track.

Fig. 3 (a), (b) and (c) shows a simplified model of the reproducing process using the transverse read MR head in the new method. In the ideal case, the readout of the MR head could be roughly expressed by equation (3).

$V =$

$$\begin{aligned}
&V_{p,max}\frac{x}{W_{MR}}\left(\frac{2(y-nL_R)}{L_R}-1\right), && \text{when } 0<x<W_{MR},\ 2(n-1)<\frac{y}{L_R}<2n-1\\
&V_{p,max}\left(\frac{2(y-nL_R)}{L_R}-1\right), && \text{when } W_{MR}<x<L_C,\ 2(n-1)<\frac{y}{L_R}<2n-1\\
&V_{p,max}\left(1-\frac{x-L_C}{W_{MR}}\right)\left(\frac{2(y-nL_R)}{L_R}-1\right), && \text{when } L_C<x<W_{MR}+L_C,\ 2(n-1)<\frac{y}{L_R}<2n-1\\
&V_{p,max}\frac{x}{W_{MR}}\left(1-\frac{2(y-(n+1)L_R)}{L_R}\right), && \text{when } 0<x<W_{MR},\ 2n-1<\frac{y}{L_R}<2n\\
&V_{p,max}\left(1-\frac{2(y-(n+1)L_R)}{L_R}\right), && \text{when } W_{MR}<x<L_C,\ 2n-1<\frac{y}{L_R}<2n\\
&V_{p,max}\left(1-\frac{x-L_C}{W_{MR}}\right)\left(1-\frac{2(y-(n+1)L_R)}{L_R}\right) && \text{when } L_C<x<W_{MR}+L_C,\ 2n-1<\frac{y}{L_R}<2n
\end{aligned} \quad \ldots\ldots (3)$$

where the $V_{p,max}$ is the maximum peak voltage reproduced by the MR head when it passes the centre of a servo pattern, W_{MR} is the trackwidth of the MR head, L_C is the servo pattern bit width, L_R is the servo pattern bit length, n is data track number, Y direction is in radial of disks. The right tip of the MR head is reference point of (x, y).

The readout of the MR head calculated by equation (3) as the MR head crossing a servo pattern along the X axis direction at different off track displacement in Y direction is shown in Fig. 3(b), which shows the readout that the transverse MR head reaches a maxima Vp when the MR head is at the X axis direction centre of a servo pattern. Such a maxima depends on the off track displacement of the MR head. Therefore, the envelope curve of Vp at different y, which is shown in Fig. 3(c), can be used as PES. The points where the PES is equal to zero are used to indicate the data track centre.

The obvious advantage of the new servo method is that the readout of the servo head width is no longer affected by the data trackwidth. Further more, the asymmetrical off-track response has no effect on the accuracy of the detected head position. Therefore such a transverse read MR servo head could reproduce high quality PES for submicron track following.

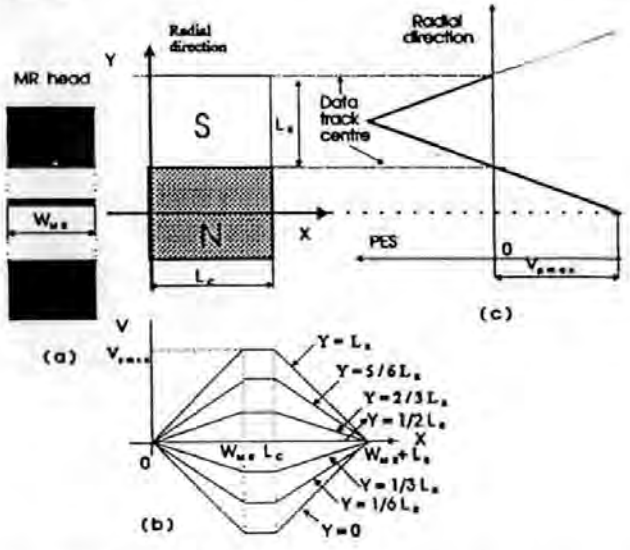

Figure 3: A simplified model for the reproducing process using transverse read MR head

III. Track Following on 0.7 μm Tracks

In the experiment, the transverse writing head is a thin film inductive head. Its gap length (0.8 μm) is in the radial direction and gap width (writing trackwidth 6.0 μm) is in the circumferential direction. The transverse MR servo head is a shielded MR head, also at a 90° angle to the conventional data head. The inter-shield gap length is 0.7 μm and MR trackwidth is 4μm. A 3.5" glass disk coated with CoCrTa single magnetic-layered perpendicular media was used. The CoCrTa media were deposited on Ti underlayers, with coercivity of 2000 Oe and thickness of 0.2 μm [6]. The writing of the servo pattern was undertaken on an air bearing disk drive spindle with nonrepeatable runout of less than 0.07 μm. An actuator with positioning accuracy of more than 0.05μm was used to move the write head along the disk radial direction as writing the servo pattern.

In order to optimise the quality of the PES, the experiment was undertaken on the disk on which one hundred transverse servo tracks with various trackwidths ranging from 0.40 μm to 8.2 μm were written. The PES was reproduced by an above shielded transverse MR head. The experiment results are show in figure 4.

Fig. 4 shows the maximum signal level and linearity of the reproduced PES as a function of servo pattern bit length.

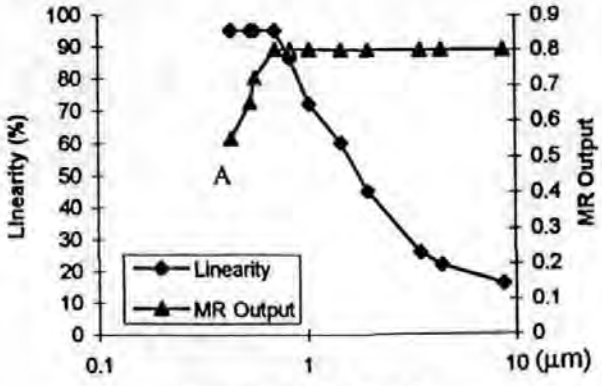

Fig. 4 readout, linearity of PES vs. servo pattern bit length

It can be seen from the figure that the maximum PES level is constant for the bit length equal to or greater than the MR head inter-shield spacing (curve A). The linearity of PES improves as the bit length is reduced. In the experiment, it was found that the S/N of the PES increases as the servo bit length is reduced for the bit length equal to or greater than the MR head inter-shield spacing. As a result, the optimum quality of the PES was obtained when servo pattern bit length is equal to the MR head inter-shield spacing.

According to the above results, the servo pattern bit length and width were designed for 0.7 and 8 μm (therefore data trackwidth is 0.7 μm). 1536 servo patterns were formatted equally on a circle path of the disk and every adjacent servo pattern is lined up radially [7]. They occupy about 9 % of the data area.

0.7 μm track following experiment was undertaken on the disk mounted on air bearing spindle. The experimental disk was running at a speed of 300 rpm and the head and the disk was in contact magnetic recording.

Because the magnetic trackwidth is of submicron size and the disk when it is running has a nonrepeatable runout, a dual-stage actuator is needed. The dual-stage actuator consists of a coarse actuator and a fine actuator in the experiment, as shown in Fig. 5 (a). A general piezoelectric bimorph element is used as a fine actuator and as a bearing spring of head slider too, as shown in Fig. 5 (b). The dimensions of the element are 9 × 1.5 × 0.6 mm. The fine actuator is part of the structure of the data / servo MR composite head.

The main performance with this piezoelectric bimorph was given below in the equation:

$$Z f_r = KE \quad \text{..... (4)}$$

Z = deflection, f_r = resonant frequency, E = electric field strength, K = constant.

This means that the product of deflection and resonant frequency is a constant for a given field strength. Therefore for driving magnetic heads any combination of deflection and resonant frequency may be chosen by varying the free length and thickness as well as material of the bimorph.

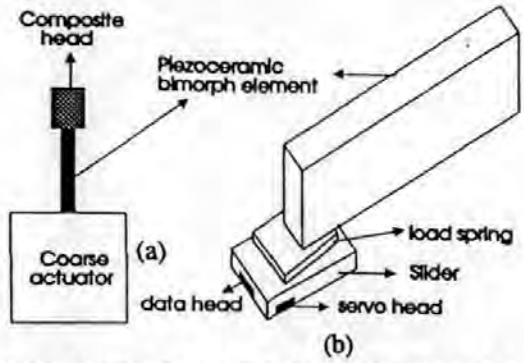

Fig. 5 (a) Diagram showing the structure of the dual-stage actuator

(b) The structure of the data/servo MR composite head

According to the above equation (4), we design a combination of bimorph characteristics and get a relationship of the fine actuator's displacement in the radial direction of the disk and the voltage supplying to the bimorph as shown in Fig. 6. Hysteresis and creep phenomena of piezoelectric bimorph plate make that 2 curve do not overlap in Fig. 6.

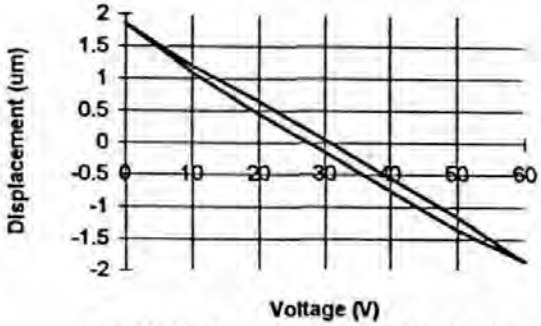

Fig.6. Displacement versus Voltage of a fine actuator

The relationship of load and resonant frequency of the fine actuator is shown in Fig. 7. In the experiment, the effective mass of the brimorph is 70 mg. As the speed of the disk is low, low resonant frequency is selected in the fine actuator. The mass of the slider and small load spring of the servo MR head is 11 mg. Then the resonant frequency of the fine actuator is about 2.4 kHz.

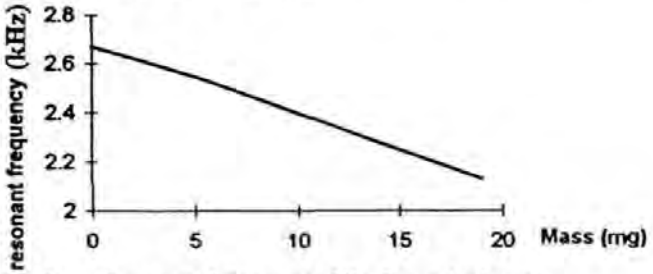

Fig. 7 Resonant frequency of the fine actuator vs. slider mass.

In the experiment of 0.7 μm track following, a PES reproduced by the servo MR head when it was seeking track is shown in Fig. 8. The S/N, linearity and servo gain of the PES is sufficient for the 0.7 μm track following.

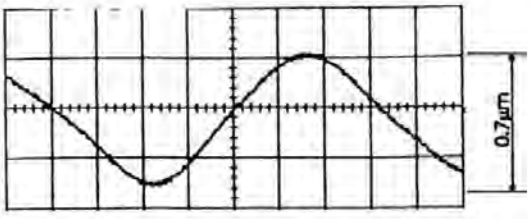

Fig. 8 A PES waveform reproduced by the servo MR head.

An output waveform of the servo MR head accessing tracks with trackwidth of 0.7μm is shown in Fig. 9. The head's seeking speed is about 10000 tracks per second. The S/N and linearity of the accessing waveform are sufficient for reliable operation and optimal seek performance.

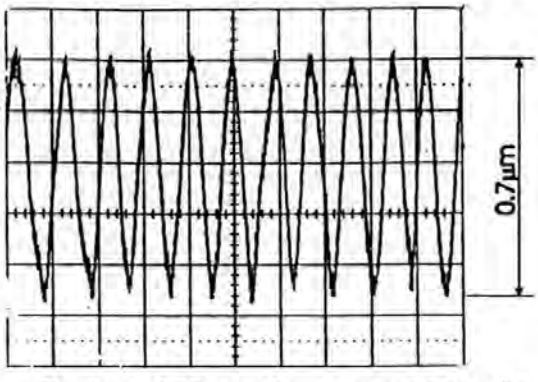

Fig. 9 A PES waveform accessed 22 tracks

Fig. 10 (a) shows the PES waveform without track following and with a degree of eccentricity as the centre of the disk as written servo pattern and the centre of rotation of the spindle motor are bound to differ. The left half of waveform (a) in Fig. 10 means that servo MR head crosses 8 tracks towards the inner; it's right half means that the MR head crosses 8 tracks towards the outside. The points A and B are points at cross direction change and points of maximum offset. The waveform (b) in Fig. 10 shows the residual following error on 0.7 μm track on the disk with

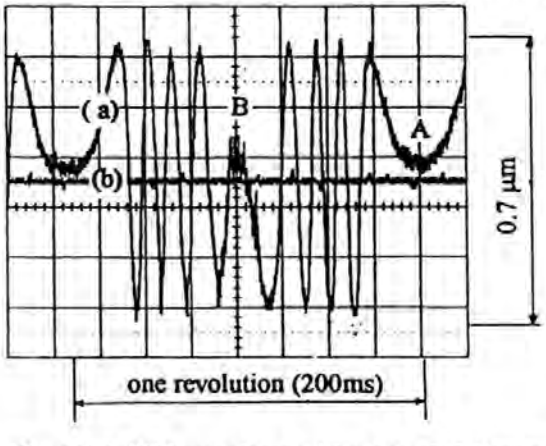

Fig. 10 (a) A PES waveform without track following, (b) A PES with track following

air bearing spindle with servo loop closed. The error is less than 0.07 μm (rms).

VI. Conclusion

A new servo system for submicron track following on perpendicular magnetic disks has been reported in the above. This uses writing and reading servo pattern magnetized along radial direction to obtain an extremely sensitive system for detecting head position. A piezoelectric bimorph element is designed as a fine actuator and as a bearing spring of the MR composite head. Track following on 0.7μm track on perpendicular rigid disks is achievable.

Furthermore, it is tendency that servo signal is reproduced by a servo head, not by a data head for submicron trackwidth following. This new head 'position detection method is based on high bit density technology of magnetic recording. Therefore the method can meet the need of ultra-high track density, along with the development of ultra-high bit density technology. The new servo method would seem to have the potential of achieving track density up to 254 K TPI (0.1μm) if the servo pattern is formatted with high accuracy.

Acknowledgement

The authors wish to thank Dr. N. Darragh and Phil Brown for their technical assistance. Special thanks are due to Prof. Jiangling Zhang for his encouragement.

References

[1] Y. Nakamura, " Theoretical and Experimental Prospects of perpendicular magnetic recording", J. Magn. Soc. Japan, vol.15, No. S2, pp.497-506, 1991.

[2]. K. Akagi, T.Nakao, Y.Miyamura," High Density Magnetic recording Tracking Method Using a Laser Diode ", IEEE Trans. Magn., vol. 27, pp.5301-5303 Nov. 1991.

[3] K.Mori, T. Munemoto, H. Otsuki, Y. Yamaguchi and K. Akagi, " A Dual-stage Magnetic Disk Drive Actuator Using a Piezoelectric Device for High Track Density ", IEEE Trans. Magn., vol. 27, pp.5298-5300, Nov. 1991.

[4] K. Watanabe, T Takeda, K. Okada and H. Takino " Demonstration of Track Following Technique Based on Discrete Track Media ", IEEE Trans. Magn., vol. 29, pp.4030-4032 (1993).

[5] B. Tan, G. Pan and D. J. Mapps, " A New MR Head Track Following Method for Submicron Track Servo on Rigid Disks ", Paper EC-05, Presented at the 6th Joint MMM-Intermag Conference (1994).

[6] D. J. Mapps, G. Pan, M. A. Akhter, S. Onodera and A.Okabe, " In-contact magnetic recording performance of Pt / CoCrTa thin films on glass computer disks ", Journal of Magnetism and Magnetic Material 120 (1993) 305-309.

[7] Baolin Tan, Z. Yang, Y. Zhu and D. He, "A New Method of Testing Servowriting Pattern", J. Magn. Soc. Japan, vol.15, No. S2, pp.331-337, 1991

ELSEVIER

Journal of Magnetism and Magnetic Materials 155 (1996) 345–347

Journal of magnetism and magnetic materials

A new servo method using servo layer and transverse MR head for submicron track servo on hard computer disks

Baolin Tan *, Desmond J. Mapps, Genhua Pan, Paul Robinson

Centre for Research in Information Storage Technology University of Plymouth, Plymouth, Devon, PL4 8AA, UK

Abstract

A disk with a data, servo and isolation layer has been fabricated with the data layer magnetized along the circumferential direction. The servo layer was recorded with servo pattern magnetized along the radial direction. A continuous servo signal is obtained and the servo does not occupy any data area. In this new method, the servo and data bits can share media surface area on the disk without interference. Track following on 0.7 μm tracks has been demonstrated using the new servo method on longitudinal rigid disks.

1. Introduction

For magnetic rigid disks, it is not only important to increase bit density, but also to increase track density. A large increase in track density is anticipated in the 21st century [1]. Akagi et al. [2] used a laser diode and pits fabricated on a magnetic disk to obtain a high quality servo signal on a 1.5 μm track. Track following on a 0.7 μm track on longitudinal and perpendicular rigid disks has been demonstrated using a transverse MR head and radially magnetised servo patterns [3,4]. In these methods, the servo signal is no longer continuous. Therefore these servo methods have narrower bandwidth, poorer transient response, and are highly sensitive to variations and medium defects as the trackwidth is reduced to submicron size. In this study, a continuous servo signal was obtained. The servo information did not occupy any data area and following on 0.7 μm tracks was demonstrated.

2. Model of new servo method

Haynes [5] used a 'buried servo' method to obtain a positioning system on 50 μm trackwidth, in which servo and data can share a media surface area by using the surface for data only and deeper positions for servo only. In our study, the medium of the disk consists of a top data layer, a middle isolation layer and a bottom servo layer, as shown in Fig. 1. The data layer contains exclusively data bits and is magnetized along the circumferential direction. The servo layer is exclusively for servo bits magnetized along the radial direction by a transverse writing head that

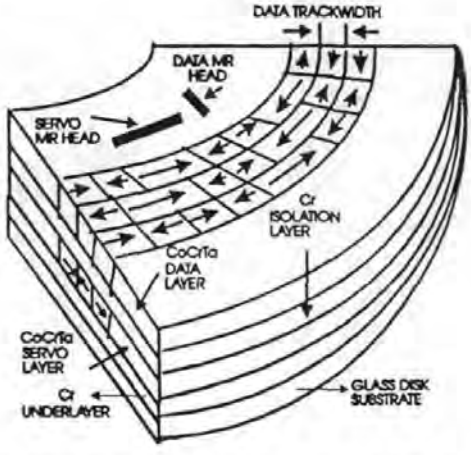

Fig. 1. Schematic diagram of the new servo method using servo layer and transverse MR head.

is aligned at right angles with the normal data head. The isolation layer is used to reduce the effect of the servo layer in reproducing data bits in the data layer and to guard against the data head re-writing servo information in the servo layer. The servo signals are reproduced by a transverse MR head with its stripe and pole gap tangential to the circumferential direction. The data signals are reproduced by a conventional MR head. The major advantages of the servo method are that the servo signal is continuous, its quality has low sensitivity to medium defects and is no longer limited by the data trackwidth.

3. Sputtering multilayer thin films on disks

In the experiment, servo layer, data layer, isolation layer and underlayer were deposited onto 2.5″ glass disks

* Corresponding author. Fax: +44-1752-232583; email: btan@plymouth.ac.uk.

0304-8853/96/$15.00
SSDI 0304-8853(95)00692-3

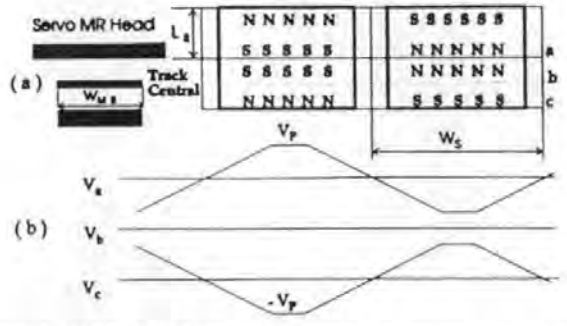

Fig. 2. (a) MR head footprint for detecting transverse magnetised servo patterns. (b) MR output voltage.

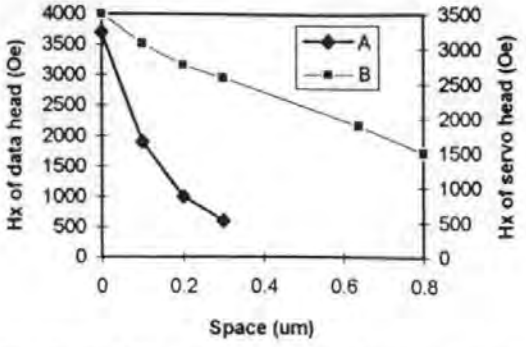

Fig. 4. Write field of servo and data head decays with spacing.

by rf sputtering. The background pressure was approximately 2×10^{-7} Torr and the sputtering pressure (Ar) was 10 mTorr. A substrate bias (-100 V) was applied during the sputtering process of CoCrTa thin film. Magnetron sputtering was used to increase deposition rate of the Cr thin film. The thickness of each layer was controlled by deposition time and using a movable shutter. The temperature of the substrate was controlled to achieve different coercivities for servo and data layers. The Cr layer was grown with a deposition rate of 1000 Å/min using a sputtering power of 600 W, while the CoCrTa layer was 200 Å/min using a sputtering power of 400 W. The structure of the multilayer thin films is shown in Fig. 1.

4. Servo pattern

In order to reduce high frequency components, any harmonics and peak shift of the servo signal, the servo pattern was designed as shown in Fig. 2(a), so that servo signals reproduced by the servo head have low frequency and are near sinusoidal.

The total (N) of servo patterns per track and servo signal frequency (f) are defined as follows:

$N = \pi R / W_s, \quad f = N \times V,$

where N must be an integer number, R is the radius of the central line of the data magnetic track and V is the rotating speed of the disk. When $W_s > W_{MR}$, the asymmetrical off-track response and the side writing phenomenon have no effect on the accuracy of the detected head position. In Fig. 2(b), V_a, V_b and V_c are waveforms when the MR head crosses the servo pattern along the circumferential direction at points of a, b and c. The peak value V_p of the position signal can be used to indicate off-track displacement. The envelope curve of V_p can therefore be used as a position error signal (PES).

5. Servo detection

In the new method, the servo signal is about 200 kHz for a 2.5″ disk and the servo pattern width (W_s) is 5 μm. The frequency of the data signal is usually over 10 MHz. This is over 50 times that of the frequency of the servo signal. The data and servo signal must occupy high and low frequency parts of the spectrum. The contributing noise from each servo and data signal to each other can be filtered out using high and low pass filters.

Curve A in Fig. 3 shows that servo signal output is increased as the MR trackwidth of the servo head is increased. In the experiment the data track was written all 1's and the data layer had H_c = 1300 Oe. The thickness of

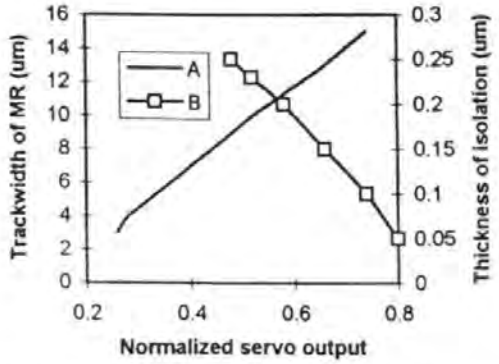

Fig. 3. Servo MR output vs. trackwidth of MR and thickness of isolation layer.

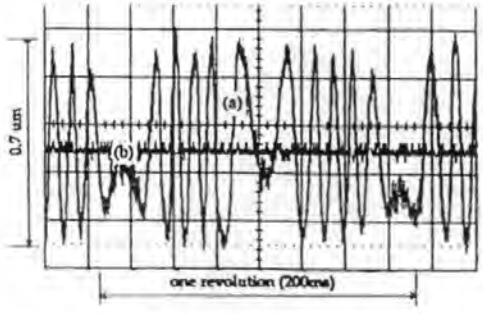

Fig. 5. PES waveform: (a) without track following, (b) with track following.

isolation layer was 0.2 μm. The coercivity of the servo layer is 1900 Oe. The widths of servo pattern in radial and circumferential directions were 0.7 and 20 μm respectively, so that the side reading effect of the MR head was removed in the experimental result. Curve B in Fig. 4 shows that servo signal output reproduced by a 10 μm trackwidth MR head is reduced as the thickness of the isolation layer is increased.

To assure the integrity of the servo layer, the data recording magnetic field produced by the data write head, H_{xd}, must be less than $0.5H_{cs}$ at the upper boundary of servo layer. On the other hand, the H_{xd} should be more than 2 times the coercive field at the bottom boundary of the data layer. The servo recording field produced by a servo write head, H_{xs}, must be greater than 1.5 times the H_{cs} of the bottom boundary of the servo layer. The write magnetic field of data and servo head used in the experiment varies with space between head and medium as shown in Fig. 4.

The experimental results of S/N studies on servo and data signals show that the S/N ratio of the servo signal is increased as the coercivity of the data layer or the thickness of isolation layer is reduced or as the coercivity of the servo layer is increased. It also shows that the S/N ratio of the data signal is increased as the coercivity of the servo layer is reduced or the thickness of isolation layer or the coercivity of data layer are increased.

To optimise the above system it is necessary to first establish the S/N ratio of the data signal by choosing H_c (data) and then adjust isolation layer thickness and H_c (servo) to increase the S/N ratio of the servo signal.

6. Track following on 0.7 μm tracks

In the following experiment on 0.7 μm tracks, a 2.5″ glass disk was made with a 400 Å thick CoCrTa film of coercivity 1900 Oe and $S^* = 0.78$ as a servo layer. The CoCrTa data layer had a coercivity of 1300 Oe, thickness 350 Å and $S^* = 0.81$. The isolation layer was 2000 Å thick and the carbon overcoat 250 Å thick. The servo bits in the servo layer on the disks were written by a thin film inductive transverse head with trackwidth of 6 μm and gap length of 0.8 μm [4]. The servo signal was reproduced by a shielded transverse MR head with trackwidth of 10 μm and an inter-shield gap length of 0.7 μm. A data write head with shorter gap length (0.25 μm) was used, so that it did not rewrite servo bits. After the servo patterns has been recorded, the data layer was dc or ac erased with a magnetic field whose strength was less than the servo write field. Then data tracks on the data layer were written with an all 1's pattern. A dual-stage actuator with piezoelectric bimorph was used in the following servo experiment [3]. The track following servo was tested on 0.7 μm servo trackwidth, as the disk was running at a speed of 300 rpm and the servo head and the disk was 'in-contact' magnetic recording. The waveform (a) in Fig. 5 shows the PES waveform without track following and with a degree of eccentricity to test the track-following properties. The waveform (b) shows that the residual following error on a 0.7 μm track is less than 0.1 μm.

7. Conclusion

A new servo method for submicron track following has been reported. A continuous servo signal is obtained which does not occupy any data area. Track following on 0.7 μm tracks has been demonstrated using the new method on longitudinal rigid disks.

Acknowledgements

The authors wish to thank Dr R. Chandrasekhar for discussions. We also wish to thank Mr. Phil Brown for his technical assistance. Special thanks to Pilkington Micronics for providing glass disks.

References

[1] H.H. Ottesen, J. Magn. Soc. Jpn. 18 (1994) 31.
[2] K. Akabi, T. Nakao, Y. Miyamura, IEEE Trans. Magn. 27 (1991) 5301.
[3] B. Tan, G. Pan and D.J. Mapps, IEEE Trans. Magn. 30 (1994) 4206.
[4] B. Tan, G. Pan and D.J. Mapps, J. Magn. Soc. Jpn. 18 (1994) 579.
[5] M.K. Haynes, IEEE Trans. Magn. 17 (1981) 2730.

CP27

Demonstration of a Magnetic Angular Position Sensor with ultra-high Accuracy

B Tan, D J Mapps*

Test Dept., Xyratex Ltd, Havant, PO9 1SA, Hampshire

**S.E.C.E.E., Unversity of Plymouth, Plymouth, PL4 8AA, Devon*

Magnetic absolute and incremental encoding systems with 500 pulses/rev and 1667/rev are reported by Campbell [1] and by Scheme [2], respectively. In this study, 160,000 pulses/rev and 0.4 accuracy are obtained using a longitudinal disk, MR sensors and a new method of formatting magnetic poles on the disk.

In this study, the magnetic poles are formatted by a thin film inductive head with a 6 μm trackwidth and 0.70 μm gap length. In order to format equally all magnetic poles (particularly the gap between the first pole and the formatted last pole) on a circular path on the disk a new method is used, in which the head is run freely at a designed signal frequency. The disk is rotated at an ideal speed with all possible small errors of the speed until an integral number of designed magnetic poles on the circular path is obtained. It will take a few seconds. An angular position signal is reproduced by two MR sensors. These are commercial MR heads with a 4μm trackwidth, 0.6 μm gap length and maintained in phase quadrature each other, to obtain signal on the direction of rotation and the counting. In the experiment, a disk with coercivity of 1800 Oe and M_r of 0.85 emu/cm^2 was maintained on an air bearing disk drive spindle and was rotating at 300 5400 rpm with 0.1% error. An integral number of 160,000 magnetic poles/rev can be successfully written when the central frequency of the writing signal is 10 Mhz and the speed of disk is 3750 rpm with 0.1% error. It takes 4.3 seconds to stabilize.

In this study, it is found that the probability of formatting an integral number (N) of poles around the track is maximum when the central frequency of the writing is matched to the central frequency of the speed of disk and the steadiness of the disk speed and writing frequency are high. The experimental results show that linearity of the angular position signal is maximum when the gap of the shielded MR head is equal to the length (L) of magnetic pole. The magnitude of angular position signal is equal to Sin^{-1} (2L/W) (W is the trackwidth of the MR head) or the gap length of the MR head is equal to twice the length of the pole.

[1] P Campbell, IEEE Trans Magn, Vol 26, No 3, pp2029-2031, 1990
[2] I H Schewe, J of the Magnetics Society of Japan, Vol 18, pp49-52, 1994